Title
Experimental Validation of Passive Safety System Models: Application to Design and Optimization of Fluoride-Salt-Cooled, High-Temperature Reactors

Author
Zweibaum, Nicolas

Publication Date
2015

Peer reviewed|Thesis/dissertation

Experimental Validation of Passive Safety System Models: Application to Design and Optimization of Fluoride-Salt-Cooled, High-Temperature Reactors

by

Nicolas Zweibaum

A dissertation submitted in partial satisfaction of the

requirements for the degree of

Doctor of Philosophy

in

Engineering – Nuclear Engineering

in the

Graduate Division

of the

University of California, Berkeley

Committee in Charge:

Professor Per F. Peterson, Chair
Professor Ehud Greenspan
Professor Arpad Horvath

Summer 2015

Experimental Validation of Passive Safety System Models: Application to Design and Optimization of Fluoride-Salt-Cooled, High-Temperature Reactors

by

Nicolas Zweibaum

Abstract

Experimental Validation of Passive Safety System Models: Application to Design and Optimization of Fluoride-Salt-Cooled, High-Temperature Reactors

by
Nicolas Zweibaum

Doctor of Philosophy in Engineering – Nuclear Engineering

University of California, Berkeley
Professor Per F. Peterson, Chair

The development of advanced nuclear reactor technology requires understanding of complex, integrated systems that exhibit novel phenomenology under normal and accident conditions. The advent of passive safety systems and enhanced modular construction methods requires the development and use of new frameworks to predict the behavior of advanced nuclear reactors, both from a safety standpoint and from an environmental impact perspective. This dissertation introduces such frameworks for scaling of integral effects tests for natural circulation in fluoride-salt-cooled, high-temperature reactors (FHRs) to validate evaluation models (EMs) for system behavior; subsequent reliability assessment of passive, natural-circulation-driven decay heat removal systems, using these validated models; evaluation of life cycle carbon dioxide emissions as a key environmental impact metric; and recommendations for further work to apply these frameworks in the development and optimization of advanced nuclear reactor designs. In this study, the developed frameworks are applied to the analysis of the Mark 1 pebble-bed FHR (Mk1 PB-FHR) under current investigation at the University of California, Berkeley (UCB).

The capability to validate integral transient response models is a key issue for licensing new reactor designs. This dissertation presents the scaling strategy, design and fabrication aspects, and startup testing results from the Compact Integral Effects Test (CIET) facility at UCB, which reproduces the thermal hydraulic response of an FHR under forced and natural circulation operation. CIET provides validation data to confirm the performance of the direct reactor auxiliary cooling system (DRACS) in an FHR, used for natural-circulation-driven decay heat removal, under a set of reference licensing basis events, as predicted by best-estimate codes such as RELAP5-3D. CIET uses a simulant fluid, Dowtherm A oil, which at relatively low temperatures (50-120°C) matches the Prandtl, Reynolds, Froude and Grashof numbers of the major liquid salts simultaneously, at approximately 50% geometric scale and heater power under 2% of prototypical conditions. The studies reported here include isothermal pressure drop tests performed during startup testing of CIET, with extensive pressure data collection to determine friction losses in the system, as well as subsequent heated tests, from parasitic heat loss tests to more complex feedback control tests and natural circulation experiments. For initial code validation, coupled steady-state single-phase natural circulation loops and simple forced cooling transients were conducted in CIET. For various heat input levels and temperature boundary conditions, fluid mass flow rates and temperatures were compared between RELAP5-3D results, analytical solutions when available, and experimental data. This study shows that RELAP5-3D provides excellent predictions of steady-state natural circulation and simple

transient forced cooling in CIET. The code predicts natural circulation mass flow rates within 8%, and steady-state and transient fluid temperatures, under both natural and forced circulation, within 2°C of experimental data, suggesting that RELAP5-3D is a good EM to use to design and license FHRs.

A key element in design and licensing of new reactor technology lies in the analysis of the plant response to a variety of potential transients. When applicable, this involves understanding of passive safety system behavior. This dissertation develops a framework to assess reliability and propose design optimization and risk mitigation strategies associated with passive decay heat removal systems, applied to the Mk1 PB-FHR DRACS. This investigation builds upon previous detailed design work for Mk1 components and the use of RELAP5-3D models validated for FHR natural circulation phenomenology. For risk assessment, reliability of the point design of the passive safety system for the Mk1 PB-FHR, which depends on the ability of various structures to fulfill their safety functions, is studied. Whereas traditional probabilistic risk assessment (PRA) methods are based on event and fault trees for components of the system that perform in a binary way – operating or not operating –, this study is mostly based on probability distributions of heat load compared to the capacity of the system to remove heat, as recommended by the reliability methods for passive safety functions (RMPS) that are used here. To reduce computational time, the use of response surfaces to describe the system in a simplified manner, in the context of RMPS, is also demonstrated. The design optimization and risk mitigation part proposes a framework to study the elements of the design of the reactor, and more specifically its passive safety cooling system, which can contribute to enhanced reliability of heat removal under accident conditions. Risk mitigation measures based on design, startup testing, in-service inspection and online monitoring are proposed to narrow probability distributions of key parameters of the system and increase reliability and safety.

Another major aspect in the development of novel energy systems is the assessment of their impacts on the environment compared to current technologies. While most existing life cycle assessment (LCA) studies have been applied to conventional nuclear power plants, this dissertation proposes a framework to extend such studies to advanced reactor designs, using the example of the Mk1 PB-FHR. The Mk1 uses a nuclear air-Brayton combined cycle designed to produce 100 MWe of base-load electricity when operated with only nuclear heat, and 242 MWe using natural gas co-firing for peaking power. The Mk1 design provides a basis for quantities and costs of major classes of materials involved in building the reactor and fabricating fuel, and operation parameters. Existing data and economic input-output LCA models are used to calculate greenhouse gas emissions per kWh of electricity produced over the life cycle of the reactor. Baseline life cycle emissions from the Mk1 PB-FHR in base-load configuration are 26% lower than average Generation II light water reactors in the U.S., 98% lower than average U.S. coal plants and 96% lower than average U.S. natural gas combined cycle plants using the same turbine technology. In peaking configuration, due to its nuclear component and higher thermal efficiency, the Mk1 plant only produces 32% of the emissions of average U.S. gas turbine simple cycle peaking plants. One key contribution to life cycle emissions results from the amount and type of concrete used for reactor construction. This is an incentive to develop innovative construction methods using optimized steel-concrete composite wall modules and new concrete mixes to reduce life cycle emissions from the Mk1 and other advanced reactor designs.

To the French and U.S. public education systems.
The passion and rigor of your professors have shaped my achievements and aspirations.

To my parents, who have always trusted my choices, and to my friends.
Thank you for making me feel home when I come back, wherever that is.

Acknowledgments

Here comes the dreaded time. Moving on to a new life, I still have one, non-peer-reviewed page to write. As a disclaimer, I should say that I am so grateful to so many people for what we have accomplished that it is impossible for me to make an exhaustive list. But... here it is.

First and foremost, I would like to thank Anne-Perrine Avrin for providing the moral, intellectual and emotional support that was well needed over these past years. You are the most amazing person I know and I am sorry if my only way to thank you has been to keep you up at night for endless conversations or lights on as I was working. I will do my best to find better ways to keep supporting you back through the great future ahead of us. I would like to thank my parents, who always supported my choices and gave me the taste of research when I was a young child by letting me play Tetris on their lab's Macintosh Classic while they were changing their cells' culture mediums. I wish I had not had to always travel so far to find inspiration but I hope you keep understanding. I would also like to thank my friends, with special mentions to Frédéric, Alice and Adrien back home, who endured Skype and phone calls at improbable hours, and my homemates Amine, Hubert and Chris, who indirectly supported this work by helping me decompress so many times.

I would like to acknowledge the exceptional leadership of Professor Peterson. I am extremely grateful that, despite your many responsibilities, you always found time to share your fundamental thoughts with me and encouraged me to do what I thought was right for this major project. Also, I would probably not be in the U.S. if it had not been for the first months I spent in Berkeley, hosted by Professor Greenspan. You were the first to teach me rigor in research and I did my best so that this project live up to the quality you instilled in my previous work. Finally, I would like to thank Professor Horvath for broadening my horizons through his remarkable teaching and for agreeing to supervise some of my research work.

I will be eternally grateful to Raluca Scarlat for being such a great mentor, peer and friend. You inspired this whole project as I saw you inspire the people who worked with you, and I am glad you will keep doing this as a professor and a parent. I also feel privileged to have crossed paths with Zhangpeng Guo, whose original mindset, curiosity and creativity permeate the quality of the work we have accomplished together. I wish you the best of luck for what awaits you and I hope our paths cross again in the near future. This project would never have taken shape absent the countless hours spent by Jeff Bickel and AJ Gubser designing and physically working on all the bits and pieces that made it a reality. In many ways you have been like big brothers to me, teaching me so much about the American culture, how to be a real engineer and how to make practical choices. Finally, I am amazed at the dedication and quality of the work performed by many students in the lab, which made a lot of things possible for this project. Special thanks go to James Kendrick, Lakshana Huddar, Rohit Upadhya, Alan Yamanaka, Aldrich Ong, Eric Yehl, Alex Chong and AJ Albaaj. You always displayed great attitudes and I am glad I got to become friends with some of you. I wish you the best in your future endeavors.

Last but not least, I would like to express my warmest thanks to Noriko Katagiri and Lisa Zemelman, who were always so dedicated and helpful guiding me through the tortuous paths of the University's administration. None of the research we have done would have been possible without them and they deserve all the credit for my PhD not having taken twice as long as it did.

Table of Contents

List of Figures

List of Tables

Acronyms

AD – Air duct
aPC – Arbitrary polynomial chaos
ASME – American Society of Mechanical Engineers
ASPRA – Assessment of passive system reliability
ATWS – Anticipated transient without scram
B&PV – Boiler and Pressure Vessel
CAD – Computer aided design
CFD – Computational fluid dynamics
CIET – Compact Integral Effects Test
CTAH – Coiled tube air heater
DAQ – Data acquisition
DHX – DRACS heat exchanger
DRACS – Direct reactor auxiliary cooling system
EIO-LCA – Economic input-output life cycle assessment
EM – Evaluation model
FANCY – FHR advanced natural circulation analysis
FHR – Fluoride-salt-cooled, high-temperature reactor
FOM – Figure of merit
GE – General Electric
GHG – Greenhouse gas
GTSC – Gas turbine simple cycle
GWP – Global warming potential
HTGR – High-temperature gas-cooled reactor
IET – Integral effects test
INL – Idaho National Laboratory
IRP – Integrated research project
LBE – Licensing basis event
LCA – Life cycle assessment
LOFC – Loss of forced cooling
LOHS – Loss of heat sink
LWR – Light water reactor
Mk1 – Mark-1
MSRE – Molten Salt Reactor Experiment
NACC – Nuclear air-Brayton combined cycle
NGCC – Natural gas combined cycle
NU – Natural uranium
OPC – Ordinary Portland cement
ORNL – Oak Ridge National Laboratory
PB-AHTR – Pebble-bed advanced high-temperature reactor
PB-FHR – Pebble-bed fluoride-salt-cooled, high-temperature reactor

PCE – Polynomial chaos expansion
PCM – Probabilistic collocation method
PIRT – Phenomena identification and ranking table
PRA – Probabilistic risk assessment
PWR – Pressurized water reactor
REPAS – Reliability evaluation of passive safety systems
RMPS – Reliability methods for passive safety functions
RSM – Response surface methodology
RTD – Resistance temperature detector
SB – Shield building
SC – Steel-concrete composite
SET – Separate effects test
SFR – Sodium-cooled fast reactor
SWU – Separative work unit
TC – Thermocouple
TCHX – Thermosyphon-cooled heat exchanger
TRISO – Tristructural isotropic
UCB – University of California, Berkeley
USNRC – U.S. Nuclear Regulatory Commission
VFD – Variable frequency drive
VI – Virtual instrument
V&V – Verification and validation

Chapter 1 Introduction

As the global population grows (over +1% per year in the past decade [1]) along with living standards and associated energy needs, energy procurement with low environmental impact has become a major challenge worldwide. In 2012, oil, coal and natural gas represented 31.4%, 29.0% and 21.3% of the world's total primary energy supply, respectively, while nuclear and renewable energies only represented 4.8% and 3.5%, respectively [2]. In a world of increasing tensions, with a weakened economy and the threat of air pollution and climate change, solutions are being sought to continuously develop and improve reliable and affordable energy sources with lower life cycle particulate pollution and carbon dioxide emissions compared to traditional fossil fuels. In this context, nuclear technology in general, and advanced nuclear reactors in particular, with increased safety, enhanced fuel use, reduced waste production and improved economics, are viewed as key players to address these challenges and provide low-carbon electricity and heat to both developed and developing countries in the decades to come. One major element in Generation III+ reactors such as Westinghouse's AP1000, and most advanced reactor designs, is the use of passive safety. Unlike their active counterparts, passive safety systems do not rely on external energy sources such as the electric grid or backup power generators to remove decay heat under accident conditions. Instead, their functionality depends purely on natural driving forces such as buoyancy, which makes them reliable, with no human intervention, in a much wider range of conditions. Combined with the traditional design approach using active systems for normal shutdown cooling, the use of passive safety is aimed at improving safety while reducing capital costs, thanks to simplified systems with a reduced need for redundant, costly, active safety trains.

One major challenge introduced by the use of novel classes of safety systems lies in the need to predict the behavior of increasingly complex, integrated systems. Before a new reactor technology is deployed at commercial scale, integral behavior of the system under a wide range of conditions must be predicted, and in particular, it must be demonstrated that safety requirements set forth by the domestic nuclear safety regulatory authority are met. While such predictions are primarily based on the use of computer codes, reliability of these codes in predicting system behavior must itself be assessed. In particular, for thermal hydraulic behavior of novel reactor designs, best-estimate codes can be validated with data from integral effects test (IET) facilities, which reproduce the integral behavior of the system of interest under a wide range of initial and boundary conditions. Design, fabrication and operation of IETs have been simplified with the advent of reduced height, reduced area and reduced power scaling. For reactors that use molten salts as coolants, the complexity of high fidelity IETs can be further decreased through the use of simulant fluids that can replicate key thermal hydraulic phenomena of a prototypical system at reduced scale, power and temperatures.

While a large set of references exist that address key challenges for a number of advanced reactor designs, this study focuses on analysis of passive safety for fluoride-salt-cooled, high-temperature reactors (FHRs) in support of design and licensing of this reactor class, as well as life cycle assessment (LCA) of this technology from an environmental standpoint. In particular,

this dissertation reports the design, construction, operation and simulation of a novel IET dedicated to FHR technology, and the use of validated models and preliminary design aspects to assess both the reliability of passive safety systems and the life cycle environmental impacts of an advanced nuclear reactor design, using the FHR as an example of a more widely applicable framework.

FHRs use a novel combination of high-temperature coated-particle fuel, initially developed for high-temperature gas-cooled reactors (HTGRs); fluoride salt coolant, first experimented in the Molten Salt Reactor Experiment (MSRE) at Oak Ridge National Laboratory (ORNL) in the 1960's; and a low-pressure primary system that delivers heat in the temperature range from 600°C to 700°C or higher, leading to improved power conversion efficiency compared to the existing fleet of light water reactors (LWRs). Recent studies of FHRs have suggested the potential to achieve attractive economic performance while meeting high standards for reactor safety and security [3-9]. Because FHRs exhibit different thermal hydraulic phenomena compared to conventional, more extensively studied advanced nuclear reactor concepts, further investigation of FHR technology requires the development of novel evaluation models (EMs) – simulation codes – to appropriately predict the behavior of this class of reactors under steady-state operation and a range of postulated licensing basis events (LBEs). Moreover, existing LCA studies of the traditional nuclear power plants that already operate must be extended to advanced reactor designs such as the FHR, as they are being designed and developed, to further reduce life cycle emissions and make nuclear power an even better option for future energy production in the context of climate change mitigation.

Section 1.1 details the methodology used for this study. In particular, it expands upon methods developed by the U.S. Nuclear Regulatory Commission (USNRC) in support of advanced reactor technology licensing, and how they apply in the context of FHR technology development. Section 1.2 provides a brief overview of the pre-conceptual design for a small, modular 236-MWth Mark-1 (Mk1) pebble-bed FHR (PB-FHR) recently developed at the University of California, Berkeley (UCB) [10,11]. Section 1.3 summarizes key thermal hydraulic figures of merit (FOMs) and phenomena in FHRs. Section 1.4 lists the various aspects in the scope of this study.

1.1 Research Methodology

Successful deployment of advanced commercial reactor designs will depend, among several key factors, on regulatory approval. In particular, in the U.S., the USNRC has developed guidelines for development and validation of advanced reactor EMs to simulate reactor response.

There are multiple reasons to rely on computer codes to simulate the behavior of large, complex systems during postulated transients instead of running such transients on a prototypical system. It is often costly to subject the prototypical system to events that would cause significant structural damage or release of radioactive material. Therefore, although one of the most important sources of data to validate the EMs is test data from the actual reactor collected during startup testing and operation, the role of EMs is to predict the system response

across a much wider range of potential operating conditions, because it is impractical to run a very large number of startup tests and to run tests that could result in significant structural damage to the reactor or fuel. Moreover, results from test facilities may not be directly applicable to the prototypical system because of scaling distortions and missing phenomena, and sometimes, postulated scenarios can only be performed and analyzed through a large number of computer code simulations. However, the capability of computer codes to scale up phenomena and processes from reduced-scale test facilities to prototypical conditions and to correct for scaling distortions must be assessed. In particular, it must be proven that empirically-derived closure relations, nodalization, and any calibration can be scaled up between the scaled experiments and the actual, prototypical reactors.

USNRC Regulatory Guide 1.203 defines a systematic process for developing EMs for the analysis of transient and accident behavior of reactors, referred to as the *EM Development and Assessment Process* [12]. The process uses the Code Scaling, Applicability, and Uncertainty methodology originally developed under USNRC research to study severe accidents in LWRs [13]. The methodology outlined in Regulatory Guide 1.203 applies a systematic approach to develop models that are appropriate for a specific system and specific transient, and incorporate a sufficient knowledge base to generate confidence in the analysis. This methodology is articulated around four elements:

1. *Establish requirements for EM capabilities*. This involves the definition of power plant and transient classes, specification of FOMs, and identification of systems and processes that must be modeled. This first step involves identification and ranking of major phenomena, usually based on expert judgment through the use of phenomena identification and ranking tables (PIRTs).
2. *Develop an assessment base*. This requires performing scaling analysis, identifying similarity criteria, identifying existing and required fundamental data, identifying applicable IETs – used to assess system interactions and global code capabilities – and separate effects tests (SETs) – used to develop and assess empirical correlations and other closure models –, and evaluating uncertainties and distortions arising from the use of such facilities to simulate prototypical transients.
3. *Develop an EM*. This model, used to predict performance of the design under consideration, must have a defined structure and incorporate adequate closure models, usually derived from SET data and, on rare occasions, from highly detailed IET data.
4. *Assess EM adequacy*. In particular, numeric solutions must represent the right processes and phenomena, and must be scalable from the SET and IET scales to the full prototypical scale. This element includes verification and validation (V&V) of the model, comparing calculated and measured test data from SET and IET facilities, benchmarking efforts through comparison to analytical solutions or results obtained with other codes, and confirmatory comparisons of EM results with startup test and operation test data collected in the prototypical reactor system after construction.

Following this methodology, significant efforts are being pursued, particularly in the U.S. and China, at universities and national laboratories to identify EM capabilities that could be used in the design and licensing phases of FHRs, as well as limitations to these capabilities for

FHR key phenomena and FOMs, existing V&V basis, and future experimental needs to fill gaps in the validation basis. This dissertation focuses on the area of thermal hydraulics, although neutronics, structural mechanics, chemistry control and mass transport are other key areas for future research in support of FHR technology.

For thermal hydraulic EMs, Regulatory Guide 1.203 recommends using a top-down scaling approach to derive non-dimensional groups governing similitude between experiments and applications, showing that these non-dimensional groups scale the results between experimental facilities, and determining whether these experiments bound the postulated events in non-dimensional space. These non-dimensional groups can be derived using the hierarchical two-tiered scaling approach that meets the requirements of severe accident scaling methodology [14]. After verification to determine that the EM is developed with the necessary degree of quality assurance, its algorithms are stable and converge to the correct solution, and it is sufficiently numerically accurate, the EM can therefore be validated using a combination of scaled SET, IET and component test data to quantify its predictive accuracy. Assessment of overall code accuracy also involves determining individual uncertainty contributions from key plant parameters – arising from the code and experimental data – using the plant's model.

In accordance with the EM Development and Assessment Process set forth by the USNRC, this study focuses on design and operation of the Compact Integral Effects Test (CIET 1.0) facility, which is the first IET that reproduces the thermal hydraulic response of FHRs under forced and natural circulation operation, using a simulant fluid that allows for reduced height and reduced power scaling. Experimental data from CIET 1.0 is used to validate best-estimate codes in support of FHR technology development. In particular, best-estimate models can then be scaled up to the full prototypical system size and used to assess reliability of safety systems, and passive systems in particular, using a methodology that can be extended to any passive system reliability assessment.

1.2 Mk1 PB-FHR Design Overview

In this Section, we review key aspects of the Mk1 PB-FHR design that are relevant for thermal hydraulic analysis and scaling leading to the design of FHR IETs. In particular, flow paths in the primary coolant system are shown, and design of the direct reactor auxiliary cooling system (DRACS) for emergency, passive decay heat removal is detailed. Additional discussions on these aspects are provided in earlier publications [11,15]. This first step, while necessarily applied to a specific design – the Mk1 PB-FHR in this case –, is part of the USNRC's EM Development and Assessment Process, which involves identification of major systems that must be modeled, as detailed in Section 1.1.

The Mk1 PB-FHR is a pebble-fueled, liquid-salt-cooled, high-temperature reactor design developed in the Department of Nuclear Engineering at UCB. The 236-MWth reactor is designed to produce 100 MWe of base-load electricity when operated with only nuclear heat, with a 42.4% net efficiency, and to increase this power output to 242 MWe using natural gas co-firing for peak electricity generation, with a 66.4% co-firing efficiency [16,17]. Buoyant fuel pebbles re-circulate slowly into the bottom and out of the top of the core in the molten salt

coolant, flibe ($^7Li_2BeF_4$). Figure 1-1 shows a flow diagram for the Mk1 reactor, main salt loop, and power conversion systems [11].

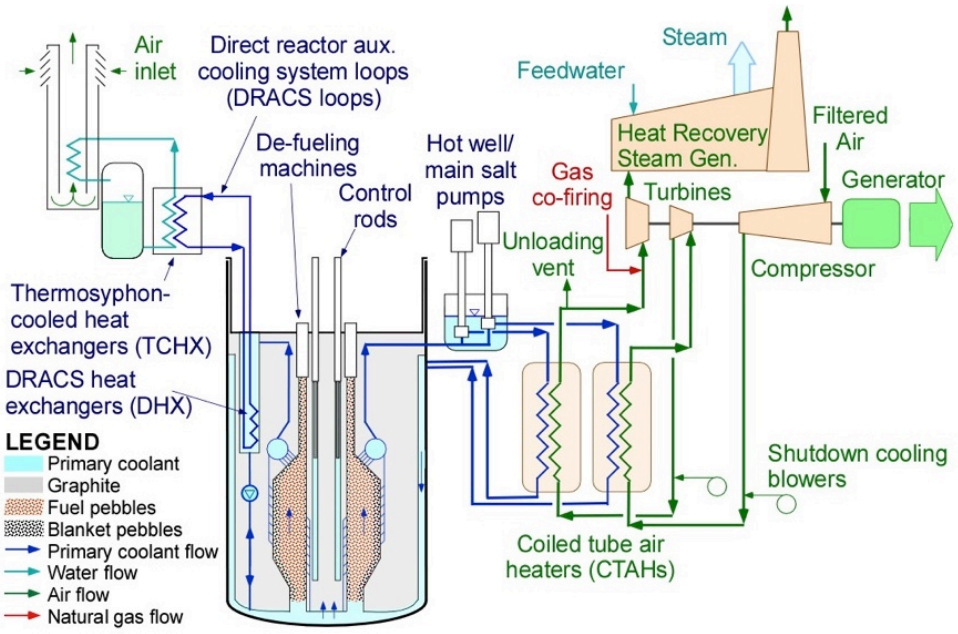

Figure 1-1. Mk1 PB-FHR flow schematic [11].

1.2.1 Primary Coolant Flow Paths

Figure 1-2 and Figure 1-3 show the primary coolant flow paths under normal power and normal shutdown cooling operation, and under natural-circulation-driven decay heat removal mode, respectively [11]. Thicker lines indicate main flow paths. Bypass flows are not shown for simplicity, although these need to be quantified and implemented in models as they can have a significant effect on the behavior of the primary coolant loop and structural materials.

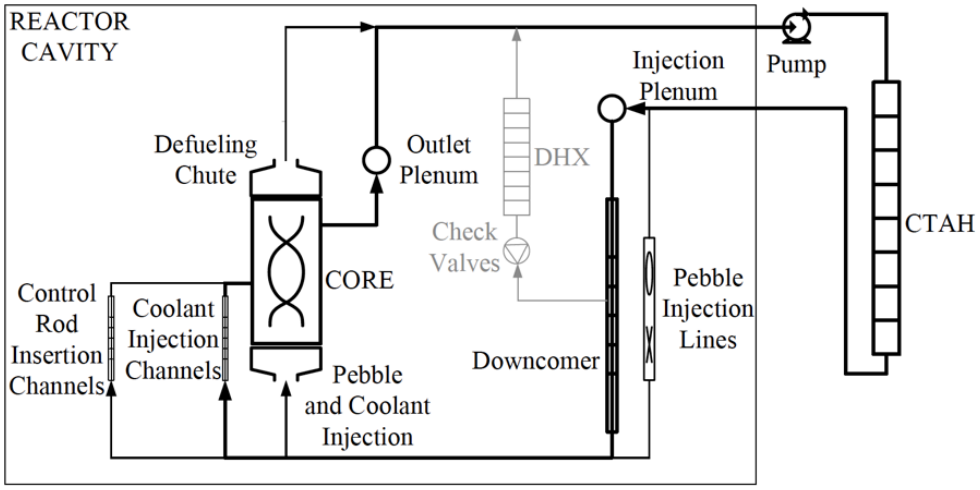

Figure 1-2. Primary coolant flow paths under normal power and normal shutdown cooling operation.

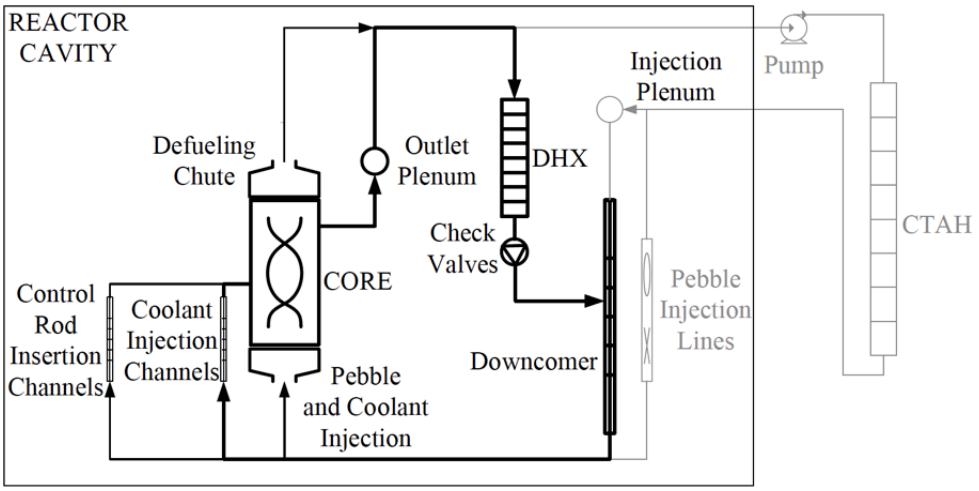

Figure 1-3. Primary coolant flow paths under natural-circulation-driven decay heat removal.

1.2.2 Direct Reactor Auxiliary Cooling System

The Mk1 PB-FHR uses three modular 50% capacity DRACS loops to remove decay heat under emergency conditions, when the normal shutdown cooling system is not functional. This 50% capacity sizing results in each DRACS loop being capable of removing 1% of nominal power (2.36 MW). This initial estimate will be refined in the future, so that the DRACS can maintain the peak bulk coolant outlet temperature – listed as the most limiting thermal hydraulic FOM in Section 1.3.1 – under a specified safety threshold, depending upon metallic structural materials limitations. The DRACS are passive and function by natural circulation. Each module consists of a DRACS heat exchanger (DHX) located inside the reactor vessel; a DRACS salt loop; a thermosyphon-cooled heat exchanger (TCHX) outside the reactor containment, which transfers heat from the DRACS salt loop to evaporate water in thermosyphons; an air-cooled condenser; a natural draft chimney to provide air flow to the condenser; and a water storage tank. Figure 1-1 shows these sub-systems and their design is detailed below.

To further reduce the probability of the primary salt becoming contaminated with other salts due to a DHX leak, the DRACS loops use the same enriched flibe salt as the primary loop. However, the use of flibe in the DRACS loops raises the issue of managing the high freezing temperature of flibe, 459°C. The intermediate water thermosyphon loop is inherited from the earlier Molten Salt Breeder Reactor drain tank design, where it was adopted to avoid coolant freezing in the DRACS loop, even under conditions where the outside ambient air temperature is very low [18].

Figure 1-4 presents both a detailed schematic view and an isometric view of a Mk1 DRACS loop. The loop has three major components: the DHX, the TCHX and the DRACS storage tank, or fill tank.

The DHX is a bayonet type of heat exchanger that uses a 2.5-m-tall bundle of twisted tubes, between a lower cold salt plenum and an upper hot salt plenum, to transfer heat from the

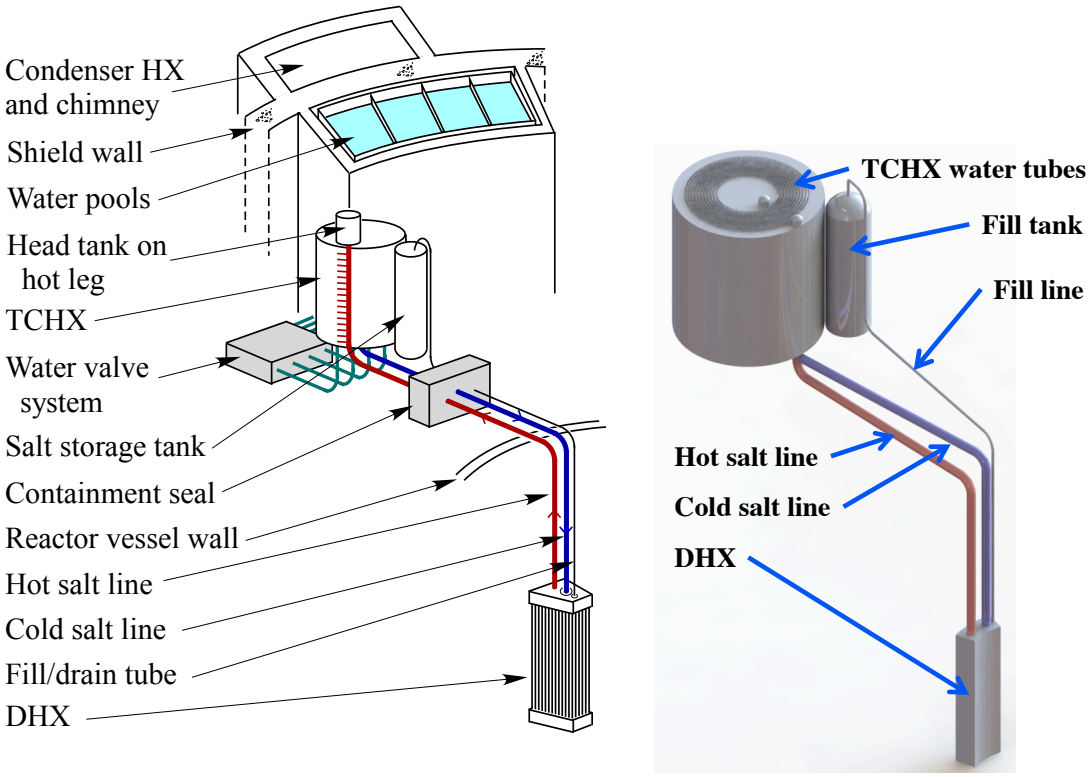

Figure 1-4. Schematic (left) and isometric view (right) of the Mk1 modular DRACS.

primary loop to the DRACS loop. Detailed parameters for a single DHX, based on a simpler, straight shell and tube heat exchanger design, are provided in Table 1-1. The geometry of the DHX bundle is selected to fit into three DHX wells in the reactor vessel upper internals structure. These wells have check valves at the bottom, which limit up flow of primary salt through the well under forced circulation operation, therefore reducing parasitic heat losses, while opening to provide a low flow resistance for natural circulation down flow. For reliability, to assure a check valve opens when needed to establish natural circulation flow, each DHX well may be equipped with more than one check valve. The redundancy and reliability requirements have not been fully defined, but should be similar to the flapper valves used in the Australian Nuclear Science and Technology Organisation's Open-Pool Australian LWR. Check valves are selected due to their capability to provide precise and predictable flow loss coefficients in both flow directions.

The TCHX is located outside of the reactor containment and transfers heat from the DRACS salt loop to a water thermosyphon loop. The salt tubes are designed with a coiled tube configuration similar to the coiled tube air heater (CTAH), with hot salt entering from a standpipe with a head tank, and the coiled tubes spiraling down into a cold salt manifold pipe. The water-cooled thermosyphon pipes are oriented vertically and go up in between the salt tube coils. Heat transfer from the salt coils to the thermosyphon is dominantly by thermal radiation, with some natural convection. One TCHX tube bundle is shown in Figure 1-5. Nine of these bundles are stacked vertically to form the TCHX, also shown in Figure 1-5. Detailed parameters for a single TCHX are provided in Table 1-2 based on an optimization study to meet desired heat

Table 1-1. Parameters for a single DHX, based on a straight shell and tube configuration.

Parameter	Value	Unit
Shell side (primary salt)		
Inlet temperature	700	°C
Outlet temperature	600	°C
Mass flow rate	9.77	kg/s
Velocity	0.045	m/s
Outside diameter	0.56	m
Inside diameter	0.548	m
Tube side (DRACS salt)		
Inlet temperature	526	°C
Outlet temperature	608	°C
Mass flow rate	11.91	kg/s
Velocity	0.065	m/s
Outside diameter	0.0127	m
Inside diameter	0.0109	m
Number of tubes	984	
Heat exchanger		
Heat load	2.36	MW
LMTD	82.7	°C
Overall U	291	$W/m^2°C$
Height	2.5	m
Heat transfer area	98	m^2

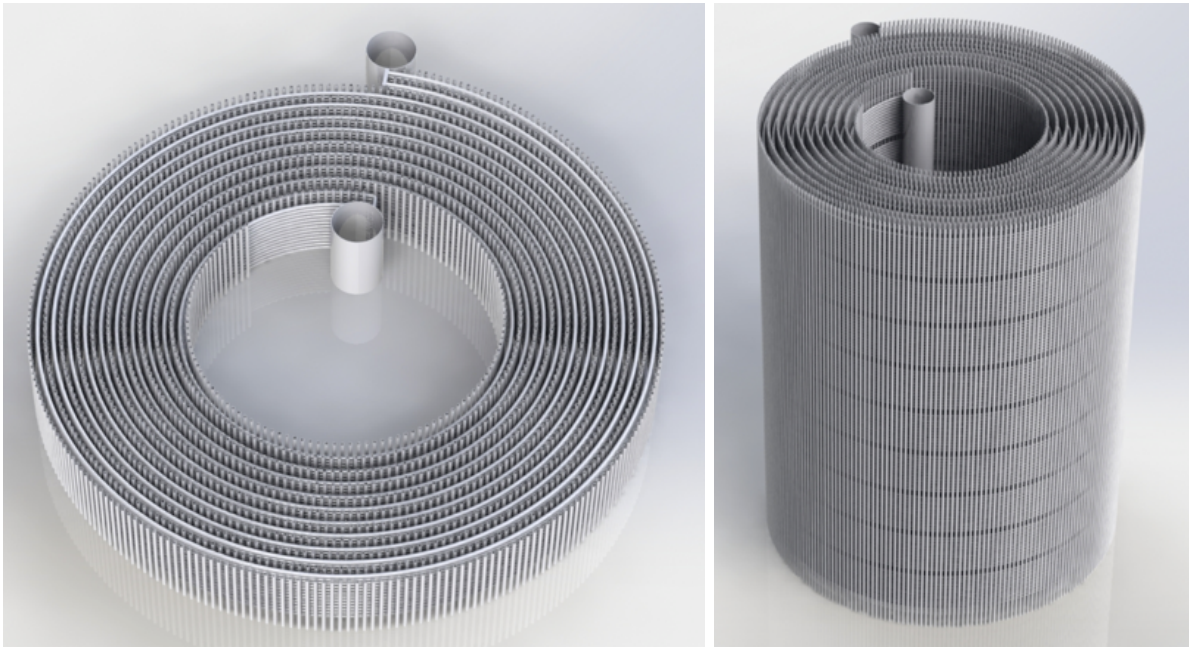

Figure 1-5. Isometric views of one TCHX bundle (left) and the full TCHX (right).

Table 1-2. Parameters for a single TCHX.

Parameter	Value	Unit
Salt side		
Inlet temperature	608	°C
Outlet temperature	526	°C
Mass flow rate	11.91	kg/s
Velocity	0.27	m/s
Outside diameter	0.0127	m
Inside diameter	0.0109	m
Number of tubes	234	
Tube length	24.0	m
Water side		
Temperature	100	°C
Mass flow rate	1.05	kg/s
Outside diameter	0.0127	m
Inside diameter	0.0109	m
Number of tubes	2050	
Tube length	2.5	m
Heat exchanger		
Heat load	2.36	MW
LMTD	465.8	°C
Overall U	22.6	$W/m^2°C$
Heat transfer area	224	m^2
Overall diameter	2.48	m

extraction requirements at steady-state. To aid natural circulation in the DRACS loop, an alternative design would consider using four hot and cold salt manifold pipes, multiplying by four the number of salt tubes and dividing each tube's length by four, therefore reducing friction losses in the coiled tubes.

The water pools, water supply valve system, steam return system, and air-cooled condensers are located at the same elevation, near the DRACS loops. The DRACS water pools are designed to have a sufficient reserve volume of water to accommodate early boil-off immediately after reactor shutdown when decay heat levels are high, and to provide gravity-driven flow to the TCHXs. Because the water pools can reach temperatures of 100°C, the vessels are insulated. Following best practice for water pools, these insulated vessels are contained inside leak-tight pool enclosures that have the capability to limit water loss if the pool vessel leaks, and provide sumps to enable leak detection.

Future modifications to the design are expected to develop a complex manifold system to supply and collect water to/from the thermosyphon water tubes, so that they can be activated in banks. For now, the tubes are simply shown protruding from the top and bottom of the TCHX shell, as seen in Figure 1-5. Future efforts will also involve detailed design of the air-cooled

condenser and natural draft chimney. This will eventually require detailed thermal hydraulic modeling to confirm performance predictions and guide design enhancements.

1.3 Key FHR Thermal Hydraulic FOMs and Phenomena

This Section highlights the most important FOMs that must be captured for FHR thermal hydraulic modeling and provides a list of key thermal hydraulic phenomena for FHR technology. A more detailed version of this discussion is presented in earlier publications [15,19].

1.3.1 Principal Thermal Hydraulic FOMs

Key FOMs that arise from FHR normal operation and thermal hydraulic transients are as follows. The most limiting FOMs are listed first:

- *Peak bulk coolant outlet temperature*, a simple metric related to structural integrity of the system;
- *Time at temperature for metallic and ceramic structures*, for long-term creep deformation and degradation of structural materials;
- *Peak thermal gradient, stress and number of cycles induced in metallic and ceramic structures*, resulting from coolant thermal shock, striping, and ratcheting;
- *Minimum coolant temperature in the DRACS loop*, to assess importance and duration of a potential overcooling transient, including freezing phenomena, reducing heat removal capacity of a safety-related component;
- *Temperature difference across the DRACS*, one of the key parameters associated with passive decay heat removal through natural circulation;
- *Time to establishment of natural circulation*, and how long it can be sustained;
- *Average fuel kernel temperature during normal operation*, which determines the peak coolant temperature reached during an anticipated transient without scram (ATWS);
- *Coolant, fuel, graphite pebbles and graphite reflectors temperature spatial distribution*, which affects reactivity;
- *Peak local power density*, which affects fuel kernel and fuel element thermal stresses;
- *Peak fuel element temperature*, to avoid fuel failure and release of radionuclides – very unlikely to govern any FHR LBE, except potentially reactivity insertion accidents, because of the large thermal margin of FHR fuel;
- *Time at temperature for the fuel*, which influences radionuclides diffusion and release.

These FOMs should be considered to be preliminary, since ultimately the concern involves the potential for structural and fuel damage. As models for structural and fuel damage become more refined, it will be appropriate to update and prioritize them. However, any thermal hydraulic code used for steady-state and transient analysis of FHRs will be required to accurately predict these principal FOMs, which depends on the capability of the code to properly account for thermal hydraulic phenomena in the system. To that effect, the following Section details FHR thermal hydraulic phenomenology.

1.3.2 FHR Thermal Hydraulic Phenomena

Fluoride salts are low-volatility fluids with high volumetric heat capacity, melting temperatures and boiling temperatures. The differences in thermal hydraulic phenomena in FHRs emerge from the differences in the thermophysical properties of the fluoride salts and the structural materials used with them, compared to other reactor coolants and their typical structural materials. Table 1-3 compares the thermophysical properties of different reactor coolants and structural materials [3,20].

Table 1-3. Thermophysical properties* of LWR, HTGR, SFR, and FHR coolants and materials.

Material	T_{melt}, °C	T_{boil}, °C	ρ, kg/m³	ρC_p, kJ/m³°C	k, W/m°C	$\nu \cdot 10^6$, m²/s	Pr
$^7Li_2BeF_4$ (flibe)	459	1,430	1,940	4,540	1.0	2.9	13
0.58 NaF-0.42 ZrF_4	500	1,290	3,140	3,583	0.49	1.6	12
Sodium	97.8	883	790	1,000	62	0.25	0.004
Lead	328	1,750	10,540	1,700	16	0.13	0.014
Helium (7.5 MPa)			3.8	20	0.29	11.0	0.76
Water (7.5 MPa)	0	290	732	4,040	0.56	0.13	0.94
Hastalloy C-276	~1,350		8,890	3,820	9.8		
Graphite			1,700	3,230	200		

* Approximate physical properties at 700°C except the pressurized water data shown at 290°C for comparison. ρ is density, C_p specific heat, k thermal conductivity, and ν viscosity.

The volumetric heat capacity of the primary coolant, flibe, exceeds even that of water; therefore, FHRs operate with lower primary coolant volumetric flow rates, pressure drops, and pumping power than LWRs, and much lower values than sodium-cooled fast reactors (SFRs) and HTGRs. The fact that low volumetric flow rates of fluoride salts can transport large amounts of heat has many implications for the design of FHRs. For example, this characteristic makes fluoride salts particularly effective in passive, buoyancy-driven natural circulation heat transfer [21]. For future FHR reactors to be commercially attractive, it is critical that FHR designers leverage the favorable thermophysical properties of the fluoride salts to the maximum degree possible, while simultaneously mitigating the impacts of the non-favorable properties – primarily the high freezing temperature of the fluoride salts.

The following subsections review key thermal hydraulic phenomena that arise from the unique thermophysical properties of the fluoride salts and FHR structural materials, and that need to be properly modeled by best-estimate codes used in the development of FHR technology.

High Prandtl Number Coolant

As seen in Table 1-3, the thermal conductivity of the baseline FHR primary coolant, flibe, is greater than water. However, flibe is also a viscous fluid, which makes it a high Prandtl (Pr) fluid (~13). Most previous nuclear experience is with moderate Pr (~1 for water/helium-) or low Pr (~10^{-3} for sodium-) cooled reactors. The greater thermal conductivity of flibe creates the potential for achieving heat transfer coefficients comparable to those for water even though the viscosity of flibe is much higher. However, the high volumetric heat capacity of flibe means that FHR convective heat transfer commonly occurs at Reynolds numbers that result in laminar or transition regime flow even under forced circulation, and natural circulation heat transfer is almost always in the transition or laminar regime. For this reason, unlike reactors using other coolants, FHR designs will commonly optimize to use enhanced heat transfer surfaces or small-diameter flow channels, such as those occurring in pebble beds.

Effective Natural Circulation for Passive Decay Heat Removal

Natural circulation is the primary passive decay heat removal method for FHRs, as explained in Section 1.2.2. Because the capability of natural circulation to remove heat is largely independent of the reactor core size, FHRs can be designed for passive safety even for large power levels. This effect is similar to LWRs, where passive heat removal can also be achieved with natural circulation. A study by the International Atomic Energy Agency reviewed experiments and the current state of the art in LWR natural circulation modeling [22]. While the steady-state flow rate in a simple natural circulation loop can be predicted easily, the flow distribution in an actual FHR will be more complex because of multiple natural circulation loops, a large decrease in coolant viscosity with increasing temperature, and significant radiative heat transfer. Typical LWR thermal hydraulic modeling codes can solve for transient flow distributions in multiple interconnected flow paths. Additionally, more complex three-dimensional flow patterns and temperature distributions can emerge in reactor cores, core outlet plena and heat exchangers. Three-dimensional computational fluid dynamics (CFD) modeling of these regions may be valuable, to assess the effectiveness of mixing. However, because of the high thermal margins of fuel and coolant in FHRs, the peak local fuel and coolant temperature FOMs are unlikely to be critical to safety, and CFD tools may not be needed for FHR technology.

Potential for Freezing (Overcooling Transients)

Mixtures of fluoride salts have high melting temperatures, typically between 320°C and 500°C, which makes overcooling transients an important topic for design and safety analysis. The 8-MWth MSRE, which operated from 1965 to 1969 at ORNL, experienced freezing in its air-cooled radiator; the radiator was then thawed without damage [23]. The lack of damage can be attributed in part to the particularly low volume change that the MSRE coolant salt, flibe, experiences upon freezing – about 2.07% [24]. Procedures developed for the MSR-FCL-2 forced circulation materials test loop, which operated with LiF-BeF_2-ThF_4-UF_4 fuel salt (71.7-16-12-0.3 mole %), to maintain reduced-speed pump circulation for a period of time after the trip of the heaters were found to be effective in preventing freezing, and serve as an important knowledge basis for FHR control strategies [25].

Bypass Flow

The graphite reflector blocks in FHRs can shrink and swell as complex functions of irradiation and temperature, and undergo much lower thermal expansion than metallic components like the Mk1 core barrel assembly. These changes can lead to the formation of gaps between the blocks through which coolant will flow. The nature of this bypass flow must be carefully studied to assess the impact on temperature profiles within the fuel blocks. Bypass flows can have significant effects on the coolant outlet temperature gradient. For fast transients, especially, detailed temperature profiles of the coolant should be taken into account for thermal stress calculations on metallic structures outside the core.

Radiative Heat Transfer

At high operating temperatures, radiative heat transfer to and from the reactor cavity, as well as total heat transfer to and from the reactor vessel, must be calculated. Likewise, wavelength-dependent absorption data are needed for coolant salts to allow their radiative interactions with heat transfer surfaces to be assessed inside the reactor.

1.4 Research Scope

The primary objective of this study is to demonstrate the value of both existing and newly developed frameworks for EM development and assessment applied to advanced nuclear reactor designs, in particular the use of scaled IET experimental data to validate best-estimate codes and the use of validated best-estimate codes in support of design and licensing of advanced reactors that incorporate passive safety systems for emergency decay heat removal.

This fundamental objective is exemplified through the development of accurate models of the thermal hydraulic behavior of FHRs, following the methodology laid out in Section 1.1. A good practice in the development of novel nuclear reactor technology is to rely on well-known modeling tools with an extensive V&V basis. Following this principle, at this point on the development path of FHR technology, all thermal hydraulic analyses have been performed using the RELAP5-3D system analysis code. Thermophysical properties for the liquid salt coolant flibe have been implemented into the code, which allows it to model thermal hydraulic steady-state and transient phenomena for FHRs [26]. RELAP5-3D has the most capabilities needed to properly model FHR key thermal hydraulic phenomena [15,19]. This work focuses on demonstrating the applicability and assessment of RELAP5-3D for a new application – safety assessment of FHRs –, similar to the adequacy evaluation of RELAP5 for simulating AP600 small-break loss of coolant accidents performed earlier at the Idaho National Laboratory (INL) [27].

However, RELAP5-3D models of FHRs lack a complete V&V basis, and experimental work is still needed to fill these gaps. Liquid salts are unique among candidate reactor coolants because simulant fluids can be used to replicate salt fluid mechanics and convective heat transfer phenomena at reduced length scales and temperature, and with greatly reduced heater and pumping power [28,29]. The availability of such simulant fluids significantly reduces the cost and difficulty of performing IETs required for system modeling code validation for reactor

licensing, compared to working at prototypical temperatures and power levels with the actual coolant. These simulant fluids can also be used in SET experiments to develop heat transfer and pressure loss correlations for use in system modeling codes.

After key FHR thermal hydraulic phenomena, listed in Section 1.3.2, and gaps in existing modeling tools to replicate these phenomena were identified, UCB built a number of SETs and IETs to fill the missing validation basis for FHR EMs [30]. This dissertation focuses on design and operation of the CIET 1.0 facility, which reproduces the integral thermal hydraulic response of FHRs under forced and natural circulation operation. CIET 1.0 provides validating data to confirm the predicted performance of the DRACS under a set of reference LBEs. CIET 1.0 uses a simulant fluid, Dowtherm A oil, which, at relatively low temperatures (50-120°C), matches the Prandtl (Pr), Reynolds (Re), Froude (Fr) and Grashof (Gr) numbers of the major liquid salts simultaneously, at approximately 50% geometric scale and heater power under 2% of prototypical conditions. In Chapter 2, the scaling methodology used to design CIET 1.0 is introduced, details on design, fabrication and startup testing in CIET 1.0 are provided, and validation of steady-state and simple transient models of CIET 1.0 in RELAP5-3D is performed.

Once EMs are fully developed and assessed, they can be used to evaluate the consequences associated with the response of advanced reactor designs to postulated transients. One key element is to perform a reliability assessment of passive safety systems, such as emergency decay heat removal through the DRACS in FHRs, following a methodology that differs from traditional probabilistic risk assessment (PRA) studies for active safety systems. This assessment is detailed in Chapter 3 and provides important information as to elements of the FHR design that require particular attention throughout the development process, due to their critical role in the performance of the DRACS, and therefore their implications on risk mitigation associated with this system.

Finally, based on life cycle carbon dioxide emissions, nuclear power plants have repeatedly been recognized as having much lower environmental impacts than fossil-fueled plants – namely coal steam plants and natural gas combined cycle (NGCC) plants. However, most existing LCA studies have only been applied to traditional, already operating nuclear power plants. In Chapter 4, we apply economic input-output LCA (EIO-LCA) methods and we use quantities and costs of major classes of materials (e.g. concrete, carbon steel and stainless steel) involved in building the reactor to calculate carbon dioxide emissions per kWh of output electricity from the Mk1 PB-FHR. While this study provides a framework for LCA of future reactor designs, the estimates developed here are used to suggest areas of improvement for the Mk1 design that can be extended to other classes of reactors, based on carbon dioxide emissions related to the construction and operation phases of the reactor.

Chapter 2 Integral Effects Testing and Code Validation for Natural Circulation Heat Transfer

The need to validate integral thermal hydraulic codes is a key issue for developing and licensing new reactor designs, particularly those using passive safety, as explained in Chapter 1 and earlier publications [15,31]. The models for heat transfer, pressure drop, and other phenomena used in these codes can be validated using SETs, where boundary and initial conditions are generated externally and may be varied over wide ranges. However, the actual boundary and initial conditions that occur in an integrated system, due to the coupling between spatial regions and the transitions from early to later phases of transients, may differ from the more idealized conditions that exist in SETs. Therefore, validation of thermal hydraulic codes for reactor safety also requires comparisons with data generated in scaled IET facilities.

Because the compact size and short height of FHRs depends upon the predicted excellent natural-circulation, single-phase decay heat transfer capability of the coolant, validating data from the UCB CIET facility, designed to reproduce the integral transient thermal hydraulic response of FHRs under forced and natural circulation operation, plays an important role in confirming the predicted performance of the DRACS used in FHRs under a set of reference LBEs. Design of the DRACS system is detailed in Section 1.2.2, and Figure 1-2 and Figure 1-3 show the coolant flow paths in the primary loop of the Mk1 PB-FHR during forced circulation and natural circulation operation, respectively. These flow paths are replicated in the CIET experiment constructed at UCB, using two coupled loops.

In this Chapter, we describe efforts to design, fabricate, and perform startup testing in the first configuration of the CIET facility (CIET 1.0) at UCB, as well as validation of RELAP5-3D steady-state and simple transient models using experimental data from CIET 1.0. The relative simplicity of construction (particularly compared to the complexity and safety requirements for high-temperature tests with the prototypical salt for FHRs, and with water, helium or sodium for LWRs, HTGRs or SFRs) was a key element in enabling the proposed experiments to be constructed and performed at much lower cost than previous IETs for other types of reactors. First-generation pressurized water reactor (PWR) IET facilities like INL's Semiscale, the Japanese Rig-of-Safety Assessment project and the French BETHSY facility were large facilities that provided data to validate integral thermal hydraulic codes for PWRs. These facilities required total budgets of several tens of millions of dollars and decade-long schedules. Improvement occurred with the advent of reduced height, accelerated time scaling (e.g., second-generation IET facilities like the Advanced Plant Experiment at Oregon State University and the Purdue University Multi-dimensional integral test Assembly), but test program costs still remained in the range of $10 million. In comparison, the use of reduced height, area and power scaling, and the use of simulant fluids in CIET 1.0 allowed the construction of this third-generation facility with a budget under $1 million.

The reference system that was used for initial scaling of CIET 1.0 was a 900 MWth pebble-bed advanced high-temperature reactor (PB-AHTR) [32]. Because the design of the FHR

commercial prototype reactor has been constantly evolving, there will be inherent distortions between the CIET 1.0 facility and a scaled version of the final FHR commercial prototype. For transient response, such distortions may arise from non-matched relative coolant residence times between the Mk1 PB-FHR and CIET 1.0 sub-systems, as well as the use of reduced flow area stainless steel piping with non-scaled thermal inertia in CIET 1.0. However, CIET 1.0 will provide useful validation data for integral transient behavior of a generic set of FHRs. Moreover, all key components of CIET 1.0 are modular, enabling easy modifications to the loop as prototypical FHR designs evolve and require new scaled parameters.

In Section 2.1, the scaling methodology developed to design CIET 1.0 is introduced. Section 2.2 details key design and fabrication aspects of the CIET 1.0 facility. In Section 2.3, the main tasks for the CIET 1.0 research plan are listed, and initial experimental results are provided. Section 2.4 includes key aspects of the computer models of CIET 1.0. Solution and code verification for natural circulation are performed in Section 2.5, and model calibration and validation efforts are detailed in Section 2.6.

2.1 Scaling and Simulant Fluids

Thermal hydraulic phenomena associated with FHR response to LBEs evolve over short time periods of minutes to days. Therefore, the major constraint on FHR thermal hydraulic experiments is not duration, but rather power and physical scale, because of the impracticality of performing IETs at the full-power level of a commercial reactor. The importance of scaling was recognized early in the pre-conceptual design of the FHR [33], and scaling methodologies were developed and applied to the design of CIET 1.0.

2.1.1 Use of Dowtherm A Oil as a Simulant Fluid for Flibe

Liquid salts are unique candidate reactor coolants because simulant fluids can replicate salt fluid mechanics and convective heat transfer phenomena at reduced length scale, temperature, and heater and pumping power, with low distortion. As mentioned in Section 1.4, in 2005, UCB identified a class of heat transfer oils that, at relatively low temperatures (50-120°C), match the Prandtl (Pr), Reynolds (Re), Froude (Fr) and Grashof (Gr) numbers of the major liquid salts simultaneously, at approximately 50% geometric scale and heater power under 2% of prototypical conditions [29]. Expressions and meanings of these non-dimensional numbers are as follows:

$$\mathrm{Pr} = \frac{\mu c_p}{k} = \frac{viscous\ diffusion\ rate}{thermal\ diffusion\ rate} \tag{2-1}$$

$$\mathrm{Re} = \frac{\rho u L}{\mu} = \frac{inertial\ forces}{viscous\ forces} \tag{2-2}$$

$$\mathrm{Fr} = \frac{u}{\sqrt{gL}} = \frac{inertial\ forces}{gravitational\ forces} \tag{2-3}$$

$$\mathrm{Gr} = \frac{\beta g \rho^2 \Delta T L^3}{\mu^2} = \beta \Delta T \cdot \frac{g \rho^2 L^3}{\mu^2} \tag{2-4}$$

where μ is the dynamic viscosity of the fluid, c_p the specific heat capacity, k the thermal conductivity, ρ the density, u the mean velocity, L the characteristic length, g the acceleration due to gravity, β the volumetric thermal expansion coefficient, and ΔT the characteristic temperature difference.

The Prandtl number, which only depends on fluid thermophysical properties as seen in Eq. (2-1), dictates the selection of the simulant liquid and its average operating temperature for scaled experiments where single-phase heat transfer phenomena are important. For forced convection, Re represents the balance between inertial and viscous forces, and therefore, matching Re allows geometrically scaled experiments to cover flow regimes of interest. If both Pr and Re are matched, the Nusselt number (Nu) for forced convection heat transfer is matched. For the case of buoyancy-driven flows, the scaling procedure is similar, except that the velocity scale emerges from the energy equation, where convective and diffusive transport must balance each other. When the velocity scale derived from the energy equation is inserted into the momentum equation, Gr emerges. Adjustment to the temperature difference scaling ratio allows Gr to be matched, and therefore, for a scaled oil system, Pr, Re, Fr and Gr of a prototypical salt system can be matched. This scaling methodology is illustrated by Eqs. (2-5)-(2-7), where the subscripts m and p are used for model and prototypical parameters, respectively.

From Eq. (2-4), the temperature difference and geometry scaling are derived, based on average fluid thermophysical properties in the model and prototypical systems:

$$(\beta \Delta T)_m = (\beta \Delta T)_p \Leftrightarrow \frac{\Delta T_m}{\Delta T_p} = \frac{\beta_p}{\beta_m} \tag{2-5}$$

$$\left(\frac{g\rho^2 L^3}{\mu^2}\right)_m = \left(\frac{g\rho^2 L^3}{\mu^2}\right)_p \Leftrightarrow \frac{L_m}{L_p} = \left(\frac{\rho_p \mu_m}{\rho_m \mu_p}\right)^{2/3} \tag{2-6}$$

From Eqs. (2-2) and (2-6), the velocity scaling is derived:

$$\begin{cases} \left(\frac{\rho u L}{\mu}\right)_m = \left(\frac{\rho u L}{\mu}\right)_p \\ \frac{L_m}{L_p} = \left(\frac{\rho_p \mu_m}{\rho_m \mu_p}\right)^{2/3} \end{cases} \Leftrightarrow \frac{u_m}{u_p} = \left(\frac{\rho_p \mu_m}{\rho_m \mu_p}\right)^{1/3} \tag{2-7}$$

If Eqs. (2-6) and (2-7) are satisfied, Fr is matched between the model and prototypical systems.

The ratios of pumping powers (P_p) and heating powers (P_q) are given by:

$$\frac{P_{p,m}}{P_{p,p}} = \frac{(Q\Delta p)_m}{(Q\Delta p)_p} = \frac{(\rho u^3 L^2)_m}{(\rho u^3 L^2)_p} \tag{2-8}$$

$$\frac{P_{q,m}}{P_{q,p}} = \frac{(Q\rho c_p \Delta T)_m}{(Q\rho c_p \Delta T)_p} = \frac{(uL^2 \rho c_p \Delta T)_m}{(uL^2 \rho c_p \Delta T)_p} \tag{2-9}$$

where Q is the volumetric flow rate and Δp the pump head.

Simplified correlations for flibe's temperature-dependent density, dynamic viscosity, specific heat capacity and thermal conductivity, based on data in the 600 to 800°C range, are as follows, with the temperature T in °C [20,34]:

$$\rho = 2279.92 - 0.488 \cdot T \ (kg/m^3) \tag{2-10}$$

$$\mu = \frac{(4.638)10^5}{T^{2.79}} \ (kg/m \cdot s) \tag{2-11}$$

$$c_p = 2415.78 \ (J/kg°C) \tag{2-12}$$

$$k = 0.7662 + 0.0005 \cdot T \ (W/m°C) \tag{2-13}$$

Dowtherm A is a eutectic mixture of two thermally stable compounds, biphenyl ($C_{12}H_{10}$) and diphenyl oxide ($C_{12}H_{10}O$). The manufacturer, Dow Chemical, recommends using this fluid in the temperature range between 15°C and 400°C. Combined with its remarkable thermophysical properties to simulate convective heat transfer in fluoride salt systems, its high stability makes Dowtherm A an ideal candidate for scaled IETs such as CIET 1.0. Dowtherm A's temperature-dependent thermo-physical properties, based on data in the 20 to 180°C range, are as follows, with the temperature T in °C [35]:

$$\rho = 1078 - 0.85 \cdot T \ (kg/m^3) \tag{2-14}$$

$$\mu = \frac{0.130}{T^{1.072}} \ (kg/m \cdot s) \tag{2-15}$$

$$c_p = 1518 + 2.82 \cdot T \ (J/kg°C) \tag{2-16}$$

$$k = 0.142 - 0.00016 \cdot T \ (W/m°C) \tag{2-17}$$

Table 2-1 shows scaled parameters for flibe and Dowtherm A oil at characteristic coolant temperatures in FHRs. These scaling parameters and the use of Dowtherm A as a simulant fuid serve as the design basis for CIET 1.0. Table 2-2 shows the impact of temperature on the range of nondimensional parameter values in the prototypical and model primary loops, using characteristic length scales and velocities in the FHR core and CIET 1.0 heater under natural circulation operation. Because it is considered to be more important to match density differences in the loop than to match Pr, the scaling for temperature differences is based on Eq. (2-5). However, Pr values still match closely, and with a 104°C temperature difference across the prototypical Mk1 PB-FHR core, matching the average Pr through average fluid temperature and Gr through temperature difference in the scaled system leads to moderate distortions for Pr at both ends of the temperature space, as shown in Figure 2-1.

IETs include the capability to vary parameters such as power, temperature, flow velocity, or geometric configuration to meet different scaling requirements. The response of the system to parametric variations can identify the relative roles of different phenomena and increase the confidence in the capability of models to predict the integral system performance. In CIET 1.0, power can be varied from 0 to 10 kW, temperatures are controlled through heat addition/rejection to/from the system through an electrical resistive heater and variable speed

Table 2-1. Scaling parameters to match average Pr, Re, Fr and Gr for flibe and Dowtherm A.

		DRACS loop		Primary coolant loop
		Normal operation	Natural circulation	
Flibe average temperature [°C]		543	567	652
Dowtherm A average temperature [°C]		51	59	95
Length scale	L_m/L_p	0.49	0.48	0.45
Velocity scale	U_m/U_p	0.70	0.69	0.67
ΔT scale	$\Delta T_m/\Delta T_p$	0.31	0.31	0.30
Transient time scale	τ_m/τ_p	0.70	0.69	0.67
Pumping power	$P_{p,m}/P_{p,p}$	-	-	3.1%
Heating power	$P_{q,m}/P_{q,p}$	-	-	1.6%

Table 2-2. Impact of temperature variations on nondimensional parameter values in the FHR core and CIET 1.0 heater under natural circulation operation.

	Flibe (600 – 704°C)	Dowtherm A (80 – 111°C)
Pr	11.7 – 18.6	12.8 – 16.9
Re	139 – 215 [a]	146 – 206 [b]
Gr	$3.65 \times 10^5 – 8.89 \times 10^5$ [a]	$3.97 \times 10^5 – 8.34 \times 10^5$ [b]

[a] L_p = 0.03 m, U_p = 0.02 m/s; [b] L_m = 0.013 m, U_m = 0.013 m/s

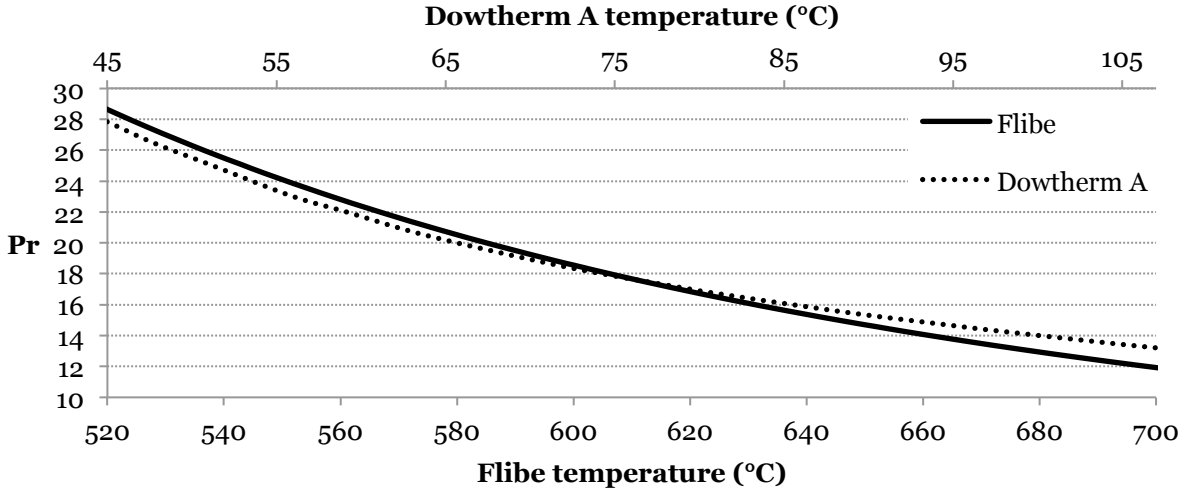

Figure 2-1. Impact of temperature on Pr in the prototypical and model systems.

fan-cooled heat exchangers, and flow velocity is varied using a variable speed motor on the primary loop's centrifugal pump. The CIET 1.0 design has extensive modularity to allow future modifications, including geometric configuration changes.

2.1.2 Scaling Methodology for CIET 1.0

In this Section, we detail the scaling methodology used in the design of CIET 1.0, including specific components such as the resistive heater, the heat exchangers and the primary pump.

Absolute heights of the primary loop heat source and sink (reactor core and DHX), and relative distances between elevations of the main heat sources and sinks for natural circulation (reactor core, DHX, and TCHX) in CIET 1.0 are scaled to ~50% of prototypical elevations in the 900-MWth channel-type PB-AHTR, following the length scales listed in Table 2-1. The prototype and model key dimensions are listed in Table 2-3.

Table 2-3. Absolute component heights and relative distances between elevations of main heat sources and sinks in 900 MWth PB-AHTR and CIET 1.0.

Absolute component heights		
	Prototype	Model
Core and upper reflector/Heater	3.27 m	1.62 m
DHX	2.60 m	1.30 m
Relative distances between elevations		
	Prototype	Model
Core-to-DHX/Heater-to-DHX	2.90 m	1.57 m
DHX-to-TCHX	8.45 m	4.23 m

Although the pre-conceptual design of a 236-MWth Mk1 PB-FHR was developed after scaling and design of CIET 1.0 were finalized [11], elevations of the main heat sources and sinks in CIET 1.0 and the Mk1 PB-FHR, shown on Figure 2-2, reveal a reasonable agreement between the scaled model and prototype.

As seen in Table 2-1, the heating power in a scaled IET facility using Dowtherm A oil is only 1.6% of the prototypical heat input into a salt system. Moreover, the CIET 1.0 heater is scaled to a prototype operating at 10% of full power. As a result, the 10-kW resistive heater installed on CIET 1.0 simulates a prototypical IET with a nominal power of 6.3 MWth. This is lower than the 236-MWth Mk1 PB-FHR, but is high compared to earlier PWR IETs and is comparable to nominal powers of planned test FHRs such as the 10-MWth solid fuel version of the Thorium Molten Salt Reactor (TMSR-SF1) experimental facility designed by the Shanghai Institute of Applied Physics in China.

Temperature scaling in CIET 1.0 is based on average temperature and temperature difference scaling factors listed in Table 2-1. Prototypical temperatures and corresponding CIET 1.0 temperatures are listed in Table 2-4. Temperatures for the primary loop are based on the Mk1 PB-FHR design [11], while values for the DRACS loop under natural circulation, and under forced circulation assuming 2% parasitic heat losses, are derived from preliminary analyses of the 900-MWth modular PB-AHTR using RELAP5 [36].

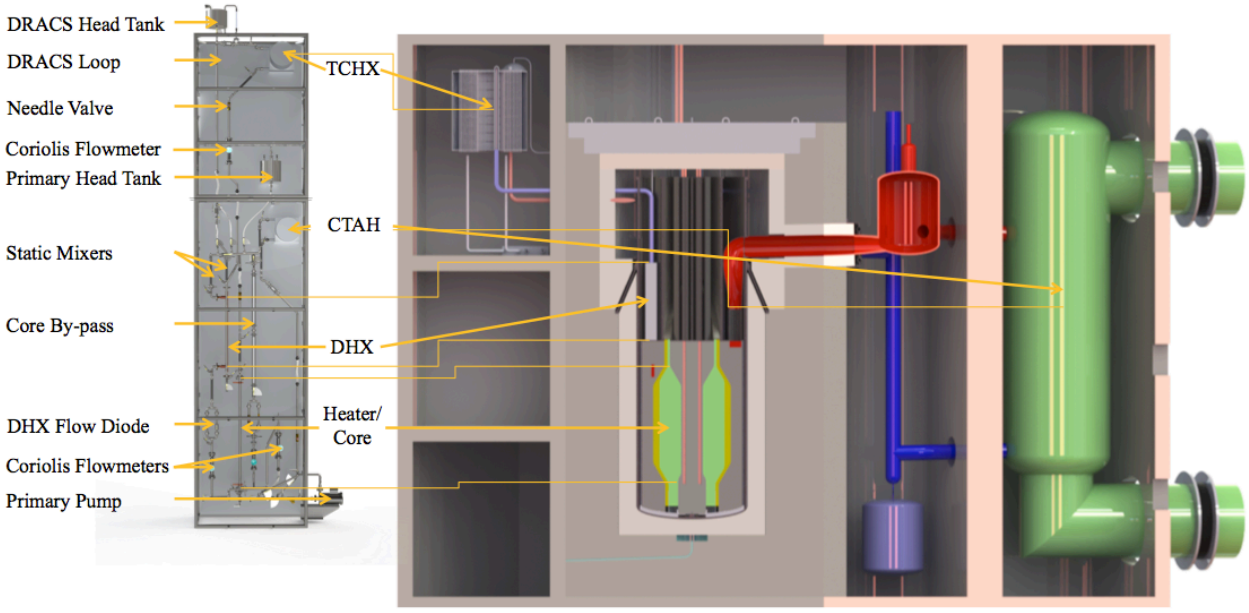

Figure 2-2. CIET 1.0 (left) 50% height scaling reasonably matches the Mk1 PB-FHR (right) design.

Table 2-4. Prototypical and CIET 1.0 temperatures.

	Mk1 PB-FHR [°C]	**CIET 1.0 [°C]**
Primary loop		
Minimum/average/maximum temperatures	600/652/704	80/95/111
DRACS loop (normal operation)		
Minimum/average/maximum temperatures	521/543/565	44/51/58
DRACS loop (natural circulation)		
Minimum/average/maximum temperatures	526/567/607	46/59/72

Resistive Heater Scaling

For CIET 1.0, it is more practical to use a straight annular tube geometry and a needle valve with Reynolds-independent friction factor located in series with the heater to replicate the heat addition, coolant residence time, and coolant pressure losses provided by the Mk1 PB-FHR pebble bed core. In this heater configuration, the outer tube is heated resistively. The natural circulation decay heat removal flow rates in the Mk1 PB-FHR correspond to the pebble bed flow regime in which both Reynolds-dependent and Reynolds-independent terms of the friction coefficient are significant [21]. To model the dynamic behavior of the natural circulation loop, the friction coefficient of the pebble bed must be replicated over the entire flow regime. The pebble bed friction factor, f_{PB}, is given by:

$$f_{PB} = \frac{f_1}{\mathrm{Re}_{PB}} + f_2 \tag{2-18}$$

where Re_{PB} is the Reynolds number in the pebble bed and various values for parameters f_1 and f_2 are found in the literature.

To match the Reynolds-dependent part of the pebble bed friction factor, the annular channel friction factor must have an inverse reciprocal dependence on Reynolds. Laminar flow through a pipe has the required 1/Re functional form, so the channel is sized to ensure that flow remains in the laminar regime. The dimensions of the CIET 1.0 resistive heater are listed in Table 2-5.

Table 2-5. CIET 1.0 resistive heater dimensions.

Annulus inner diameter [m]	3.18×10^{-2}
Annulus outer diameter [m]	3.81×10^{-2}
Channel length [m]	1.62
Hydraulic diameter [m]	6.40×10^{-3}
Cross-sectional area [m^2]	3.48×10^{-4}

The natural circulation mass flow rate in the heater is 0.036 kg/s and the average dynamic viscosity is $\mu(95°C) = 9.86 \times 10^{-4}$ Pa-s. Therefore, Re = 667 and we can conclude that flow is indeed in the laminar regime.

To match the Reynolds-independent part of the pebble bed friction factor, a needle valve in series with the heater is convenient to adjust pressure drop. The needle valves used in CIET 1.0 have Reynolds-independent loss coefficients. Pressure drop through the valve, Δp_{valve}, depends on fluid mass flow rate, $\dot{m}$, fluid density, ρ, and valve coefficient, C_v, through:

$$\Delta p_{valve} = \frac{\dot{m}^2}{\rho {C_v}^2} \tag{2-19}$$

Valve curves provided by the manufacturer give the value of C_v as a function of the percent opening of the valve, and were validated through isothermal pressure drop tests.

Heat Exchangers Scaling

CIET 1.0 is equipped with three heat exchangers that were modeled after the three heat exchangers in a prototypical reactor design: a CTAH, a DHX and a TCHX. In CIET 1.0, the DHX is a copper single-pass straight shell-and-tube heat exchanger, and the CTAH and TCHX are identical oil-to-air fan-cooled heat exchangers. Their designs are based on functional requirements for heat transfer performance, and only relative elevations of the heat sources and sinks are scaled to the 900-MWth modular PB-AHTR. It is important to note, however, that the ability to control the fan speed for each of the oil-to-air heat exchangers, as well as to interchange the current DHX with another heat exchanger design, leaves great flexibility in heat removal options for the CIET 1.0 system.

Pump Scaling

Similar to the heat exchangers, due to the lack of a detailed pump design for a prototypical PB-FHR, the primary pump on CIET 1.0 is not scaled to any prototypical pump. Instead, its

design is based on functional requirements for pump head and resulting flow rates in the system. Knowing the motor speed and pump head, flow rates can be determined using a pump performance curve. The desired range of flow rates is obtained by controlling the pump motor speed with a variable frequency drive (VFD).

2.2 Design and Fabrication of CIET 1.0

This Section details the design and fabrication phases of the CIET 1.0 experiment. This includes good practice in the design of CIET 1.0 that is applicable to future iterations of CIET and other FHR IETs.

2.2.1 Design of CIET 1.0

Flow paths in the CIET 1.0 fluid loop, controlled through valve alignments, replicate the primary and DRACS flow paths of the Mk1 PB-FHR. Figure 2-3 shows the CIET 1.0 piping and instrumentation diagram. The primary flow loop consists of the pump manifold, electrical heater branch and CTAH branch. The DHX branch of the primary circuit, similar to the prototypical DHX branch in the Mk1 PB-FHR, has high flow resistance for upwards flow through the DHX during forced convection, therefore limiting bypass flow under power operation. Similarly, this leg has low flow resistance for downwards flow through the DHX, and can simulate natural circulation decay heat removal if the reactor primary pumps were to stop in a prototypical reactor. The limited bypass flow of 1-3% of full flow through the DHX, which supplies heated primary salt to prevent overcooling of the DRACS loop, is also sufficient to remove decay heat with a reasonable temperature difference under loss of heat sink (LOHS) without a primary pump trip. The primary circuit is also equipped with a bypass branch, which simulates the bypass paths in the Mk1 PB-FHR. Relative flow resistances between all branches are regulated with needle valves, which provide Reynolds-independent flow losses. The computer aided design (CAD) rendering of the CIET 1.0 loop is shown in Figure 2-2 (left) with the main components labeled. Practical design aspects for some of these components are detailed herein. While vendor-provided information was key in supporting the design phase of CIET 1.0, all design values have subsequently been experimentally validated and, if necessary, updated.

Electrical Heater

A resistance-heated annular electric heater simulates heat generation in the core. The scaling methodology for the CIET 1.0 heater is detailed in Section 2.1.2. The computer-controlled direct-current power supply is designed to supply up to 10 kW of heat input to the fluid while not exceeding a surface temperature of 250°C in all operating modes of the facility. Additionally, the controller can provide time-dependent power profiles to the heater to simulate reactor scram and decay heat generation in the FHR core. The heater is equipped with five surface thermocouples (TCs) and several other in-line TCs at the fluid inlet and outlet for further characterization of heat transfer performance.

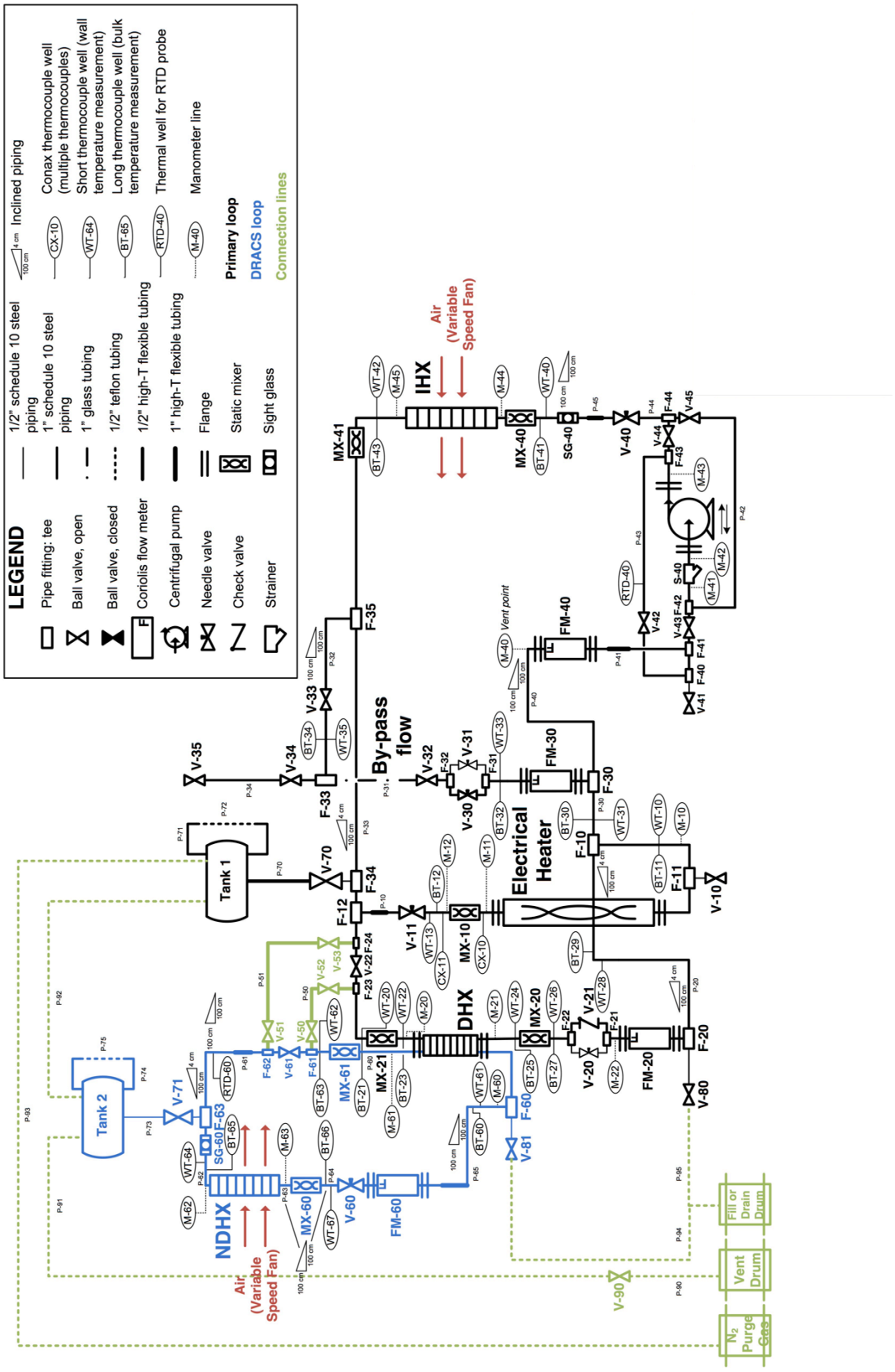

Figure 2-3. CIET 1.0 piping and instrumentation diagram.

CTAH and TCHX

Commercial air-cooled heat exchangers simulate heat extraction from two locations on CIET 1.0: the power conversion system through the CTAH in the primary loop, and the TCHX in the DRACS loop. They are designed to extract up to 10 kW under forced circulation and 2 kW under natural circulation, or 10% and 2% of scaled reactor full power, respectively. Computer-controlled VFDs connected to the fan-cooled heat exchangers allow for automated control strategies for various LBEs, where fan speed is varied to match the predicted heat load in the prototypical CTAH and TCHX. Appropriate heat exchangers were selected based on the temperature requirements listed in Table 2-4. Inlet and outlet temperatures and fan motor speeds are recorded continuously through the CIET 1.0 data acquisition (DAQ) system.

DHX

The DHX is designed to transfer up to 2 kW with a logarithmic mean temperature difference of 36°C, based on the temperature values listed in Table 2-4. This design therefore provides minimal thermal resistance between the primary loop and the DRACS loop. The modularity of CIET 1.0 can accommodate testing of several DHX designs. The initial (CIET 1.0) configuration of the DHX includes a baffled tube-in-shell heat exchanger.

Flow Diode

The DRACS in FHRs require flow diodes to restrict upward primary coolant flow through the DHX under forced circulation, but to provide low downward flow resistance for natural circulation. Flow diode options include check valves, flapper valves, and fluidic diodes. The flow diode in the CIET 1.0 DHX branch is simulated using two valves in parallel. For flow control, a needle valve is used to ensure the desired amount of bypass flow in the upwards direction during forced circulation. On a parallel branch, a check valve is used to block flow in the upwards direction and allow free flow in the other direction.

2.2.2 Good Practice in the Design of CIET 1.0

Several noteworthy elements are included into the design of CIET 1.0, which help with modularity and interchangeability of components, and extend the service life of the facility, allowing for future research.

Sight Glasses and Gas Entrainment

Gas entrainment in the oil loop must be avoided to prevent distortions in pressure drop and heat transfer. In order to monitor for entrained gas during forced circulation operation, sight glasses are installed in two locations on the CIET 1.0 flow loop: one on the primary loop, and one on the DRACS loop. Gas entrainment can be visually monitored through these sight glasses, which are located near the high points of each loop. These 20-cm-long glass sections connect to the piping with Viton double-o-ring seals. In addition to monitoring entrained gas, the ability to vent gas bubbles from the loop is critical. Vent points, using manometer ports or vent valves, are located at almost every local high point in the loop. A small volume of residual gas remained trapped in the commercial fan-cooled heat exchangers after filling, and was removed using a

degassing procedure that involved starting and stopping the primary pump, with the loop configured to provide forced flow through both the primary and DRACS loop sections, with venting being performed after each pumping cycle.

Moreover, every horizontal length of piping is sloped with a minimum of 4.0 cm rise per 100 cm of horizontal distance to enable entrained gas to rise to a local high point (and vent location). All vent valves are connected to the manometer manifold purge system, to contain any overflow and to control the release of Dowtherm A vapor. The use of sloped lines is also key in enabling complete draining of the loop for maintenance and repairs.

Thermal Insulation and Guard Heating

It is desirable to minimize heat losses from the loop to the ambient surroundings. Although the piping has been fully insulated, there remain some non-negligible parasitic heat losses from protruding metal parts such as uninsulated manometer ports and valve handles. To limit heat losses, an infrared camera has been used to identify hot spots that require additional insulation, and subsequently guard heating will be used to further reduce parasitic heat losses. Two sets of transparent polycarbonate panels are installed on the sides of the CIET frame. Each panel is 0.635 cm thick and the air layer between the two panels provides effective thermal insulation. Rubber gasket material seals the interstitial space between each panel and the steel CIET frame. The front of the CIET enclosure is also sealed by an insulated rolling-shutter door system. Extruded aluminum panels with foam cores can be raised to adjust valves or provide sight access to components inside the frame. A space heater circulates heated air inside the CIET enclosure.

Modularity

The DHX and the resistive heater on the flow loop were designed so that they can easily be removed from the loop piping. As the point design for a commercial FHR develops further, new DHX designs (e.g., twisted tube heat exchangers) can be investigated. Similarly, the resistive heater design can easily be modified to better match relative residence times in key sub-systems.

Shutdown Rod Channel and Core Bypass Line

A bypass flow line in the CIET 1.0 loop runs parallel to the resistive heater branch. This flow path simulates core bypass flow, and therefore has a needle valve to allow the flow resistance and bypass flow rate to be adjusted. Furthermore, it is instrumented with a Coriolis flowmeter to measure mass flow rate. In the initial configuration of CIET 1.0, this leg of the flow loop was constructed of the same stainless steel piping used for the rest of the loop. However, in subsequent iterations of the CIET experiment, this branch will be replaced with glass tubing so that the flow line will be transparent. A neutrally-buoyant element will be inserted in this channel, simulating a shutdown rod in prototypical FHRs, observed through the glass tubing. This work will continue research started at UCB in 2008 investigating buoyancy-driven passive safety shutdown rod insertion [37].

Centrifugal Pump

A single pump is needed and was included on the primary coolant loop of CIET 1.0. Bypass connections and valves between the primary loop and the DRACS loop permit forced circulation through the DRACS for isothermal pressure drop measurements. The pump speed is computer-controlled through a VFD, so that feedback control can be done on the primary coolant flow rate for steady-state operation and various simulated LBEs. A pump manifold is included in the design, to run the primary loop flow in both directions for pressure measurements across the DHX.

2.2.3 Instrumentation and Data Acquisition

This Section describes instrumentation and the DAQ system used to collect data from CIET 1.0.

TCs, RTD Probes, and Temperature Measurements

CIET 1.0 uses type-T sheathed TCs, which are best suited for measurements in the -200 to +250°C range. Small-sheath-diameter (0.02") TCs were chosen for their fast response time. All TC junctions are ungrounded to minimize signal noise. In total, 47 TCs are positioned at various locations around the CIET 1.0 loop. In-line TCs are used to measure bulk fluid temperatures. At each measurement point, two TCs are installed at different radial locations in the flow, to indicate any temperature non-homogeneity (e.g., thermally stratified flow). Static mixers are installed upstream of in-line TCs to ensure accurate measurements of bulk fluid temperatures. Surface TCs measure external surface temperature of the heater at five different axial locations, and ambient condition temperatures inside the CIET frame.

TCs must be calibrated at least yearly against a resistance temperature detector (RTD) measurement system. While calibration was initially done off the loop before the TCs were installed on CIET 1.0, after installation, calibration can be redone in-situ against two RTD probes installed in two thermowells on the loop, located in the pump manifold and in the DRACS loop (low and high elevations). This option allows for frequent recalibration by running the loop with isothermal conditions. The on-loop RTDs are designed to be easily removable from their thermowells and sent to the vendor for recalibration, but are left installed under normal operation to provide a diverse measurement of temperature to verify proper operation of the TCs in the loop.

Pressure Measurements

All pressure measurements taken from the CIET 1.0 flow loop are direct head measurements read through 16 transparent manometers with an inner diameter of 3/16" (4.76 mm) and an outer diameter of 1/4" (6.35 mm). All manometer lines connect to the same 3.34-cm-outer-diameter (1.315" OD, 1" nominal) Schedule 10 (0.28-cm-wall-thickness) piping. Therefore, at the connection point on the loop, the flow cross-sectional area is the same for all manometer lines, and for pressure drop measurements across major components in individual branches, the dynamic pressure term of the Bernoulli equation can be disregarded. Manometers from both the primary and DRACS loop use transparent Teflon tubing, routed to a vertical manometer board.

Two digital cameras are used to record oil levels in the primary and DRACS loop manometers. These cameras are remotely operated from the computer control station. Pictures are taken and digitally transmitted to the CIET computer, and fluid levels are converted to relative pressure measurements with a partly automated script.

Flow Rate Measurements

Four Coriolis flowmeters provide direct, dynamic, bidirectional mass flow rate measurements in each branch of CIET 1.0. They were sized to provide accurate measurements within ±2% uncertainty of the mass flow over the expected flow range of the loop. By appropriate valve alignment, CIET 1.0 allows forced circulation flow to be induced through multiple flowmeters in series. Comparison of the measured flow rates can confirm that individual flowmeter calibrations are not drifting.

DAQ System and Interface with LabVIEW Software

CIET 1.0 is equipped with a National Instruments DAQ system, which sends data to the CIET control computer. With a total of 64 input channels, the DAQ system can accommodate the 47 TCs and 4 flowmeters used for temperature and fluid mass flow rate measurements. The DAQ system takes the signals generated from the TCs and flowmeter transmitters, and writes the data to individual files. On the CIET 1.0 control station, the National Instruments LabVIEW 2013 software has been installed for optimal integration with the DAQ system. LabVIEW has a series of key virtual instruments (VIs) for control and data acquisition from CIET 1.0:

- The "DAQ Assistant" VI is used to calibrate and coordinate instrumentation, and properly process TC and flowmeter transmitter signals through LabVIEW;
- Three VFDs, used to control the pump motor and the CTAH and TCHX fan speeds, are controlled, manually or through automatic feedback, through LabVIEW. By integrating VFD control and data acquisition, LabVIEW is a powerful tool to test control strategies on CIET 1.0.

2.2.4 Fabrication of CIET 1.0

CIET 1.0 uses modular construction, with piping subassembly sections installed inside a steel frame 7.6 m in height and 1.8 m in width. The experimental loop uses 3.34-cm-outer-diameter (1.315" OD, 1" nominal) Schedule 10 (0.28-cm-wall-thickness) 304L stainless steel piping. Due to the large size of the experiment, it was split into upper and lower modules that were mated together during final assembly, using flexible hose sections to connect pipes. Figure 2-4 shows the timeline of the CIET project. In particular, Figure 2-5 shows various stages of the piping thermal insulation process, and Figure 2-6 shows the lower and upper frame assemblies and piping being placed in their final location.

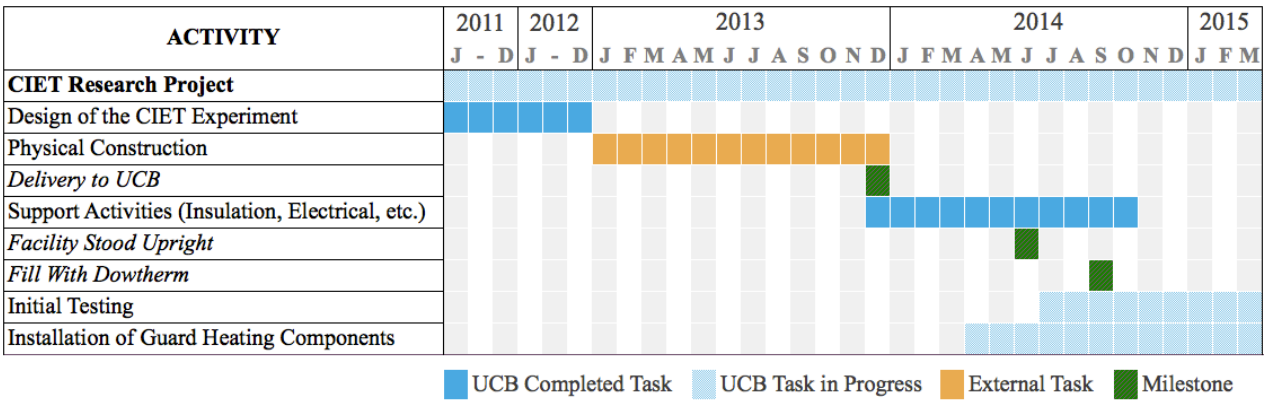

Figure 2-4. CIET project timeline.

Figure 2-5. CIET 1.0 piping insulation in progress, February 2014 (left), March 2014 (center) and April 2014 (right).

Figure 2-6. CIET 1.0 lower (left) and upper (right) frame assemblies being set in place, June 2014.

2.2.5 Initial Fill-up

The CIET loop was first filled up with Dowtherm A on September 15th, 2014. A fill tank was slowly pressurized with nitrogen, using a regulator and a control valve, to push the oil into the CIET loop. Throughout the process, all transparent lines (i.e. manometer lines and sight glasses) were monitored to verify the absence of entrained gas bubbles, as shown in Figure 2-7, and fluid inventory in the loop, measured by the weight of oil removed from the fill tank, was recorded. In total, 51.4 kg of Dowtherm A oil, or a total volume of 48.4 L, were loaded into the CIET 1.0 loop.

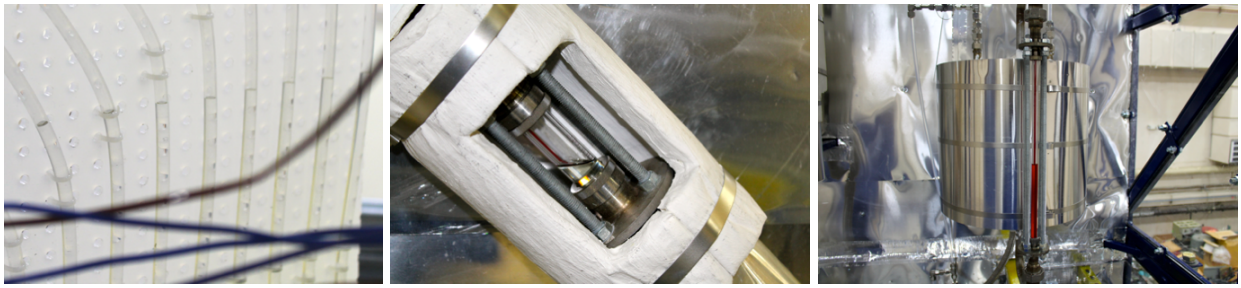

Figure 2-7. CIET 1.0 transparent sections monitored during fill-up to verify absence of gas bubbles.

2.3 Research Plan and Initial Results

The formal research program for CIET was planned as follows, with specific objectives associated to each step. Completed stages of the research plan, as of May 2015, are italicized.

1. *Isothermal, forced circulation flow around the loop, with pressure data collection to determine friction losses in the system: CIET-specific friction loss correlations have been compared with handbook values, and empirically measured values have been implemented in the system codes that are to be validated by data from CIET 1.0.*
2. *Steady-state single loop and coupled natural circulation in the primary loop and the DRACS loop: collected data has been compared to predicted performance and forms the validation basis for best-estimate steady-state models.*
3. Thermal transients, including *startup, shutdown, power step changes*, loss of forced cooling (LOFC) with scram and LOHS with scram: the set of collected data serve the double purpose of confirming strategies for operation of FHRs, and validating best estimate transient models.

2.3.1 Isothermal Pressure Drop Tests

In this series of tests, pressure drop was measured at various flow rates in each branch of the CIET 1.0 loop at room temperature, and CIET-specific pressure loss correlations were implemented in CIET system modeling codes. Flow rates in the loop were controlled through pump speed and, secondarily, by throttling flow through needle valves. Flow paths were controlled through valve line-up and enforced by the use of check tables included in a quality-controlled test procedure. Pressure drop in the loop was measured directly through fluid level

differences in manometer lines. Ambient air and fluid temperatures were continuously measured with TCs. The flow rate ranges selected for this series of tests covered expected Reynolds numbers in each branch during forced and natural circulation operation of CIET 1.0. Pump speeds were varied both up and down to verify reproducibility of the results and absence of hysteresis. As an example, fluid levels in the CTAH and heater branch manometer lines at various flow rates and ambient temperature of 20°C are shown in Figure 2-8. The free surface is located in the primary loop expansion tank.

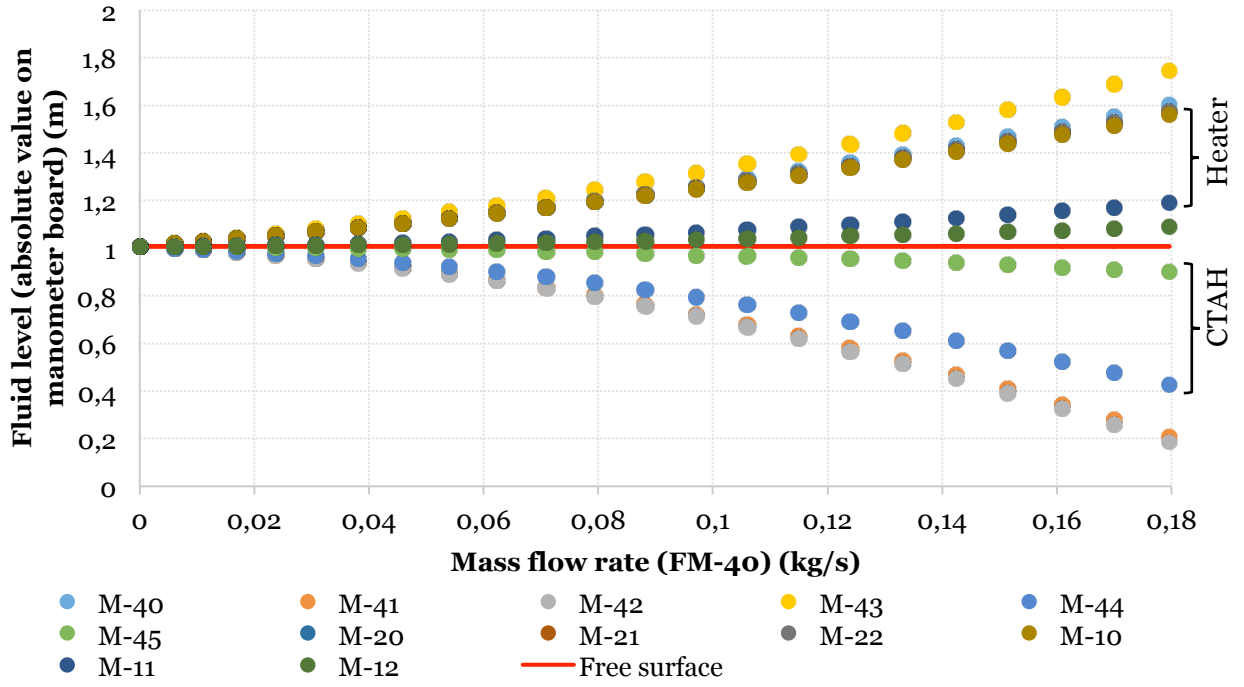

Figure 2-8. Fluid levels in the CTAH and heater branch manometers at various flow rates.

The goal of this series of tests was to generate CIET-specific component-scale friction number correlations in the following non-dimensional form, which can subsequently be implemented in system modeling codes such as RELAP5-3D:

$$K + f\frac{L}{D} = A + B\mathrm{Re}^{-C} \tag{2-20}$$

where f is the friction factor, L the component length, D the component hydraulic diameter, K the sum of form losses, and A, B and C empirically-derived coefficients. The following equations were used to calculate friction and Reynolds numbers for each set of data, based on measured fluid levels, mass flow rates $\dot{m}$ and temperatures (dynamic viscosity μ and density ρ are temperature-dependent):

$$\Delta p = \frac{\rho u^2}{2}\left(f\frac{L}{D} + K\right) \Rightarrow f\frac{L}{D} + K = \frac{2\Delta p}{\rho u^2} = \frac{2\rho A^2 \Delta p}{\dot{m}^2} \tag{2-21}$$

$$\mathrm{Re} = \frac{\rho u D}{\mu} = \frac{\dot{m} D}{A \mu} \tag{2-22}$$

where Δp is pressure drop, u fluid velocity and A flow cross-sectional area.

CIET-specific correlations for static mixers, Coriolis flowmeters and fan-cooled heat exchangers, derived from these tests, are listed in Table 2-6. Table 2-6 also lists the values of A and D used to calculate Re in Eq. (2-22).

Table 2-6. CIET-specific friction number correlations for static mixers, Coriolis flowmeters and fan-cooled heat exchangers.

Component	A (m²)	D (m)	Friction number correlation
Static mixer	$6.11 \cdot 10^{-4}$	$2.79 \cdot 10^{-2}$	$K + f\frac{L}{D} = 21 + \frac{4{,}000}{\mathrm{Re}}$
Coriolis flowmeter	$6.11 \cdot 10^{-4}$	$2.79 \cdot 10^{-2}$	$K + f\frac{L}{D} = 18 + \frac{93{,}000}{\mathrm{Re}^{1.35}}$
Fan-cooled heat exchanger	$1.33 \cdot 10^{-3}$	$1.19 \cdot 10^{-2}$	$K + f\frac{L}{D} = 400 + \frac{52{,}000}{\mathrm{Re}}$

These correlations were based on optimal fits of calibration data collected from static mixer MX-10, flowmeter FM-40, and both fan-cooled heat exchangers (see locations on Figure 2-3). The corresponding fitting curves are shown in Figure 2-9, Figure 2-10 and Figure 2-11, respectively, and compared to vendor-provided values when available.

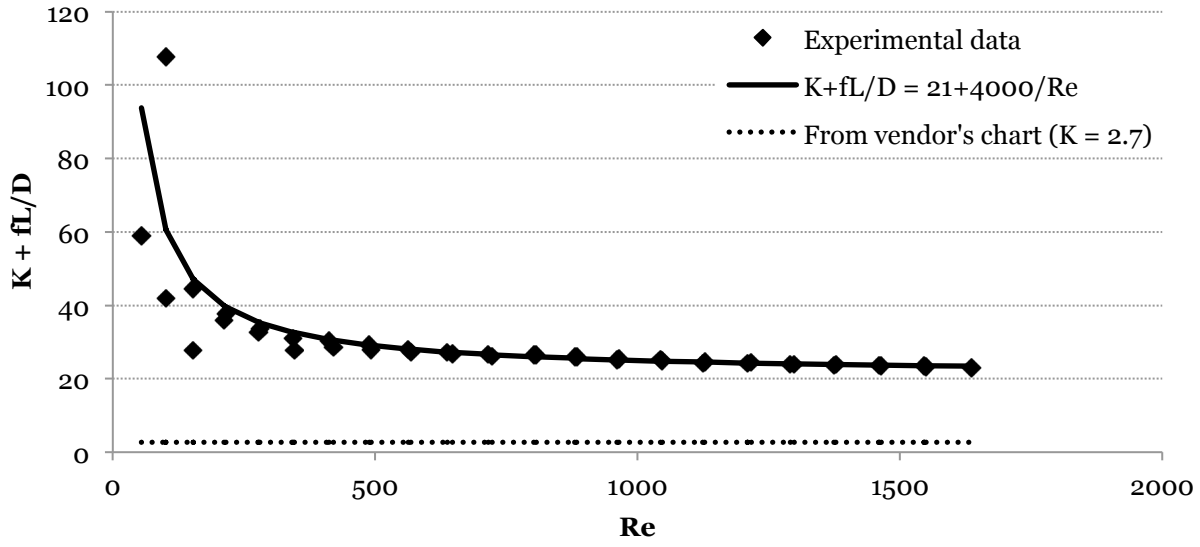

Figure 2-9. Friction number correlation for static mixer MX-10.

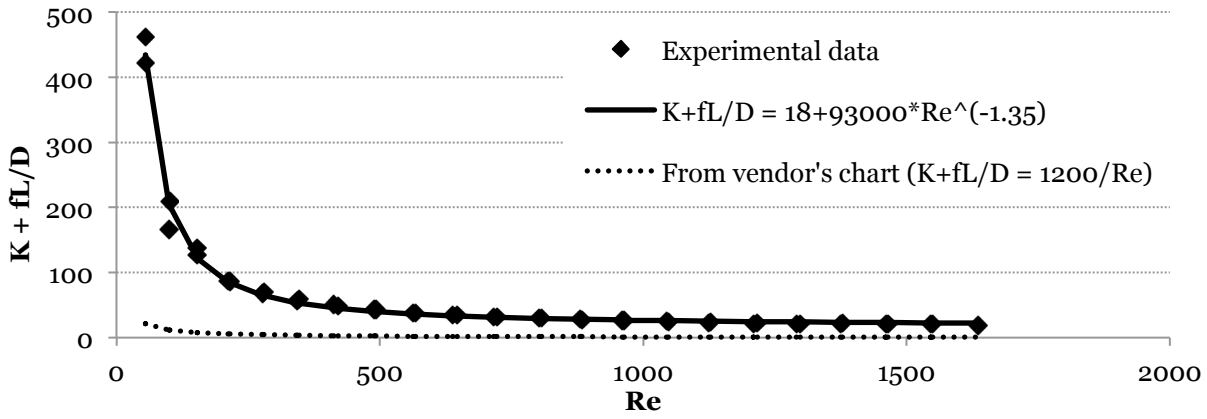

Figure 2-10. Friction number correlation for Coriolis flowmeter FM-40.

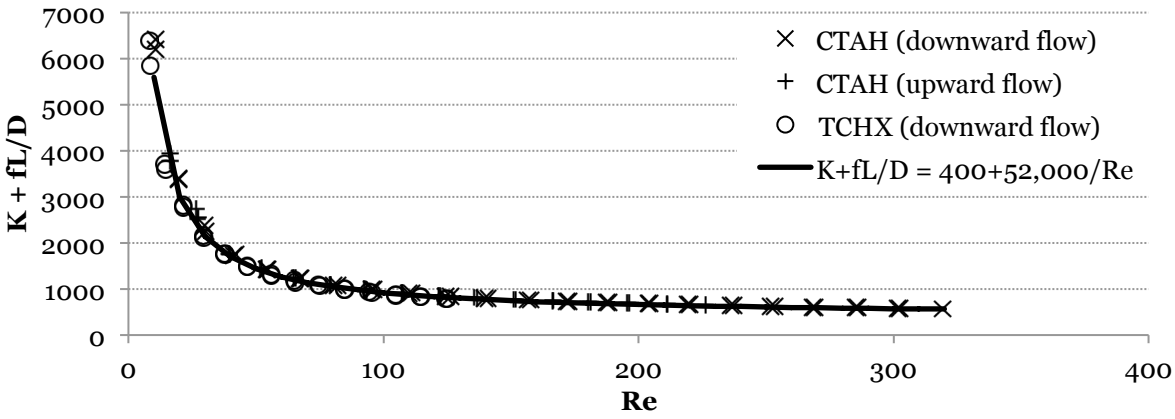

Figure 2-11. Friction number correlation for fan-cooled heat exchangers.

This series of tests also validated the analytical correlation for laminar flow friction factor in straight, cylindrical pipes ($f = 64/\mathrm{Re}$) and its applicability to the CIET 1.0 annular heater, with an agreement within 10% between experimental data and the analytical correlation, as shown in Figure 2-12.

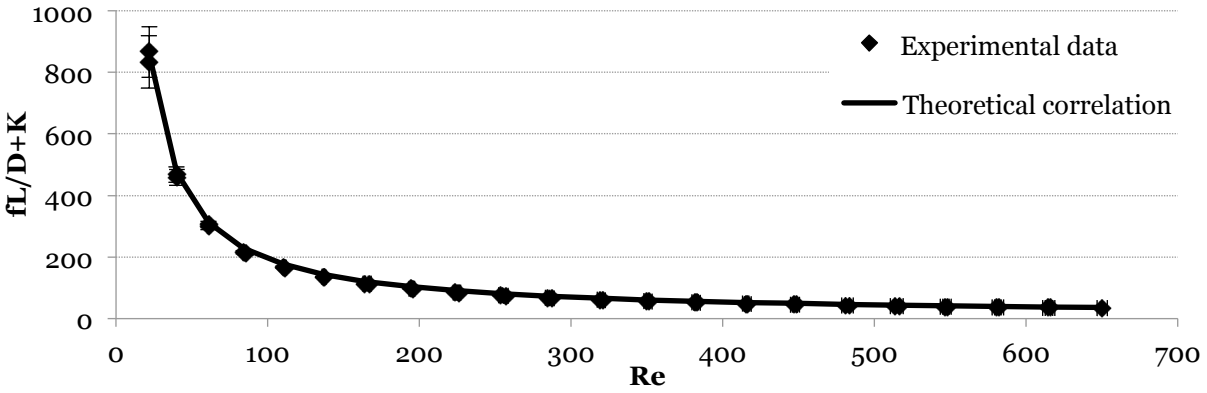

Figure 2-12. Friction number correlation for the CIET 1.0 annular heater.

These tests confirmed that analytical correlations can be used for regular piping sections of CIET 1.0, and component-scale correlations for static mixers, Coriolis flowmeters and heat exchangers have been developed and match experimental data with an agreement within 10%.

2.3.2 Initial Heated Tests

Before steady-state forced and natural circulation, and eventually transient tests were performed on the CIET 1.0 facility, a series of initial heated tests were performed to confirm performance and the ability to control various key components of the experiment.

Heater Control Trials, Parasitic Heat Losses

One series of experiments was aimed at testing the CIET 1.0 power supplies and heater functionality, and determining parasitic heat losses from the oil loop to ambient air through the piping thermal insulation without guard heating. This was done by varying power input from the heater and recording steady-state mass flow rates and bulk fluid temperatures in the loop with no active heat rejection. The energy conservation equation applied between consecutive temperature measurement points was used to calculate local heat losses from individual sections of the loop, and thermal insulation was enhanced in locations where high parasitic heat losses were observed. An infrared camera was used to identify specific locations where these losses occurred and to reduce them by adding thermal insulation.

CTAH Control Trials

For automated operation of the CIET 1.0 facility and optimized response to transients, feedback control must be implemented on the fan-cooled heat exchangers to vary fan motor speed. The initial control algorithm was developed to vary fan speed to control the average fluid outlet temperatures of the TCHX and CTAH heat exchangers. An additional benefit from the development of this feedback control system involves the opportunity to collect extensive heat transfer data for these heat exchangers. This data can be used to improve models to better characterize heat rejection from the CIET 1.0 fan-cooled heat exchangers at various fan speeds, and oil and air temperatures. Throughout these tests, the heater power input was manually varied, and the CTAH feedback control system was used to control the CTAH steady-state outlet temperature. Several options were examined for feedback control of the CTAH, including proportional, proportional-integral and proportional-integral-derivative controllers.

Figure 2-13 shows results obtained using a simple proportional controller to vary CTAH fan speed based on CTAH outlet temperature set-points, with a fixed heat input of 1.06 kW through the resistive heater. The proportional controller, activated 4000 seconds into the test, was successful in reaching steady CTAH outlet temperatures of 40°C (step up), 38°C (step down) and 41.5°C (step up), successively.

2.3.3 Best-Estimate Code Validation Tests

As part of the CIET research plan, steady-state single loop natural circulation in the DRACS loop, coupled DRACS and primary natural circulation loops, and simple, forced cooling power step change transients in the heater and CTAH loop have been studied using CIET 1.0. For

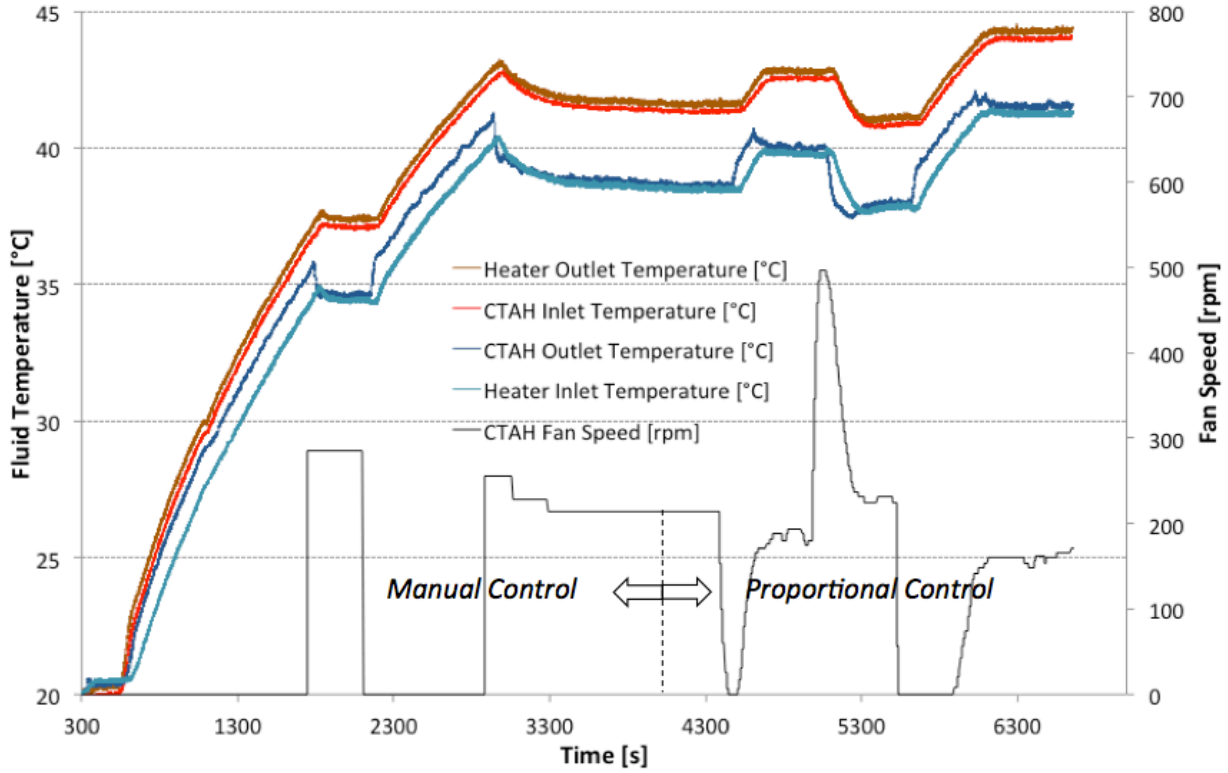

Figure 2-13. CTAH proportional feedback control test.

validation purposes, computational results from RELAP5-3D/Ver. 4.0.3 have been compared against experimental data. Experimental data and results from V&V of RELAP5-3D models are detailed in the following Sections. Reproducing such experimental setups in RELAP5-3D is key to better understanding thermal hydraulic phenomena specific to FHRs and how to best model them. Part of the V&V effort also included code-to-code comparisons with the FHR advanced natural circulation analysis (FANCY) code specifically developed at UCB for CIET and FHR natural circulation modeling.

2.4 RELAP5-3D and FANCY Models of CIET 1.0

While a detailed discussion of the CIET 1.0 design is provided in the previous Sections, this Section introduces key aspects of the CIET 1.0 geometry and boundary conditions relevant to the RELAP5-3D and FANCY models of the facility. These models are also described here.

2.4.1 CIET 1.0 Steady-State Natural Circulation Loops

As mentioned earlier, the CIET 1.0 facility replicates the main flow paths in the primary loop and the DRACS loop of prototypical FHRs. In particular, for emergency decay heat removal through the DRACS, natural circulation is established in the primary system, with flow upwards through the core, then downwards through the DHX and downcomer. This natural circulation loop, simply called *primary loop* in the remainder of this Chapter, consists of a vertical annular heated section, the shell side of a vertical single-pass straight shell-and-tube DHX, and the

connected piping. For simplicity in these experiments, the segment of the primary system that includes the primary pump and the primary loop oil cooler was valved off. The primary loop hot leg is the piping connecting the top of the heater to the top of the DHX. The primary loop cold leg is the piping connecting the bottom of the DHX to the bottom of the heater. Similarly, the DRACS loop consists of the tube side of the DHX, the TCHX, and the connected piping. The DRACS hot leg is the piping connecting the top of the DHX to the inlet of the TCHX. The DRACS cold leg is the piping connecting the outlet of the TCHX to the bottom of the DHX. Table 2-7 gives the physical dimensions of each segment. A detailed list of all input parameters to the CIET 1.0 model in RELAP5-3D and an example input deck are provided in Appendix A.

Table 2-7. Physical parameters of the CIET 1.0 natural circulation loops.

	Primary Loop				**DRACS Loop**			
	Heater	Hot Leg	DHX shell	Cold Leg	DHX tubes	Hot Leg	TCHX	Cold Leg
Length [m]	1.924	3.521	1.187	3.165	1.483	4.274	1.564	4.915
Elevation Change [m]	1.924	1.276	-1.187	-2.013	1.483	3.696	-0.416	-4.763
Hydraulic Diameter [mm]	6.6	27.9	5.7	27.9	6.9	27.9	11.9	27.9
Flow Area [10^{-4} m^2]	3.64	6.11	9.43	6.11	7.18	6.11	13.3	6.11

In modeling the steady-state behavior of the loops, it is assumed that the boundary conditions are:

- Adiabatic on the inner tube of the annular heater;
- Uniform heat flux inside the outer tube of the annular heater;
- Stainless steel piping with 5-cm-thick fiberglass insulation on the hot and cold legs of each loop;
- Copper piping with 5-cm-thick fiberglass insulation on the shell side of the DHX;
- Bare copper piping on the TCHX;
- Controlled bulk oil outlet temperature at the TCHX;
- 20°C ambient temperature around the rest of the loop;
- Atmospheric absolute pressure at the free surface of each expansion tank;
- Bypass branch, CTAH branch and primary pump manifold valved off (valves V-30, V-31, V-32, V-33, V-34, V-40, V-50, V-51, V-52 and V-53 closed – see locations on Figure 2-3).

As mentioned in Section 2.2.3, the loop is instrumented with inline TCs to measure bulk fluid temperatures at the inlets and outlets of the heater, DHX shell side, DHX tube side and TCHX. The type-T TCs accuracy is ±0.5°C in the 0-200°C range. Mass flow rates are directly measured in each loop using Coriolis flowmeters with accuracies of ±2% over the range of flow rates of interest. For each run, the heat input is set through the power supplies' controls. To collect the data used in this study, temperatures and mass flow rates in each loop are recorded when steady-state conditions have been reached. The coolant mass flow rate is the main metric of interest for steady-state natural circulation studies, since higher mass flow rates remove heat from the system with a smaller temperature difference between the hot and cold parts of the loop.

2.4.2 CIET 1.0 Forced Cooling Loop

The CIET 1.0 facility also replicates forced cooling in the heater and CTAH loop, simply called *CTAH loop* in the remainder of this Chapter. This loop consists of a vertical annular heated section, the oil side of the CTAH, and the connected piping, including the primary pump. For simplicity in forced cooling power step change transient experiments, the segment of the primary system that includes the DHX was valved off. The CTAH loop hot leg is the piping connecting the top of the heater to the inlet of the CTAH. The CTAH loop cold leg is the piping connecting the outlet of the CTAH to the bottom of the heater, including the primary pump.

In modeling the transient behavior of the loop for simple, forced cooling power step changes, it is assumed that the boundary conditions are:

- Adiabatic on the inner tube of the annular heater;
- Uniform heat flux inside the outer tube of the annular heater, controlled through the CIET LabVIEW station and varied with step changes over time;
- Stainless steel piping with 5-cm-thick fiberglass insulation on the hot and cold legs of the loop;
- Bare copper piping on the CTAH;
- Controlled CTAH bulk oil outlet temperature at 80°C, using the control strategy illustrated in Section 2.3.2;
- 20°C ambient temperature around the rest of the loop;
- Atmospheric absolute pressure at the free surface of the primary expansion tank;
- Controlled oil mass flow rate at 0.18 kg/s, using a proportional controller that continuously reads flow rates through the CTAH branch Coriolis flowmeter and adjusts primary pump speed with a VFD accordingly;
- Bypass branch and DHX branch valved off (valves V-22, V-30, V-31, V-32, V-33, V-34, V-50, V-51, V-52 and V-53 closed – see locations on Figure 2-3).

To collect the data used in this study, temperatures in the loop are continuously recorded as power input to the outer tube of the annular heater is varied. Coolant temperatures are the main metric of interest for transient tests since, as mentioned in Section 1.3.1, the main FOM related to structural integrity of metallic structural components in FHRs is expected to be the peak bulk coolant outlet temperature.

2.4.3 CIET 1.0 RELAP5-3D and FANCY Models

The RELAP5-3D and FANCY models of CIET 1.0 reproduce its geometry (i.e. components lengths, elevations, hydraulic diameters and flow areas listed in Table 2-7), pressure and temperature boundary conditions, and working fluid thermophysical properties. Material properties for the stainless steel and copper tubing, as well as the fiberglass insulation, are manually implemented in the models. In particular, thermal mass of the system has an impact on transient modeling and validation. Therefore, masses of individual components were measured and recorded throughout the assembly process of CIET 1.0, and these individual masses are added to heat structures in the RELAP5-3D and FANCY models when transient model validation is performed. Figure 2-14 shows a labeled 3-dimensional model of CIET 1.0

and the corresponding nodalization diagram for the RELAP5-3D and FANCY models. On the diagram, the primary loop and the DRACS loop, used for natural circulation validation tests, are highlighted in green. A more detailed nodalization diagram, as well as a detailed list of input parameters to the CIET 1.0 model in RELAP5-3D and an example input deck are provided in Appendix A.

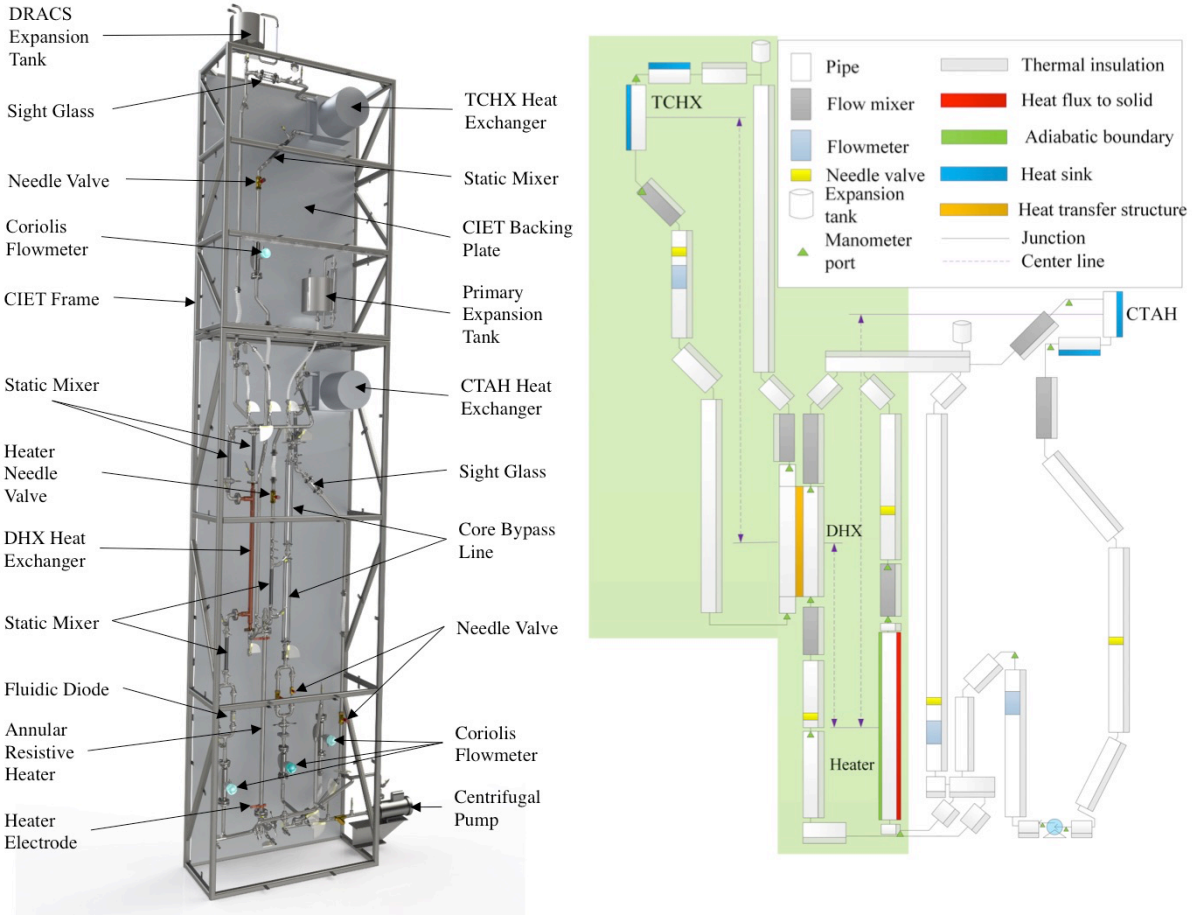

Figure 2-14. CIET 1.0 3-dimensional model, not showing insulation (left) and corresponding nodalization diagram for the RELAP5-3D and FANCY models (right).

For this study, all calculations are run with RELAP5-3D/Ver. 4.0.3 and FANCY/Ver. 2.0 in transient mode. For steady-state calculations, the models are run until steady-state conditions are reached for fluid temperatures and mass flow rates in each loop.

2.5 Solution and Code Verification for Steady-State Natural Circulation

Verification is “the process of determining that a model implementation accurately represents the developer’s conceptual description of the model and the solution to the model” [38]. Verification efforts are divided between solution verification, assessing the numerical

accuracy of the solution to a computational model, and code verification, assessing the reliability of the software coding. Such efforts are pursued here, to the extent possible for end users of the executable version of the RELAP5-3D code.

2.5.1 Solution Verification

For solution verification purposes, sensitivity of the steady-state natural circulation mass flow rate to a set of initial and boundary conditions, as well as model discretization, is assessed in RELAP5-3D and FANCY. This sensitivity analysis is performed using models of the DRACS loop with a constant power input of 1 kW. The results are summarized in Table 2-8, where solutions are reported as *not sensitive* to a parameter when they vary by less than 1% for any value of the parameter in the range of interest.

Table 2-8. Sensitivity of steady-state natural circulation mass flow rates calculated by RELAP5-3D and FANCY to a set of model parameters.

Model input parameter	Parameter range	Sensitivity
Expansion tank temperature [°C]	25 – 185	Not sensitive
Loop initial temperature [°C]	25 – 185	Not sensitive
Loop initial pressure [kPa]	100 – 200	Not sensitive
Loop initial mass flow rate [kg/s]	0.01 – 1.0	Not sensitive
Wall radial discretization [meshes]	3 – 20	Not sensitive
Hot/cold leg axial discretization [control volumes]	10 – 50	Not sensitive
Heater/heat exchangers axial discretization [control volumes]	5 – 55	Not sensitive
TCHX outlet temperature [°C]	35 – 70	Sensitive

As expected, the steady-state natural circulation mass flow rate is not sensitive to the expansion tank fixed temperature, since at steady-state, there is no flow going in or out of the tank. It is not sensitive to initial conditions, which should not impact steady-state behavior of the loop. It is not sensitive to radial discretization of the walls, nor to axial discretization of the hot and cold legs, heater and heat exchangers, because temperature distributions are approximately linear. However, the natural circulation mass flow rate is sensitive to the TCHX outlet temperature boundary condition. Indeed, higher temperature boundary conditions lead to a higher average fluid temperature in the loop at steady-state. Because viscosity of the oil decreases at higher temperature, friction losses are reduced, which leads to higher natural circulation mass flow rates. This result is shown in Figure 2-15, where mass flow rates in the DRACS loop are obtained with RELAP5-3D for TCHX outlet temperatures in the range of 35-70°C. This confirms the necessity to properly account for the impact of this boundary condition on natural circulation problems solved with RELAP5-3D and FANCY.

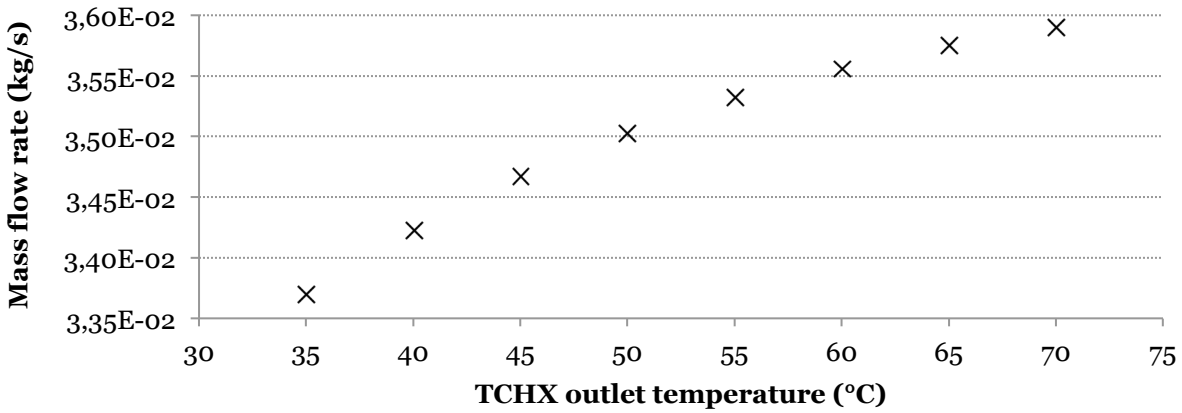

Figure 2-15. Sensitivity of DRACS steady-state natural circulation mass flow rate to TCHX outlet temperature with a constant power input of 1 kW.

2.5.2 Code Verification

For code verification, the following tests are performed at steady-state:

- Is the heat input to the fluid equal to the sum of the heat removed through the TCHX and parasitic heat losses along the loop?
- Is the mass flow rate uniform in each loop?
- Is the following equation verified in each loop:

$$Q_h = \dot{m} c_{p,av} \Delta T_h \tag{2-23}$$

where Q_h is the heat input from the heat source (i.e. the heater in the primary loop and the DHX in the DRACS loop), $\dot{m}$ the loop mass flow rate, $c_{p,av}$ the average specific heat capacity of the fluid in the heat source, and ΔT_h the temperature change of the fluid across the heat source. The code results have passed these tests, hence partly verifying proper solving of the fundamental conservation equations.

The CIET 1.0 models in RELAP5-3D and FANCY have therefore been developed to a point where they are only sensitive to relevant physical parameters for our application, such as heat input to the fluid, and heat exchanger outlet temperature boundary condition. The next step of the V&V exercise is model validation.

2.6 Model Calibration and Validation

Validation is "the process of determining the degree to which a model is an accurate representation of the real world from the perspective of the intended uses of the model" [38]. The validation effort is performed here by comparing computational results from RELAP5-3D and FANCY to experimental data from CIET 1.0 for single loop steady-state natural circulation in the DRACS, coupled steady-state natural circulation in the primary loop and the DRACS, and forced cooling at constant mass flow rate with heat input step changes in the CTAH loop.

2.6.1 Model Calibration

There is a distinction between model validation and calibration efforts, where validation is an assessment of the model in a "blind" test with experimental data, whereas the key issue in calibration is to adjust the physical modeling parameters to improve agreement with experimental data [38]. For this V&V study, four different sets of natural circulation data were collected on CIET 1.0. The first dataset is used for model calibration, while the three remaining datasets are used for model validation. In this case, the calibration effort consists in correcting for the overall heat transfer coefficient of the DHX and the piping thermal insulation. It was observed that default heat transfer coefficient correlations in RELAP5-3D and FANCY systematically underestimate parasitic heat losses in the primary loop by ~75% and in the DRACS loop by ~50%, likely due to additional losses through metallic components protruding from the thermal insulation (e.g. TC ports and manometer valves), even after these protrusions were insulated based on image data from an infrared camera. Conversely, default heat transfer coefficient correlations overestimate overall heat transfer coefficient in the DHX by ~45%. These effects are easily corrected by using multiplication factors on heat transfer coefficients in each major section of the coupled loops.

2.6.2 Model Validation

For model validation, computational results from RELAP5-3D and FANCY are compared to experimental data from CIET 1.0. This is first done for single loop, steady-state natural circulation in the DRACS, where analytical solutions for mass flow rate in a loop with no parasitic heat losses exist. Then, model validation is performed for coupled natural circulation in the primary loop and the DRACS loop. Finally, validation of simple transient models in RELAP5-3D is achieved by comparing experimental data and code results for forced cooling with heat input step changes in the CTAH loop.

DRACS Loop Steady-State Natural Circulation Model Validation

Three sets of experimental data have been collected for model validation at various heat input levels and TCHX outlet temperatures. Corresponding boundary conditions have been reproduced in RELAP5-3D and FANCY.

For single-phase natural circulation loops with no parasitic heat losses, Scarlat has derived the following expression from the mass, momentum and energy conservation equations for mass flow rate, based on fluid average thermophysical properties and loop geometry [21]:

$$\dot{m}^3 = \frac{2{\rho_{av}}^2 g \beta_{av}}{c_{p,av}} \cdot \frac{\Delta z_{NC} Q_h}{F'} \tag{2-24}$$

$$F' = \sum_{i=1}^{N} \left(\frac{1}{{A_i}^2} \cdot \frac{L_i}{D_i} \right) f_i \tag{2-25}$$

where ρ_{av} is the average density of the fluid, g the gravity constant, β_{av} the average volumetric expansion coefficient of the fluid, Δz_{NC} the buoyancy head, defined as the elevation difference between the centerlines of the heated and cooled sections, A_i the cross-sectional area of section

i, L_i the length of section i, D_i the hydraulic diameter of section i, f_i the friction factor in section i, and N the total number of sections in the loop.

Equation (2-24) is implicit since f_i depends on Re_i, the Reynolds number in section i, which in turn depends on $\dot{m}$ through:

$$\mathrm{Re}_i = \frac{1}{\mu_i}\dot{m}\frac{D_i}{A_i} \tag{2-26}$$

where μ_i is the dynamic viscosity of the fluid in section i. However, using the analytical correlation for laminar flow friction factor in straight, cylindrical pipes ($f = 64/\mathrm{Re}$), Eq. (2-24) can be solved. This correlation is valid here. Indeed, the DRACS loop always operates in the laminar regime, and it has been measured that friction losses make up to 98% of total losses in the loop, while form losses only contribute to 2% of total losses. Therefore, the analytical solution is expected to be close to the correct solution.

Figure 2-16 shows the comparison of experimental data, RELAP5-3D and FANCY results, and analytical solutions for various heat inputs and two different TCHX outlet temperatures. Since Eq. (2-24) uses average fluid thermophysical properties, analytical results are calculated at the average fluid temperatures obtained from RELAP5-3D. All analytical solutions use the temperature-dependent thermophysical properties for Dowtherm A listed in Eqs. (2-14)-(2-17). It has been verified that Dowtherm A thermophysical properties at atmospheric pressure, implemented in RELAP5-3D, lie within ±0.4% of the values obtained with Eqs. (2-14)-(2-17) in the 20-180°C temperature range [39]. Moreover, the oil used in CIET 1.0 was sent to the manufacturer for analysis prior to filling the loop, and it was confirmed that it had the correct composition.

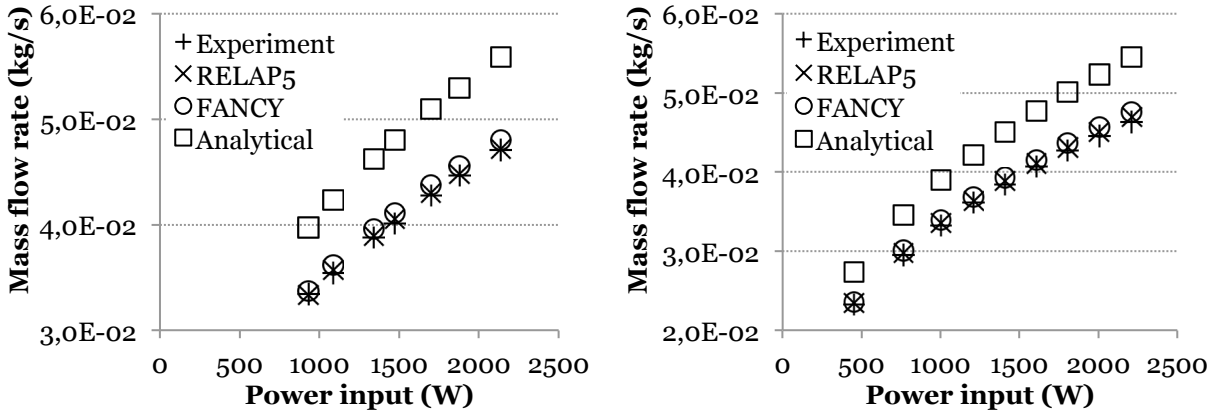

Figure 2-16. Comparison of experimental, RELAP5-3D, FANCY and analytical steady-state natural circulation mass flow rates for various heat inputs and TCHX outlet temperatures of 46°C (left) and 35°C (right).

At all power input levels and TCHX outlet temperatures, the agreement between RELAP5-3D and experimental data is within 1% and the agreement between FANCY and experimental data is within 3%. Figure 2-16 also shows that analytical solutions overestimate natural circulation mass flow rates in the DRACS loop by ~18%. Indeed, analytical solutions are only

valid for ideal loops with no parasitic heat losses from the hot and cold legs, while for these tests, parasitic heat losses ranging from ~50% at a power input of 450 W to ~5% at a power input of 2,200 W result in reduced natural circulation mass flow rates in the DRACS. The parasitic heat loss effect, typical of scaled IETs with reduced flow area, is properly taken into account by the RELAP5-3D and FANCY models, where properties of the fiberglass thermal insulation and ambient temperatures are included, and overall heat transfer coefficients of piping thermal insulation have been calibrated.

The direct comparisons shown in Figure 2-16 are not optimal since a new graph must be generated when experimental boundary conditions are varied. Vijayan proposes a non-dimensional, generalized correlation of the following form for steady flow in a fully laminar or fully turbulent natural circulation loop [40]:

$$\mathrm{Re} = C\left[\frac{(Gr_m)_{\Delta z_{NC}}}{N_G}\right]^r \tag{2-27}$$

$$\mathrm{Re} = \frac{D_r \dot{m}}{A_r \mu_{av}} \tag{2-28}$$

$$(\mathrm{Gr}_m)_{\Delta z_{NC}} = \frac{{D_r}^3 {\rho_{av}}^2 \beta_{av} g Q_h \Delta z_{NC}}{A_r {\mu_{av}}^3 c_{p,av}} \tag{2-29}$$

$$N_G = \frac{L_t}{D_r}\sum_{i=1}^{N}\left(\frac{l_{eff}}{d^{1+b}a^{2-b}}\right)_i \tag{2-30}$$

where $L_t = \sum_{i=1}^{N} L_i$ is the total length of the loop, $D_r = \frac{1}{L_t}\sum_{i=1}^{N} D_i L_i$ the reference hydraulic diameter of the loop, $A_r = \frac{1}{L_t}\sum_{i=1}^{N} A_i L_i$ the reference flow area of the loop, $d_i = \frac{D_i}{D_r}$ the relative hydraulic diameter of section i, $a_i = \frac{A_i}{A_r}$ the relative flow area of section i, $\left(l_{eff}\right)_i = \left(L_{eff}\right)_i / L_t$ the relative effective length of section i, $\left(L_{eff}\right)_i = L_i + Le_i$ the effective length of section i, and $Le_i = \frac{K_i D_i}{f_i}$ with K_i the sum of form loss coefficients in section i.

The correlation is applicable if a friction law of the form $f = \frac{p}{\mathrm{Re}^b}$ is valid throughout the loop with the same values of p and b. Then, Vijayan shows that:

$$C = \left(\frac{2}{p}\right)^r \tag{2-31}$$

$$r = \frac{1}{3-b} \tag{2-32}$$

For fully laminar flow ($p = 64$, $b = 1$), as in the DRACS loop, $C = 0.1768$ and $r = 0.5$.

Figure 2-17 shows results of the comparison between RELAP5-3D and FANCY calculations, experimental data, and the correlation proposed by Vijayan (Eq. (2-27)) in the non-dimensional space. Figure 2-17 uses a logarithmic scale to exemplify the linear trend predicted by Eq. (2-27). Throughout the range of interest, Figure 2-17 shows an excellent agreement between RELAP5-

3D and FANCY solutions, experimental data, and the correlation proposed by Vijayan with $C = 0.1768$ and $r = 0.5$.

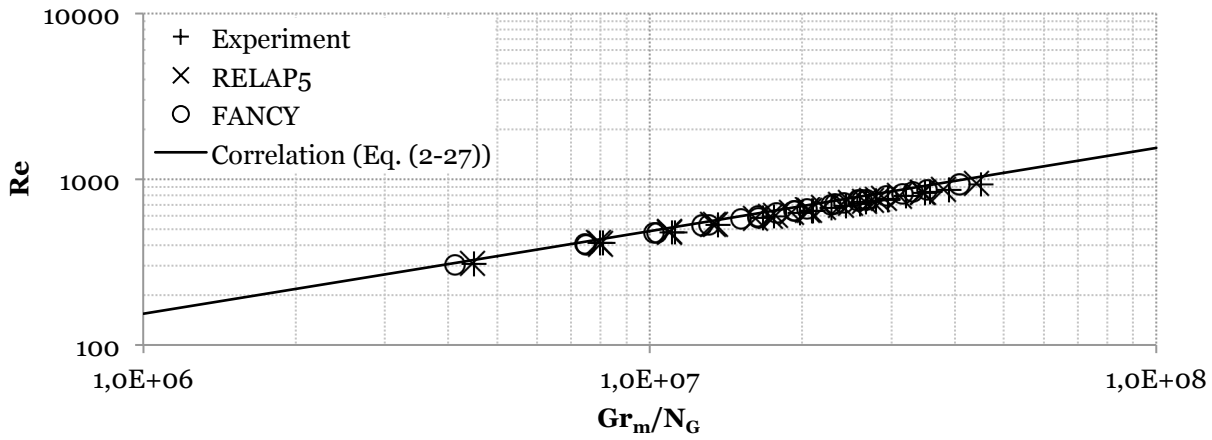

Figure 2-17. DRACS experimental data, RELAP5-3D and FANCY steady-state natural circulation models.

Coupled Loops Steady-State Natural Circulation Model Validation

The same three sets of experimental data are used to validate RELAP5-3D and FANCY models of coupled, steady-state natural circulation in the primary loop and the DRACS loop. At all power input levels and TCHX outlet temperatures, the agreement between RELAP5-3D and experimental data is within 8% in both loops and the agreement between FANCY and experimental data is within 13% in both loops. Figure 2-18 and Figure 2-19 show results of the comparison between RELAP5-3D and FANCY calculations, experimental data, and the correlation proposed by Vijayan (Eq. (2-27)) in the non-dimensional space for the primary loop and the DRACS loop, respectively. Throughout the ranges of interest, Figure 2-18 and Figure 2-19 show excellent agreements between RELAP5-3D and FANCY solutions, experimental data, and the correlation proposed by Vijayan with $C = 0.1768$ and $r = 0.5$.

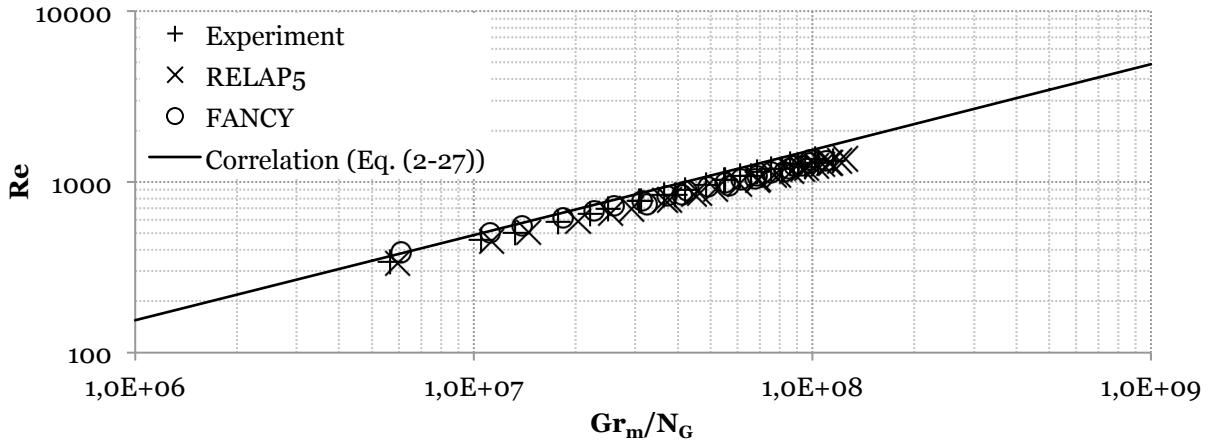

Figure 2-18. Primary loop experimental data, RELAP5-3D and FANCY steady-state natural circulation models.

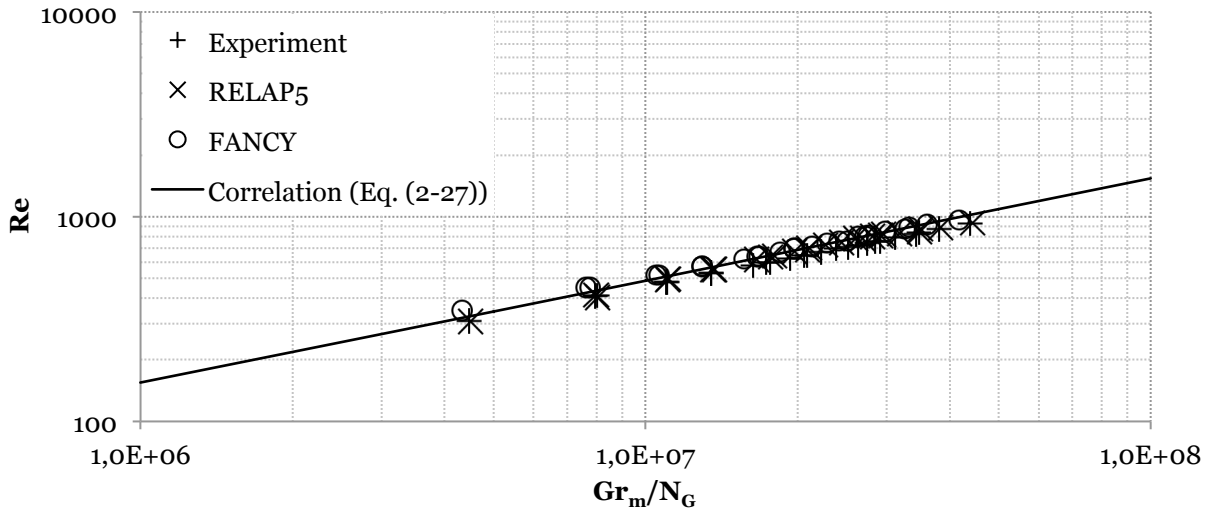

Figure 2-19. DRACS loop experimental data, RELAP5-3D and FANCY steady-state natural circulation models.

Forced Cooling, Power Step Change Model Validation

Experimental data has been collected for transient, forced cooling model validation using heat input step changes, a fixed coolant mass flow rate of 0.18 kg/s in the CTAH loop and a controlled CTAH outlet temperature of 80°C. Corresponding boundary conditions have been reproduced in RELAP5-3D, as listed in Section 2.4.2. The only discrepancy between the model and the experiment is that RELAP5-3D uses a fixed CTAH outlet temperature boundary condition of 80°C instead of the more complex real evolution resulting from the CTAH controller on CIET, because of the lack of a detailed model for the CTAH at the time of this study. Power step changes under forced cooling operation with a fixed mass flow rate are aimed at validating the model for thermal inertia of the system's solid structures and fluid, which affects its response time to such transients. Thermal capacities for each heat structure are documented in the RELAP5-3D input deck provided in Appendix A. In particular, because the thermal capacity of the solid structures in the loop – ~50 kJ/K – is of the same order of magnitude as the thermal capacity of the oil – ~20 kJ/K –, it is important to account for both types of heat structures to accurately predict the system's transient behavior.

Figure 2-20 shows a comparison of RELAP5-3D results and experimental data for an entire test, and Figure 2-21 shows details of this comparison for a selection of power step changes up and down. Throughout the test, the agreement between RELAP5-3D results and experimental data is within 2°C. More specifically, the agreement is within instrumentation accuracy (±0.5°C) for the heater outlet temperature and there is a delay of ~100 s in the response of the CTAH inlet temperature to power step changes compared to experimental data. The agreement between code results and experimental data for the CTAH outlet and heater inlet temperatures is within instrumentation accuracy, except for the short periods during which the code uses an idealized CTAH outlet temperature boundary condition of 80°C instead of the more complex controller implemented on CIET 1.0.

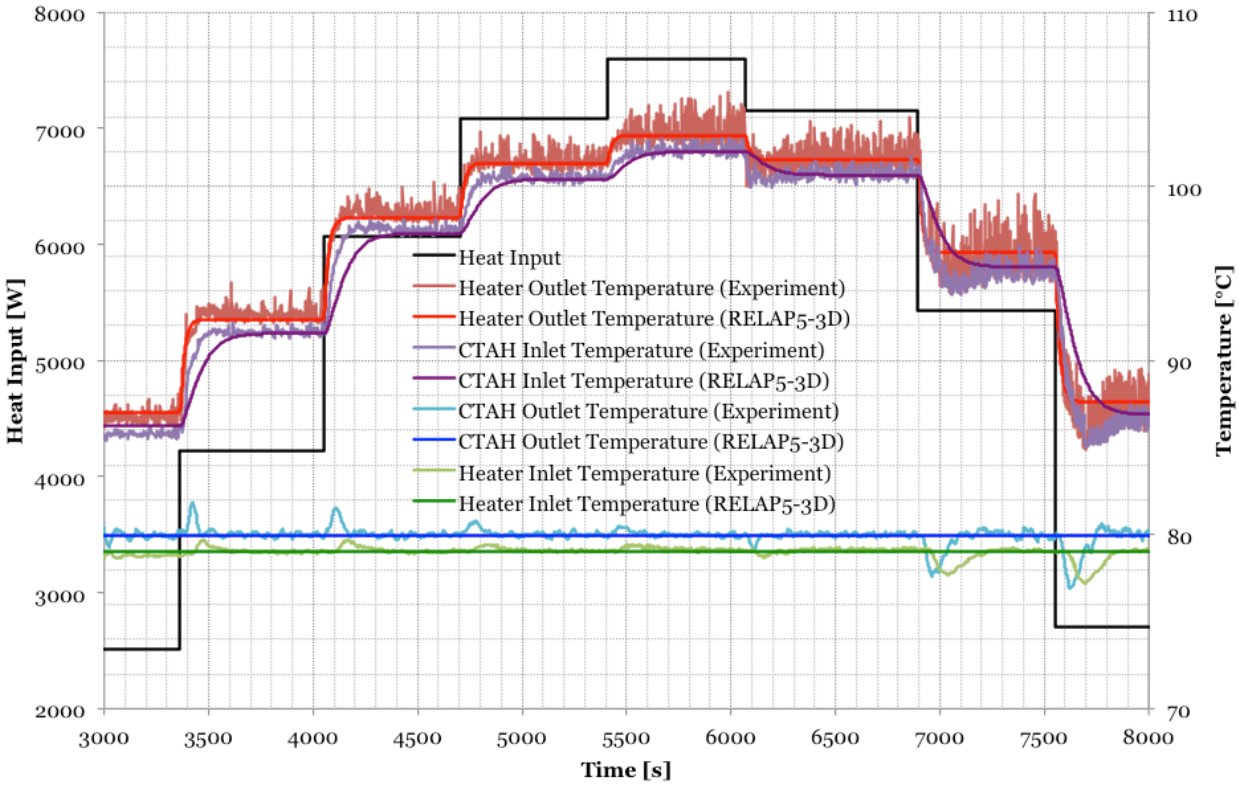

Figure 2-20. Experimental data and RELAP5-3D results for transient forced cooling in the CTAH loop.

The fact that RELAP5-3D accurately predicts the transient increase of the heater outlet temperature indicates that the model has the correct thermal capacity for the heater element. Conversely, the thermal capacity between the heater outlet and the CTAH inlet does not appear to be modeled perfectly, since RELAP5-3D predicts a slower response of the CTAH inlet temperature than CIET produces. Because accurate data for the masses of the CIET thermal structures, and therefore for their thermal capacities, was measured during fabrication of the CIET 1.0 facility and implemented in the code, this disagreement may be due to the approach to modeling these structures, and the fact that some of the thermal structures (e.g. pipe walls), which have a large surface area compared to their thermal inertia, are more tightly coupled to the fluid than components with small surface areas compared to their thermal inertia (e.g. flanges, valves). As shown in Figure 2-22, closer agreement between code results and experimental data is indeed obtained by separating the weakly and the strongly coupled thermal masses into separate heat structures in the RELAP5-3D model, based upon measured values for weights of individual components and the fact that weakly coupled thermal masses account for ~20% of the total weight of the system's solid structures.

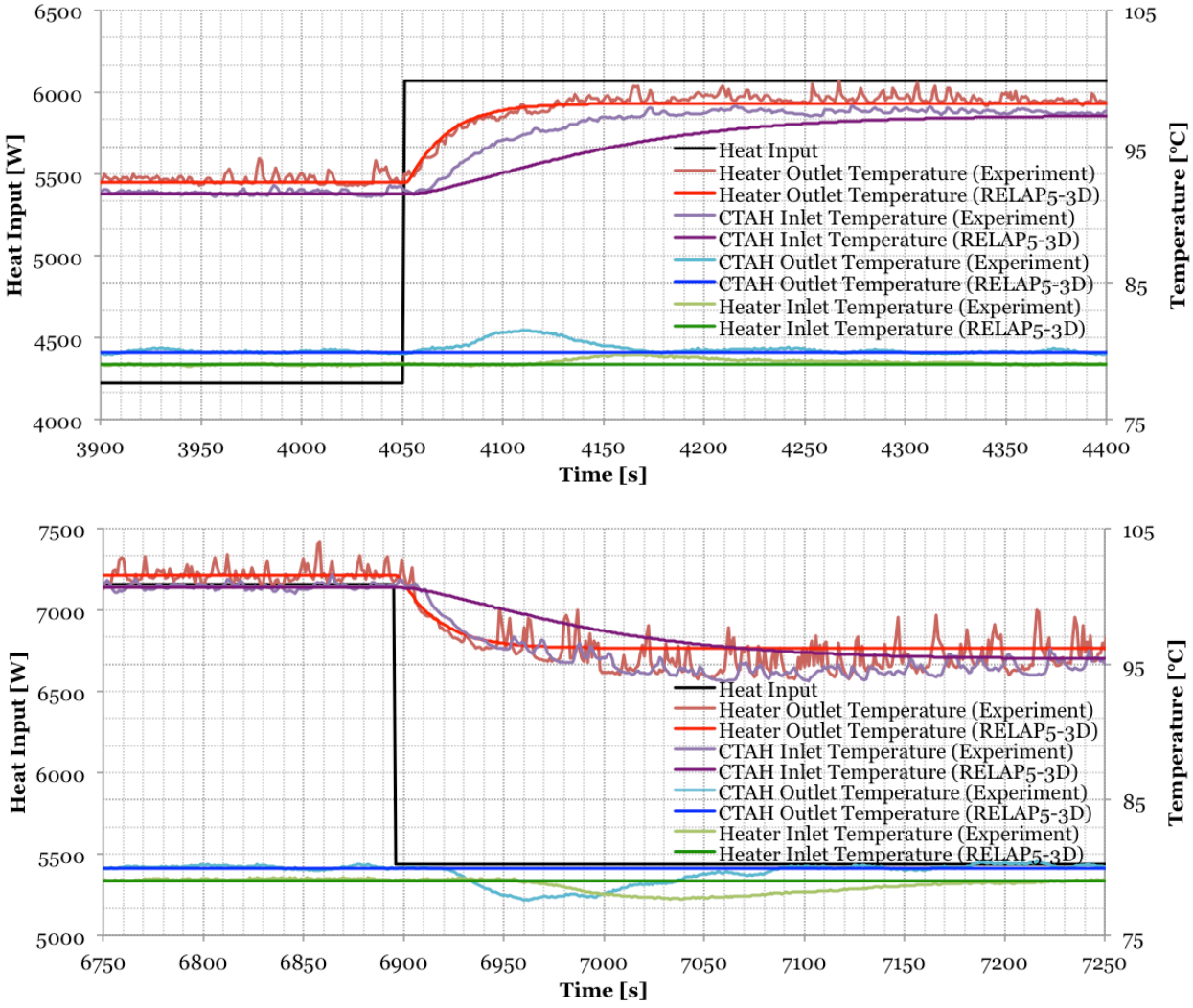

Figure 2-21. Experimental data and RELAP5-3D results for transient forced cooling in the CTAH loop (details).

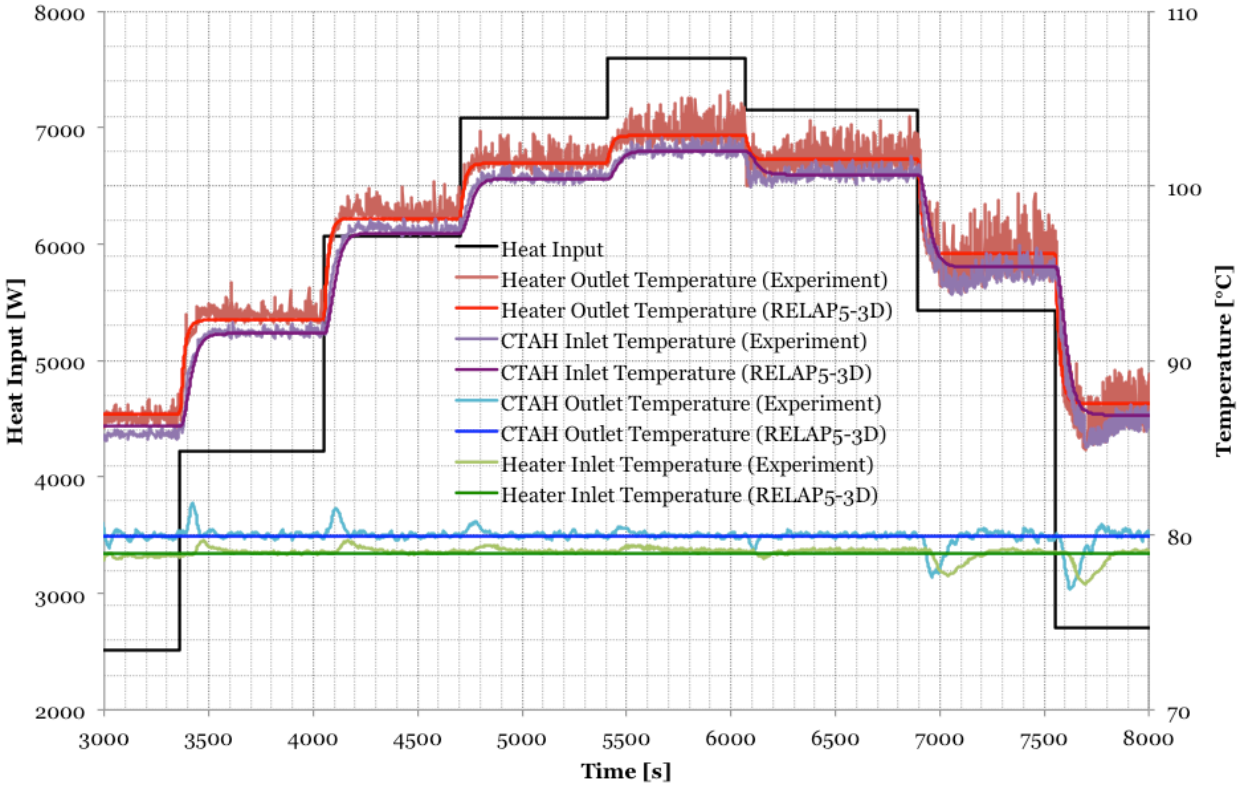

Figure 2-22. Experimental data and RELAP5-3D results for transient forced cooling in the CTAH loop using decoupled heat structures.

2.6.3 Conclusions of the Validation Effort

For single, steady-state natural circulation loops, at all power input levels and TCHX outlet temperatures tested for this study, the agreement between RELAP5-3D and experimental data for the loop mass flow is within 1% and the agreement between FANCY and experimental data is within 3%. For coupled, steady-state natural circulation between the primary loop and the DRACS loop, the agreement between RELAP5-3D and experimental data remains within 8% and the agreement between FANCY and experimental data remains within 13% in both loops. Equation (2-27) provides a means to properly compare best-estimate steady-state code solutions to experimental data in the non-dimensional space. This comparison shows an excellent agreement between both code calculations and experimental data in the coupled loops, where flow is in the fully laminar regime. The results also show remarkable agreement with the correlation proposed by Vijayan for steady-state flow in a fully laminar natural circulation loop, which is the case here.

For transient, forced cooling in the CTAH loop using heat input step changes, a fixed coolant mass flow rate of 0.18 kg/s and a controlled CTAH outlet temperature of 80°C, the agreement between RELAP5-3D results and experimental data is within 2°C when all thermal masses are modeled as tightly coupled to fluid structures. This agreement falls to within 1°C when components with small surface areas compared to their thermal inertia (e.g. flanges, valves) are modeled as separate heat structures in RELAP5-3D.

This study demonstrates the value of following the individual steps listed below, in the order shown, for proper validation of best-estimate models, which is key to FHR safety analysis, using scaled IETs such as the CIET 1.0 facility or future full scale salt loops:

1. Isothermal, forced circulation flow around the loop, with pressure data collection to determine friction losses in the system. When handbook values are not applicable (e.g. for complex-shaped components), empirically measured values must be implemented in the best-estimate codes used for integral system modeling.
2. Steady-state single and coupled natural circulation. Collected data, compared to predicted performance, forms the validation basis for best-estimate steady-state models. In particular, steady-state experimental data is used to develop overall heat transfer coefficient correlations for heat exchangers and parasitic heat losses in major sections of the fluid loops.
3. Transient tests, starting with forced cooling at fixed mass flow rate and heat input step changes or other, more complex power profiles. This series of tests is used to characterize thermal response of the loop and provide insight for modeling of heat structures more or less tightly coupled to the fluid.

Chapter 3 Reliability of Passive Safety Systems and Application to the Mk1 PB-FHR DRACS

In the aftermath of the Fukushima accident of March 2011, where reactor cores were severely damaged due to an inability to provide external power to active equipment to remove decay heat from the shut down cores, the advantages of using passive safety cooling systems for new generation nuclear power plants have become more obvious than ever. However, the current framework used to assess risks in nuclear reactors, using a combination of deterministic approaches and PRA, is not adapted to assessment of the performance of these passive safety systems, which would inform risk mitigation measures.

The goal of this study is to show that novel methodologies to assess the reliability of passive safety systems have been proposed and successfully implemented, and that they can be implemented again to reactor designs under current development, using the example of the PB-FHR and its natural-circulation-driven DRACS loops. Although FHR designs are continuing to evolve, all use passive safety for emergency decay heat removal. The analysis for the Mk1 PB-FHR provides important information as to elements of the system that require particular attention throughout the development process, due to their critical role in the performance of the DRACS, and therefore their implications on risk mitigation associated with this system. A number of elements in this analysis are based on personal engineering judgment, which would not be sufficient if such a study were to be used towards licensing of an FHR.

Expert judgment emerges as one of the critical elements throughout the study, in order to identify and rank key phenomena involved in the behavior of the DRACS, and more generally in the global behavior of the reactor. Therefore, although some of the conclusions from this study may be used to inform regulatory work on licensing new generation nuclear power plants such as the Mk1 PB-FHR, most of the work remains gathering experts to discuss functional requirements and run PIRT-type exercises for this novel design, in order to identify phenomena and points of the design that merit particular attention to reduce risks associated with the reactor and its passive safety cooling system to a minimum. This study is not primarily valuable for the results of the risk assessment performed here, which is only a preliminary attempt. It rather aims at showing that the framework for risk analysis of new generation nuclear power plants can and should be updated, and that recommendations for risk mitigation can be informed by analyses as preliminary as those presented in this Chapter.

Previous studies, based on the earlier design of a 900-MWth PB-AHTR, have found that the system could adequately respond to severe accidents such as LOFC and LOHS by relying on emergency decay heat removal through the DRACS [32,36]. However, these deterministic studies relied on non-validated models and, as importantly, did not include a discussion on actual reliability of the DRACS based on epistemic – or state-of-knowledge – uncertainties on parameters affecting natural circulation in the DRACS loop. An important challenge when assessing the reliability of passive safety systems such as natural-circulation-driven decay heat removal systems is that both driving forces – buoyancy forces in this case – and counter-forces

– friction losses here – are small and dependent on a wide diversity of phenomena. As a result, performance of the natural circulation system strongly depends on plant conditions and configurations when the system needs to be called upon for safety purposes, and in particular, on deviations of some key parameters from their nominal values due to failure of either active components (e.g. control valves, pumps and electric signals) or passive components, as well as uncertainties associated with factors on which the magnitudes of these forces and counter-forces depend (e.g. values of heat transfer coefficients and pressure losses).

Several methods have been proposed to assess the reliability of passive safety systems involving a moving working fluid – one representative example being natural-circulation-driven decay heat removal systems such as the Mk1 DRACS. A first class of methods uses propagation of uncertainties from key input parameters to system response. These methods were first developed as the reliability evaluation of passive safety systems (REPAS) methodology [41], which later evolved to become the reliability methods for passive safety functions (RMPS) [42]. A second class of methods, known as the assessment of passive system reliability (APSRA) methodology, uses failure surfaces predicted with best-estimate codes, considering deviations of operating parameters from their nominal states that affect system response [43]. The state of the art for these methods has recently been summarized in a technical document by the International Atomic Energy Agency [44]. For this study, we focus on adapting the RMPS to the DRACS of the Mk1 PB-FHR to address the following problems:

- Identification and quantification of the sources of uncertainty and determination of key parameters for passive system reliability;
- Propagation of the uncertainties through thermal hydraulic models and assessment of thermal hydraulic passive system reliability;
- Introduction of passive system reliability in accident sequence analyses.

To illustrate the possibilities of this methodology, each step and application to the DRACS for the PB-FHR is presented in Section 3.1. An alternative approach using response surfaces, aimed at reducing the computation time required by extensive use of best-estimate calculations while introducing more statistically significant results, is developed in Section 3.2. Measures and design improvements informed by this risk assessment analysis, which constitute a risk mitigation study, are proposed in Section 3.3.

3.1 RMPS Methodology and Application to the DRACS

This Section summarizes each step of the RMPS and develops their application to the DRACS for the Mk1 PB-FHR. These steps are shown in the RMPS methodology roadmap in Figure 3-1 [42].

3.1.1 Definition of the Transient Scenario

Results from the reliability analysis of a given passive safety system and its sensitivity to a set of key parameters are specific to a postulated transient scenario. Therefore, the first step of the methodology is the definition of the transient scenario in which the passive system is relied upon for safety. Specific failure criteria, relevant parameters and quantified uncertainties are

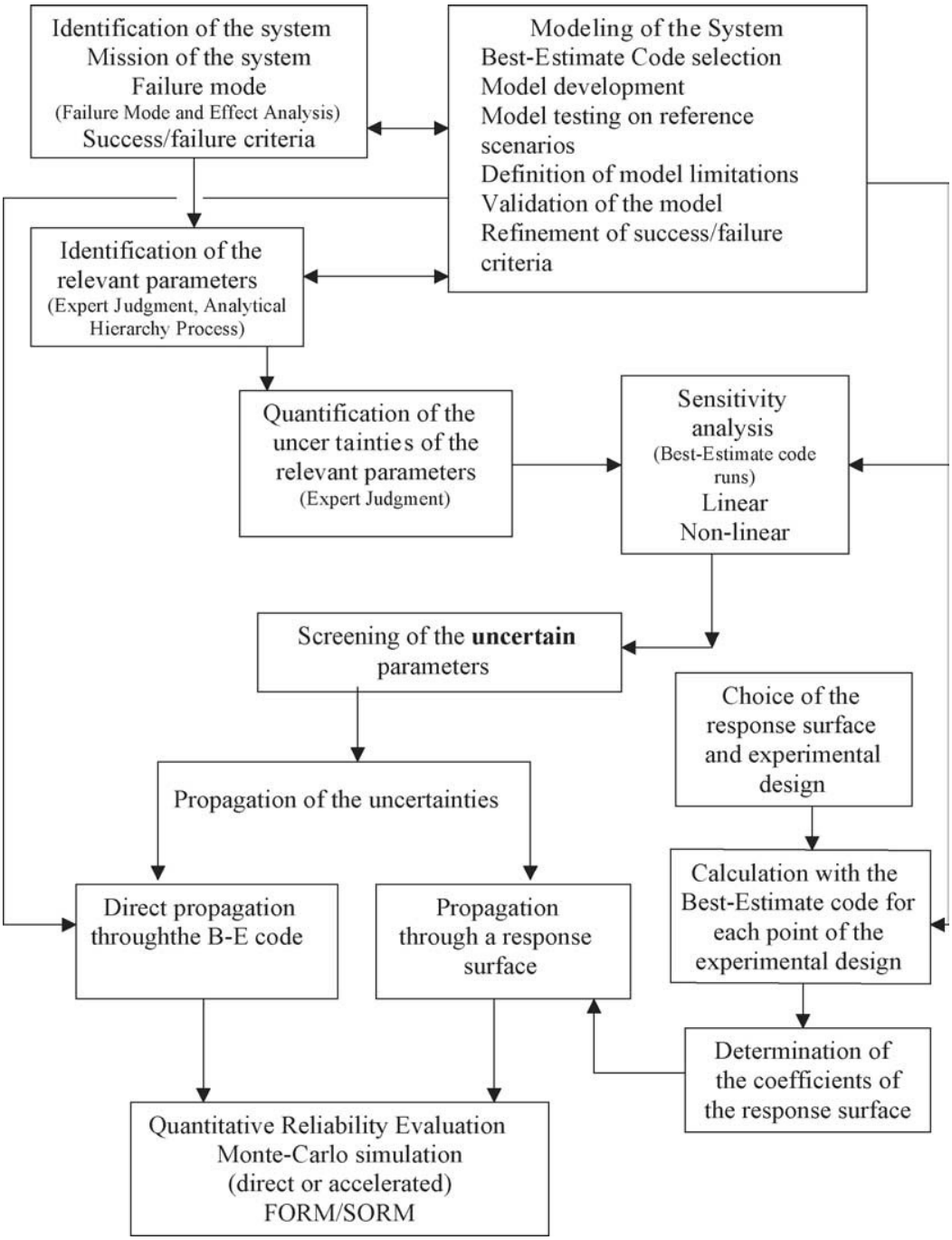

Figure 3-1. RMPS methodology roadmap [42].

subsequently tied to the postulated scenario. At the end of the RMPS, reliability of the passive system is obtained by integration of all transient scenarios for which this system plays a role, through a conventional PRA.

The design basis for the DRACS in the Mk1 PB-FHR considers performance during challenging transient scenarios. In this sense, one severe event has been determined to be protected LOFC, where forced primary cooling stops and the reactor is shut down automatically,

associated with the normal shutdown cooling system not functioning, which leaves coupled natural circulation in the primary loop and the DRACS loops as the sole cooling mechanism [31]. This is the transient scenario under consideration for this study.

3.1.2 Identification of the System

The purpose of the study is to gather quantitative information on reliability of the passive safety system during postulated transient scenarios and to identify the conditions for potential failures of the functions of this system. In this context, the mission of the system must be defined, and failure modes and failure criteria must be listed.

Mission of the System

The mission of the passive system is the goal for which it has been designed. One of the key safety design criteria for FHRs is control of heat removal and addition [31]. The DRACS plays a key role by providing means of control of decay heat removal in case of failure of normal shutdown cooling. For the transient scenario under consideration here, the mission of the DRACS is to prevent any structural damage if the normal shutdown cooling system does not function (investment protection function) and to prevent damage to fuel and release of radionuclides (safety function). However, because the fuel failure temperature (~1,600°C) is higher than the boiling point of flibe (1,430°C), damage to fuel is impossible if the fuel remains covered by the coolant. Therefore, the main safety function of the DRACS is to maintain integrity of the primary coolant boundary such that primary salt inventory is maintained.

The nominal, combined heat load capacity of the DRACS was selected to be 2% of the nominal reactor power as a preliminary surrogate for a final design capacity number that will be selected in detailed design. However, the actual functional requirement for the DRACS is to limit peak bulk coolant outlet temperatures reached during severe transients, based on the Mk1 PB-FHR decay heat curve shown in Figure 3-2 [45].

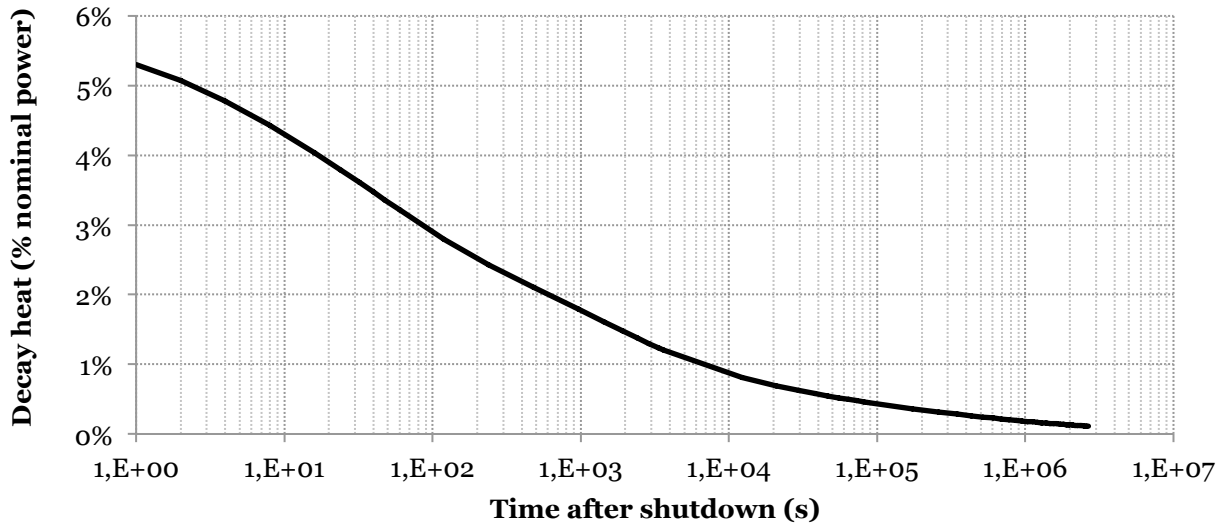

Figure 3-2. Mk1 PB-FHR decay heat curve [45].

Success/Failure Criteria

Failure criteria are obtained by comparing key FOMs characterizing the performance of the system with expected values of these FOMs. In some cases, a global failure criterion for the whole system is more appropriate than a specific criterion for the passive system. For instance, the failure criterion can be based on the peak primary loop structure temperature during a specified period.

A number of safety concerns arise due to a failed control of heat removal in FHRs. The fuel and graphite core structures have significant margins to thermal damage, and therefore cannot be easily damaged. Instead, overheating of the primary system would begin by causing accelerated thermal creep and mechanical failure of the metallic materials with the lowest thermal limits, compromising the physical functions of these components [15]. Accelerated creep, fracture, deformation, rupture and melting are all potential mechanical failure modes if temperatures or thermal gradients exceed specific thresholds.

Among metallic structural materials under current consideration for the design of the PB-FHR, 316 stainless steel is a key candidate alloy, along with Alloy N. 316 stainless steel is an attractive candidate material for use in FHRs due to the extensive experience for nuclear applications, its good tolerance for neutron irradiation and the well developed American Society of Mechanical Engineers (ASME) Boiler and Pressure Vessel (B&PV) Code, Section III case for high temperature use [46]. 316 stainless steel is allowed for use at temperatures up to 816°C in Subsection NH and Code Case N-201-5, which comprise extensions to Subsections NB and NG, respectively [47]. These parts of the ASME B&PV Code cover type 316H stainless steel in terms of high-temperature strength, creep, and creep-fatigue effects up to a design life of 300,000 hours (~35 years). As mentioned in Section 1.3.1, the main FOM related to structural integrity of metallic structural components is the peak bulk coolant outlet temperature. Therefore, for the purpose of this study, failure of the system is assumed to occur if the peak coolant temperature exceeds 816°C during evolution of the transient of interest. Detailed stress calculations have not yet been performed to support this value at this feasibility study level and will need to be performed at a next stage of the analysis. Future mechanistic analyses could show that the 816°C limit may have to be corrected if only considering peak temperatures rather than time at temperature, or if other structural materials such as Alloy N are used in the design of the reactor.

3.1.3 Modeling of the System

Because no FHR has been built to-date, there are no existing experimental databases to assess the reliability of the DRACS for passive decay heat removal from the reactor core. This is an inherent challenge for all advanced reactor designs for which such a study would be performed. Therefore, initial evaluation of system reliability, which provides a basis for licensing, must rely on numerical modeling, using qualified thermal hydraulic best-estimate codes. Calculations must first be carried out on a reference case, using nominal values for all key parameters that define the state of the system. Whenever possible, best-estimate codes and models must be validated with experimental data if any exist. After a first reactor is built, startup testing will be required prior to operation, and ongoing testing as defined in Technical

Specifications (e.g., online monitoring, functional tests and in-service inspection) will be mandated during operation, which will provide additional validation data. Eventually, for multi-unit small modular reactor stations like the Mk1 PB-FHR, an approach will need to be developed to collect validation data from many similar units.

In Chapter 2, the methodology to develop IETs for characteristic FHR thermal hydraulic phenomena was introduced, and the example of successful validation of steady-state and simple transient RELAP5-3D models for both forced cooling and natural circulation in the CIET facility are encouraging for the use of this best-estimate code to evaluate safety, and in particular assess reliability of the DRACS, in full-scale FHR systems. While transient data from CIET simulating the reference LOFC scenario is not available at the time of this study, the methodology introduced here serves as a framework and can be refined for future studies, once more experimental data is available for code and model validation.

Preliminary modeling of the complete Mk1 PB-FHR primary loop and DRACS loop has been performed in RELAP5-3D. Figure 2-2 shows the high level model of the Mk1 PB-FHR system and Figure 3-3 shows the corresponding simplified nodalization diagram in RELAP5-3D, based on an equivalent model of the reactor. In this equivalent model, the two CTAH loops, which transfer heat from the primary loop of the reactor to air in the nuclear air-Brayton combined cycle (NACC), are combined into one equivalent loop. Similarly, two of the three DRACS loops of the Mk1 design are reduced to one loop with equivalent heat removal capacity to that of the two loops combined. This strategy could eventually support the redundant safety design of the Mk1 PB-FHR, where two out of three DRACS loops must be sufficient to extract decay heat from the reactor. For this proof-of-concept analysis, the reactor core is modeled as an equivalent one-dimensional component along the axial direction, and radial flow and bypass flows are not modeled, although they will have an impact on integral behavior of the system and will need to be taken into account as part of future studies. Appendix B provides details about modeling of the Mk1 core in RELAP5-3D. The TCHX is modeled as an open loop rather than a closed loop with recondensing of water in a chimney in the real system. The only heat structures modeled for this analysis are the pebble bed core and the three heat exchangers – CTAH, DHX and TCHX. This simplification of the Mk1 PB-FHR thermal hydraulic systems into an equivalent model is the first step in analyzing transient response of this class of reactors. Detailed parameters for the Mk1 equivalent model, and a RELAP5-3D input deck for the transient scenario studied here, are provided in Appendix B. It is worth noting that failures of individual CTAH or DRACS loops cannot be studied using the equivalent model. For example, during an LOFC transient, both main salt pumps, combined into a single pump, will coast down at the same time in the model. Future analyses will use refined models that take all individual systems into account, including heat structures related to structural materials. A key task will then be to quantify distortions when using simplified rather than detailed models, and implications on overall safety assessment.

Before running transient calculations of the model based on the transient scenario of interest, a steady-state calculation is performed to adjust the characteristic parameters identified in the study to their target values. The following assumptions are taken into account for the reference calculation:

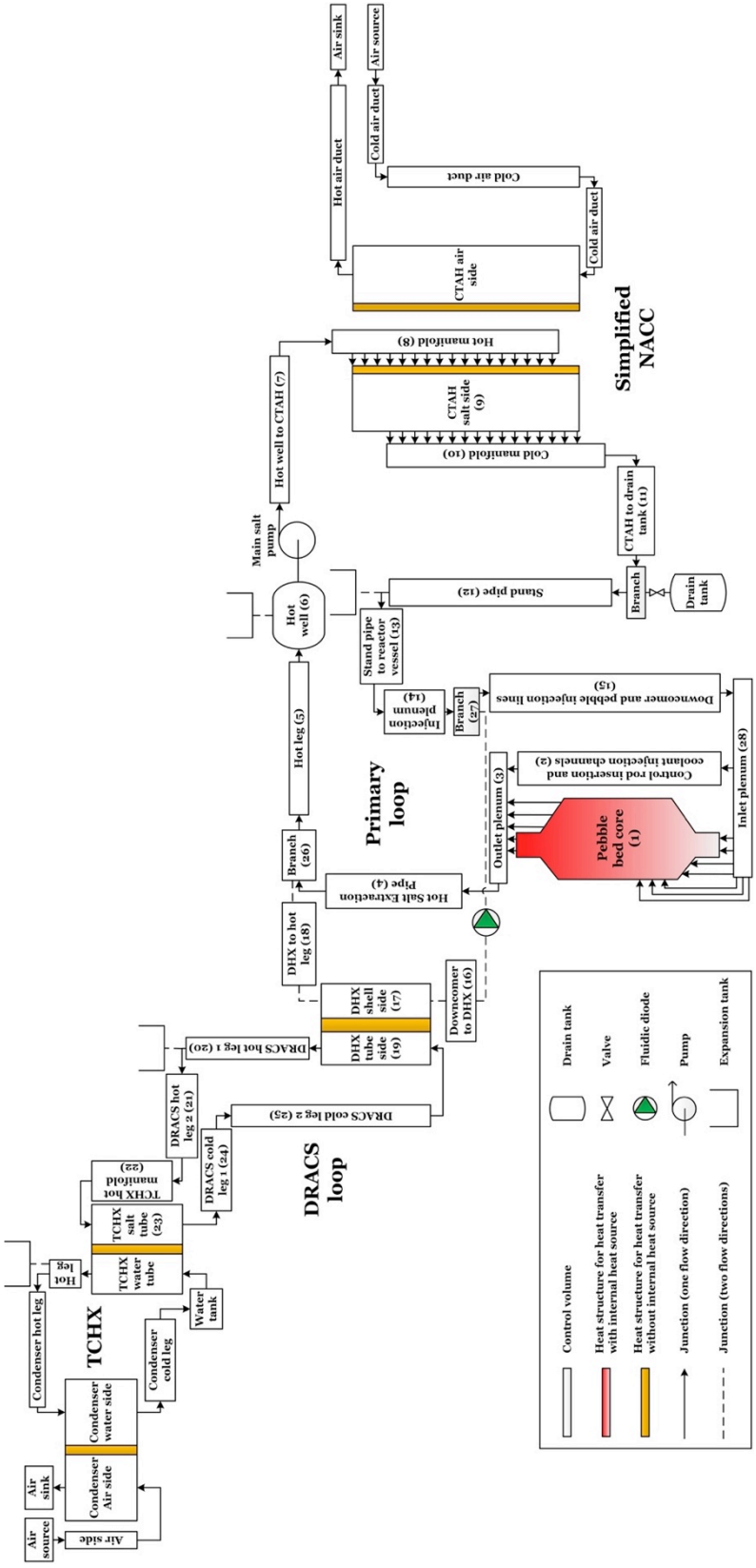

Figure 3-3. Simplified nodalization of the Mk1 RELAP5-3D equivalent model.

- Steady-state initiation with core power at 100% nominal power (236 MWth) and axial power distribution based on neutronic models of the Mk1 PB-FHR core [45];
- At steady-state, primary pumps forcing a total coolant mass flow rate of 1,033 kg/s through the core, resulting in inlet and outlet coolant temperatures of 600°C and 700°C, respectively;
- Total bypass channels area – simulating control rod insertion channels, bypass flow paths, etc. – adjusted such that 25% of total flow in the primary loop bypasses the core during normal operation;
- Form losses in the upward flow direction in the DHX branch adjusted such that 1% of the total thermal power generated in the core is lost as parasitic heat losses through the DRACS during normal operation. This preliminary value, which may be refined in future analyses, provides enough heat to the DRACS loop to prevent overcooling of the salt there when the reactor operates normally, while limiting the amount of heat that does not get transferred to the NACC to produce power from the reactor.

The following assumptions are used once the transient scenario starts:

- The transient is initiated by a primary pump trip. A specific pump is not modeled at this point, and instead, a coast down time of 4.5 s, corresponding to the amount of time it takes for the forced flow in the primary loop to be reduced by 50%, is simulated using a time-dependent junction in RELAP5-3D, where forced flow rates follow the desired trend. This also simulates failure of the normal shutdown cooling system – which would rely on reduced-speed operation of the primary pumps – to start;
- Simultaneously, a scram of the reactor is simulated, with thermal power generation in the core following the Mk1 PB-FHR decay heat curve shown in Figure 3-2.

Starting from normal, steady-state operation, the transient is initiated after 100 s in the RELAP5-3D model, and resulting coolant mass flow rates and temperatures over time are shown in Figure 3-4 and Figure 3-5, respectively, for the main sub-systems of the reactor.

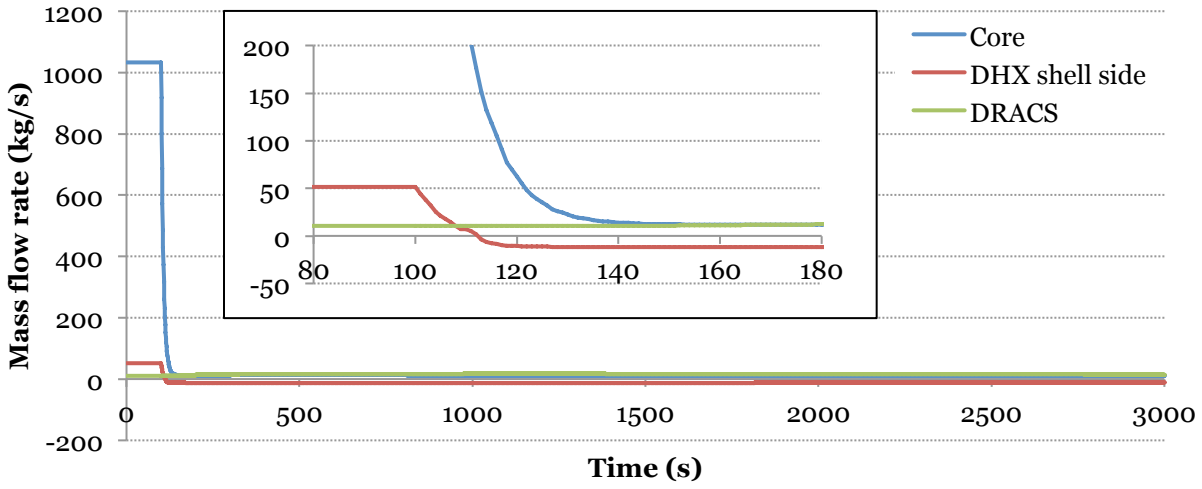

Figure 3-4. Coolant mass flow rates in the main Mk1 PB-FHR sub-systems following a protected LOFC transient.

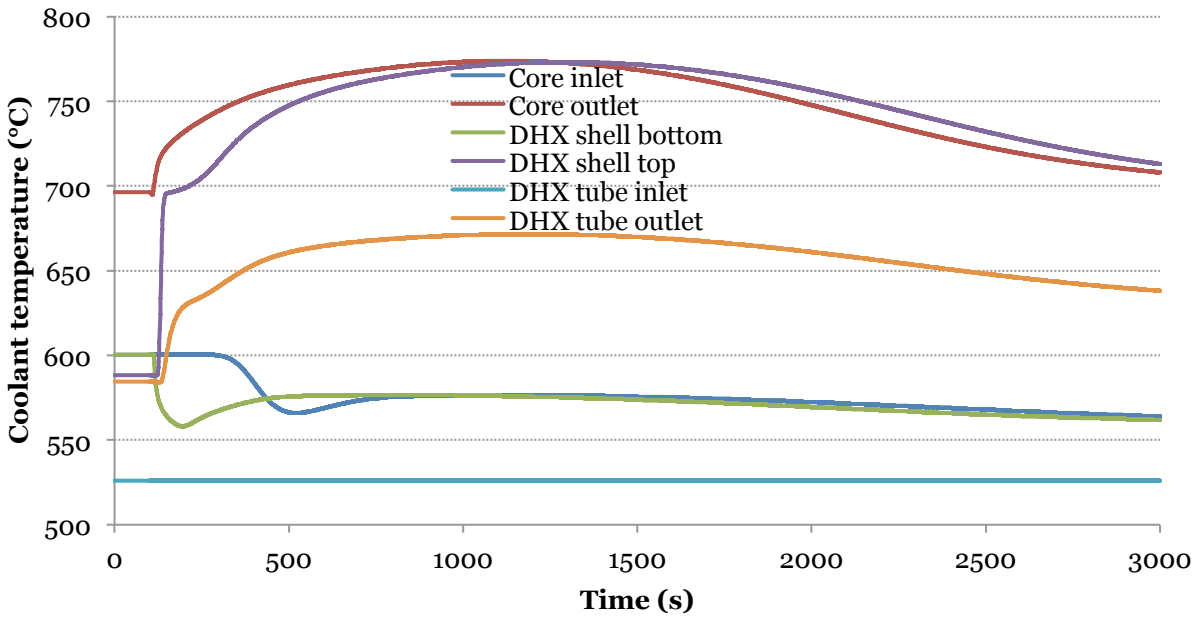

Figure 3-5. Coolant temperatures in the main Mk1 PB-FHR sub-systems following a protected LOFC transient.

Once the transient is initiated, Figure 3-4 shows that coolant mass flow rate in the core decreases quickly as a result of the primary pump trip. Flow reversal occurs in the primary (shell) side of the DHX as natural circulation is initiated between the core and the DHX and the coolant starts flowing downwards through the DHX while it was flowing upwards during normal operation. The coolant mass flow rate slowly increases in the DRACS as natural circulation there provides the only mean to reject decay heat from the reactor, while during normal operation, the DRACS was only rejecting parasitic heat. The coolant mass flow rate in the DRACS then starts to decrease as decay heat slowly decreases.

Figure 3-5 shows that the peak bulk coolant outlet temperature in this reference case is 774°C, reached 985 s into the transient, which provides a margin of 42°C below the failure criterion listed in Section 3.1.2. Prior to initiation of the transient, the temperature at the bottom of the shell side of the DHX is above the temperature at the top, due to the minimal amount of flow that runs parallel to the core and transfers heat to the DRACS. Once the transient is initiated, as flow reversal occurs, the temperature at the top of the DHX reaches a maximum of 774°C 177 s after this peak occurs at the core outlet, which is consistent with the fluid residence time between the core outlet and the DHX inlet, and the fact that no heat structures are modeled between these two points, which would reduce the peak temperature of the fluid reaching the DHX. Finally, as the transient occurs, the DHX switches from a parallel flow to a counter flow heat exchanger configuration, and temperatures on the shell side become higher than during steady state operation. As a result, the temperature at the outlet of the tube side of the DHX quickly rises, then starts to drop as natural circulation is established in the DRACS loop.

The results from this reference case provide a starting point for future studies to optimize the Mk1 DRACS design based upon more detailed analysis of the effects of peak coolant

temperatures on coolant boundary and other structures. Performance of the DRACS depends on the configuration of the system as the transient occurs, and in particular, on the values of some parameters assumed in the best-estimate model. In the following Sections, some sources of uncertainty in the results of the model, and therefore in the actual performance of the DRACS, are listed as examples, and their impacts on reliability of the passive system are assessed.

3.1.4 Identification of the Sources of Uncertainty

A number of parameters can be identified as potentially important contributors to uncertainty of the code results. Among such parameters, Marquès et al. [42] list:

- Model uncertainties due to approximations in modeling physical processes (e.g. through the use of uncertain empirical correlations);
- Approximations in modeling the system geometry (e.g. through finite discretization of continuous regions, and uncertainty in the actual as-built geometry due to finite tolerances for fabrication of components);
- Uncertainties in input variables (e.g. initial and boundary conditions such as plant temperatures and reactor power, physical properties such as densities, thermal conductivities and specific heats, and thermal hydraulic parameters such as heat transfer coefficients and friction factors).

Some parameters are likely to be more or less uncertain at the time of the DRACS passive system startup and significantly influencing the performance of this system. A preliminary assessment of this set of parameters, their variation range, and the importance of their influence on the global behavior of the system strongly relies on expert judgment. Typically, this kind of assessment is associated with a PIRT exercise, which goes beyond the scope of this study when it comes to the incomplete design of a very important sub-system of a novel reactor design, like the DRACS system for the PB-FHR. However, several characteristic parameters that have been identified for this study are listed below. After a first prototypical reactor is built, startup testing data, if properly measured, can be used to reduce certain types of uncertainty:

- *PUI*: percentage of nominal power actually generated in the core during normal operation. For a given DRACS geometry, as this value increases, because the system is not optimized to extract higher amounts of thermal power, the peak bulk coolant outlet temperature is expected to be higher.
- *CDT*: coast down time for the primary pumps. This parameter affects the time to establishment of natural circulation in the loop between the core and the DHX. Uncertainties may result from uncertainties in measurement of the moment of inertia of the pumps.
- *DHS*: heat transfer surface area between the shell side and the tube side of the DHX. This parameter – a proxy for overall heat transfer coefficient in the heat exchanger, easier to vary in the RELAP5-3D model – had to be adjusted through the calibration process of the CIET model in RELAP5-3D, and similarly, the heat transfer coefficient in a prototypical DHX will need to be carefully evaluated and uncertainties in this evaluation may lead to significant uncertainties in code results.

- *FLD*: total form losses in the DRACS loop. This parameter directly affects counter-forces to natural circulation in the DRACS and, if underestimated, leads to an overestimate of the coolant mass flow rate in the DRACS loop and an underestimate of the peak bulk coolant outlet temperature.
- *FLP*: total form losses in the DHX branch. This parameter has similar effects as form losses in the DRACS loop for natural circulation. Uncertainties in its value could result, for instance, from uncertainties in the friction factor through the fluidic diode or check valve at the bottom of the shell side of the DHX.

3.1.5 Identification of Relevant Parameters

Once sources of uncertainty have been identified, assessment of the reliability of a passive safety system requires identification of the most relevant parameters, which have dominant effects on the system goal. In this effort, phenomena identification and ranking can be helpful. However, absent a well-developed PIRT for a system in its early design stage such as the Mk1 PB-FHR, the use of sensitivity studies based on best-estimate models can provide valuable information to identify the relevant parameters. This is the object of the following steps of the RMPS methodology.

3.1.6 Quantification of Uncertainties

One of the most important challenges in applying the RMPS methodology is to adequately select distributions for each of the relevant input parameters, based on epistemic uncertainties. These distributions, propagated through best-estimate models, must be carefully chosen as they strongly affect the estimated reliability of the passive system. Most of the time, as little data is available to characterize the parameters of interest, expert judgment must be called upon to associate probability distributions that best fit the data for each parameter. Alternatively, if only the first statistical moments of the distributions of parameters are known through experimental data rather than entire probability distributions, advanced response surface methods, detailed in Section 3.2, can also be used to propagate parameter uncertainties to system performance reliability assessment. Finally, in the case where no preferred distribution can be justified, Marquès et al. suggest to use a uniform distribution where each value between minimum and maximum is equally likely [42].

Within the scope of this study, only preliminary reliability and sensitivity analyses of the DRACS system can be carried out, by considering broad ranges of variation for the characteristic parameters mentioned in Section 3.1.4. These ranges are supposed to represent the whole set of initial and boundary conditions to which the system could be subjected. The idea behind these first evaluations is to make a single reliability analysis of the system and in this way, limit the number of uncertainty calculations. The drawbacks of this unique evaluation are that the obtained results can be overly conservative and not realistic, and that this method does not allow testing of the influence of the passive system on different transient scenarios. However, absent extensive expert judgment regarding the DRACS system within the PB-FHR phenomenology at this point, this preliminary methodology still provides valuable information as to the sensitivity of the system response and its reliability depending on the characteristic parameters that are being varied.

A preliminary choice for the ranges of variation and probability density functions of the characteristic parameters identified in Section 3.1.4 is given in Table 3-1, based on reasonable assumptions. The list provided here would merit further investigation when the design of the reactor is more mature, the components used in the system are better known, and expert judgment is called upon for a PIRT-type exercise. Most importantly, the requirements of the methodology developed here indicate that throughout the design process, assumptions such as those already used in the best-estimate models built for this study must be made and clearly documented. As more information is obtained about the design (e.g. through IET data, startup testing, in-service inspection, etc.), these assumptions can be validated, or the assessment must be modified, based upon the new information.

Here, for illustration purposes mainly, truncated normal distributions are chosen by default so that all parameters lie within a reasonable range. The highest probability value for each parameter is its design basis nominal value, based on the Mk1 PB-FHR design.

Table 3-1. Probabilistic model of the characteristic parameters in the global reliability analysis.

Variable (unit)	Distribution	Nominal value	Standard deviation	ω_{min}	ω_{max}
PUI (%)	Truncated normal	100.0	1.0	98.0	102.0
CDT (s)	Truncated normal	4.5	1.0	3.0	6.0
DHS (m^2)	Truncated normal	196.0	15.0	162.0	230.0
FLD	Truncated normal	50.0	10.0	35.0	90.0
FLP	Truncated normal	100.0	10.0	80.0	140.0

3.1.7 Sensitivity Analysis

One important outcome of the RMPS methodology is to evaluate uncertainties in performance of the passive system, and in particular, sensitivity to input parameter uncertainties. Sensitivity analysis provides a ranking of input parameters in this respect. In particular, results of the sensitivity analysis inform future studies to reduce state-of-knowledge uncertainties (through further design, experimental tests, etc.) and increase confidence in reliability of the passive system.

At first, when little is known about the passive system being considered and limited data on system performance, either from operational experience or best-estimate models, is available, the sensitivity analysis may be performed in a qualitative way. Similar to a PIRT exercise, in a qualitative sensitivity analysis, phenomena and parameters are ranked in terms of the level of uncertainties associated with them, and sensitivity of the overall performance of the passive system to these phenomena and parameters. In this respect, the higher the ranking, the more important it is to properly characterize a given phenomenon or parameter to evaluate overall reliability of the passive system.

Additionally, quantitative sensitivity analyses can be performed using best-estimate models of the passive system under consideration. Various quantitative measures of sensitivity can be obtained depending on the methodology used. One simple method is developed in this Section, and a more advanced method based on Sobol indices derived from a response surface is detailed in Section 3.2.

To assess the sensitivity of the performance of the passive system to each of the characteristic parameters listed in Section 3.1.4, the first method proposed here is to calculate the range of peak bulk coolant outlet temperatures reached when each single parameter varies from its minimum value to its maximum value, while all other parameters are set at their reference values as listed in Table 3-1. Each parameter is therefore associated with a range of peak bulk coolant outlet temperatures, and these temperature ranges are then weighted by the percent variation of their associated parameters and normalized, so that eventually, each characteristic parameter i is associated with its normalized sensitivity index calculated as follows:

$$Sensitivity\ index_i = (T_{max} - T_{min})_i \cdot \left(\frac{\omega_{nominal}}{\omega_{max} - \omega_{min}}\right)_i \quad (3\text{-}1)$$

$$Normalized\ sensitivity\ index_i = \frac{Sensitivity\ index_i}{\sum_i Sensitivity\ index_i} \quad (3\text{-}2)$$

Table 3-2 shows, for each characteristic parameter, its minimum and maximum values (from Table 3-1) and the associated peak bulk coolant outlet temperature ranges while other parameters are set at their reference values, calculated with RELAP5-3D. Figure 3-6 shows the resulting normalized sensitivity indices for the chosen characteristic parameters.

Table 3-2. Peak bulk coolant outlet temperature ranges when characteristic parameters vary.

Variable (unit)	ω_{min}	ω_{max}	T_{min} (°C)	T_{max} (°C)
PUI (%)	98.0	102.0	770.8	776.7
CDT (s)	3.0	6.0	765.8	782.7
DHS (m²)	162.0	230.0	772.8	775.1
FLD	35.0	90.0	773.3	779.0
FLP	80.0	140.0	768.4	812.5

As can be seen on Figure 3-6, the most important parameters, from the preliminary set identified at this point, are the thermal power of the core (as a fraction of the 236 MWth nominal power), the total form losses in the DHX branch and the pump coast down time.

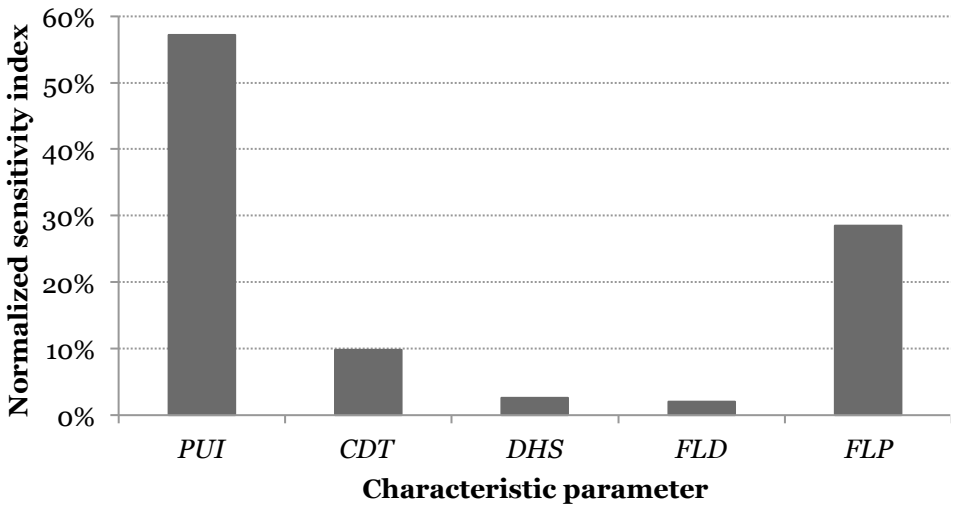

Figure 3-6. Normalized sensitivity indices for performance of the Mk1 DRACS.

3.1.8 Reliability Evaluation

The most important goal of the methodology is to provide a quantitative evaluation of the reliability of the passive system of interest. The performance function of the passive system for a specified mission is given by [42]:

$$f(\omega_1, \dots, \omega_N) = performance\ criterion - limit \tag{3-3}$$

where the ω_j $(j = 1, \dots, N)$ are the N characteristic parameters and $f(\cdot)$ is the functional relationship between the characteristic parameters and the performance of the system. This function can be defined so that the failure surface is given by $f(\omega_1, \dots, \omega_N) = 0$. In this case, failure is defined as the space where $f(\omega_1, \dots, \omega_N) > 0$, and success is defined as the space where $f(\omega_1, \dots, \omega_N) \leq 0$. Therefore, the probability of failure is evaluated by the following integral:

$$P_f = \int \dots \int f_\omega(\omega_1, \dots, \omega_N) d\omega_1 \dots d\omega_N \tag{3-4}$$

where f_ω is the joint density function of $\omega_1, \dots, \omega_N$, and the integration is performed over the region where $f(\omega_1, \dots, \omega_N) > 0$.

For the Mk1 PB-FHR, the performance function of the DRACS is given by:

$$f(\omega_1, \dots, \omega_5) = peak\ bulk\ coolant\ outlet\ temperature - 816°C \tag{3-5}$$

Because the characteristic parameters listed in Section 3.1.4 are independent variables, the expression for the probability of failure given in Eq. (3-4) can be expressed as:

$$P_f = \int f_\omega(\omega_1) d\omega_1 \times \dots \times \int f_\omega(\omega_{10}) d\omega_{10} \tag{3-6}$$

Direct Monte Carlo simulation techniques can be used to estimate the probability of failure given in Eq. (3-6). However, due to the variability of the characteristic parameters and the necessity to run best-estimate codes (RELAP5-3D here) to calculate the value of the

performance function of the DRACS in each configuration of the system used in Monte Carlo simulations, calculating P_f may require a large amount of computation time to obtain an accurate result. Instead, Jafari et al. have developed a simplified method detailed here, which can be complemented by response surface approximation methods developed in Section 3.2.

First, the continuous range of values for each of the characteristic parameters is discretized into 4 point values, and the associated probability density functions are also broken into 4 probability values that sum up to 1. The result of this discretization is shown in Table 3-3, where probability values for each status of the characteristic parameters are reported in italics. Although this process introduces arbitrariness through the selection of discrete values for each parameter, it greatly reduces the amount of computation time needed to get at least a good estimate of the performance of the system.

Table 3-3. Discretized probabilistic model of the characteristic parameters in the global reliability analysis.

Variable (unit)	Nominal value	Range	Discrete values and associated probabilities			
PUI (%)	100.0	98.0-102.0	98.0 *0.07*	100.0 *0.53*	101.0 *0.33*	102.0 *0.07*
CDT (s)	4.5	3.0-6.0	3.0 *0.13*	4.0 *0.35*	4.5 *0.39*	6.0 *0.13*
DHS (m^2)	196.0	162.0-230.0	162.0 *0.05*	178.0 *0.29*	196.0 *0.61*	230.0 *0.05*
FLD	50.0	35.0-90.0	35.0 *0.22*	50.0 *0.68*	70.0 *0.09*	90.0 *0.01*
FLP	100.0	80.0-140.0	80.0 *0.10*	100.0 *0.78*	120.0 *0.11*	140.0 *0.01*

It should be noted that the combination of all discrete parameter values in Table 3-3 yields more than 1,000 ($4^5 = 1{,}024$) possible scenarios for the DRACS system, which would still require a considerable amount of computation time to model. Therefore, a meaningful selection of system scenarios is necessary. For the statistic selection, Jafari points out that the analyst should select a "reasonable" number of parameter sets, which are representative of the general, physical behaviors of the passive system [41]. This is achieved by a random selection through the 4^5 possible scenarios, performed by a proper computational tool (a Matlab code adopting a Monte Carlo procedure is chosen for this study). 100 sets of parameters are selected through this process. The 100 statistically selected sets ensure a "high confidence level," typically greater than 95%, from the application of the Wilks formula [41]. The selected parameters are then used in the RELAP5-3D model of the system, and the performance of the system is assessed for each of the 100 scenarios.

From the 100 scenarios randomly tested, only 1 scenario (combining high initial thermal power in the core, large form losses in the DHX branch and high primary pump coast down time) fails to fulfill the performance criterion and has a peak bulk coolant outlet temperature of

820°C during transient evolution, which exceeds the safety criterion of 816°C. Therefore, we can conclude that the DRACS system, with the preliminary ranges of parameters selected for this study through basic engineering judgment, has a reliability of about 99% with a confidence level greater than 95%.

3.1.9 Integration of Passive System Reliability in PRA

The final step in assessing the reliability of a passive safety system is to implement its estimated reliability in a PRA model for the plant. Most existing PRA studies for advanced reactors do not take into account the risk of failure of the physical phenomena on which passive systems rely, such as natural circulation. Only recently has the international community started to recognize the importance of this effort and suggested unified methods to address this challenge [44]. In the RMPS methodology, an event tree representation of the transient sequences is chosen [42]. The consequences of various sequences in Level 1 PRA are defined as degrees of reactor core damage, including "safe" state and "severe accident" state. These consequences are generally evaluated through conservative thermal hydraulic calculations. Events corresponding to the failure of a passive safety system to fulfill its mission are added to the event tree and results from system reliability evaluation are used as the corresponding failure probability.

The simplified PRA carried out in this study consists in analyzing an accident, defined as an initiating event – LOFC when the reactor is running at full power – and the associated transient management for which, in the case where normal shutdown cooling does not function, decay heat removal relies on the DRACS passive safety system. The accident sequences are defined using an event tree, taking into account the success or failure of the components and physical processes involved in the DRACS. Knowing the occurrence frequency of each accident sequence and considering that all the events are independent, estimation of the probability of structural damage to the primary coolant boundary – which occurs before core damage and can compromise the capability of the reactor safety systems to remove decay heat in FHRs – can be carried out by summing up the probabilities of each sequence leading to structural damage to the primary coolant boundary. At this point, one very important note is that, due to many uncertainties in the detailed design of the Mk1 PB-FHR, most event and component failure probabilities are unknown, and some of them could be the object of future studies similar to this one (e.g., system response to an ATWS). The main objective of this study is to show the applicability of the RMPS methodology to the DRACS system, and the event tree in Figure 3-7 is only a simplified version of what the actual event tree for the LOFC transient should eventually be.

The LOFC transient involves shutdown of both main salt pumps, and the inability to activate the normal shutdown cooling system. If coolant flow is lost in one pump, the second pump will be stopped to avoid back-flow. Since the Mk1 uses a primary pump operating at low speed to circulate primary coolant to a CTAH for normal shutdown cooling, if one primary pump fails, the ability to establish normal shutdown cooling depends upon the ability of the other pump and other equipment needed for shutdown cooling (e.g., an air-blower to circulate air through the CTAH) to function. The frequency of a running motor-driven pump failing to keep running is

estimated at $4.54 \cdot 10^{-6}$/reactor-hr or $\sim 4 \cdot 10^{-2}$/reactor-yr [48]. For two independent running pumps failing to run at the same time, this frequency falls to $1.6 \cdot 10^{-3}$/reactor-yr. Therefore, the probability of occurrence of this initiating event is estimated to be $1.6 \cdot 10^{-3}$ per reactor-year. The scram that should follow an LOFC, either by active or passive means, has a probability of success P_S that is not estimated in this study. The probability of the normal shutdown cooling system functioning after the reactor has been scrammed – P_{NS} in the event tree in Figure 3-7 – is another unknown whose evaluation goes beyond the scope of this study. Finally, in a more complete event tree, one should consider the possibility that only a fraction of the DRACS loops operate, due to some TCHX water feed valves or condenser air dampers not functioning properly. In the interest of computation time, all DRACS loops were combined into a single loop in the RELAP5-3D equivalent model of the system, and therefore, both automatic activation and operator action to open the dampers are not considered here. Figure 3-7 shows the subsequent simplified event tree.

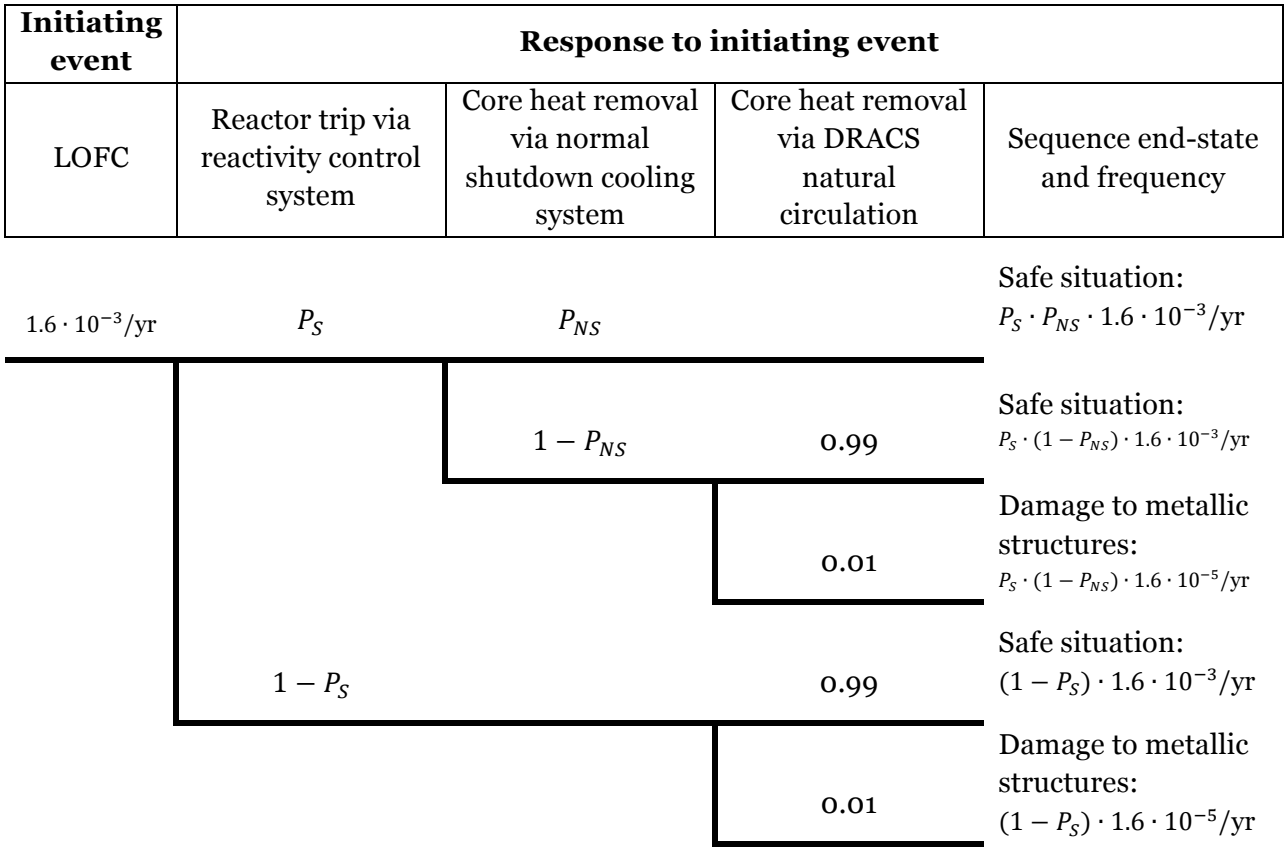

Figure 3-7. Preliminary event tree of LOFC on a Mk1 PB-FHR.

Several limitations, which should be eliminated in subsequent, more detailed PRAs, are:

- The analysis only concerns a single initiating event, LOFC. Even if this transient is the reference transient used for the design basis of the safety systems dedicated to residual heat removal, other initiating events have to be analyzed [31];

- No aggravating event is considered, relative to the initiating event of LOFC with failure of normal shutdown cooling, apart from the DRACS thermal hydraulic process failures;
- Human factors are not explicitly taken into account. However, the periodic maintenance and inspection of passive systems introduces particular constraints. Unlike an active system that can be more easily isolated or inspected during shutdown periods, a passive system requires to be tested under its real physical conditions of utilization, and this may generate implementation and safety problems. Conversely, due to their great complexity, active systems may be more susceptible to failures caused by human errors, such as mispositioning of valves or electrical breakers. Online monitoring of temperatures and other state parameters in a passive system may allow certain types of degradation, such as flow blockage, to be detected, increasing the system reliability. Likewise, periodic functional testing may increase reliability. The question of whether it is an advantage or a disadvantage that passive systems may not allow operator intervention during operation as readily as active systems should also be investigated. Likewise, operator intervention to restore the function of the normal shutdown cooling system may affect the predicted overall system reliability;
- No common cause failure between the actual three DRACS loops has been considered, and redundancy brought by this number of loops has disappeared through the modeling of a single combined DRACS loop in the RELAP5-3D equivalent model. This was done to save computation time while providing conservative results as to the performance of the passive system. However, further best-estimate code studies should include a more detailed analysis of the interaction between the loops and the capacity of the system not to fail if one or two of the three loops are unavailable or have degraded performance for decay heat removal.

Reactor damage frequency after an LOFC event can hardly be estimated based on this preliminary study. Indeed, many uncertainties remain as to the performance of other components and sub-systems in the reactor, which would require separate studies. Eventually, the frequency of primary coolant boundary structural damage should correspond to the sum of the probabilities of each accident sequence leading to primary coolant boundary structural damage for the LOFC transient with the assumption that all the events are independent. At this point, however, the results provide us with valuable information as to the performance of the DRACS system in order to fill in such an event tree when more information about the design and component options becomes available. Besides, it should be noted that this analysis shows that the passive operation of the DRACS allows for a significant reduction of the risks of reactor component damage initiated by a LOFC. Section 3.2 develops the response surface methodology (RSM) used to derive more statistically meaningful results from this study, and as a result of these analyses, Section 3.3 focuses on design optimization and risk mitigation methods that would allow for the DRACS system to be more reliable and further contribute to safety of the FHR.

3.2 The Role of Response Surfaces in Reliability Assessment of Passive Systems

Although simple, straightforward methods to perform safety analysis and reliability evaluation of passive systems were introduced in Section 3.1, these methods may not be physically meaningful for complex, heterogeneous distributions of input parameters to the system behavior, especially when little data is known about these parameters and significant approximations are introduced. Moreover, the approach developed in Section 3.1 does not address the issue of potential interactions between input factors that may affect overall system performance. In this context, response surfaces can be developed to assess response of the passive system – e.g. peak bulk coolant outlet temperature – to uncertain distributions of input parameters and derive more statistically meaningful sensitivity indices and reliability results. One important, additional benefit from this approach is to provide meaningful system response metrics in a relative rather than an absolute sense, by comparing variations in the performance function of the passive system when examining modifications from the baseline design, and detecting cliff edge regions where system response presents sharp evolutions (e.g. peak bulk coolant outlet temperature grows rapidly and exceeds a certain threshold) for relatively small changes of input parameters (e.g. heat transfer coefficients).

The new, mathematically and physically consistent tools presented in this study involve the use of RSM, more specifically arbitrary polynomial chaos (aPC) expansion [49-51], whose practical applications are so far limited to the aerospace engineering [52] and petroleum engineering [53] fields. In statistics, RSM explores the relationship between several controlled variables (input parameters for physical models) and one or more response variables [54]. In the context of passive system reliability assessment, we are interested in the relationship between uncertain input parameters (e.g. heat transfer coefficients, pump coast down time) and system response (e.g. peak bulk coolant outlet temperature). By building a simplified representation of the relationship between given input parameters and system response while conserving key characteristics of this relationship, one can easily explore the space of multiple input parameter values to identify system failure regions, detect cliff edge regions and perform sensitivity analysis.

3.2.1 Technical Challenges in System Response Characterization

As exemplified in Section 3.1.4, a number of highly heterogeneous factors can be taken into account when evaluating the performance function for a given passive safety system and a specific mission. One critical task is to identify how many and what input parameters must be considered in such analyses, and based on expert judgment and PIRT exercises, the actual list of relevant parameters can be expected to be significantly longer than that proposed in this preliminary study.

Once a list of all relevant input parameters has been established, the large number of these parameters – potentially several hundreds – can itself be a significant challenge, with computation time for traditional system response quantification methods using best-estimate codes that may exceed acceptable limits if appropriate screening methods are not applied. While

at least some cliff edge effects may be caused by combinations of parameters, exploring all such combinations to detect critical regions for passive system performance might then be impractical if surrogate models are not used.

Another challenge arises from heterogeneity of input parameters in best-estimate models (e.g. heat transfer coefficient vs. pump coast down time). Heterogeneity factors involve the nature of the input parameters and the magnitude of uncertainties among them.

These classes of challenges call for the use of RSM, which is capable of handling a large number of uncertain parameters in a mathematically and physically consistent manner, therefore complementing traditional or overly simplified reliability assessment methods.

3.2.2 Objective and Proposed Method

As mentioned in Section 3.1.8, the most straightforward and widely used option to propagate uncertainties from all model input parameters to the performance function of interest is to use Monte Carlo sampling methods to select sets of representative values for each input parameter, taking each parameter's probability distribution into account. A potential issue with this approach is that for models with a large number of input variables, such as typical best-estimate models for a complex passive system, finding a converging response using Monte Carlo sampling can become computationally intensive, unless a surrogate response function can be found. The alternative method, suggested by Jafari et al. [41], to use a reduced subset of randomly selected input parameters and to characterize system performance for these parameter sets, may not be physically meaningful for highly heterogeneous parameters and only provides discrete evaluations of the performance function for which failure probability distributions may not be statistically representative. Therefore, our objective is to build simplified but accurate representations of best-estimate models, using generic functions, to gain insight on overall system performance and to identify cliff edge regions in the context of a large number of uncertain input parameters.

This can be done through RSM, by building a surrogate (usually polynomial) response function. The polynomial functions can be constructed to provide an optimal representation of the best-estimate model up to a pre-established, mathematically defined level of approximation. The polynomial response surface is "fitted" to the actual response function (i.e. the original best-estimate model solutions) calculated at a finite number of points (called collocation points). Once the surrogate response function has been built, useful information about system response to input parameters is readily derived. Most importantly, the simplicity of the polynomial representation compared to typical best-estimate models greatly facilitates the exploration of parameter changes or combinations of parameter changes leading to sharp gradients in the performance function (cliff edges).

3.2.3 Application of RSM to Passive System Reliability Assessment

While RSM has been considered in the past for component-level risk analysis of nuclear power plants (e.g. [55-57]), here we demonstrate the benefits of its application to plant-level analysis involving passive system reliability assessment.

In both traditional and RSM approaches, the passive system reliability analysis is based on best-estimate models and calculations of the performance function for the system response of interest. The traditional approach, developed in Section 3.1, then uses Monte Carlo sampling to vary all input parameters in the best-estimate model following defined uncertainty distributions, and quantification of the original performance function to characterize system response in terms of mean value, probability distribution, simplified sensitivity indices, etc. With RSM, the surrogate system response function is also built by quantifying the original performance function for a subset of input parameters. However, the resulting continuous response surface provides more insight on plant risk, in addition to mean values and probability distributions, such as characterization of cliff edges and statistically meaningful sensitivity indices.

Let $\omega = \{\omega_1, \dots, \omega_N\}$ represent the vector of N input parameters (e.g. heat transfer coefficients, main salt pumps coast down time, etc.) for some model $\Omega = f(\omega)$ (e.g. Ω represents the performance function introduced in Section 3.1.8). To perform passive system reliability assessment, sensitivity analysis and uncertainty quantification, we wish to investigate the influence of all parameters ω on the model output Ω.

The polynomial chaos expansion (PCE) method is an example of RSM where the model response is approximated by a truncated polynomial expansion, using multivariate polynomials $\Psi_k(\omega) = a_0 + a_1\omega + a_2\omega^2 + \cdots$:

$$\Omega(\omega) \approx \sum_{k=1}^{M} c_k \Psi_k(\omega) \tag{3-7}$$

where the number M of polynomials depends on the total number N of analyzed input parameters and the order d of the polynomial representation through the combinatoric formula:

$$M = \frac{(N+d)!}{N!d!} \tag{3-8}$$

The coefficients c_k in Eq. (3-7) quantify the dependence of the model output Ω on the input parameters ω. The symbol Ψ_k is a simplified notation of the multivariate orthonormal polynomial basis for ω including all cross-terms between different parameters.

Traditional PCE methods and their extension to the generalized polynomial chaos framework assume an exact knowledge of the probability density functions of all input parameters and are optimal only when applied to certain parametric probability distributions (uniform, normal, gamma and beta distributions) [58,59]. Application to passive system reliability assessment, where only scarce data exists to describe some input parameter distributions, calls for further generalization of the method. Such generalization is achieved with aPC [49-51]. While existing practical applications of aPC are so far limited to aerospace engineering [52] and petroleum engineering [53], the method yields interesting results in the context of this study.

With aPC, only low-order statistical moments of input parameter probability distributions – up to order $(2d - 1)$ where d is the order of the polynomial expansion – are needed instead of full probability density functions to build the orthogonal polynomial basis Ψ_k [49-51]. For instance, to use a 2nd order polynomial expansion, one needs to know the mean, variance and

skewness of each input parameter distribution. This better applies to most input parameters encountered in passive system reliability assessment applications, where limited data is available and ideal, arbitrarily-chosen probability distributions might have wrong high-order moments compared to reality. Once the orthogonal polynomial basis has been built, the performance function only has to be calculated at a subset of collocation points in the space of input parameters to build the response surface. aPC has proven to be more accurate than classic RSM included in the RMPS methodology, using experimental-design methods (see Figure 3-1), while providing high-order approximation of error propagation in earlier applications [53].

Detailed mathematical descriptions of aPC, including methods to derive the polynomial basis Ψ_k and the expansion coefficients c_k from low-order moments of input parameter probability distributions, are available in the literature [49-51] and summarized in Appendix C. The resulting algorithm for integrated implementation with best-estimate codes such as RELAP5-3D is presented in Figure 3-8. Appendix C details the derivation of all symbols in Figure 3-8, and for illustration purposes, a simple, generic example is provided, using a 2nd order polynomial expansion for a model with two input parameters that can be generalized to higher-order, larger-dimension cases.

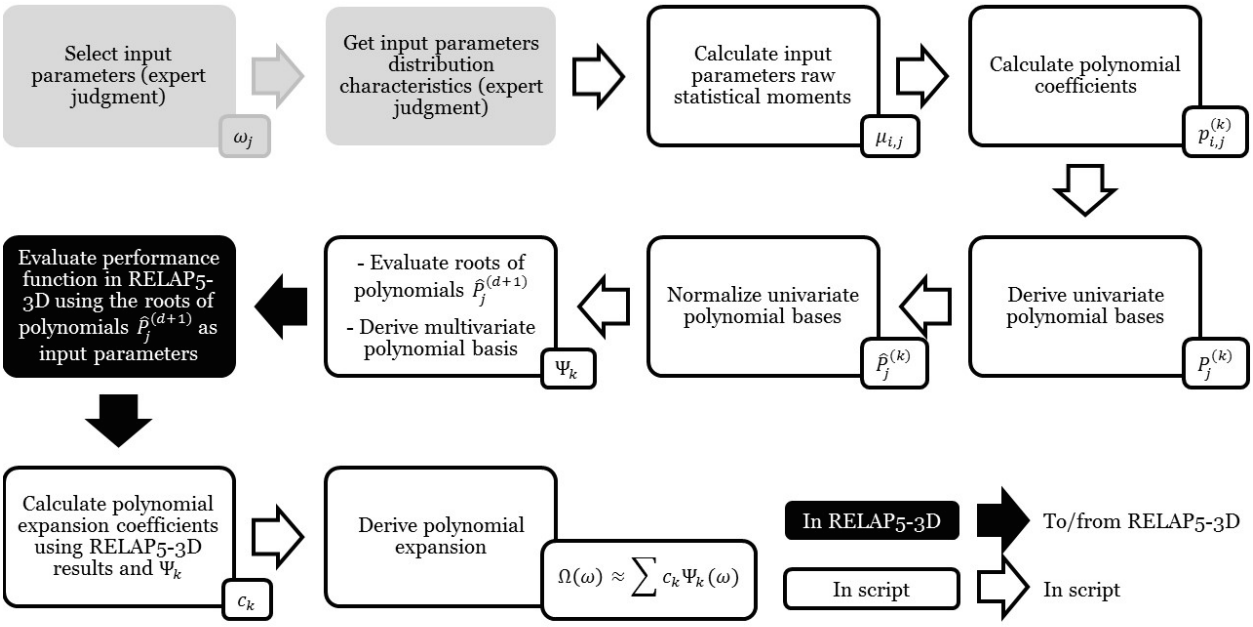

Figure 3-8. aPC implementation algorithm integrated with RELAP5-3D for passive system reliability assessment.

In the light of its minimal requirements and powerful results in past applications to other domains, RSM using aPC appears as a promising approach for some aspects of passive system reliability assessment and cliff edge effects identification. The following is a non-exhaustive list of its benefits in the context of this study:

- **aPC is capable of handling models with a very large number of input parameters.** As mentioned in Section 3.2.1, one of the main challenges in passive

system reliability assessment is the quantity and diversity of modeling variables. In this regard, aPC provides an algorithm to handle large numbers of input variables, each with their associated uncertainties, and reproduce performance function quantification at minimal computational cost once the response surface has been built. This needs to be compared with Monte Carlo sampling used to quantify response uncertainty based on input parameter distributions in the traditional approach developed in Section 3.1;

- **aPC constructs an optimal response surface for any desired distribution of data.** Another challenge in passive system reliability assessment is heterogeneity of the types and magnitudes of uncertainties associated with all input parameters. Since only low-order statistical moments are needed in the aPC algorithm, a large variety of input distributions can be taken into account in the analysis;
- **aPC provides information on system response without requiring intensive Monte Carlo simulation.** Once the response surface has been built, simple analytical expressions of the mean and variance of the performance function are readily obtained [51]:

$$mean(\Omega) = c_1, \;\; Var(\Omega) = \sum_{k=2}^{M} c_k^2 \tag{3-9}$$

and more complex information, such as the probability of failure defined in Eq. (3-4), can be obtained at reduced computational cost by quantifying the surrogate response function rather than the original model;

- **aPC can be used for global sensitivity analysis.** Analytical expressions are derived from the aPC expansion coefficients and polynomial basis for global sensitivity indices in Section 3.2.4. These indices yield more physically significant information than the simple indices developed in Section 3.1.7. This aspect makes aPC a promising approach to identify major contributors to overall passive system reliability;
- **aPC can be applied to any best-estimate model following a simple algorithm, without any deep mathematical knowledge.**

3.2.4 Sensitivity Analysis Using aPC

Global sensitivity analysis is used to rank input parameters in terms of their overall impacts on passive system performance and to identify what combinations of input parameters have the highest impacts on overall risk.

For instance, the Sobol index $S_{i_1,\dots,i_s}$ indicates what fraction of the total variance of the performance function can be traced back to the joint contributions of input parameters $\omega_{i_1}, \dots, \omega_{i_s}$ [60,61]. It has a simple analytical expression based on aPC expansion coefficients [51], provided in Appendix C.

A complementary metric for global sensitivity analysis is the *Total Index*, which indicates the total contribution to the variance of the performance function from an individual uncertain parameter in all cross-combinations with other parameters [62]. It is expressed, for each input parameter ω_j, as:

$$S_{\omega_j}^{T} = \sum_{(i_1,\dots,i_S):\, j \in (i_1,\dots,i_S)} S_{(i_1,\dots,i_S)} \tag{3-10}$$

$S_{\omega_j}^T$ sums up all Sobol indices in which the variable ω_j appears, both as univariate and joint influences. In the context of passive system reliability assessment, the Total Index can help identify major *individual* contributors to overall system performance, while the Sobol index can indicate what *combinations* of input parameters have the greatest impact on system response.

The weighted sensitivity index is another global sensitivity metric that reflects the square gradient of the performance function $\partial\Omega(\omega)/\partial\omega_j$ averaged over the statistical distributions $\Gamma(\omega_j)$ of all input parameters [49]:

$$S_{\omega_j}^2 = \int_{\omega_1} \dots \int_{\omega_N} \left[\frac{\partial\Omega(\omega)}{\partial\omega_j}\right]^2 d\Gamma(\omega_1) \dots d\Gamma(\omega_N) \tag{3-11}$$

Expressions based on aPC are provided in the literature [51] and summarized in Appendix C. In Appendix C, a simple, generic example is also derived using a 2nd order polynomial expansion for a model with two input parameters, which can be generalized to higher-order, larger-dimension cases.

The weighted index does not rely on comparison among different parameters, and is rather an absolute measure of parameter contribution to gradients of the performance function. This is an advantage over the Total Index, which is only a relative measure. Therefore, weighted sensitivity indices complement the more widely used Sobol indices for global sensitivity analysis.

3.2.5 Application to the Mk1 PB-FHR DRACS

For reliability assessment of the Mk1 PB-FHR DRACS, relevant inputs to the model are listed in Section 3.1.4. Based on their probability distributions detailed in Section 3.1.6, the first raw statistical moments μ_i of all input parameters are calculated, listed in Table 3-4, and used to build the orthonormal polynomial basis associated with each parameter, using the Matlab script provided in Appendix C.

Table 3-4. First raw statistical moments of input parameters.

	μ_1	μ_2	μ_3	μ_4	μ_5
PUI	100.0	1.00 x 10^4	1.00 x 10^6	1.00 x 10^8	1.00 x 10^{10}
CDT	4.5	20.8	98.9	481	2,390
DHS	196.0	3.86 x 10^4	7.65 x 10^6	1.52 x 10^9	3.04 x 10^{11}
FLD	50.0	2,670	1.45 x 10^5	8.06 x 10^6	4.62 x 10^8
FLP	100.0	1.01 x 10^4	1.03 x 10^6	1.06 x 10^8	1.11 x 10^{10}

Based on Eq. (3-8), with 5 input parameters, only 21 RELAP5-3D runs are required to build a second order polynomial response surface. Table 3-5 lists the values of each parameter for the 21 runs and the resulting performance function, given by Eq. (3-5) and calculated with RELAP5-3D. The second part of the Matlab script provided in Appendix C is then used to calculate the polynomial expansion coefficients c_k and, based on Eq. (3-9), the calculated mean of the performance function is -40°C and its standard deviation is 10°C. The mean of the performance

function, associated with a peak bulk coolant outlet temperature of 776°C, is consistent with the peak bulk coolant outlet temperature of 774°C obtained in Section 3.1.3, when all parameters are set to their nominal values. The standard deviation obtained here means that, considering the probability distributions of input parameters selected for this preliminary study, the peak bulk coolant outlet temperature lies in an interval between 756°C and 796°C with a confidence level of 95%, leaving a margin of 20°C below the failure criterion of 816°C identified in Section 3.1.2.

Table 3-5. Collocation points and performance function calculated by RELAP5-3D.

PUI (%)	*CDT* (s)	*DHS* (m²)	*FLD*	*FLP*	Performance function (°C)
100	3.9	182	43	91	-40.9
100	3.9	210	43	91	-41.9
141	5.4	182	43	91	5.1
141	3.9	182	62	91	18.7
100	5.4	182	43	91	-49.6
100	3.9	210	43	111	-36.9
100	5.4	210	62	111	-44.2
141	5.4	182	43	111	11.9
141	3.9	182	62	111	25.2
141	3.9	210	43	111	22.9
100	3.9	210	62	111	-35.9
100	5.4	182	62	91	-48.6
141	5.4	210	43	111	10.7
141	3.9	182	43	91	17.6
141	3.9	210	62	111	23.9
100	3.9	182	62	111	-34.9
141	3.9	210	43	91	16.4
100	5.4	210	62	91	-49.6
141	3.9	182	43	111	24.1
141	5.4	210	62	111	11.9
141	5.4	182	62	111	13.1

Once the response surface is built, the Total Index and the weighted sensitivity index for each parameter, which are defined by Eqs. (3-10) and (3-11) and provide complementary global sensitivity indices, can be calculated using expressions provided in Appendix C. These expressions have been implemented in a Matlab script (see Appendix C) and the calculated global sensitivity indices for the characteristic parameters studied here are shown in Figure 3-9.

Figure 3-9 shows that, both in combination with all other parameters – as expressed by the Total Index – and in terms of absolute contribution to the variance of the performance function – expressed by the weighted sensitivity index –, the performance of the DRACS primarily depends on the thermal power of the core (as a fraction of the 236 MWth nominal power), followed by the total form losses in the DHX branch and the DRACS loop, then the pump coast

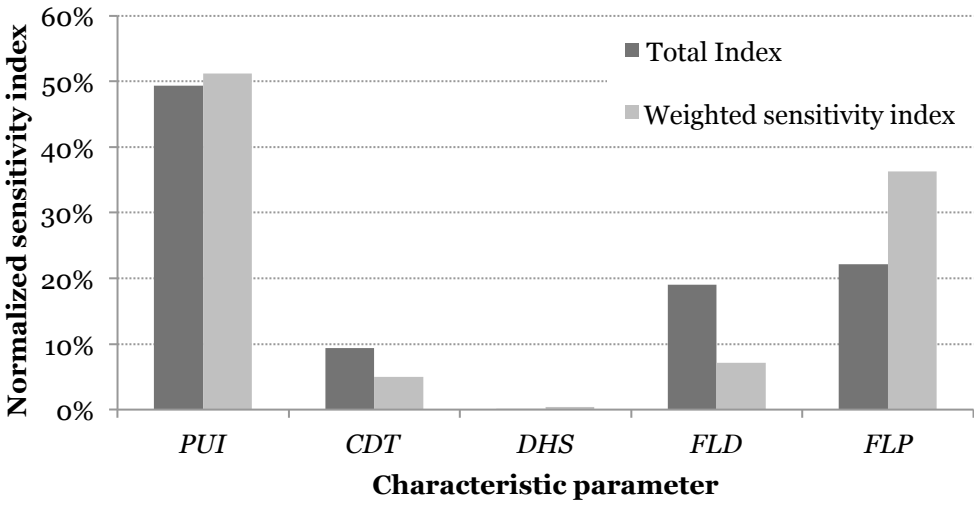

Figure 3-9. Normalized sensitivity indices from aPC method.

down time. Conversely, the heat transfer surface area of the DHX seems to play a minor role in the overall performance of the passive system. This result, obtained through physically and mathematically more meaningful methods, is partly consistent with the simple ranking of parameters shown in Figure 3-6, although the new indices show the important role of friction losses in the DRACS loop, which was underestimated in Figure 3-6. It is interesting to note that, although the contributions of friction losses in the DHX branch and the DRACS loop are similar when considered in combination with other parameters through the Total Index, friction losses in the DHX branch have an impact more than four times greater than friction losses in the DRACS loop in terms of absolute contribution to the total variance of the performance function expressed through the weighted sensitivity index. This insight is an incentive to study such sub-systems both individually and combined into the larger Mk1 PB-FHR plant.

3.2.6 Future Research Path

As the method to apply aPC to passive system reliability assessment matures, it needs to be implemented for increasingly complex models to prove its value and applicability compared to more traditional methods. Most importantly, as the number of input parameters grows, computational costs must be assessed against classic uncertainty propagation methods using Monte Carlo sampling. While only 5 input parameters were used in this study, future work may consider variations of up to several hundred uncertain parameters.

Also, low-order polynomials may not exhibit steep enough gradients to detect cliff edge effects with the proposed method. Moreover, when using a polynomial response surface, the approximated performance function always extrapolates to plus or minus infinity at the boundaries of the input parameters domain, which is unphysical and therefore bounds applications to the physically significant cases of small perturbations around mean values of the input parameters. One solution, which should be investigated as the method matures further, is to include both ordinary and inverse polynomials in the response surface. Inverse polynomials would better characterize the performance function at the edge of the input parameters domain

[55]. However, fitting methods for inverse polynomials are based on a weighted least-squares criterion and a more complicated iterative method based on maximum likelihood [63,64], making them less straightforward to implement than aPC.

As models and surrogate functions used in RSM become more complex, it will become more and more critical to reduce computation time by screening input parameters. This will primarily involve PIRT-type exercises based on expert judgment and the use of fixed (mean) values for input parameters with low levels of uncertainty to exclude them from the list of uncertain variables.

3.3 Design Optimization and Risk Mitigation

In this Section, design optimization and risk mitigation elements are suggested in order to allow for the DRACS to fulfill its decay heat removal function in a more reliable way, and therefore further contribute to the overall safety of the PB-FHR.

3.3.1 Results of the Sensitivity Analysis

The sensitivity analysis performed in Sections 3.1.7 and 3.2.5 shows that the most important parameters affecting the performance of the DRACS, from the set of parameters identified at this point, are the thermal power of the core (as a fraction of the 236 MWth nominal power) at steady-state, friction losses in the system – both in the DHX branch and in the DRACS loop – and pump coast down time. Therefore, to reduce the risks associated with the performance of the passive safety cooling system, one should make sure that these parameters stay close to their nominal values. In order to test this assumption, the same reliability evaluation as that performed in Section 3.1.8 was performed again, this time allowing *PUI* to vary only between 99% and 101% of the 236 MWth nominal power, *CDT* between 4.0 s and 5.0 s, FLP between 80.0 and 120.0, and FLD between 35.0 and 70.0. Running the model again for 100 random sets of the characteristic parameters defined in this study, the failure criterion was never reached, and the reliability of the system was therefore proven to increase from 99% to 100% with a confidence level greater than 95%.

This result shows that a critical element in mitigating the risks associated with the performance of the DRACS is indeed to make sure that the thermal power of the core, friction losses in the system and primary pump coast down time stay close to their nominal values.

The requirement on core thermal power reliability is partly addressed by the use of pebble fuel instead of fixed fuel, which allows for constant adjustability of the core reactivity, and therefore finer control on the power generated during normal operation. Further design of the control rods should be aimed at allowing for even more precise control of the thermal power generated in the core.

The requirement on primary pump coast down time essentially depends on the reliability of the pump itself, and could easily be addressed by using pumps that have high enough reliability, based on risk assessment methods. This parameter is related to the inertial mass of the rotating

parts of the pump, which can be adjusted by adding more or less large flywheels to the relatively small FHR pumps.

Finally, friction losses in the primary loop and the DRACS loop can be accurately measured in non-nuclear salt loops, similar to the characterization that was performed as a first step towards validation of best-estimate models of the CIET facility, as explained in Section 2.3.1. More generally, as the methodology developed here matures and is applied to a larger set of input parameters, the values of these parameters and their probability distributions can be estimated early in the development and operation phases of the reactor, through validation and startup testing, and yield refined sensitivity indices related to reliability of the DRACS.

3.3.2 Risk Mitigation through Further Design Analysis

A very important point to make in this study is that risk assessment was only based on a preliminary design of the DRACS and the Mk1 PB-FHR itself. Therefore, at this development stage of the reactor, many efforts can be made towards further design of sub-systems of the plant that play a critical role in overall safety of the system.

The failure criterion was based on thermal limits of metallic components that are currently considered for use in parts of the reactor. However, one could envision using other materials with higher thermal limits close to the outlets of the core, where coolant temperature reaches its highest value, which would reduce risks of failure as they have been identified to-date. A noteworthy element is that, although 1 test out of 100 proved to lead to failure of the system in the preliminary risk assessment performed for this study, the peak temperatures reached by the coolant were only a few degrees higher than the limit set, which would actually probably not lead to serious failure of the metallic components in the reactor, and could still allow for proper decay heat removal through the DRACS in accidental situations.

As importantly, the annular core design allows for optimization of the design of the coolant outlets and the outlet plenum to enhance coolant mixing, and therefore reduce outlet coolant temperature gradients and average temperature. Having most of the coolant flow entering the core through the inner reflector and leaving the core through the outer reflector, instead of having mostly axial flow, helps to reduce coolant outlet temperature for most of the outlets while maintaining the desired average temperature differential between inlet and outlet during steady-state operation. Moreover, using inert graphite pebbles as an outer layer in the core serves both purposes of neutron shielding of the outer reflector – which is the primary purpose of this layer – and enhancing coolant mixing before it exits the core, therefore reducing temperature gradients at the outlets and allowing for an easier design of the outlet plenum where thermal stresses due to inflows of coolant at different temperatures would be reduced. Ultimately, one should still design the outlets to reduce temperature differences between the different flows of coolant reaching the outlet plenum, for instance by achieving intermediate mixing of coolant flows that exit the core in neighboring locations before they reach the outlet plenum, while only reduced flow of coolant at higher temperatures exits the core through the defueling chute.

Finally, and in a more general way, the performance of the DRACS relies on proper activation of natural circulation, which in turn strongly relies on the geometry of the system. If the design of the system has been developed so that the DRACS performs its safety function properly in a specific geometrical configuration, then one should ensure that this geometry is not compromised by the initiating event and throughout transient evolution of the system, which can be very complicated. One way to mitigate risks associated with geometrical configuration of the system would be to design the DRACS with large margins as to geometry, so that it can still remove sufficient heat from the core even if it is not in its reference configuration.

However, at this point, only few sub-systems of the Mk1 PB-FHR design have been thoroughly studied, as would be the case for any advanced reactor design under early development, and proper risk mitigation related to the performance of the DRACS can only be achieved by further analyzing the designs of all sub-systems of the PB-FHR and their impacts on the way the DRACS ensures decay heat removal in transient situations.

3.3.3 Risk Mitigation through a Better Understanding of the System

Because the PB-FHR design is still in an early phase of its development path, risk mitigation still mainly relies on a better understanding of system response to transient situations.

As pointed out in Section 3.1.4, uncertainties in the performance of a system that is not yet fully developed can be assessed, and therefore risks can be mitigated in a better way, through a novel approach to PIRT-type exercises. By relying on expert judgment to identify phenomena that will have the strongest influence on the capacity of the passive safety cooling system to perform its functions, and the sub-systems that are associated with this performance, engineers are given the capacity to know which elements of the system need further analysis before they come up with a final design, and operators have the ability to know which sub-systems and associated key parameters need closer monitoring while the reactor is operating. This process, which combines pre- and post-construction considerations, eventually leads to better risk mitigation. This is especially true for the performance of the DRACS, which can only be tested under its real physical conditions of utilization, and for which risk assessment and mitigation therefore strongly depend on past experience in the industry.

At the development stage, in which the PB-FHR design is currently standing, better understanding of the DRACS behavior, related to the behavior of the whole system, can be achieved through computational models that need to be validated with scaled experiments. The process of code validation, developed in Chapter 2, is a first approach to risk mitigation after important phenomena have been identified through expert judgment, since it allows engineers to constantly upgrade their design in order for the passive safety cooling system to eventually reach its performance goals.

As a result of the risk assessment analysis performed in this study, several elements of the design, apart from the DRACS itself, have been identified and need further analysis in order to ensure proper risk mitigation in the case of an LOFC initiating event. As can be seen on Figure 3-7, one first unknown is the probability that reactor trip via the reactivity control system

occurs, should an initiating event such as LOFC occur. Furthermore, at this point in the design of the PB-FHR, response of the core to an ATWS is still not fully characterized. Proper risk mitigation related to LOFC could be achieved by first identifying these consequences and reducing the importance of damage caused to the core, and more importantly, by reducing the probability of ATWS. Again, this requires further studies of the design of the whole system, not only the DRACS sub-system by itself. Another important element that has been identified on Figure 3-7 is the probability of the normal shutdown cooling system to operate if the reactor is properly scrammed after LOFC occurs, which would contribute to decreasing the risks associated with this initiating event. Once again, increasing this probability is a critical element in helping to mitigate the risks associated with LOFC, and it requires further analysis of the performance of the normal shutdown cooling system itself, not the DRACS. These examples show that, when trying to mitigate the risks associated with one initiating event, one cannot rely on risk assessment associated with only one sub-system such as the DRACS, but should rather get a better understanding of the response of the system as a whole, in which the passive safety cooling system plays a critical role.

3.3.4 Risk Mitigation through Redundancy of Safety Cooling Systems

As with the current generation of nuclear power plants, whose risk assessment has been achieved through traditional PRA, one of the most important points for risk mitigation associated with passive safety cooling systems is redundancy.

As can be seen on the event tree in Figure 3-7, safe situations for the core can be achieved without DRACS operation in the case of an LOFC initiating event, if the normal shutdown cooling system is properly activated. That system and the DRACS are redundant in the sense that they serve the same goal of decay heat removal – one in an active way and the other in a passive way. However, having both sub-systems implemented in an FHR reduces the risks of severe core damage, should an LOFC occur.

It is also worth noting that, from the sensitivity analysis performed in Sections 3.1.7 and 3.2.5, it appears that the performance of the DRACS is not highly sensitive to the heat transfer surface area in the DHX, compared to the impacts of core power, friction losses and primary pump coast down time on the response of the system. This is because during the first seconds of the transient, when natural circulation in the DRACS loops is slowly starting and the coolant outlet temperature reaches its highest value, the rest of the system, including the CTAH and other structural materials, plays a more important role than the DRACS itself for decay heat removal through thermal inertia. Therefore, the rest of the system completes the role of the DRACS for decay heat removal, and one should investigate its performance and enhance it in order to mitigate the risks associated with the sole performance of the DRACS. For instance, one could consider using a reactor cavity cooling system similar to those used in more conventional reactor designs, which would allow to remove heat absorbed by the reactor cavity during transients through water boiling.

Finally, one should not forget that the risk assessment study performed here was done by combining two out of three DRACS loops that would be present in the actual system into one for the RELAP5-3D equivalent model used. Having several DRACS loops in the PB-FHR, with only

part of them being required to operate to properly remove heat from the core when needed, is a strong element for risk mitigation, which prevents damage to the core, should some of the DRACS loops be unable to perform their safety function during transients.

3.3.5 Risk Mitigation through Inspection and Monitoring

One final consideration regarding risk mitigation is that, once the reactor is operating, one should always be able to repair components while their degradation is incipient rather than at an advanced stage, when they are about to fail completely, or have failed already. This is true for every component of the reactor, and especially relevant for safety systems such as the DRACS, which must serve as final risk mitigation elements during transient situations.

One way of detecting small damage to structural components early is through online monitoring of material defects. Several methods exist for this purpose: small holes can be drilled in critical components, where coupons are inserted and then extracted to monitor irradiation; optical methods can be used to measure geometry deformation of these same small holes, therefore assessing thermal expansion of the materials, which is especially relevant for metallic components, which have the lowest thermal limits and highest thermal expansion coefficients; finally, acoustic methods can be used to hear cracks due to corrosion propagating in structural materials [65]. Another method that can be used on a regular basis is direct inspection of the components of the reactor. This is facilitated by the fact that liquid flibe is transparent in the visible spectrum at temperatures at which the Mk1 PB-FHR is operating. Therefore, one could send probes into the coolant that take pictures of structural components, and those pictures could be used to determine if some components need short term replacement.

These are methods that complete all the risk mitigation elements presented in previous Sections once the reactor is operating. They can be applied to the whole reactor, and more specifically to the DRACS, for which geometry integrity is one of the critical parameters for natural circulation, and therefore for proper decay heat removal.

Chapter 4 A Framework for Life Cycle Assessment of Advanced Reactor Designs

In the context of increasing concerns with global greenhouse gas (GHG) emissions and depletion of hydrocarbon fuel reserves, more and more countries are investigating low-GHG energy portfolios. Based on life cycle CO_2 emissions, nuclear power plants have repeatedly been recognized as having much lower environmental impacts than fossil-fueled plants – namely coal steam plants, NGCC plants and gas turbine simple cycle (GTSC) plants. However, previous LCA studies have only been applied to existing, conventional nuclear power plants. Extending such studies to advanced reactor designs earlier rather than later in their development process could lead to further life cycle emissions reduction and make nuclear power an even better option for climate change mitigation, beyond the safety case supported by the methods introduced in Chapter 2 and Chapter 3.

In this Chapter, we establish the framework and prove the value of performing LCA in the early design phase of advanced nuclear reactor technology. As an example, we apply EIO-LCA methods to the Mk1 PB-FHR design. Results of this study allow us to suggest areas for future improvement of the PB-FHR design, based on estimated CO_2 emissions related to the construction and operation phases of the reactor. For the rest of the nuclear fuel cycle, GHG emission calculations are based on available data for conventional nuclear technology, adapted to the Mk1 design. This study can be extended to any novel nuclear reactor concept, provided that the design is mature enough that approximate construction material inventories are available and operation modes are defined.

Elements of the baseline Mk1 PB-FHR design that are not already listed in Chapter 1 are first introduced in Section 4.1, as they provide a basis for estimating quantities and costs of major classes of materials involved in building and operating the reactor. We then detail the methodology developed to derive average GHG emissions per kWh of electricity produced over the lifetime of the reactor in Section 4.2. Results of this study are provided in Section 4.3 for the baseline case. In Section 4.4, sensitivity of the LCA results to a number of parameters, including uranium enrichment method, primary energy mix, concrete inventories and concrete mix, is evaluated, and life cycle GHG emissions from the Mk1 PB-FHR are compared to LCAs for traditional base-load power sources – coal, NGCC and conventional nuclear power plants – and peaking power sources – GTSC plants. In Section 4.5, these results are used to inform enhancements in the approaches to design and operate this new class of reactors from the perspective of climate change mitigation, and suggest areas for future research to further reduce GHG emissions from the nuclear power industry.

4.1 Mk1 PB-FHR Design

The Mk1 PB-FHR design differs from previous FHR designs developed and published by UCB and others. It uses a NACC based upon a modified General Electric (GE) 7FB gas turbine,

designed to produce 100 MWe of base-load electricity when operated with only nuclear heat, with a 42.4% net efficiency, and to increase this power output to 242 MWe using natural gas co-firing for peak electricity generation, with a 66.4% co-firing efficiency [16,17]. Therefore, the NACC provides flexible grid support services to handle the ever-increasing demand for dispatchable peak power, in addition to traditional base-load electric power generation. In this Section, we detail some specific aspects of the Mk1 PB-FHR design that are useful for LCA studies. Similar design considerations would need to be taken into account to perform LCA for other advanced reactor technologies.

4.1.1 Mk1 PB-FHR Reference Configuration and Material Inventories

The reference configuration for the Mk1 site uses 12 Mk1 units, capable of producing 1200 MWe of base-load electricity, and ramping to a peak power output of 2900 MWe using natural gas co-firing [11]. The Mk1 design, shown in Figure 4-1, uses the same steel-concrete composite (SC) wall modular construction methods as the Westinghouse AP1000, and its modular components can be manufactured in the same factories. A Mk1 reactor uses 7 structural modules for the shield building (SB) and 3 modules for the below-grade air duct (AD) vault, as shown in Figure 4-2. The reactor cavity is located in the SB4 module.

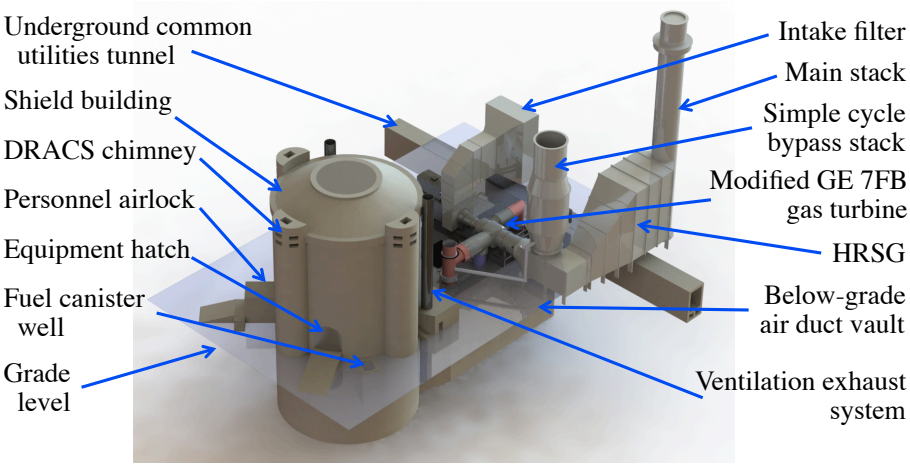

Figure 4-1. The Mk1 PB-FHR reactor shield building adjacent to the power conversion system.

For performing LCA, it is helpful to have estimates for total quantities of materials used in reactor designs. Table 4-1 presents the quantities of stainless steel, high-alloy steel, graphite and flibe salt used in the main components of the Mk1 reactor system. These quantities are calculated by the SolidWorks CAD program used to develop the system models [11], except for the quantity of high-alloy steel in the NACC power conversion system, which is based on values from the THERMOFLEX power system modeling software. This approach demonstrates the value of using well-organized CAD models throughout the advanced reactor design process, as it allows for easy accounting of material inventories and automatic updates as the design matures. To enable near-term deployment, the Mk1 design uses a core barrel and other core internal structures fabricated from the same metallic material as the reactor vessel and main salt piping.

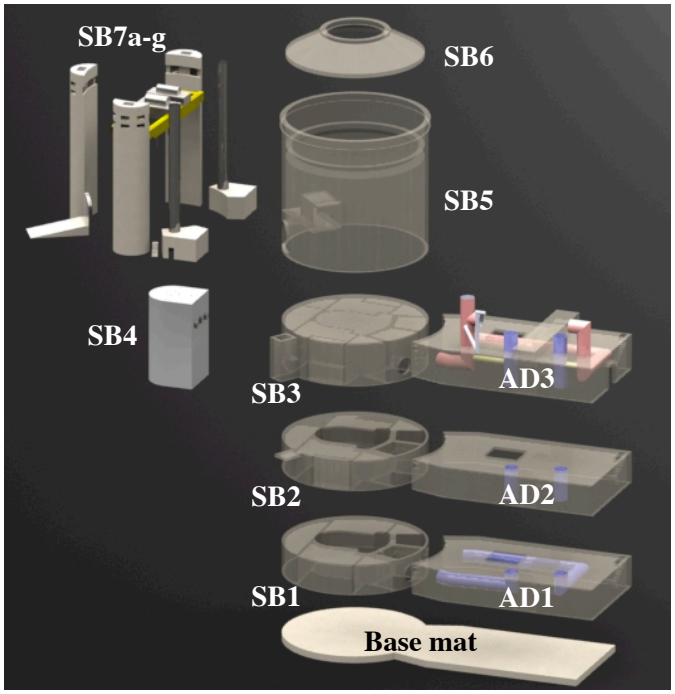

Figure 4-2. The Mk1 PB-FHR uses 10 primary structural modules.

Table 4-1. Mk1 reactor system steel, graphite and salt inventories.

	Mass (kg)
316 Stainless Steel	**238,420**
Reactor vessel (6.0 cm wall below ring, 4.0 cm wall above)	57,150
Upper internals	49,160
Core barrel (3.0 cm wall)	13,290
Lower outer reflector support skirt	9,640
Lower center reflector support ring	133
Hot leg and cross-over leg piping (3.0 cm wall)	5,690
Hot well (5.0 cm wall)	18,990
Cold legs and standpipes (3.0 cm wall)	11,624
Drain tanks (3.0 cm wall)	9,240
CTAH tube bundles	63,500
High-Alloy Steel	**797,800**
NACC power conversion system	638,250
All other uses in plant (assume 25% addition)	159,550
Graphite (density of 1,740 kg/m^3)	**49,250**
Outer reflector	43,310
Center reflector	5,940
Flibe (density of 1,962.7 kg/m^3)	**91,900**
Core, reactor internals and DHX wells (11.67 m^3)	22,900
Main salt piping, hot well and CTAHs (31.59 m^3)	62,010
DRACS (3.56 m^3)	6,990

Table 4-2 presents the quantities of carbon steel (density of 7,800 kg/m^3) and concrete (density of 2,400 kg/m^3) used to construct the base mat, the SC walls for the reactor SB and AD vaults and other structures, shown in Figure 4-2, again using values derived from the CAD model [11], except for the NACC power conversion system, which uses values from THERMOFLEX. Figure 4-3 shows the CAD model of the SB7 module with the concrete mass listed among other properties on the left. The steel masses are calculated based on the surface area of each module, assuming that the steel plates used in the modules are 1.25-cm thick everywhere except on the outside of the shield building and the inside of the CTAH cavities, where the steel plates are 2.50-cm thick. The total mass of steel calculated is increased by 10% to account for additional tie rods and other fixtures between the plates. The mass of steel used in the base mat, which uses conventional reinforcing bar, is assumed based upon the use of 18 gage (5.73-cm-diameter) rebar (20.3 kg/m) used in two layers in a square pattern with a spacing of 0.30 m.

Table 4-2. Mk1 reactor building and air duct vault steel and concrete.

	Carbon Steel (1,000 kg)	**Concrete (1,000 kg)**
Base mat	336.8	3,601.5
Shield building level 1 (SB1) module	163.8	1,638.1
Shield building level 2 (SB2) module	163.8	2,293.0
Shield building level 3 (SB3) module	202.6	2,994.0
Reactor cavity module (SB4)	111.9	1,674.0
Shield building upper ring (SB5)	598.8	3,498.7
Shield building roof (SB6)	166.0	680.2
Shield building external structures SB7a-g (DRACS chimneys, etc.)	305.8	1,954.1
Polar crane*	200.0	0.0
Air duct vault level 1 (AD1) module**	258.2	1,713.3
Air duct vault level 1 (AD2) module**	180.6	1,713.3
Air duct vault level 1 (AD3) module**	335.4	2,267.4
Underground common tunnel	0.0	2,075.0
NACC power conversion system***	2,512.0	3,663.0
Vehicle barrier system (1.7 m W x 1.2 m H x 3400 m L)/12 units	54.0	578.0
Support buildings (25% of total)	1,397.4	7,585.9
TOTALS	**6,987.1**	**37,929.5**

* Polar crane mass assumed to be 2 times its 100 t capacity.

** Includes steel mass of 2.5-cm-thick air duct pipes preinstalled in module.

*** Concrete is 50% of conventional NGCC plant to reflect the fact that the Mk1 AD vault replaces the foundation needed for a conventional NGCC plant.

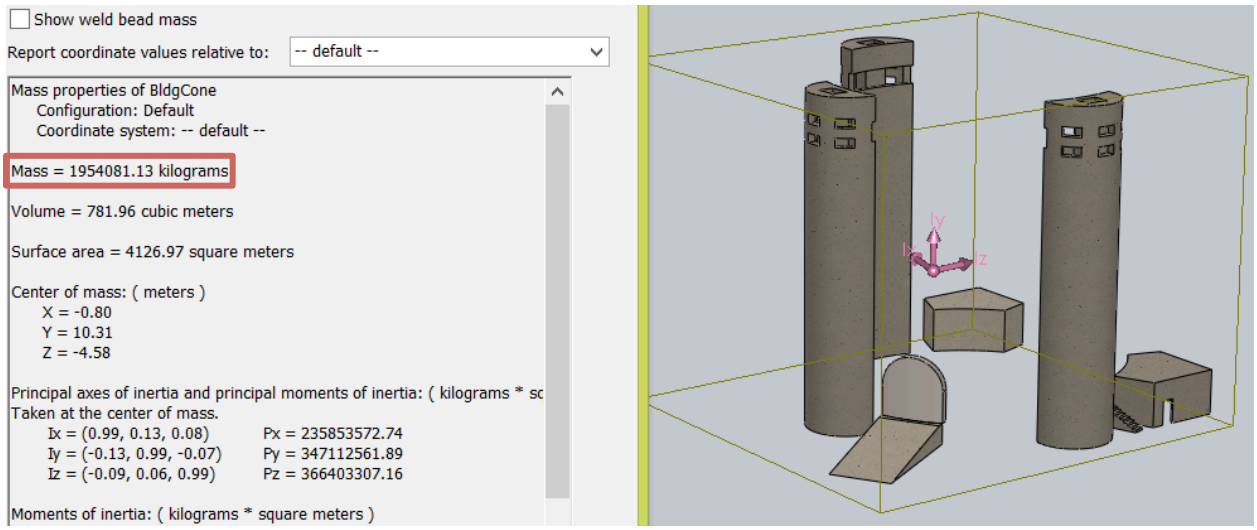

Figure 4-3. CAD model of the SB7 module, listing concrete mass.

4.1.2 Mk1 PB-FHR Fuel

As with earlier UCB designs, the Mk1 PB-FHR uses 3.0-cm-diameter, spherical pebble fuel elements with coated particles in an annular fuel zone, and a low-density center graphite core. Fuel kernels are the same tristructural-isotropic (TRISO) fuel used in HTGRs, and therefore, similar methods as those developed here could easily be adapted to LCA of HTGR technology. Fuel pebbles are continuously circulated through the core at a slow pace. Because of their buoyancy in the salt coolant, they move upward through the core and are removed at the top of the core.

Inert graphite reflector pebbles surround the annular fuel region in the core to provide shielding to the fixed outer radial graphite reflector and allow it to be used for the full operating lifetime of the plant. Figure 4-4 shows the design of the Mk1 PB-FHR fuel pebbles, and key parameters for the Mk1 fuel and core design used for LCA studies are listed in Table 4-3 [11].

4.1.3 Mk1 PB-FHR Coolant

The high volumetric heat capacity of the salt coolant enables FHRs to maintain a high average temperature – 650°C – and small temperature rise across the core – 100°C. This mode of operation yields thermal efficiencies similar to HTGRs while operating within a temperature regime covered by the ASME B&PV Code to enable faster development and deployment.

The flibe coolant in the Mk1 PB-FHR requires a ^{7}Li enrichment of 99.995%. The costs of the major constituents of flibe, beryllium and lithium, are approximately $770/kg and $63/kg, respectively, or $79/kg of flibe (2002$) [20]. The cost to enrich lithium is uncertain. With the concentration of ^{7}Li in natural lithium being 92.41%, and for a tails assay of 85% (the tails can be sold for essentially the same price as the natural lithium is purchased for), the separative work to produce 99.995%-enriched ^{7}Li is 0.97 SWU/kg of flibe [11]. As a possible metric for cost, worldwide prices for uranium enrichment in 2010 ranged from $40 to $160/SWU. Lithium is

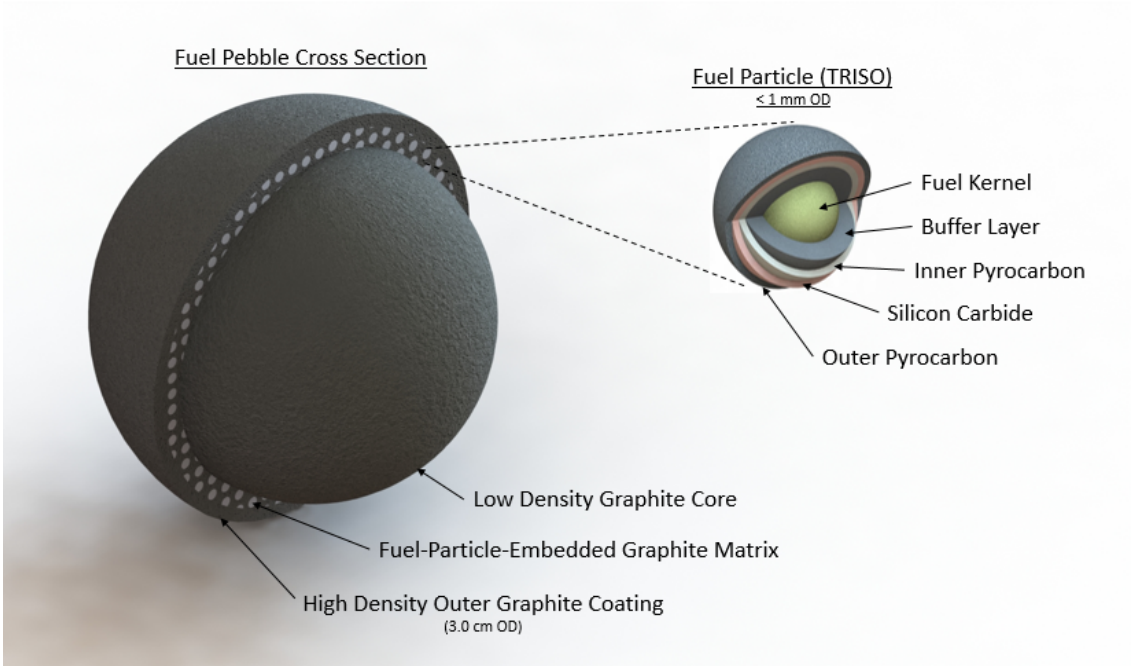

Figure 4-4. A Mk1 PB-FHR pebble fuel element.

Table 4-3. Mk1 PB-FHR fuel and core design parameters.

Fuel pebble design	
Pebble diameter	30.0 mm
Graphite coating thickness	1.0 mm
Inner graphite core diameter	25.0 mm
Uranium enrichment	19.90%
Coated particle packing fraction in fuel layer	40%
Average pebble discharge burnup	180 MWth-d/kg-HM
Separative work	1.98 MWe-d/kg-SWU
Pebble consumption rate	920/full power day
Fuel kernel design	
Fuel kernel diameter	400 μm
Fuel kernel composition	$UC_{1.5}O_{0.5}$
Graphite buffer layer thickness	100 μm
PyC inner layer thickness	35 μm
SiC layer thickness	35 μm
PyC outer layer thickness	35 μm
Core design	
Thermal power	236 MWth
Electrical power	100 MWe
Power conversion efficiency	42.4%
Number of fuel pebbles in core	470,000
Number of graphite pebbles in core	218,000

easier to enrich than uranium, but costs to develop infrastructure for this purpose must be incurred. If lithium enrichment were to cost $100/SWU, then the total cost of flibe would contribute about $20 million – or about 8% – to the total direct cost of the 236-MWth Mk1 PB-FHR.

4.1.4 NACC Power Conversion

The NACC is a novel power conversion system under current development at UCB, which combines two traditional electricity generation heat sources, namely nuclear and natural gas, into a single hybrid system. A conventional, industrial, frame-type gas turbine (GE 7FB) is modified to accept heat from an external source, while also maintaining its ability to combust natural gas rapidly on demand. The resulting combination allows for the production of 100 MWe from an inexpensive base-load nuclear source for low demand periods and the option to co-fire natural gas to a power of 242 MWe during peak demand periods. Conversion of natural gas to electricity in the proposed system is achieved with 66.4% efficiency, higher than state-of-the-art NGCC.

These operating and physical characteristics place the NACC in a unique position in a competitive electricity market. Depending on market conditions, the NACC can operate at full electric output or throttle down and sell process heat from its Rankine bottoming cycle for steam production, distillation technology, hydrogen production, or other chemical processes. Additionally, the NACC can generate revenues from providing grid support and resource adequacy services to the transmission system operator. Such services become even more valuable as variable generation sources penetrate the market, with the implementation of renewable portfolio standards, and as the transmission system operator introduces flexible capacity ancillary services. This is a significant departure from traditional nuclear power plants' role in an electricity market.

4.2 Methodology and Assumptions

Several LCA studies and meta-analyses are available in the literature for conventional nuclear power plants [66-70]. These studies set the basis for detailed technology-to-technology comparisons in the electric power sector. In addition, UCB published a report that provided an analysis of trends in material inventories from Generation II LWRs to Generation III advanced LWRs and an early AHTR design [71]. However, there has not been any detailed LCA study for advanced nuclear reactor concepts to-date. Such analyses are critical to support the claim that nuclear power, and especially Generation IV reactors, could play a key role in reducing GHG emissions from the power sector and mitigating climate change in the future. Here, we use the same breakdown of the nuclear fuel cycle as used in earlier nuclear LCA studies, and we apply it to advanced reactor technologies, using the FHR example.

Wherever possible, we use available information from the Mk1 PB-FHR design to calculate GHG emissions on a per-kWh basis, using the EIO-LCA method. This method estimates the environmental emissions resulting from economic activities, based on specific sectors and economic values, which are directly related to material inventories and costs [72]. It is

important to note that, while material costs are used as inputs to the EIO-LCA method to derive GHG emissions, these costs cannot be used directly to estimate total plant capital cost as they do not include other significant factors such as financing, engineering work, construction, quality assurance, nuclear grade material qualification, etc. Where detailed information on material input requirements is not available from the current Mk1 design, a scaling method is used to infer GHG emissions for the Mk1 PB-FHR life cycle based on data from earlier studies of Generation II LWRs. However, these earlier studies show significant variability in their results. The main variability factors include the primary source energy mix for uranium enrichment, uranium ore grade, and the selected LCA method to perform the analysis, with results ranging from 4 to 110 g CO_2-eq/kWh for Generation II LWRs [69].

4.2.1 General Assumptions on Reactor Operation

A number of assumptions on reactor operation are useful throughout the life cycle study to assess costs and GHG emissions per kWh of electricity produced. These assumptions address concerns about the major sources of uncertainty related to nuclear LCAs as listed in the literature [70].

In the case of the Mk1 PB-FHR, the lifetime of the plant is estimated to be 60 years. This number is consistent with the current push by the U.S. nuclear industry to extend existing plant operating licenses from 40 years to 60 years, and all Mk1 reactor internals have been designed for a 60-year lifetime, except for the center graphite reflector and graphite reflector pebbles, which must be replaced every 10 years because of neutron irradiation [45]. A similar assumption would apply to most advanced reactor designs under current investigation.

The capacity factor for the plant is estimated to be 92.5%. This is a conservative value for PB-FHRs, based on an average capacity factor of 90% for the U.S. nuclear fleet over the past 6 years [73], and recognizing that online refueling is likely to lead to higher capacity factors. Similar capacity factors could be expected from advanced reactor designs refueled online, such as pebble-bed HTGRs, while fixed fuel designs would likely be closer to conventional plants' capacity factors.

The net efficiency of the reactor with the NACC power conversion system is 42.4% when operated with only nuclear heat (100 MWe base-load electric output), and 66.4% for natural gas co-firing (additional 142 MWe electric output). These values were estimated from a detailed analysis of the NACC using THERMOFLEX, a heat balance modeling and engineering program [16,17]. For this LCA study, continuous base-load operation and continuous co-fired operation are used as bounding cases, resulting in total electricity productions of $4.86 \cdot 10^{10}$ kWh and $1.18 \cdot 10^{11}$ kWh throughout the lifetime of the plant, respectively, or $2.40 \cdot 10^{6}$ kWh and $5.81 \cdot 10^{6}$ kWh of daily electricity productions, respectively. In real markets, the co-firing capability would only be used part of the time, for conventional load-following and to compensate for the introduction of significant intermittent electricity generation by nondispatchable wind and solar [74].

4.2.2 Mk1 PB-FHR Fuel Life Cycle

In this Section, we list the methods and assumptions specific to each stage of the nuclear fuel cycle for the Mk1 PB-FHR, used to calculate GHG emissions per kWh of electricity produced over the 60-year lifetime of the plant. The breakdown of the fuel cycle is adapted from the conventional nuclear fuel cycle and would apply to any LCA for reactors using low enriched uranium fuel.

Uranium Mining and Milling

Uranium is extracted from ores using either open pit, underground excavation, in situ leaching, or as a by-product in other mining. GHG emissions from the mining stage of the fuel cycle are highly dependent on the technique used, as well as ore grade and fuel utilization [68]. The baseline GHG factor for mining and milling in the U.S. nuclear fuel cycle is estimated to be 1.7 g CO_2-eq/kWh, calculated from an average uranium ore grade of 0.2% U_3O_8 [67]. GHG emissions are proportional to the energy required for mining and milling, which is itself proportional to the mass of ore that is mined and milled, and therefore inversely proportional to natural uranium (NU) utilization in the reactor. The Mk1 PB-FHR produces 1.56 MWe-d/kg-NU, while a typical Westinghouse 4-loop PWR produces 1.46 MWe-d/kg-NU [11]. It is important to note that one can trade off consumption of NU and consumption of separative work units (SWU) for the subsequent enrichment stage by changing the enrichment tails assay. While this is normally done to minimize cost, it could also be done to minimize life cycle GHG emissions.

Conversion to Uranium Hexafluoride (UF_6)

After milling or in situ leaching, uranium is converted to gaseous UF_6 to enable enrichment. This process occurs in several stages, leading to a wide range of GHG emission values [68]. For the current U.S. nuclear fuel cycle, the GHG factor is estimated to be 0.8 g CO_2-eq/kWh [67]. Again, these GHG emissions are proportional to the energy required for conversion, which is itself proportional to the mass of converted uranium, and therefore inversely proportional to NU utilization in the reactor.

Enrichment

Several processes can be used for uranium enrichment, with gaseous diffusion and gas centrifuge being the two most widely used options worldwide. The amounts of electricity required for theses methods range from 50 kWh/SWU for gas centrifuge to 2,500 kWh/SWU for gaseous diffusion [75]. As a baseline, we use the 50 kWh/SWU value, which is representative of the U.S. context since the last U.S. gaseous diffusion plant in Paducah, Kentucky, was shut down in 2013. GHG emissions related to the enrichment stage of the fuel cycle depend on the method used, but also on the SWU required for a given electric output. The Mk1 PB-FHR produces 1.98 MWe-d/kg-SWU (or 47,520 kWh/SWU), while a typical Westinghouse 4-loop PWR produces 2.43 MWe-d/kg-SWU [11]. Finally, GHG emissions are proportional to the GHG emission factor of upstream electricity used for enrichment. As a baseline, we use the 2009 average U.S. GHG emission factor of 554 g CO_2-eq/kWh [76], although this value could vary significantly

depending on the region of the world – and the state in the U.S. – where enrichment occurs. Another approach would be to treat the electricity consumed for the enrichment phase as a house load – substracting the power needed for enrichment from net plant power generation – and therefore to use the GHG emission factor from base-load operation of a Mk1 PB-FHR rather than the average GHG emission factor of the current grid. Sensitivity of life cycle GHG emissions from a Mk1 PB-FHR to some of these assumptions is evaluated in Section 4.4.

Fuel Fabrication

The fuel fabrication stage is one of the main differentiating factors between conventional nuclear power plants and advanced reactors such as the Mk1 PB-FHR, because of the very different fuel form used in PB-FHRs and other advanced reactor concepts compared to conventional fuel rods. Because little data is available for industrial scale production of TRISO fuel and pebble compacts, we use material inventories and EIO-LCA to calculate GHG emissions from the Mk1 fuel fabrication stage. All fuel parameters used for this calculation are listed in Table 4-3. Densities and prices for corresponding materials, as well as related GHG emissions, are listed in Table 4-4. GHG emissions are obtained through the online EIO-LCA tool, which lists graphite under "Carbon and graphite product manufacturing" and silicon carbide under "Electrometallurgical ferroalloy product manufacturing." [77]

Table 4-4. Mk1 PB-FHR fuel characteristics.

	Inner core	Fuel matrix and coating	Buffer	PyC	SiC
Material	Graphite				Silicon carbide
Density (g/cm^3)	1.59	1.74	1.05	1.90	3.18
Price ($/kg) [78]	18				0.9
GHG emissions (g CO_2-eq/$) [77]	876				2,567

Plant Construction

The plant construction stage is another important differentiating factor between Generation II LWRs and advanced reactors such as the Mk1 PB-FHR. While past internal studies have tried to estimate material inputs for several FHR designs based on scaling from conventional power plants [45,71], here we use baseline material inventories from the Mk1 design, listed in Table 4-1 and Table 4-2, to derive life cycle GHG emissions using the EIO-LCA method. Densities and prices for corresponding materials, as well as related GHG emissions, are listed in Table 4-5. Both prices for raw materials and scaled prices from known costs for a conventional NGCC plant, using the THERMOFLEX/PEACE software, are listed in Table 4-5. The large discrepancy comes from costs related to civil labor, transportation, excavation, etc. Therefore, scaled prices are used rather than raw materials prices as inputs to the EIO-LCA tool. GHG emissions are obtained through the online EIO-LCA tool, which lists all steels under "Iron and steel mills," graphite under "Carbon and graphite product manufacturing" and concrete under "Concrete product manufacturing." [77]

Table 4-5. Mk1 PB-FHR construction materials characteristics.

Material	316 stainless steel	High-alloy steel	Carbon steel	Graphite	Concrete
Raw materials price ($/kg) [78]	3.7	1.0	0.6	18	0.04
Scaled price ($/kg)	67	22	15	384	0.9
GHG emissions (g CO_2-eq/$) [77]	2,567			876	250

Plant Operation

In conventional nuclear LCA studies, GHG emissions are estimated based on the plant's running expenses, replacement of reactor materials, non-radioactive waste management and other miscellaneous supplies. Because actual modes of operation of the PB-FHR and maintenance requirements are speculative in the Mk1 design, GHG emissions from the reactor operation stage in base-load mode are conservatively assumed to be identical to baseline values for conventional designs, at 3.9 g CO_2-eq/kWh [67]. The same assumption can be used for LCA of any advanced reactor design in its early development phase, when detailed operation characteristics are not defined. For the Mk1 PB-FHR, additional emissions result from natural gas burning in co-firing configuration. These emissions are estimated at 171 g CO_2-eq/kWh, using a THERMOFLEX model of the NACC power conversion system. LCA studies for NGCC plants have shown that production and distribution of natural gas result in GHG emissions up to 33% of the sole burning of natural gas [79]. This factor is added to the direct emissions factor provided by THERMOFLEX.

Back End and Decommissioning

The final steps of conventional nuclear LCA include nuclear waste storage, re-processing (if applicable) and disposal, and plant decommissioning. In total, these stages emit ~4 g CO_2-eq/kWh [67]. Because these aspects of the design of the PB-FHR have not been investigated yet, the same value is used as a baseline for the Mk1 reactor.

4.3 Results

Based on the assumptions listed in Section 4.2.2, GHG emissions from the various stages of the Mk1 PB-FHR fuel cycle are calculated as follows and summarized in Table 4-6:

Mining and milling:

$$Baseload\ emissions = Conventional\ emissions \cdot \frac{Conventional\ NU\ utilization}{Mk1\ PB{-}FHR\ NU\ utilization} = 1.7 \cdot \frac{1.46}{1.56} = 1.6\ g\ CO2eq/kWh \quad (4\text{-}1)$$

$$Cofiring\ emissions = Baseload\ emissions \cdot \frac{Baseload\ production}{Cofiring\ production} = 1.6 \cdot \frac{100}{242} = 0.66\ g\ CO2eq/kWh \quad (4\text{-}2)$$

Conversion to UF_6:

$$Baseload\ emissions = Conventional\ emissions \cdot \frac{Conventional\ NU\ utilization}{Mk1\ PB{-}FHR\ NU\ utilization} = 0.8 \cdot \frac{1.46}{1.56} = 0.7\ g\ CO2eq/kWh \quad (4\text{-}3)$$

$$Cofiring\ emissions = Baseload\ emissions \cdot \frac{Baseload\ production}{Cofiring\ production} = 0.7 \cdot \frac{100}{242} = 0.3\ g\ CO2eq/kWh \quad (4\text{-}4)$$

Enrichment:

$$Baseload\ emissions = \frac{Primary\ mix\ emission\ factor \cdot Enrichment\ electricity\ consumption}{Electricity\ produced/SWU} = \frac{554 \cdot 50}{1.98 \cdot 10^3 \cdot 24} = 0.58\ g\ CO2eq/kWh \quad (4\text{-}5)$$

$$Cofiring\ emissions = Baseload\ emissions \cdot \frac{Baseload\ production}{Cofiring\ production} = 0.58 \cdot \frac{100}{242} = 0.24\ g\ CO2eq/kWh \quad (4\text{-}6)$$

Fuel fabrication:

$$Emissions = Pebble\ consumption\ rate \cdot \sum_{i \in Pebble\ constituents} m_i C_i E_i \quad (4\text{-}7)$$

where m_i is the mass of constituent i in one pebble, based on composition and dimensions in Table 4-3 and material densities in Table 4-4, C_i the cost of constituent i per unit mass as listed in Table 4-4, and E_i the emission factor for production of constituent i per unit cost as listed in Table 4-4.

$$Pebble\ consumption\ rate\ [pebbles/kWh] = \frac{Pebble\ consumption\ rate\ [pebbles/full\ power\ day]}{Daily\ power\ production\ [kWh/day]} \quad (4\text{-}8)$$

Therefore:

$$Baseload\ emissions = \frac{920}{2.40 \cdot 10^6}[(2.15 \cdot 10^{-2} + 1.00 \cdot 10^{-3}) \cdot 18 \cdot 876 + 8.28 \cdot 10^{-4} \cdot 0.9 \cdot 2567] = 0.13\ g\ CO2eq/kWh \quad (4\text{-}9)$$

$$Cofiring\ emissions = Baseload\ emissions \cdot \frac{Baseload\ production}{Cofiring\ production} = 0.13 \cdot \frac{100}{242} = 0.055\ g\ CO2eq/kWh \quad (4\text{-}10)$$

Plant construction:

$$Emissions = \frac{\sum_{i \in Construction\ materials} m_i C_i E_i}{Lifetime\ power\ production} \quad (4\text{-}11)$$

where m_i is the mass of material i in the plant as listed in Table 4-1 and Table 4-2, C_i the scaled cost of material i per unit mass as listed in Table 4-5, and E_i the emission factor for production of material i per unit cost as listed in Table 4-5.

Therefore:

$$Baseload\ emissions = \frac{(2.38 \cdot 10^5 \cdot 67 + 7.98 \cdot 10^5 \cdot 22 + 6.99 \cdot 10^6 \cdot 15) \cdot 2567 + 4.33 \cdot 10^4 \cdot 384 \cdot 876 + 3.79 \cdot 10^7 \cdot 0.9 \cdot 250}{4.86 \cdot 10^{10}} = 8.3\ g\ CO2eq/kWh \quad (4\text{-}12)$$

$$Cofiring\ emissions = Baseload\ emissions \cdot \frac{Baseload\ production}{Cofiring\ production} = 8.3 \cdot \frac{100}{242} = 3.4\ g\ CO2eq/kWh \quad (4\text{-}13)$$

Plant operation:

$$Baseload\ emissions = Conventional\ emissions = 3.9\ g\ CO2eq/kWh \quad (4\text{-}14)$$

$$Cofiring\ emissions = Baseload\ emissions \cdot \frac{Baseload\ production}{Cofiring\ production} + Emissions\ from\ gas\ burning \quad (4\text{-}15)$$

$$Cofiring\ emissions = 3.9 \cdot \frac{100}{242} + 171 \cdot 1.33 = 230\ g\ CO2eq/kWh \quad (4\text{-}16)$$

Back end and decommissioning

$$Baseload\ emissions = Conventional\ emissions = 4.0\ g\ CO2eq/kWh \quad (4\text{-}17)$$

$$Cofiring\ emissions = Baseload\ emissions \cdot \frac{Baseload\ production}{Cofiring\ production} = 4.0 \cdot \frac{100}{242} = 1.7\ g\ CO2eq/kWh \quad (4\text{-}18)$$

Table 4-6. Mk1 base-load and co-firing emissions for each stage of the fuel cycle.

	Base-load emissions (g CO_2-eq/kWh)	**Co-firing emissions (g CO_2-eq/kWh)**
Mining and milling	1.6	0.66
Conversion to UF_6	0.7	0.3
Enrichment	0.58	0.24
Fuel fabrication	0.13	0.055
Plant construction	8.3	3.4
Plant operation	3.9	230
Back end and decommissioning	4.0	1.7
TOTALS	**19.3**	**236.2**

4.4 Sensitivity Analysis

As observed through the methodology developed in Section 4.2 and the results listed in Section 4.3, GHG emissions from the Mk1 PB-FHR system depend on a variety of factors, some of which can take a large range of values, or be adjusted through design changes. In this Section, we evaluate the sensitivity of the results obtained in Section 4.3 to some of these factors, namely the enrichment method, the primary energy mix used for the front end of the fuel cycle, and the amount of concrete and type of concrete mix used for plant construction.

4.4.1 Sensitivity to the Enrichment Method

As mentioned in Section 4.2, the amounts of electricity required for fuel enrichment range from 50 kWh/SWU for gas centrifuge to 2,500 kWh/SWU for gaseous diffusion [75]. While the 50 kWh/SWU value is used as a baseline for this study, the use of gaseous diffusion, with 50 times higher emissions, would lead to increases of total base-load and co-firing emissions by 148% and 5%, respectively, compared to the values listed in Table 4-6. This demonstrates the value of using gas centrifuge rather than gaseous diffusion for fuel enrichment from an environmental standpoint.

4.4.2 Sensitivity to the Primary Energy Mix

Mining and milling of uranium, conversion to UF_6 and fuel enrichment require the use of electricity. Therefore, related GHG emissions are proportional to the GHG emission factor of the

grid used for these processes. While this study uses the average U.S. GHG emission factor of 554 g CO_2-eq/kWh as a baseline, emission factors vary widely across the U.S. because of variations in energy mixes, from 227 g CO_2-eq/kWh in upstate New York to 831 g CO2-eq/kWh in the Rocky Mountains [76]. While it is unlikely that any step of the front end of the fuel cycle would happen in these areas, their GHG emission factors are representative of the range of values one might want to consider when performing a thorough LCA study. Using these lower and upper bounds would lead to decrease or increase of total base-load emissions by 9.0% and 7.6%, respectively, and to decrease or increase of total co-firing emissions by 0.3%. This shows a relatively low sensitivity of total life cycle GHG emissions to the primary energy mix. However, this factor would have a much higher impact if cumulated with the use of gasous diffusion rather than gas centrifuge for uranium enrichment. In this case, increases of total base-load and co-firing emissions could reach 229.9% and 7.8%, respectively, compared to the values listed in Table 4-6.

4.4.3 Sensitivity to the Amount of Concrete Used for Plant Construction

Table 4-6 shows that the construction phase contributes to a large share of total life cycle GHG emissions from the Mk1 PB-FHR plant – 43.1% of total base-load emissions and 1.5% of total co-firing emissions. Figure 4-5 shows the contributions of the various construction materials used in the Mk1 design to emissions from the construction phase. In particular, concrete structures contribute to 31.3% of emissions from the construction phase. This indicates that the ability to reduce GHG emissions resulting from concrete use, for instance by reducing the amount of concrete used for construction of the plant, bears significant environmental benefits. Figure 4-5 breaks down concrete emissions between various plant structures, based on the amounts of concrete used for these structures as listed in Table 4-2.

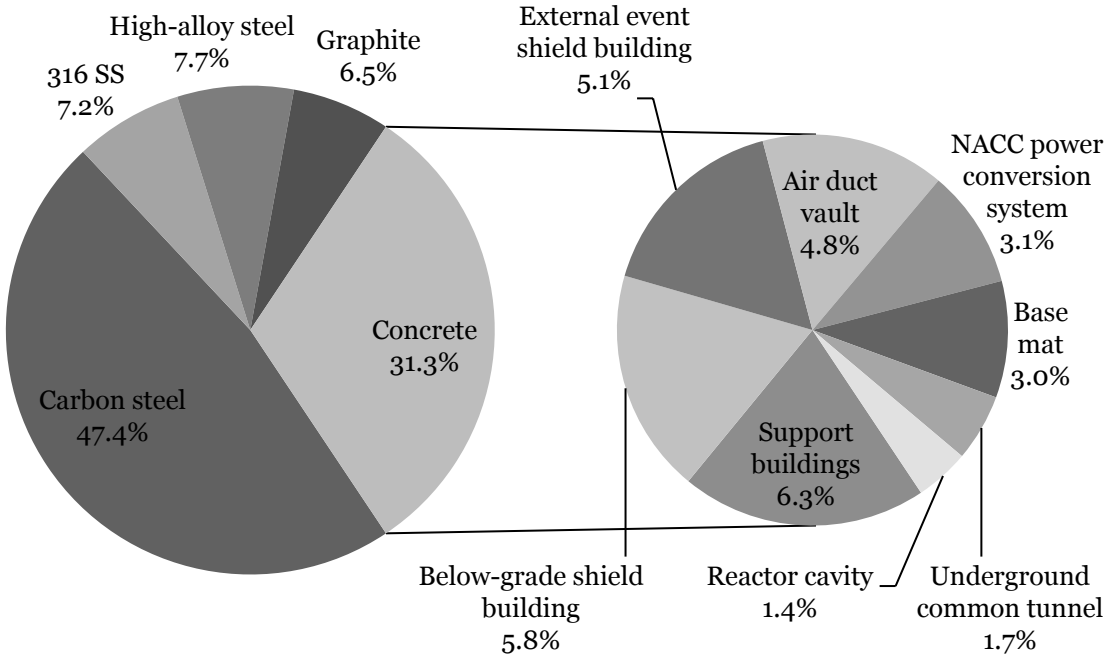

Figure 4-5. Main contributors to GHG emissions from the Mk1 construction phase.

The amount of concrete used in support buildings and other structures such as vehicle barriers around the plant owner controlled area is assumed to be ~25% of total other concrete inventories. Therefore, it represents the highest share of concrete inventories. However, this number could easily be reduced through optimization of the overall Mk1 site layout.

The amount of concrete used for the below-grade shield building is based on wall thicknesses, driven by soil support requirements. Future studies may conclude that thinner walls are acceptable while maintaining structural integrity of the below-grade external shield.

The main requirement driving the thickness, and therefore the concrete mass used for construction of the external event shield building is protection against missile impact. Studies have shown that SC walls have a missile impact resistance comparable to 30% thicker reinforced concrete walls [80]. A reduction of 30% in the amount of concrete used for construction of the external event shield building would lead to reductions of total base-load and co-firing emissions by 0.7% and 0.02%, respectively, compared to the values listed in Table 4-6.

Like most foundations, the base mat is designed to be able to spread weight loads if there is a weak area in the soil. The basis for determining what distance the foundation must be able to spread load is defined by codes, and future studies may conclude that a thinner base mat is acceptable to address this functional requirement. The same applies to all floor thicknesses, based on floor loading criteria.

In the end, if the total amount of concrete used in constructing the plant can be reduced by up to 30%, total base-load and co-firing emissions can be reduced by 4.0% and 0.1%, respectively, compared to the values listed in Table 4-6.

4.4.4 Sensitivity to the Type of Concrete Mix Used for Plant Construction

While the characteristics of construction steels are relatively uniform between various applications, the type of concrete mix used, and associated life cycle GHG emissions, strongly depends on the considered application. For nuclear construction, the most important factor to take into account is compressive strength, and standard values for compressive strengths in various plant designs range from 4000 psi (27.6 MPa) to 6000 psi (41,4 MPa).

Studies suggest that annual savings of up to 1 billion tons of CO_2 could be reached through the concrete sector if 50% of ordinary Portland cement (OPC) were replaced by a low-carbon alternative [81]. In particular, the capability to replace OPC with high-volume fly ash and limestone powder in self-consolidating concrete mixtures while conserving acceptable mechanical properties and durability performance is a key step towards achieving GHG emission reductions from the construction phase of nuclear power plants. A study by Celik et al. [82], using the GreenConcrete LCA tool [83] and experimental data, has compiled compressive strenghts and global warming potential (GWP) for concrete mixes replacing various proportions of OPC with high-volume fly ash and limestone powder. Their results are shown in Figure 4-6, where concrete mixes are ranked based on their compressive strength after 365 days of curing time. Each mix is labeled in terms of its content of OPC, high-volume fly ash and limestone powder, in this order (i.e. 55-30-15 means 55% OPC, 30% fly ash and 15% limestone).

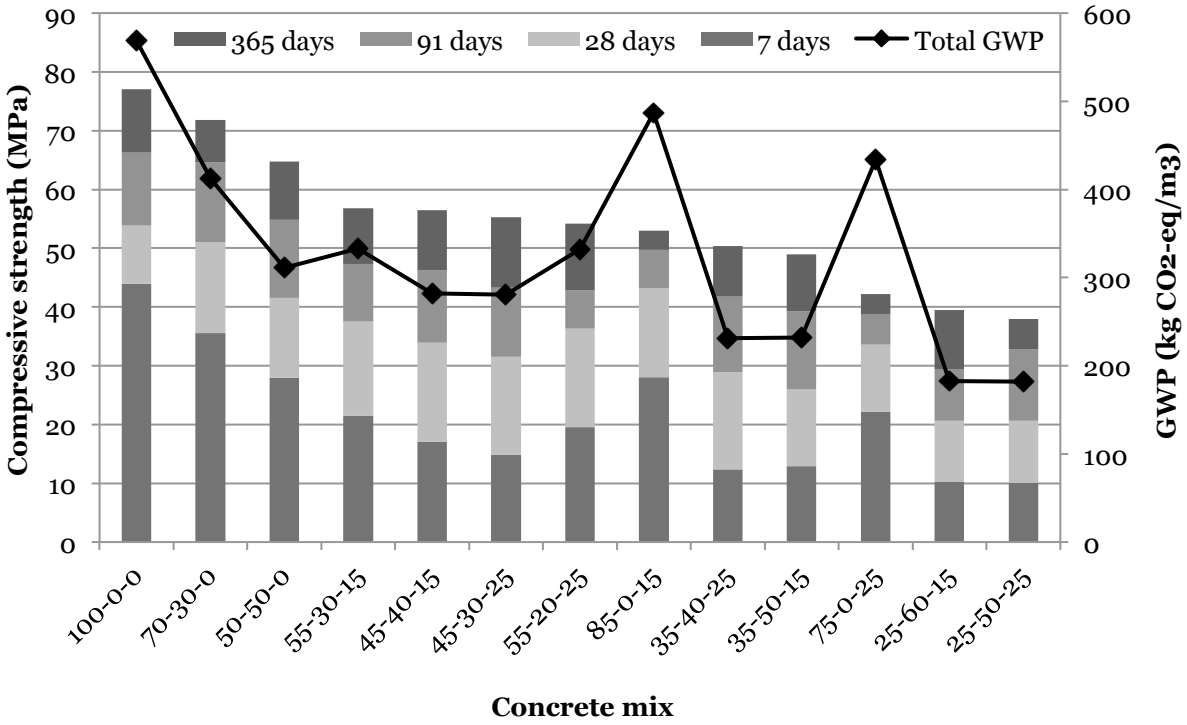

Figure 4-6. Comparison of average compressive strength of various concrete mixtures over time and associated GWP [82].

The study shows that compressive strengths higher than 4000 psi (27.6 MPa) are achieved by 91 days for all mixtures considered, compressive strengths higher than 5000 psi (34.5 MPa) are achieved after 91 days for mixtures with OPC proportions higher or equal to 35%, and compressive strengths higher than 6000 psi (41.4 MPa) are achieved after 365 days for mixtures with OPC proportions higher or equal to 35%. Most interestingly, the 35-40-25 mix has the third lowest GWP – 231 kg CO_2-eq/m^3 – among all considered mixtures, and its compressive strength exceeds the 6000 psi threshold by 91 days, making it an excellent candidate for nuclear construction with lower GHG emissions. With a 59% reduction in GWP compared to the baseline case, using this concrete mix rather than conventional concrete would reduce total base-load and co-firing emissions from the Mk1 PB-FHR by 8.0% and 0.3%, respectively, compared to the values listed in Table 4-6. This is a significant, achievable improvement over the baseline case considered for this study, which merits further investigation to verify that such concrete mixtures would satisfy code requirements for nuclear construction beyond the single compressive strength metric.

4.4.5 Results

Aggregated results from Section 4.3, including results from the sensitivity analysis performed in this Section, are shown in Figure 4-7, where they are compared to average values for the U.S. conventional nuclear fleet, as well as a range of values from the literature for nuclear power LCA [66-70]. The plant construction stage is the single largest contributor to life cycle

GHG emissions from both conventional nuclear power plants and the Mk1 PB-FHR in base-load configuration. Baseline life cycle emissions from the Mk1 PB-FHR in base-load configuration add up to 19.3 g CO_2-eq/kWh, which is 26% lower than average Generation II LWRs in the U.S., and well within the range of values reported in the literature. In comparison, because the Mk1 PB-FHR under co-firing configuration produces 59% of its electricity from natural gas burning, GHG emissions from the plant operation stage are 236.2 g CO_2-eq/kWh.

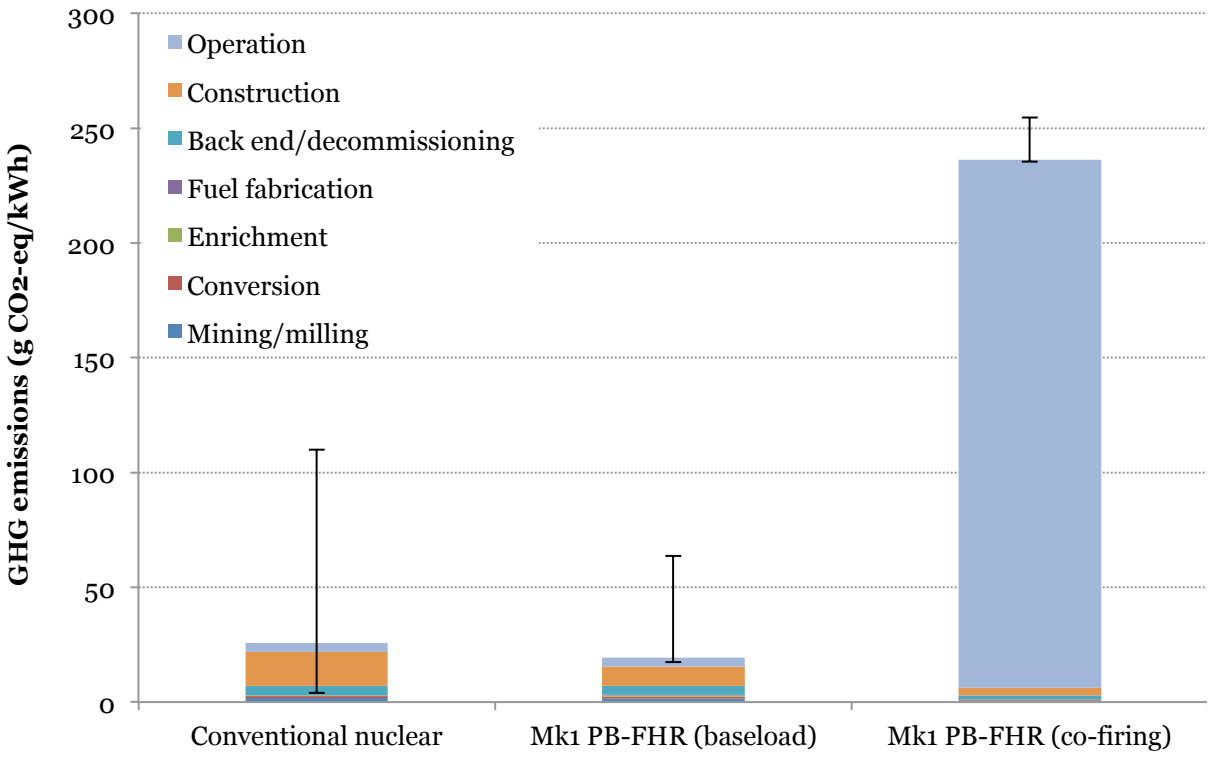

Figure 4-7. GHG emissions from conventional nuclear plants and the Mk1 PB-FHR in base-load and co-firing configurations.

With its base-load and power peaking capabilities, the Mk1 PB-FHR could compete with both traditional base-load power plants such as coal steam plants and NGCC plants, and peaking power plants such as GTSC plants to back up the increasing penetration of intermittent renewable energy sources such as wind and solar in electricity markets. Figure 4-8 shows a comparison of total emissions from conventional nuclear plants, Mk1 PB-FHR under base-load configuration, NGCC plants and coal plants on the left, and Mk1 PB-FHR under co-firing configuration and GTSC plants on the right. For fossil-fueled power plants, emission ranges and average U.S. values are obtained from the literature [66,70]. While GHG emissions from the Mk1 PB-FHR under base-load configuration are only 1.9% of emissions from average U.S. coal plants and 4.2% of emissions from average U.S. NGCC plants, it is also interesting to note that, due to its nuclear component and higher thermal efficiency, the Mk1 plant under co-firing configuration only produces 32% of GHG emissions of average U.S. GTSC plants.

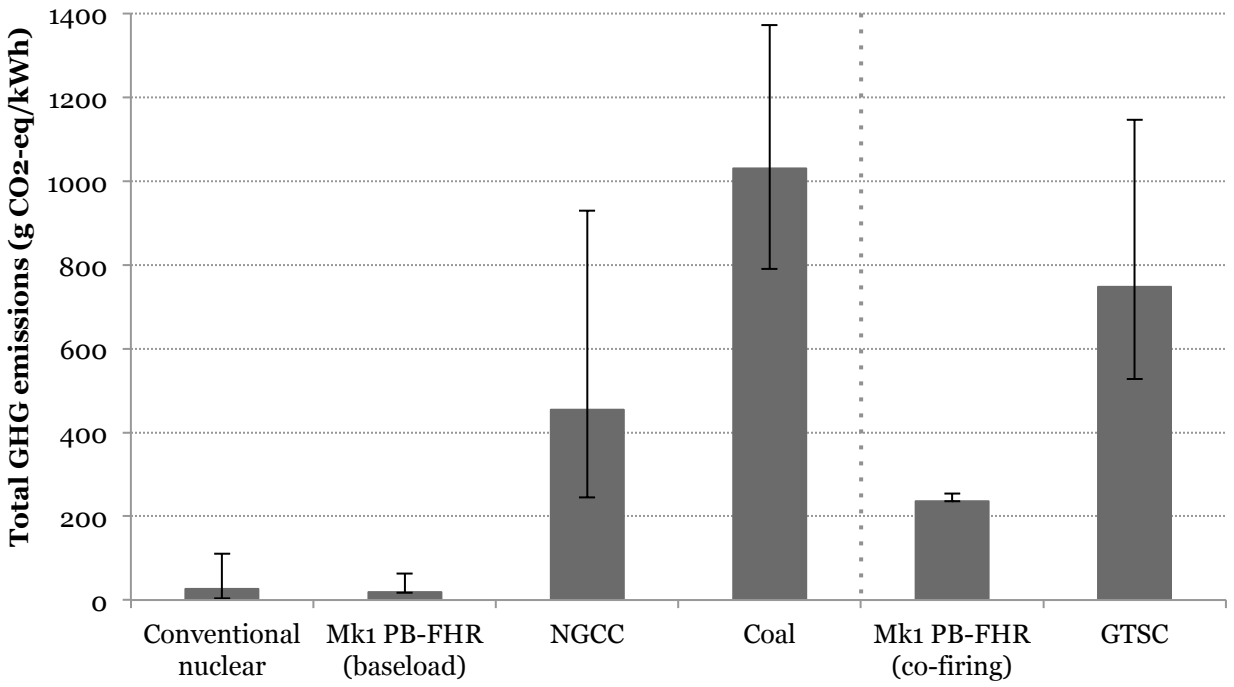

Figure 4-8. GHG emissions from a set of base-load (left) and peaking (right) power plants.

4.5 Discussion

This study shows that, while offering new proposition values for nuclear power such as peaking power capabilities through natural gas co-firing, advanced nuclear reactor designs like the Mk1 PB-FHR still compare favorably with other base-load plants – conventional nuclear, and especially NGCC and coal power plants – and peaking power plants such as GTSC plants in terms of GHG emissions per amount of electricity produced. Baseload operation of the Mk1 PB-FHR cuts GWP by 98.1% and 95.8% compared to production from average U.S. coal steam plants and NGCC plants, respectively, and co-firing operation of the Mk1 cuts GWP by 68.4% compared to production from average U.S. GTSC plants. To illustrate the strong potential of such a reduction in GHG emissions, should a reasonable carbon tax of \$30/t CO_2-eq be implemented in the U.S., baseload operation of the Mk1 PB-FHR would cut the additional cost related to this carbon tax by ¢3.0/kWh and ¢1.3/kWh compared to production from average U.S. coal steam plants and NGCC plants, respectively, and co-firing operation of the Mk1 would cut this additional cost by ¢1.5/kWh compared to production from average U.S. GTSC plants. These amounts are not negligible compared to levelized costs of electricity of ¢96/kWh for conventional coal plants, ¢66/kWh for conventional NGCC plants and ¢128/kWh for conventional GTSC plants [84]. Moreover, because co-firing will occur during periods of peak demand when electricity prices are generally much higher than low demand periods, the economic performance of the Mk1 PB-FHR will remain excellent even under significantly higher carbon taxes.

The use of a novel fuel form and higher uranium enrichment does not lead to significantly higher life cycle emissions from the front end of the fuel cycle, because of the optimized fuel utilization in the Mk1 design. The reactor construction phase also emits less GHG on a life cycle basis than conventional nuclear plants. Indeed, the loss of economies of scale with the use of 12 small units on a Mk1 site, which can be expected for all small modular reactor designs, is compensated by other design aspects, such as passive safety, which eliminates the need for bulky, expensive and redundant safety systems as well as complex equipment and power supplies. Additional material input reductions, and therefore life cycle GHG emission reductions, result from operation at near ambient pressures, reducing the complexity of construction and associated capital costs. Finally, from an environmental standpoint, higher net efficiencies of the Mk1 PB-FHR compared to conventional nuclear plants and fossil-fueled plants result in less waste heat, which lessens the thermal environmental impact and the costs of dealing with that waste heat.

This study shows that GHG emissions in the construction phase result primarily from the amounts of carbon steel and concrete used in the Mk1 design. Therefore, an important aspect for future studies will be to investigate how to reduce these amounts without compromising plant safety, and how to reduce life cycle emissions from the concrete used in future nuclear construction. In particular, modularity allows whole reactors or their components to be mass-produced and assembled uniformly, with materials being shipped to centralized factories and whole systems then being shipped to construction sites. This new trend could lead to significant improvements. Additional improvements would result from further optimizing the vertical stacking of major components to reduce the total height of the reactor building, optimizing the arrangement of equipment to reduce the building footprint, reducing the thickness of walls and floors, and eventually implementing larger design changes, such as having multiple reactor vessels inside a single reactor building.

Other aspects are not covered in this study because of insufficient information in the current Mk1 design, which need to be investigated in future analyses and similar analyses for other advanced reactor concepts. Most importantly, fuel cycle back end- and decommissioning-related emissions cannot be estimated at this point and may contribute to higher life cycle emissions. Also, no facility exists in the U.S. today to produce enriched lithium for flibe in industrial quantities. Therefore, it is difficult to estimate GHG emissions related to coolant production, which may further contribute to overall life cycle emissions of the PB-FHR. Finally, this study uses the current U.S. energy mix as a basis for most calculations. This is a common shortcoming of LCA studies, which neglect the fact that, if nuclear power, and high temperature reactors in particular, were to expand in the energy mix, the electricity and process heat required for major steps such as fuel enrichment and materials manufacturing would produce much lower GHG emissions.

Chapter 5 Conclusions and Future Work

The fundamental goal of this study was to demonstrate the value of both existing and newly developed frameworks for EM development and assessment applied to advanced nuclear reactor simulation, in particular the use of scaled IET experimental data to validate best-estimate codes, the use of validated best-estimate codes in support of design and licensing of advanced reactors that incorporate passive safety systems, and the use of LCA based on a pre-conceptual reactor design to inform design optimization at early stages of the development of advanced reactors. These methods were applied to the design of the PB-FHR under current development across several institutions in the U.S. and abroad.

The CIET 1.0 facility, which reproduces the thermal hydraulic response of an FHR under forced and natural circulation operation at reduced power, temperature and geometric scales, was designed, fabricated, filled up with Dowtherm A oil, and operated, using extensive instrumentation and automated controls. Isothermal, forced circulation flow tests around the loop were completed, with pressure data collection to determine friction losses in the system. CIET-specific friction loss correlations were compared with handbook values, and empirically measured values were implemented in the system codes that are to be validated by data from CIET 1.0. Simple, initial heated tests were also completed, including parasitic heat loss tests at nominal flow rates and heat inputs from the resistive heater, and feedback control tests on the primary pump and fan-cooled heat exchangers. Further heated tests included steady-state natural circulation in the primary loop and the DRACS loop, and simple power step change transients under forced cooling regime. Collected data was compared to predicted performance and forms the validation basis for best-estimate steady-state models in RELAP5-3D and FANCY.

The V&V study detailed here shows that both RELAP5-3D and FANCY are appropriate tools to model single loop and coupled natural circulation in the primary loop and the DRACS loop of CIET 1.0, as a first step towards predicting the performance of passive decay heat removal systems in FHRs. RELAP5-3D shows agreement within 1% and 8% with experimental data in the DRACS loop alone and coupled loops, respectively, and FANCY shows agreement within 3% and 13% with experimental data in the DRACS loop alone and coupled loops, respectively. This performance remains valid across the whole range of power inputs and temperature boundary conditions investigated for this study, which covers the range of values expected for natural circulation in CIET 1.0. For transient, forced cooling in the CTAH loop using heat input step changes, the agreement between RELAP5-3D results and experimental data is within 1°C when components with small surface areas compared to their thermal inertia (e.g. flanges, valves) are modeled as separate heat structures in the code. This further demonstrates that RELAP5-3D is a key tool to simulate the behavior of the oil loop in CIET 1.0, and could be appropriate to simulate similar behavior in FHRs.

The methodology developed for this study demonstrates the value of following the individual steps listed below, in the order shown, for proper validation of best-estimate models, which is

key to FHR safety analysis, using scaled IETs such as the CIET 1.0 facility or future full scale salt loops:

1. Isothermal, forced circulation flow around the loop, with pressure data collection to determine friction losses in the system. When handbook values are not applicable (e.g. for complex-shaped components), empirically measured values must be implemented in the best-estimate codes used for integral system modeling.
2. Steady-state single and coupled natural circulation. Collected data, compared to predicted performance, forms the validation basis for best-estimate steady-state models. In particular, steady-state experimental data is used to develop overall heat transfer coefficient correlations for heat exchangers and parasitic heat losses in major sections of the fluid loops.
3. Transient tests, starting with forced cooling at fixed mass flow rate and heat input step changes or other, more complex power profiles. This series of tests is used to characterize thermal response of the loop and provide insight for modeling of heat structures more or less tightly coupled to the fluid.

This study is the first iteration of a series of benchmarking thermal hydraulic exercises in support of FHR technology development. The extensive modularity of the CIET 1.0 facility makes it a test rig of choice for a variety of FHR benchmarking exercises, and future work will involve similar validation efforts using other best-estimate codes. Thermal transients (startup, shutdown, LOFC with scram and LOHS with scram) will also be run on CIET 1.0. The set of collected data will serve the double purpose of confirming strategies for operation of FHRs, and validating best estimate transient models. CIET 1.0 is equipped with all necessary instrumentation and controls to analyze control logic for prototypical FHRs. To this effect, an initial control logic strategy has already been implemented for startup of the facility, and future tests will include load following and more complex transients.

With the detailed design of the 236-MWth Mk1 PB-FHR now available, modifications can be made to the CIET 1.0 facility to enhance scaling properties between the model and full scale prototype. Modifications will include testing of various DHX designs, including twisted tube heat exchangers, based on performance data collected from the current CIET 1.0 DHX. The resistive heater will also be modified to better match friction losses and relative residence time in the prototypical Mk1 PB-FHR core. Finally, the primary loop head tank will be integrated into the flow loop to replicate the location of the main salt pumps hot well on the hot leg of the Mk1 PB-FHR. All these modifications will be implemented during the second phase of a U.S.-Department-of-Energy-sponsored integrated research project (IRP), while data from CIET 1.0 is used for benchmarking of various thermal hydraulic codes used or developed by the members of the IRP and their partners.

In order to further assess the reliability of the DRACS, which serves as a passive safety cooling system for FHRs, the RMPS methodology was summarized and implemented for a preliminary risk assessment of the performance of the Mk1 PB-FHR DRACS. The performance of the DRACS was assessed under an LOFC transient with the normal shutdown cooling system not functioning, leaving natural circulation as the sole cooling mechanism. The failure criterion

was identified to be the peak bulk coolant outlet temperature exceeding 816°C, because of metallic components thermal limits. A model of the Mk1 PB-FHR reactor, including the DRACS, in RELAP5-3D was used to perform a sensitivity and reliability analysis of the passive safety cooling system performance under various sets of key parameters. The performance of the DRACS appeared to be mainly dependent on core thermal power during normal operation, friction losses in the system and primary pumps coast down time. With the probability distributions of key parameters used in this study, based on preliminary assumptions, the reliability of the DRACS was estimated to be 99%, with a confidence level greater than 95%.

RSM using aPC expansions was also summarized, implemented in a custom algorithm and applied to the RELAP5-3D model of the Mk1 PB-FHR to calculate the mean and standard deviation of the performance function, defined here as the margin between the peak bulk coolant outlet temperature and the failure criterion of 816°C, as well as physically and mathematically meaningful sensitivity indices associated with the probability distributions of the preliminary set of characteristic input parameters used for this reliability study. Using aPC, the mean value and standard deviation of the performance function are evaluated as -40°C and 10°C, respectively. Therefore, the mean peak bulk coolant outlet temperature is expected to be 776°C and, considering the probability distributions of input parameters selected for this preliminary study, the peak bulk coolant outlet temperature is expected to lie in an interval between 756°C and 796°C with a confidence level of 95%, leaving a margin of 20°C below the failure criterion of 816°C. The complementary sensitivity indices calculated using aPC confirm that the performance – and the variance in the performance – of the DRACS is mainly dependent on core thermal power during normal operation, friction losses in the system and primary pumps coast down time.

As a result, this reliability assessment study proved that an efficient way to reduce risks associated with operation of the DRACS would be to reduce uncertainty related to the performance of the most impactful parameters, identified here as the actual core thermal power during normal operation, friction losses in the DHX branch and the DRACS, and primary pumps coast down time. Because the PB-FHR design is still in an early development phase, risk mitigation can be further achieved by properly designing key sub-systems, such as the outlet plenum or air dampers on the condenser for the TCHX. Moreover, in order to ensure proper natural circulation in the DRACS, geometrical integrity of key components must be preserved, which can be ensured by clever design. A better understanding of the core behavior, through expert judgment and PIRT-type exercises, will help engineers and operators identify key components for proper operation of the DRACS, inform their designs, and eventually monitor their associated parameters throughout the lifetime of the reactor. As with all nuclear power plants, further risk mitigation can be achieved through redundancy of safety systems. Regarding the DRACS, such systems include, but may not be limited to, the normal shutdown cooling system, and a reactor cavity cooling system. These sub-systems need further design analysis and should eventually contribute to reducing the risks associated with operation of the DRACS. Finally, constant monitoring and inspection methods should be investigated, as they are the best way to prevent damage from occurring during operation of the reactor.

This novel approach of risk assessment and mitigation of a passive safety cooling system, though preliminary, for a reactor design that is still in its early development phase, should be considered with interest regarding the ultimate goal of licensing FHRs and other advanced reactor designs. In particular, as the design matures, additional validation data is collected from IETs and eventually from startup testing and online monitoring, PRA including results from RMPS must be considered and used as a living tool that informs design upgrades, maintenance and best operational practice.

Beyond the importance of safety in design and optimization of advanced nuclear reactors, costs and environmental impacts also play a key role. In this study, we expanded the scope of LCA for conventional nuclear power plants to an advanced nuclear reactor design, using the example of the Mk1 PB-FHR. Using both data from the literature for conventional nuclear fuel cycle LCA and the EIO-LCA method applied to well-developed aspects of the Mk1 design, we showed that the Mk1, when used as a base-load plant, achieves life cycle GHG emissions comparable to those of conventional nuclear power plants, and only 1.9% of emissions from average U.S. coal plants and 4.2% of emissions from average U.S. NGCC plants using the same turbine technology. The Mk1 PB-FHR, with its NACC power conversion cycle, can also operate as a peaking power plant, and we showed that in natural gas co-firing configuration, the plant only produces 32% of GHG emissions of average U.S. GTSC plants, due to its nuclear component and higher thermal efficiency.

One important share of the life cycle GHG emissions for the Mk1 PB-FHR is related to concrete use during construction of the reactor. This finding suggests that improvements in the design of the plant could arise from better construction methods, including further development of SC wall modular construction, and other concrete inventory reductions, including optimized elevations for the reactor building based on better arrangements of reactor internals.

Overall, this study shows that the Mk1 PB-FHR could be a key player in addressing climate change issues from global GHG emissions, by serving both as a base-load plant displacing conventional coal steam plants, and as a peaking power plant displacing natural gas plants to compensate for intermittency of the increasing share of variable renewable energy in the U.S. and global energy mixes.

References

1. The World Bank, "Population Growth (Annual %)," *http://data.worldbank.org/indicator/SP.POP.GROW*. Accessed: April 11, 2015.
2. International Energy Agency, "Key World Energy Statistics 2014" (2014).
3. C. Forsberg, P. F. Peterson, and P. S. Pickard, "Molten-Salt-Cooled Advanced High-Temperature Reactor for Production of Hydrogen and Electricity," *Nuclear Technology*, **144** (3), pp. 289-302 (2003).
4. D. T. Ingersoll et al., "Status of Preconceptual Design of the Advanced High-Temperature Reactor (AHTR)," Oak Ridge National Laboratory, ORNL/TM-2004/104 (2004).
5. P. F. Peterson and H. Zhao, "A Flexible Base-Line Design for the Advanced High-Temperature Reactor Utilizing Metallic Reactor Internals (AHTR-MI)," *Proceedings of the 2006 International Congress on Advances in Nuclear Power Plants (ICAPP '06)*, Reno, Nevada, June 4-8, 2006, American Nuclear Society (2006).
6. T. Fei et al., "A Modular Pebble-Bed Advanced High Temperature Reactor," Department of Nuclear Engineering, University of California, Berkeley, UCBTH-08-001 (2008).
7. S. R. Greene et al., "Pre-Conceptual Design of a Fluoride-Salt-Cooled Small Modular Advanced High-Temperature Reactor (SmAHTR)," Oak Ridge National Laboratory, ORNL/TM-2010/199 (2010).
8. D. E. Holcomb, F. J. Peretz, and A. L. Qualls, "Advanced High Temperature Reactor Systems and Economics Analysis," Oak Ridge National Laboratory, ORNL/TM-2011/364 (2011).
9. V. K. Varma, D. E. Holcomb, F. J. Peretz, E. C. Bradley, D. Ilas, A. L. Qualls, and N. M. Zaharia, "AHTR Mechanical, Structural, and Neutronic Preconceptual Design," ORNL/TM-2012/320 (2012).
10. D. L. Krumwiede et al., "Design of a pre-conceptual pebble-bed, fluoride-salt-cooled, high-temperature reactor commercial power plant," *Proceedings of the 2014 International Congress on Advances in Nuclear Power Plants (ICAPP '14)*, Charlotte, North Carolina, April 6-9, 2014, American Nuclear Society (2014).
11. C. Andreades et al., "Technical Description of the 'Mark 1' Pebble-Bed Fluoride-Salt-Cooled High-Temperature Reactor (PB-FHR) Power Plant," Department of Nuclear Engineering, University of California, Berkeley, UCBTH-14-002 (2014).
12. U.S. Nuclear Regulatory Commission, "Regulatory Guideline 1.203. Transient and Accident Analysis Methods" (2005).
13. U.S. Nuclear Regulatory Commission, "Quantifying Reactor Safety Margins. Application of Code Scaling, Applicability, and Uncertainty Evaluation Methodology to a Large-Break, Loss-of-Coolant Accident," NUREG/CR-5249 (1989).
14. N. Zuber, "A Hierarchical, Two-Tiered Scaling Analysis," Appendix D to *An Integrated Structure and Scaling Methodology for Severe Accident Technical Issue Resolution*, NUREG/CR-5809 (1991).
15. N. Zweibaum et al., "Phenomenology, Methods and Experimental Program for Fluoride-Salt-Cooled, High-Temperature Reactors (FHRs)," *Progress in Nuclear Energy*, **77**, pp. 390-405 (2014).

16. C. Andreades, R. O. Scarlat, L. Dempsey, and P. F. Peterson, “Reheat Air-Brayton Combined Cycle Power Conversion Design and Performance under Nominal Ambient Conditions,” *Journal of Engineering for Gas Turbines and Power*, **136** (7) (2014).
17. C. Andreades, L. Dempsey, and P. F. Peterson, “Reheat Air-Brayton Combined Cycle Power Conversion Off-Nominal and Transient Performance,” *Journal of Engineering for Gas Turbines and Power*, **136** (7) (2014).
18. M. W. Rosenthal et al., “Molten Salt Reactor Program Semiannual Progress Report for the Period Ending August 31, 1969,” Oak Ridge National Laboratory, ORNL-4449, pp. 52-56 (1970).
19. A. T. Cisneros et al., “Fluoride-Salt-Cooled, High-Temperature Reactor (FHR) Methods and Experiments Program White Paper,” Department of Nuclear Engineering, University of California, Berkeley, UCBTH-12-002 (2013).
20. D. F. Williams, L. M. Toth, and K. T. Clarno, “Assessment of Candidate Molten Salt Coolants for the Advanced High-Temperature Reactor (AHTR),” Oak Ridge National Laboratory, ORNL/TM-2006/12 (2006).
21. R. O. Scarlat, “Design of Complex Systems to Achieve Passive Safety : Natural Circulation Cooling of Liquid Salt Pebble Bed Reactors,” PhD Dissertation, Department of Nuclear Engineering, University of California, Berkeley (2012).
22. International Atomic Energy Agency, “Natural Circulation in Water Cooled Nuclear Power Plants: Phenomena, Models, and Methodology for System Reliability Assessments,” International Atomic Energy Agency, IAEA-TECDOC-1474 (2005).
23. R. B. Briggs, “Molten-Salt Reactor Program: Semiannual Progress Report For Period Ending August 31, 1966,” Oak Ridge National Laboratory, ORNL-4037, p. 42 (1967).
24. R. E. Thoma, “Chemical Aspects of MSRE Operations,” Oak Ridge National Laboratory, ORNL-4658, p. 116 (1971).
25. L. E. McNeese, “Molten-Salt Reactor Program: Semiannual Progress Report for Period Ending February 29, 1976,” Oak Ridge National Laboratory, ORNL-5132, p. 20 (1976).
26. C. B. Davis, “Implementation of Molten Salt Properties into RELAP5-3D/ATHENA,” Idaho National Laboratory, INEEL/EXT-05-02658 (2005).
27. C. D. Fletcher et al., “Adequacy Evaluation of RELAP5/MOD3, Version 3.2.1.2 for Simulating AP600 Small Break Loss-of-Coolant Accidents,” INEL-96/0400 (1997).
28. C. J. Cavanaugh and P. F. Peterson, “Scale Modeling of Oscillating Sheet Jets for the HYLIFE-II Inertial Confinement Fusion Reactor,” *Fusion Technology*, **26**, pp. 917-921 (1994).
29. P. Bardet and P. F. Peterson, “Options for Scaled Experiments for High Temperature Liquid Salt and Helium Fluid Mechanics and Convective Heat Transfer,” *Nuclear Technology*, **163** (3), pp. 344-357 (2008).
30. N. Zweibaum et al., "Role and Status of Scaled Experiments in the Development of Fluoride-Salt-Cooled, High-Temperature Reactors," *Proceedings of the 2015 International Congress on Advances in Nuclear Power Plants (ICAPP '15)*, Nice, France, May 3-6, 2015, French Society of Nuclear Energy (2015).
31. R. O. Scarlat et al., “Design and Licensing Strategies for the Fluoride-Salt-Cooled, High-Temperature Reactor (FHR) Technology,” *Progress in Nuclear Energy*, **77**, pp. 406-420 (2014).

32. P. M. Bardet, E. D. Blandford, M. Fratoni, A. Niquille, E. Greenspan, and P. F. Peterson, "Design, Analysis and Development of the Modular PB-AHTR," *Proceedings of the International Congress on Advances in Nuclear Power Plants (ICAPP '08),* Anaheim, California, June 8-12, 2008, American Nuclear Society (2008).
33. E. D. Blandford and P. F. Peterson, "Global Scaling Analysis for the Pebble-Bed, Advanced High-Temperature Reactor," *Proceedings of NURETH-13*, Kanazawa City, Ishikawa Prefecture, Japan, September 27-October 2, 2009, American Nuclear Society (2009).
34. M. S. Sohal, M. A. Ebner, P. Sabharwall, and P. Sharpe, "Engineering Database of Liquid Salt Thermophysical and Thermochemical Properties," Idaho National Laboratory, INL/EXT-10-18297 (2013).
35. The Dow Chemical Company, "Dowtherm A Heat Transfer Fluid Product Technical Data" (1997).
36. C. Galvez, "Design and Transient Analysis of Passive Safety Cooling Systems for Advanced Nuclear Reactors," Ph.D. Dissertation, Department of Nuclear Engineering, University of California, Berkeley (2011).
37. E. D. Blandford and P. F. Peterson, "A Novel Buoyantly-Driven Shutdown Rod Design for Passive Reactivity Control of the PB-AHTR," *Fourth International Topical Meeting on High Temperature Reactor Technology, Volume 2*, Washington, DC, September 28-October 1, 2008, American Society of Mechanical Engineers (2008).
38. W. L. Oberkampf and T. G. Trucano, "Verification and Validation Benchmarks," *Nuclear Engineering and Design*, **238**, pp. 716-743 (2008).
39. R. L. Moore, "Implementation of Dowtherm A Properties into RELAP5-3D/ATHENA," Idaho National Laboratory, INL/EXT-10-18651 (2010).
40. P. K. Vijayan, "Experimental Observations on the General Trends of the Steady State and Stability Behaviour of Single-Phase Natural Circulation Loops," *Nuclear Enginering and Design*, **215**, pp. 139-152 (2002).
41. J. Jafari, F. D'Auria, H. Kazeminejad, and H. Davilu, "Reliability Evaluation of a Natural Circulation System," *Nuclear Engineering and Design*, **224**, pp. 79-104 (2003).
42. M. Marquès et al., "Methodology for the Reliability Evaluation of a Passive System and its Integration into a Probabilistic Safety Assessment," *Nuclear Engineering and Design*, **235**, pp. 2612-2631 (2005).
43. A. K. Nayak, M. R. Gartia, A. Antony, G. Vinod, and R. K. Sinha, "Passive System Reliability Analysis Using the APSRA Methodology," *Nuclear Engineering and Design*, **238**, pp. 1430-1440 (2008).
44. International Atomic Energy Agency, "Progress in Methodologies for the Assessment of Passive Safety System Reliability in Advanced Reactors," IAEA-TECDOC-1752 (2004).
45. A. T. Cisneros, "Development of Depletion Analysis Methods and Design Optimization Methods for Pebble Bed Reactors Applied to the Design of the Pebble Bed Fluoride Salt Cooled High Temperature Reactor (PB-FHR)," Ph.D. dissertation, University of California, Berkeley (2013).
46. G. Cao et al., "Fluoride-Salt-Cooled High Temperature Reactor (FHR) Materials, Fuels and Components White Paper," Department of Nuclear Engineering, University of California, Berkeley, UCBTH-12-003 (2013).

47. ASME Boiler & Pressure Vessel Code, Section III, Division 1, "Rules for Construction of Nuclear Facility Components," American Society of Mechanical Engineers (2007).
48. S. A. Eide, T. E. Wierman, C. D. Gentillon, D. M. Rasmuson, and C. L. Atwood, "Industry-Average Performance for Components and Initiating Events at U.S. Commercial Nuclear Power Plants," U.S. Nuclear Regulatory Commission, NUREG/CR-6928, and Idaho National Laboratory, INL/EXT-06-11119 (2007).
49. S. Oladyshkin, F. P. J. de Barros, and W. Nowak, "Global Sensitivity Analysis: a Flexible and Efficient Framework with an Example from Stochastic Hydrogeology," *Advances in Water Resources*, **37**, pp. 10-22 (2012).
50. S. Oladyshkin and W. Nowak, "Data-Driven Uncertainty Quantification Using the Arbitrary Polynomial Chaos Expansion," *Reliability Engineering and System Safety*, **106**, pp. 179-190 (2012).
51. S. Oladyshkin and W. Nowak, "Polynomial Response Surfaces for Probabilistic Risk Assessment and Risk Control via Robust Design," Novel Approaches and Their Applications in Risk Assessment, Dr. Yuzhou Luo, pp. 317-344 (2012).
52. J. A. S. Witteveen, S. Sarkar, and H. Bijl, "Modeling Physical Uncertainties in Dynamic Stall Induced Fluid-Structure Interaction of Turbine Blades Using Arbitrary Polynomial Chaos," *Computers and Structures*, **85**, pp. 866-887 (2007).
53. H. Li, P. Sarma and D. Zhang, "A Comparative Study of the Probabilistic-Collocation and Experimental-Design Methods for Petroleum-Reservoir Uncertainty Quantification," *Society of Petroleum Engineers Journal*, **16** (2), pp. 429-439 (2011).
54. G. E. P. Box and K. B. Wilson, "On the Experimental Attainment of Optimum Conditions," *Journal of the Royal Statistical Society. Series B (Methodological),* **13** (1), pp. 1-45 (1951).
55. L. Olivi, "Response Surface Methodology - Handbook for Nuclear Reactor Safety," Luxembourg: Commission of the European Communities (1985).
56. M. Brandyberry and G. Apostolakis, "Response Surface Approximation of a Fire Risk Analysis Computer Code," *Reliability Engineering & System Safety*, **29** (2), pp. 153-184 (1990).
57. C. J. Fong, "Reliability Analysis of a Passive Cooling System Using a Response Surface with an Application to the Flexible Conversion Ratio Reactor," M.S. Thesis, Massachusetts Institute of Technology (2008).
58. N. Wiener, "The Homogeneous Chaos," *American Journal of Mathematics*, **60** (4), pp. 897-936 (1938).
59. D. Xiu, "Numerical Methods for Stochastic Computations: A Spectral Method Approach," Princeton University Press (2010).
60. I. M. Sobol, "Sensitivity Estimates for Nonlinear Mathematical Models," *Mathematical Modeling and Computational Experiments*, **1**, pp. 407-414 (1993).
61. I. M. Sobol, "Global Sensitivity Indices for Nonlinear Mathematical Models and their Monte Carlo Estimates," *Mathematics and Computers in Simulation*, **55** (1-3), pp. 271-280 (2001).
62. T. Homma and A. Saltelli, "Importance Measures in Global Sensitivity Analysis of Nonlinear Models," *Reliability Engineering & System Safety*, **52** (1), pp. 1-17 (1996).
63. F. S. G. Richards, "A Method of Maximum-Likelihood Estimation," *Journal of the Royal Statistical Society. Series B (Methodological)*, **23** (2), pp. 469-475 (1961).

64. J. A. Nelder, “Inverse Polynomials, a Useful Group of Multi-Factor Response Functions,” *Biometrics*, **22** (1), pp. 128-141 (1966).
65. American Society for Testing and Materials, “Corrosion Monitoring in Industrial Plants Using Nondestructive Testing and Electrochemical Methods” (1986).
66. P. J. Meier, “Life-Cycle Assessment of Electricity Generation Systems and Applications for Climate Change Policy Analysis,” Ph.D. dissertation, University of Wisconsin, Madison, WI (2002).
67. V. M. Fthenakis and H. C. Kim, “Greenhouse-Gas Emissions from Solar Electric- and Nuclear Power: A Life-Cycle Study,” *Energy Policy*, **35**, pp. 2549-2557 (2007).
68. M. Lenzen, “Life Cycle Energy and Greenhouse Gas Emissions of Nuclear Energy: A Review,” *Energy Conversion and Management*, **49**, pp. 2178-2199 (2008).
69. E. S. Warner and G. A. Heath, “Life Cycle Greenhouse Gas Emissions of Nuclear Electricity Generation: Systematic Review and Harmonization,” *Journal of Industrial Ecology*, **16** (S1), pp. S73-S92 (2012).
70. E. Masanet et al., “Life-Cycle Assessment of Electric Power Systems,” *Annual Review of Environment and Resources*, **38**, pp. 107-136 (2013).
71. P. F. Peterson, H. Zhao, and R. Petroski, “Metal And Concrete Inputs For Several Nuclear Power Plants,” Department of Nuclear Engineering, University of California, Berkeley, UCBTH-05-001 (2005).
72. C. T. Hendrickson, A. Horvath et al., “Economic Input-Output Models for Environmental Life-Cycle Assessment,” *Environmental Science and Technology*, **4**, pp. 184A-191A (1998).
73. U.S. Energy Information Administration, “Electric Power Monthly with Data for November 2014,” U.S. Department of Energy (2015).
74. C. W. Forsberg and D. Curtis, “Meeting the Needs of a Nuclear-Renewables Electrical Grid With a Fluoride-Salt-Cooled High-Temperature Reactor Coupled to a Nuclear Air-Brayton Combined-Cycle Power System,” *Nuclear Technology*, **185** (3), pp. 281-295 (2014).
75. World Nuclear Association, “Uranium Enrichment,” http://www.world-nuclear.org/info/Nuclear-Fuel-Cycle/Conversion-Enrichment-and-Fabrication/Uranium-Enrichment/. Accessed: April 18, 2015.
76. U.S. Environmental Protection Agency, “eGRID2012 Version 1.0: Year 2009 Summary Tables” (2012).
77. Carnegie Mellon University Green Design Institute, “Economic Input-Output Life Cycle Assessment (EIO-LCA), US 1997 Industry Benchmark Model,” *http://www.eiolca.net* (2008).
78. A. Gandrik, B. Wallace, L. Demick, S. Melancon, and M. Patterson, “Assessment of High Temperature Gas-Cooled Reactor (HTGR) Capital and Operating Costs,” Idaho National Laboratory, TEV-1196 (2011).
79. P. L. Spath and M. K. Mann, “Life Cycle Assessment of a Natural Gas Combined-Cycle Power Generation System,” National Renewable Energy Laboratory, NREL/TP-570-27715 (2000).
80. J. C. Bruhl, A. H. Varma, and W. H. Johnson, “Design of Composite SC Walls to Prevent Perforation from Missile Impact,” *International Journal of Impact Engineering*, **75**, pp. 75-87 (2015).

81. C. D. Tomkins, “Redefining What’s Possible for Clean Energy by 2020, *Gigaton Throwdown*, San Francisco (2009).
82. K. Celik, C. Meral, A. P. Gursel, P. K. Mehta, A. Horvath, and P. J. M. Monteiro, “Mechanical Properties, Durability, and Life-Cycle Assessment of Self-Consolidating Concrete Mixtures Made with Blended Portland Cements Containing Fly Ash and Limestone Powder,” *Cement & Concrete Composites*, **56**, pp. 59-72 (2015).
83. A. P. Gursel and A. Horvath, “GreenConcrete LCA Tool,” University of California, Berkeley (2012).
84. U.S. Energy Information Administration, “Annual Energy Outlook 2015 with projections to 2040,” DOE/EIA-0383 (2015).
85. D.A. Nield and A. Bejan, “Convection in Porous Media,” New York, NY: Springer (1999).
86. J. Villadsen and M. L. Michelsen, “Solution of Differential Equation Models by Polynomial Approximation,” Englewood Cliffs, NJ: Prentice-Hall (1978).

Appendix A RELAP5-3D Model of CIET 1.0

This Appendix lists all parameters – for both hydrodynamic components and heat structures – used to build the model of the CIET 1.0 facility in RELAP5-3D, represented by the detailed nodalization diagram in Figure A-1. For reproducibility purposes, the RELAP5-3D input deck used to generate the results shown in Figure 2-22 is also included in Section A.2.

A.1 Detailed Nodalization Diagram and List of Parameters Used in the RELAP5-3D CIET Model

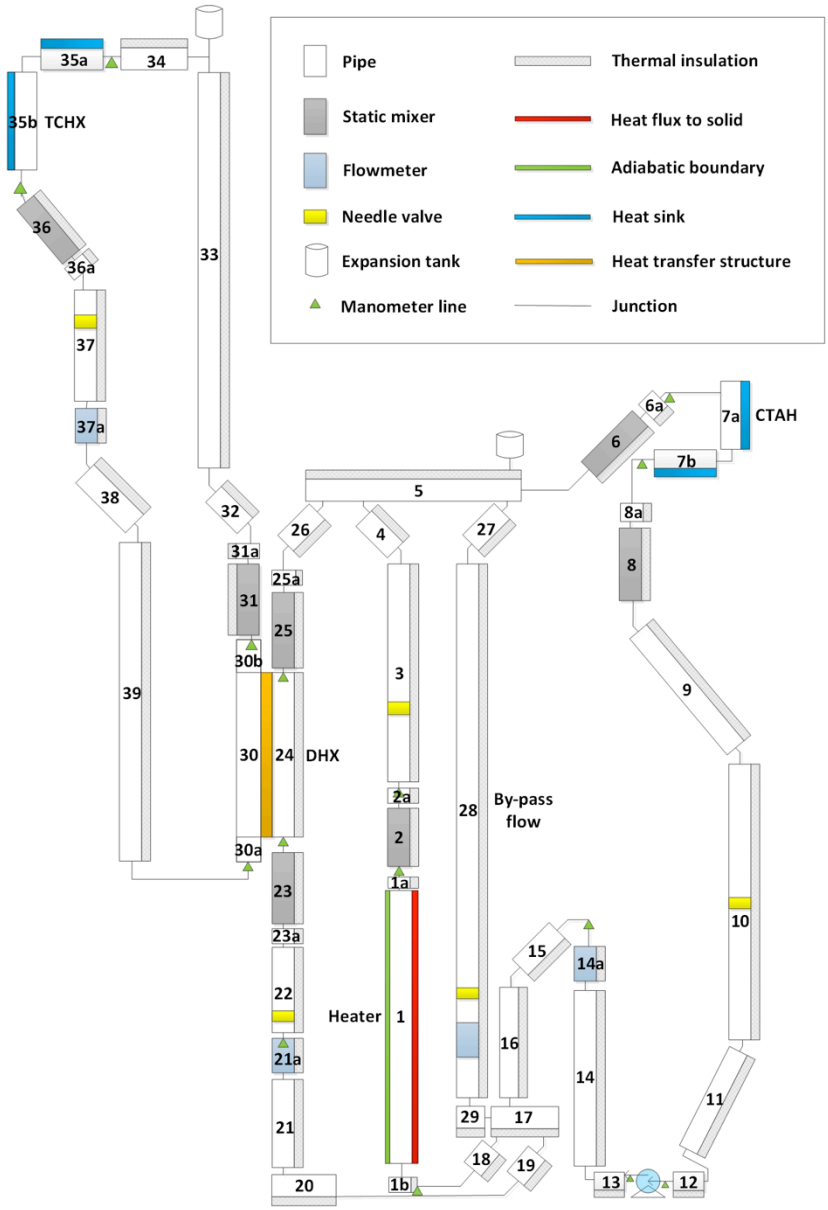

Figure A-1. Detailed CIET 1.0 nodalization diagram for RELAP5-3D and FANCY.

Table A-1. Hydrodynamic component parameters of the RELAP5-3D CIET model.

Component	Number on diagram	RELAP volume number	Length (m)	Vertical angle (°)	Hydraulic diameter (m)	Flow area (m²)	Form losses
Heater branch (bottom to top)							
Heater bottom head	1b	11	0.19685	90	6.60E-03	3.64E-04	3.95
Heater	1	10	1.6383	90	6.60E-03	3.64E-04	
Heater top head	1a	12	0.0889	90	6.60E-03	3.64E-04	3.75
Static mixer pipe	2a	20	0.149425	90	2.79E-02	6.11E-04	1.8
Static mixer	2	21	0.33	90	2.79E-02	6.11E-04	*
Pipe	3	30	1.2827	90	2.79E-02	6.11E-04	3.15
Pipe	4	40	0.2413	49.743387	2.79E-02	6.11E-04	2.4
Branch	5	50	0.7493	0	2.79E-02	6.11E-04	
CTAH branch (top to bottom)							
Static mixer pipe	6a	60	0.1526	51.526384	2.79E-02	6.11E-04	5.05
Static mixer	6	61	0.33	51.526384	2.79E-02	6.11E-04	*
CTAH (vertical)	7a	71	0.3302	-90	1.19E-02	1.33E-03	3.9
CTAH (horizontal)	7b	72	1.2342	0	1.19E-02	1.33E-03	*
Static mixer pipe	8a	80	0.22245	-90	2.79E-02	6.11E-04	3.75
Static mixer	8	81	0.33	-90	2.79E-02	6.11E-04	*
Pipe	9	90	0.7112	-42.73211	2.79E-02	6.11E-04	0.8
Pipe	10	100	2.4511	-90	2.79E-02	6.11E-04	0.45
Pipe	11	110	0.4826	-63.47465	2.79E-02	6.11E-04	2.4
Pipe	12	120	0.333375	0	2.79E-02	6.11E-04	21.65
Pipe	13	130	1.273175	0	2.79E-02	6.11E-04	12.95
Pipe	14	140	0.6687	90	2.79E-02	6.11E-04	2.4
Flowmeter	14a	141	0.36	90	2.79E-02	6.11E-04	*
Pipe	15	150	0.3556	-49.36983	2.79E-02	6.11E-04	0.8
Pipe	16	160	0.644525	-90	2.79E-02	6.11E-04	1.9
Branch	17	170	0.473075	0	2.79E-02	6.11E-04	
DHX branch (bottom to top)							
Pipe	19	190	0.219075	-31.44898	2.79E-02	6.11E-04	7.5
Pipe	20	200	0.33655	0	2.79E-02	6.11E-04	
Pipe	21	210	0.487725	90	2.79E-02	6.11E-04	4.4
Flowmeter	21a	211	0.36	90	2.79E-02	6.11E-04	*
Pipe	22	220	0.69215	90	2.79E-02	6.11E-04	9.95
Static mixer pipe	23a	230	0.0891	90	2.79E-02	6.11E-04	1.35
Static mixer	23	231	0.33	90	2.79E-02	6.11E-04	*
DHX shell side	24	240	1.18745	90	5.65E-03	9.43E-04	23.9
Static mixer pipe	25a	250	0.22245	90	2.79E-02	6.11E-04	1.35
Static mixer	25	251	0.33	90	2.79E-02	6.11E-04	*
Pipe	26	260	0.2159	52.571994	2.79E-02	6.11E-04	1.75
Pipe	18	180	0.1778	-40.00520	2.79E-02	6.11E-04	5.15
DRACS loop (counterclockwise)							
DHX tube side	30a	301	0.111125	90	6.93E-03	7.18E-04	
DHX tube side	30	300	1.18745	90	6.93E-03	7.18E-04	3.3
DHX tube side	30b	302	0.18415	90	6.93E-03	7.18E-04	
Static mixer pipe	31a	310	0.143075	90	2.79E-02	6.11E-04	1.35
Static mixer	31	311	0.33	90	2.79E-02	6.11E-04	*
Pipe	32	320	0.238125	54.422897	2.79E-02	6.11E-04	0.8
Pipe	33	330	3.0099	90	2.79E-02	6.11E-04	2.75

Component	Number on diagram	RELAP volume number	Length (m)	Vertical angle (°)	Hydraulic diameter (m)	Flow area (m²)	Form losses
Pipe	34	340	0.55245	0	2.79E-02	6.11E-04	4.25
NDHX (horizontal)	35a	351	1.148475	0	1.19E-02	1.33E-03	*
NDHX (vertical)	35b	352	0.415925	-90	1.19E-02	1.33E-03	5.8
Static mixer pipe	36a	360	0.2034	-58.99728	2.79E-02	6.11E-04	3.75
Static mixer	36	361	0.33	-58.99728	2.79E-02	6.11E-04	*
Pipe	37	370	1.7736	-90	2.79E-02	6.11E-04	
Flowmeter	37a	371	0.36	-90	2.79E-02	6.11E-04	*
Pipe	38	380	0.33655	-52.41533	2.79E-02	6.11E-04	0.8
Pipe	39	390	1.91135	-80.64882	2.79E-02	6.11E-04	2.65

* For these components, form losses have been measured experimentally. Correlations are provided in Table 2-6.

Table A-2. Heat structure parameters of the RELAP5-3D CIET model.

Component	Number on diagram	RELAP volume number	Length (m)	Insulation wall thickness (m)	Pipe wall thickness (m)	Left boundary (m)
Heater branch (bottom to top)						
Heater bottom head	1b	11	0.19685	0.0508	0.001905	1.92E-02
Heater	1	10	1.6383	0.0508	0.001905	1.92E-02
Heater top head	1a	12	0.0889	0.0508	0.001905	1.92E-02
Static mixer pipe	2a	20	0.149425	0.0508	0.0027686	0.01393195
Static mixer	2	21	0.33	0.0508	0.0027686	0.01393195
Pipe	3	30	1.2827	0.0508	0.0027686	0.01393195
Pipe	4	40	0.2413	0.0508	0.0027686	0.01393195
Branch	5	50	0.7493	0.0508	0.0027686	0.01393195
CTAH branch (top to bottom)						
Static mixer pipe	6a	60	0.1526	0.0508	0.0027686	0.01393195
Static mixer	6	61	0.33	0.0508	0.0027686	0.01393195
CTAH (vertical)	7a	71	0.3302		0.000406	5.95E-03
CTAH (horizontal)	7b	72	1.2342		0.000406	5.95E-03
Static mixer pipe	8a	80	0.22245	0.0381	0.0027686	0.01393195
Static mixer	8	81	0.33	0.0381	0.0027686	0.01393195
Pipe	9	90	0.7112	0.0381	0.0027686	0.01393195
Pipe	10	100	2.4511	0.0381	0.0027686	0.01393195
Pipe	11	110	0.4826	0.0381	0.0027686	0.01393195
Pipe	12	120	0.333375	0.0508	0.0027686	0.01393195
Pipe	13	130	1.273175	0.0508	0.0027686	0.01393195
Pipe	14	140	0.6687	0.0508	0.0027686	0.01393195
Flowmeter	14a	141	0.36			
Pipe	15	150	0.3556	0.0508	0.0027686	0.01393195
Pipe	16	160	0.644525	0.0508	0.0027686	0.01393195
Branch	17	170	0.473075	0.0508	0.0027686	0.01393195
DHX branch (bottom to top)						
Pipe	19	190	0.219075	0.0508	0.0027686	0.01393195
Pipe	20	200	0.33655	0.0508	0.0027686	0.01393195
Pipe	21	210	0.487725	0.0508	0.0027686	0.01393195
Flowmeter	21a	211	0.36			

Component	Number on diagram	RELAP volume number	Length (m)	Insulation wall thickness (m)	Pipe wall thickness (m)	Left boundary (m)
Pipe	22	220	0.69215	0.0508	0.0027686	0.01393195
Static mixer pipe	23a	230	0.0891	0.0508	0.0027686	0.01393195
Static mixer	23	231	0.33	0.0508	0.0027686	0.01393195
DHX shell side	24	240	1.18745	0.0508	0.0016	2.82E-03
Static mixer pipe	25a	250	0.22245	0.0508	0.0027686	0.01393195
Static mixer	25	251	0.33	0.0508	0.0027686	0.01393195
Pipe	26	260	0.2159	0.0508	0.0027686	0.01393195
Pipe	18	180	0.1778	0.0508	0.0027686	0.01393195
DRACS loop (counterclockwise)						
DHX tube side	30a	301	0.111125		0.00079375	3.47E-03
DHX tube side	30	300	1.18745		0.00079375	3.47E-03
DHX tube side	30b	302	0.18415		0.00079375	3.47E-03
Static mixer pipe	31a	310	0.143075	0.0508	0.0027686	0.01393195
Static mixer	31	311	0.33	0.0508	0.0027686	0.01393195
Pipe	32	320	0.238125	0.0508	0.0027686	0.01393195
Pipe	33	330	3.0099	0.0508	0.0027686	0.01393195
Pipe	34	340	0.55245	0.0508	0.0027686	0.01393195
NDHX (horizontal)	35a	351	1.148475		0.000406	5.95E-03
NDHX (vertical)	35b	352	0.415925		0.000406	5.95E-03
Static mixer pipe	36a	360	0.2034	0.0508	0.0027686	0.01393195
Static mixer	36	361	0.33	0.0508	0.0027686	0.01393195
Pipe	37	370	1.7736	0.0508	0.0027686	0.01393195
Flowmeter	37a	371	0.36			
Pipe	38	380	0.33655	0.0508	0.0027686	0.01393195
Pipe	39	390	1.91135	0.0508	0.0027686	0.01393195

A.2 Example of a RELAP5-3D Input Deck Used to Model a Simple Transient on CIET 1.0

```
=CIET 1.0 Facility Model
* Parameters to be adjusted before each run:
* - Heater power in general table (end of input)
* - CTAH and TCHX outlet temperatures in general tables (end of input)
* - K for each needle valve, based on number of turns open (cards 5050101, 5250101 and 5410101)
* - Trip valve parameters for open/closed branches (look for 'vlv')
* - Initial temperatures in all components for transients (cards CCC1201)
* - Initial mass flow rates in all components for transients (cards CCC1301)
* - Initial mass flow rates at all junctions for transients (cards CCC0201)
* - Initial mass flow rates in all branches for transients (cards CCCN201)
* - Ambient temperature in general table (end of input)
* Future updates:
* - Add pump physical model
* - Add by-pass line (not used for tests to-date)
* - Implement empirical heat transfer correlations for fan-cooled heat exchangers
* New problem using non-standard fluid; transient mode
100 newath transnt
* SI units for input; SI units for output
102 si si
* Reference volume; reference elevation; fluid (Dowtherm A)
120   10010000 0.0000  dowa
121  300010000 1.8701  dowa
```

```
* End time; min time step; max time step; control option; minor edit frequency; major edit frequency; restart
frequency
201  3000.000   1.0e-7 0.1  15011  100 1000 1000
202  10000.00   1.0e-6 1.0  15011    1 1000 1000
* Minor edit requests: variable request code; parameter
301  mflowfj  10010000
302  mflowfj 300010000
303  tempf    11020000
304  tempf    12010000
305  tempf    61010000
306  tempf    81010000
*******************************************************
* Hydrodynamic components
*******************************************************
*
* Heater Bottom
* Component name; component type
110000 heat_bot pipe
* Number of elements
110001 2
* Volume flow area; which elements
110101 3.64e-4,2
* Volume length; which elements
110301 0.09843,2
* Volume azimuthal angle; which elements (optional card)
110501 0.0,2
* Volume inclination angle; which elements (required)
110601 90.0,2
* Wall roughness; hydraulic diameter; which elements
* Here for stainless steel: k=0.015mm
110801 1.5e-5,6.60e-3,2
* tlpvbfe (see p.130 of Manual Appendix A); which elements
111001 0,2
* jefvcahs (see p.132 of Manual Appendix A); which elements
111101 0,1
* ebt (initial conditions options); P; T; 0; 0; 0; which elements
111201 3,1.45e5,325.0,0.,0.,0.,2
* Junction initial conditions control option (0 for velocities, 1 for mass flow rates)
111300 1
* Initial liquid velocity; initial gas velocity; interface velocity (enter 0.0); junction number
111301 0.18,0.18,0.,1
*
* Heater
* Component name; component type
100000 heater pipe
* Number of elements
100001 15
* Volume flow area; which elements
100101 3.64e-4,15
* Volume length; which elements
100301 0.10922,15
* Volume azimuthal angle; which elements (optional card)
100501 0.0,15
* Volume inclination angle; which elements (required)
100601 90.0,15
* Wall roughness; hydraulic diameter; which elements
* Here for stainless steel: k=0.015mm
100801 1.5e-5,6.60e-3,15
* tlpvbfe (see p.130 of Manual Appendix A); which elements
101001 0,15
* jefvcahs (see p.132 of Manual Appendix A); which elements
101101 0,14
```

```
* ebt (initial conditions options); P; T; 0; 0; 0; which elements
101201 3,1.41e5,325.0,0.,0.,0.,15
* Junction initial conditions control option (0 for velocities, 1 for mass flow rates)
101300 1
* Initial liquid velocity; initial gas velocity; interface velocity (enter 0.0); junction number
101301 0.18,0.18,0.,14
*
* Heater Top
* Component name; component type
120000 heat_top pipe
* Number of elements
120001 1
* Volume flow area; which elements
120101 3.64e-4,1
* Volume length; which elements
120301 0.08890,1
* Volume azimuthal angle; which elements (optional card)
120501 0.0,1
* Volume inclination angle; which elements (required)
120601 90.0,1
* Wall roughness; hydraulic diameter; which elements
* Here for stainless steel: k=0.015mm
120801 1.5e-5,6.60e-3,1
* tlpvbfe (see p.130 of Manual Appendix A); which elements
121001 0,1
* ebt (initial conditions options); P; T; 0; 0; 0; which elements
121201 3,1.4e5,325.0,0.,0.,0.,1
* Junction initial conditions control option
*
* Heater Mixer Pipe
* Component name; component type
200000 heatmix1 pipe
* Number of elements
200001 1
* Volume flow area; which elements
200101 6.11e-4,1
* Volume length; which elements
200301 0.14943,1
* Volume azimuthal angle; which elements (optional card)
200501 0.0,1
* Volume inclination angle; which elements (required)
200601 90.0,1
* Wall roughness; hydraulic diameter; which elements
* Here for stainless steel: k=0.015mm
200801 1.5e-5,2.79e-2,1
* tlpvbfe (see p.130 of Manual Appendix A); which elements
201001 0,1
* ebt (initial conditions options); P; T; 0; 0; 0; which elements
201201 3,1.39e5,325.0,0.,0.,0.,1
*
* Heater Mixer
* Component name; component type
210000 heatmix2 pipe
* Number of elements
210001 1
* Volume flow area; which elements
210101 6.11e-4,1
* Volume length; which elements
210301 0.33000,1
* Volume azimuthal angle; which elements (optional card)
210501 0.0,1
* Volume inclination angle; which elements (required)
```

```
210601 90.0,1
* Wall roughness; hydraulic diameter; which elements
* Here for stainless steel: k=0.015mm
210801 1.5e-5,2.79e-2,1
* tlpvbfe (see p.130 of Manual Appendix A); which elements
211001 10,1
* ebt (initial conditions options); P; T; 0; 0; 0; which elements
211201 3,1.38e5,325.0,0.,0.,0.,1
*
* Hot Leg 1
* Component name; component type
300000 hotleg1 pipe
* Number of elements
300001 12
* Volume flow area; which elements
300101 6.11e-4,12
* Volume length; which elements
300301 0.10689,12
* Volume azimuthal angle; which elements (optional card)
300501 0.0,12
* Volume inclination angle; which elements (required)
300601 90.0,12
* Wall roughness; hydraulic diameter; which elements
* Here for stainless steel: k=0.015mm
300801 1.5e-5,2.79e-2,12
* tlpvbfe (see p.130 of Manual Appendix A); which elements
301001 0,12
* jefvcahs (see p.132 of Manual Appendix A); which elements
301101 0,11
* ebt (initial conditions options); P; T; 0; 0; 0; which elements
301201 3,1.3e5,325.0,0.,0.,0.,12
* Junction initial conditions control option (0 for velocities, 1 for mass flow rates)
301300 1
* Initial liquid velocity; initial gas velocity; interface velocity (enter 0.0); junction number
301301 0.18,0.18,0.,11
*
* Hot Leg 2
* Component name; component type
400000 hotleg2 pipe
* Number of elements
400001 2
* Volume flow area; which elements
400101 6.11e-4,2
* Volume length; which elements
400301 0.12065,2
* Volume azimuthal angle; which elements (optional card)
400501 180.0,2
* Volume inclination angle; which elements (required)
400601 49.74338742,2
* Wall roughness; hydraulic diameter; which elements
* Here for stainless steel: k=0.015mm
400801 1.5e-5,2.79e-2,2
* tlpvbfe (see p.130 of Manual Appendix A); which elements
401001 0,2
* jefvcahs (see p.132 of Manual Appendix A); which elements
401101 0,1
* ebt (initial conditions options); P; T; 0; 0; 0; which elements
401201 3,1.2e5,325.0,0.,0.,0.,2
* Junction initial conditions control option (0 for velocities, 1 for mass flow rates)
401300 1
* Initial liquid velocity; initial gas velocity; interface velocity (enter 0.0); junction number
401301 0.18,0.18,0.,1
```

```
*
* CTAH Inlet Mixer Pipe
* Component name; component type
600000 CTAHmix1 pipe
* Number of elements
600001 1
* Volume flow area; which elements
600101 6.11e-4,1
* Volume length; which elements
600301 0.15260,1
* Volume azimuthal angle; which elements (optional card)
600501 0.0,1
* Volume inclination angle; which elements (required)
600601 51.52638425,1
* Wall roughness; hydraulic diameter; which elements
* Here for stainless steel: k=0.015mm
600801 1.5e-5,2.79e-2,1
* tlpvbfe (see p.130 of Manual Appendix A); which elements
601001 0,1
* ebt (initial conditions options); P; T; 0; 0; 0; which elements
601201 3,1.15e5,325.0,0.,0.,0.,1
*
* CTAH Inlet Mixer
* Component name; component type
610000 CTAHmix2 pipe
* Number of elements
610001 1
* Volume flow area; which elements
610101 6.11e-4,1
* Volume length; which elements
610301 0.33000,1
* Volume azimuthal angle; which elements (optional card)
610501 0.0,1
* Volume inclination angle; which elements (required)
610601 51.52638425,1
* Wall roughness; hydraulic diameter; which elements
* Here for stainless steel: k=0.015mm
610801 1.5e-5,2.79e-2,1
* tlpvbfe (see p.130 of Manual Appendix A); which elements
611001 10,1
* ebt (initial conditions options); P; T; 0; 0; 0; which elements
611201 3,1.12e5,325.0,0.,0.,0.,1
*
* CTAH Vertical
* Component name; component type
710000 CTAH_ver pipe
* Number of elements
710001 3
* Volume flow area; which elements
710101 1.33e-3,3
* Volume length; which elements
710301 0.11007,3
* Volume azimuthal angle; which elements (optional card)
710501 0.0,3
* Volume inclination angle; which elements (required)
710601 -90.0,3
* Wall roughness; hydraulic diameter; which elements
* Here for stainless steel: k=0.015mm
710801 1.5e-5,1.19e-2,3
* tlpvbfe (see p.130 of Manual Appendix A); which elements
711001 10,3
* jefvcahs (see p.132 of Manual Appendix A); which elements
```

```
711101 0,2
* ebt (initial conditions options); P; T; 0; 0; 0; which elements
711201 3,1.15e5,325.0,0.,0.,0.,3
* Junction initial conditions control option (0 for velocities, 1 for mass flow rates)
711300 1
* Initial liquid velocity; initial gas velocity; interface velocity (enter 0.0); junction number
711301 0.18,0.18,0.,2
*
* CTAH Horizontal
* Component name; component type
720000 CTAH_hor pipe
* Number of elements
720001 11
* Volume flow area; which elements
720101 1.33e-3,11
* Volume length; which elements
720301 0.11220,11
* Volume azimuthal angle; which elements (optional card)
720501 180.0,11
* Volume inclination angle; which elements (required)
720601 0.0,11
* Wall roughness; hydraulic diameter; which elements
* Here for stainless steel: k=0.015mm
720801 1.5e-5,1.19e-2,11
* tlpvbfe (see p.130 of Manual Appendix A); which elements
721001 10,11
* jefvcahs (see p.132 of Manual Appendix A); which elements
721101 0,10
* ebt (initial conditions options); P; T; 0; 0; 0; which elements
721201 3,1.2e5,325.0,0.,0.,0.,11
* Junction initial conditions control option (0 for velocities, 1 for mass flow rates)
721300 1
* Initial liquid velocity; initial gas velocity; interface velocity (enter 0.0); junction number
721301 0.18,0.18,0.,10
*
* CTAH Outlet Mixer Pipe
* Component name; component type
800000 CTAHmix3 pipe
* Number of elements
800001 2
* Volume flow area; which elements
800101 6.11e-4,2
* Volume length; which elements
800301 0.11123,2
* Volume azimuthal angle; which elements (optional card)
800501 0.0,2
* Volume inclination angle; which elements (required)
800601 -90.0,2
* Wall roughness; hydraulic diameter; which elements
* Here for stainless steel: k=0.015mm
800801 1.5e-5,2.79e-2,2
* tlpvbfe (see p.130 of Manual Appendix A); which elements
801001 0,2
* jefvcahs (see p.132 of Manual Appendix A); which elements
801101 0,1
* ebt (initial conditions options); P; T; 0; 0; 0; which elements
801201 3,1.2e5,325.0,0.,0.,0.,2
* Junction initial conditions control option (0 for velocities, 1 for mass flow rates)
801300 1
* Initial liquid velocity; initial gas velocity; interface velocity (enter 0.0); junction number
801301 0.18,0.18,0.,1
*
```

```
* CTAH Outlet Mixer
* Component name; component type
810000 CTAHmix4 pipe
* Number of elements
810001 1
* Volume flow area; which elements
810101 6.11e-4,1
* Volume length; which elements
810301 0.33000,1
* Volume azimuthal angle; which elements (optional card)
810501 0.0,1
* Volume inclination angle; which elements (required)
810601 -90.0,1
* Wall roughness; hydraulic diameter; which elements
* Here for stainless steel: k=0.015mm
810801 1.5e-5,2.79e-2,1
* tlpvbfe (see p.130 of Manual Appendix A); which elements
811001 10,1
* ebt (initial conditions options); P; T; 0; 0; 0; which elements
811201 3,1.2e5,325.0,0.,0.,0.,1
*
* Cold Leg 1
* Component name; component type
900000 coldleg1 pipe
* Number of elements
900001 7
* Volume flow area; which elements
900101 6.11e-4,7
* Volume length; which elements
900301 0.10160,7
* Volume azimuthal angle; which elements (optional card)
900501 0.0,7
* Volume inclination angle; which elements (required)
900601 -42.73211004,7
* Wall roughness; hydraulic diameter; which elements
* Here for stainless steel: k=0.015mm
900801 1.5e-5,2.79e-2,7
* tlpvbfe (see p.130 of Manual Appendix A); which elements
901001 0,7
* jefvcahs (see p.132 of Manual Appendix A); which elements
901101 0,6
* ebt (initial conditions options); P; T; 0; 0; 0; which elements
901201 3,1.3e5,325.0,0.,0.,0.,7
* Junction initial conditions control option (0 for velocities, 1 for mass flow rates)
901300 1
* Initial liquid velocity; initial gas velocity; interface velocity (enter 0.0); junction number
901301 0.18,0.18,0.,6
*
* Cold Leg 2
* Component name; component type
1000000 coldleg2 pipe
* Number of elements
1000001 22
* Volume flow area; which elements
1000101 6.11e-4,22
* Volume length; which elements
1000301 0.11141,22
* Volume azimuthal angle; which elements (optional card)
1000501 0.0,22
* Volume inclination angle; which elements (required)
1000601 -90.0,22
* Wall roughness; hydraulic diameter; which elements
```

```
* Here for stainless steel: k=0.015mm
1000801 1.5e-5,2.79e-2,22
* tlpvbfe (see p.130 of Manual Appendix A); which elements
1001001 0,22
* jefvcahs (see p.132 of Manual Appendix A); which elements
1001101 0,21
* ebt (initial conditions options); P; T; 0; 0; 0; which elements
1001201 3,1.4e5,325.0,0.,0.,0.,22
* Junction initial conditions control option (0 for velocities, 1 for mass flow rates)
1001300 1
* Initial liquid velocity; initial gas velocity; interface velocity (enter 0.0); junction number
1001301 0.18,0.18,0.,21
*
* Cold Leg 3
* Component name; component type
1100000 coldleg3 pipe
* Number of elements
1100001 4
* Volume flow area; which elements
1100101 6.11e-4,4
* Volume length; which elements
1100301 0.12065,4
* Volume azimuthal angle; which elements (optional card)
1100501 180.0,4
* Volume inclination angle; which elements (required)
1100601 -63.47464798,4
* Wall roughness; hydraulic diameter; which elements
* Here for stainless steel: k=0.015mm
1100801 1.5e-5,2.79e-2,4
* tlpvbfe (see p.130 of Manual Appendix A); which elements
1101001 0,4
* jefvcahs (see p.132 of Manual Appendix A); which elements
1101101 0,3
* ebt (initial conditions options); P; T; 0; 0; 0; which elements
1101201 3,1.41e5,325.0,0.,0.,0.,4
* Junction initial conditions control option (0 for velocities, 1 for mass flow rates)
1101300 1
* Initial liquid velocity; initial gas velocity; interface velocity (enter 0.0); junction number
1101301 0.18,0.18,0.,3
*
* Pump Suction
* Component name; component type
1200000 pumpsuc pipe
* Number of elements
1200001 3
* Volume flow area; which elements
1200101 6.11e-4,3
* Volume length; which elements
1200301 0.11113,3
* Volume azimuthal angle; which elements (optional card)
1200501 180.0,3
* Volume inclination angle; which elements (required)
1200601 0.0,3
* Wall roughness; hydraulic diameter; which elements
* Here for stainless steel: k=0.015mm
1200801 1.5e-5,2.79e-2,3
* tlpvbfe (see p.130 of Manual Appendix A); which elements
1201001 0,3
* jefvcahs (see p.132 of Manual Appendix A); which elements
1201101 0,2
* ebt (initial conditions options); P; T; 0; 0; 0; which elements
1201201 3,1.45e5,325.0,0.,0.,0.,3
```

```
* Junction initial conditions control option (0 for velocities, 1 for mass flow rates)
1201300 1
* Initial liquid velocity; initial gas velocity; interface velocity (enter 0.0); junction number
1201301 0.18,0.18,0.,2
*
* Pump Discharge
* Component name; component type
1300000 pumpdis pipe
* Number of elements
1300001 12
* Volume flow area; which elements
1300101 6.11e-4,12
* Volume length; which elements
1300301 0.10610,12
* Volume azimuthal angle; which elements (optional card)
1300501 180.0,12
* Volume inclination angle; which elements (required)
1300601 0.0,12
* Wall roughness; hydraulic diameter; which elements
* Here for stainless steel: k=0.015mm
1300801 1.5e-5,2.79e-2,12
* tlpvbfe (see p.130 of Manual Appendix A); which elements
1301001 0,12
* jefvcahs (see p.132 of Manual Appendix A); which elements
1301101 0,11
* ebt (initial conditions options); P; T; 0; 0; 0; which elements
1301201 3,1.45e5,325.0,0.,0.,0.,12
* Junction initial conditions control option (0 for velocities, 1 for mass flow rates)
1301300 1
* Initial liquid velocity; initial gas velocity; interface velocity (enter 0.0); junction number
1301301 0.18,0.18,0.,11
*
* Cold Leg 4
* Component name; component type
1400000 coldleg4 pipe
* Number of elements
1400001 6
* Volume flow area; which elements
1400101 6.11e-4,6
* Volume length; which elements
1400301 0.11145,6
* Volume azimuthal angle; which elements (optional card)
1400501 0.0,6
* Volume inclination angle; which elements (required)
1400601 90.0,6
* Wall roughness; hydraulic diameter; which elements
* Here for stainless steel: k=0.015mm
1400801 1.5e-5,2.79e-2,6
* tlpvbfe (see p.130 of Manual Appendix A); which elements
1401001 0,6
* jefvcahs (see p.132 of Manual Appendix A); which elements
1401101 0,5
* ebt (initial conditions options); P; T; 0; 0; 0; which elements
1401201 3,1.4e5,325.0,0.,0.,0.,6
* Junction initial conditions control option (0 for velocities, 1 for mass flow rates)
1401300 1
* Initial liquid velocity; initial gas velocity; interface velocity (enter 0.0); junction number
1401301 0.18,0.18,0.,5
*
* CTAH Flowmeter
* Component name; component type
1410000 CTAHflo pipe
```

```
* Number of elements
1410001 1
* Volume flow area; which elements
1410101 6.11e-4,1
* Volume length; which elements
1410301 0.36,1
* Volume azimuthal angle; which elements (optional card)
1410501 0.0,1
* Volume inclination angle; which elements (required)
1410601 90.0,1
* Wall roughness; hydraulic diameter; which elements
* Here for stainless steel: k=0.015mm
1410801 1.5e-5,2.79e-2,1
* tlpvbfe (see p.130 of Manual Appendix A); which elements
1411001 10,1
* ebt (initial conditions options); P; T; 0; 0; 0; which elements
1411201 3,1.35e5,325.0,0.,0.,0.,1
*
* Cold Leg 5
* Component name; component type
1500000 coldleg5 pipe
* Number of elements
1500001 3
* Volume flow area; which elements
1500101 6.11e-4,3
* Volume length; which elements
1500301 0.11853,3
* Volume azimuthal angle; which elements (optional card)
1500501 180.0,3
* Volume inclination angle; which elements (required)
1500601 -49.36983394,3
* Wall roughness; hydraulic diameter; which elements
* Here for stainless steel: k=0.015mm
1500801 1.5e-5,2.79e-2,3
* tlpvbfe (see p.130 of Manual Appendix A); which elements
1501001 0,3
* jefvcahs (see p.132 of Manual Appendix A); which elements
1501101 0,2
* ebt (initial conditions options); P; T; 0; 0; 0; which elements
1501201 3,1.35e5,325.0,0.,0.,0.,3
* Junction initial conditions control option (0 for velocities, 1 for mass flow rates)
1501300 1
* Initial liquid velocity; initial gas velocity; interface velocity (enter 0.0); junction number
1501301 0.18,0.18,0.,2
*
* Cold Leg 6
* Component name; component type
1600000 coldleg6 pipe
* Number of elements
1600001 6
* Volume flow area; which elements
1600101 6.11e-4,6
* Volume length; which elements
1600301 0.10742,6
* Volume azimuthal angle; which elements (optional card)
1600501 0.0,6
* Volume inclination angle; which elements (required)
1600601 -90.0,6
* Wall roughness; hydraulic diameter; which elements
* Here for stainless steel: k=0.015mm
1600801 1.5e-5,2.79e-2,6
* tlpvbfe (see p.130 of Manual Appendix A); which elements
```

```
1601001 0,6
* jefvcahs (see p.132 of Manual Appendix A); which elements
1601101 0,5
* ebt (initial conditions options); P; T; 0; 0; 0; which elements
1601201 3,1.4e5,325.0,0.,0.,0.,6
* Junction initial conditions control option (0 for velocities, 1 for mass flow rates)
1601300 1
* Initial liquid velocity; initial gas velocity; interface velocity (enter 0.0); junction number
1601301 0.18,0.18,0.,5
*
* Cold Leg 7
* Component name; component type
1800000 coldleg7 pipe
* Number of elements
1800001 1
* Volume flow area; which elements
1800101 6.11e-4,1
* Volume length; which elements
1800301 0.17780,1
* Volume azimuthal angle; which elements (optional card)
1800501 180.0,1
* Volume inclination angle; which elements (required)
1800601 -40.00520088,1
* Wall roughness; hydraulic diameter; which elements
* Here for stainless steel: k=0.015mm
1800801 1.5e-5,2.79e-2,1
* tlpvbfe (see p.130 of Manual Appendix A); which elements
1801001 0,1
* ebt (initial conditions options); P; T; 0; 0; 0; which elements
1801201 3,1.41e5,325.0,0.,0.,0.,1
*
* DHX Leg 1
* Component name; component type
1900000 DHXleg1 pipe
* Number of elements
1900001 2
* Volume flow area; which elements
1900101 6.11e-4,2
* Volume length; which elements
1900301 0.10954,2
* Volume azimuthal angle; which elements (optional card)
1900501 180.0,2
* Volume inclination angle; which elements (required)
1900601 -31.44898139,2
* Wall roughness; hydraulic diameter; which elements
* Here for stainless steel: k=0.015mm
1900801 1.5e-5,2.79e-2,2
* tlpvbfe (see p.130 of Manual Appendix A); which elements
1901001 0,2
* jefvcahs (see p.132 of Manual Appendix A); which elements
1901101 0,1
* ebt (initial conditions options); P; T; 0; 0; 0; which elements
1901201 3,1.41e5,325.0,0.,0.,0.,2
* Junction initial conditions control option (0 for velocities, 1 for mass flow rates)
1901300 1
* Initial liquid velocity; initial gas velocity; interface velocity (enter 0.0); junction number
1901301 0.,0.,0.,1
*
* DHX Leg 2
* Component name; component type
2000000 DHXleg2 pipe
* Number of elements
```

```
2000001 3
* Volume flow area; which elements
2000101 6.11e-4,3
* Volume length; which elements
2000301 0.11218,3
* Volume azimuthal angle; which elements (optional card)
2000501 180.0,3
* Volume inclination angle; which elements (required)
2000601 0.0,3
* Wall roughness; hydraulic diameter; which elements
* Here for stainless steel: k=0.015mm
2000801 1.5e-5,2.79e-2,3
* tlpvbfe (see p.130 of Manual Appendix A); which elements
2001001 0,3
* jefvcahs (see p.132 of Manual Appendix A); which elements
2001101 0,2
* ebt (initial conditions options); P; T; 0; 0; 0; which elements
2001201 3,1.45e5,325.0,0.,0.,0.,3
* Junction initial conditions control option (0 for velocities, 1 for mass flow rates)
2001300 1
* Initial liquid velocity; initial gas velocity; interface velocity (enter 0.0); junction number
2001301 0.,0.,0.,2
*
* DHX Leg 3
* Component name; component type
2100000 DHXleg3 pipe
* Number of elements
2100001 4
* Volume flow area; which elements
2100101 6.11e-4,4
* Volume length; which elements
2100301 0.12193,4
* Volume azimuthal angle; which elements (optional card)
2100501 0.0,4
* Volume inclination angle; which elements (required)
2100601 90.0,4
* Wall roughness; hydraulic diameter; which elements
* Here for stainless steel: k=0.015mm
2100801 1.5e-5,2.79e-2,4
* tlpvbfe (see p.130 of Manual Appendix A); which elements
2101001 0,4
* jefvcahs (see p.132 of Manual Appendix A); which elements
2101101 0,3
* ebt (initial conditions options); P; T; 0; 0; 0; which elements
2101201 3,1.4e5,325.0,0.,0.,0.,4
* Junction initial conditions control option (0 for velocities, 1 for mass flow rates)
2101300 1
* Initial liquid velocity; initial gas velocity; interface velocity (enter 0.0); junction number
2101301 0.,0.,0.,3
*
* DHX Flowmeter
* Component name; component type
2110000 DHXflo pipe
* Number of elements
2110001 1
* Volume flow area; which elements
2110101 6.11e-4,1
* Volume length; which elements
2110301 0.36,1
* Volume azimuthal angle; which elements (optional card)
2110501 0.0,1
* Volume inclination angle; which elements (required)
```

```
2110601 90.0,1
* Wall roughness; hydraulic diameter; which elements
* Here for stainless steel: k=0.015mm
2110801 1.5e-5,2.79e-2,1
* tlpvbfe (see p.130 of Manual Appendix A); which elements
2111001 10,1
* ebt (initial conditions options); P; T; 0; 0; 0; which elements
2111201 3,1.35e5,325.0,0.,0.,0.,1
*
* DHX Leg 4
* Component name; component type
2200000 DHXleg4 pipe
* Number of elements
2200001 6
* Volume flow area; which elements
2200101 6.11e-4,6
* Volume length; which elements
2200301 0.11536,6
* Volume azimuthal angle; which elements (optional card)
2200501 0.0,6
* Volume inclination angle; which elements (required)
2200601 90.0,6
* Wall roughness; hydraulic diameter; which elements
* Here for stainless steel: k=0.015mm
2200801 1.5e-5,2.79e-2,6
* tlpvbfe (see p.130 of Manual Appendix A); which elements
2201001 0,6
* jefvcahs (see p.132 of Manual Appendix A); which elements
2201101 0,5
* ebt (initial conditions options); P; T; 0; 0; 0; which elements
2201201 3,1.3e5,325.0,0.,0.,0.,6
* Junction initial conditions control option (0 for velocities, 1 for mass flow rates)
2201300 1
* Initial liquid velocity; initial gas velocity; interface velocity (enter 0.0); junction number
2201301 0.,0.,0.,5
*
* DHX Outlet Mixer Pipe
* Component name; component type
2300000 DHXmix1 pipe
* Number of elements
2300001 1
* Volume flow area; which elements
2300101 6.11e-4,1
* Volume length; which elements
2300301 0.08910,1
* Volume azimuthal angle; which elements (optional card)
2300501 0.0,1
* Volume inclination angle; which elements (required)
2300601 90.0,1
* Wall roughness; hydraulic diameter; which elements
* Here for stainless steel: k=0.015mm
2300801 1.5e-5,2.79e-2,1
* tlpvbfe (see p.130 of Manual Appendix A); which elements
2301001 0,1
* ebt (initial conditions options); P; T; 0; 0; 0; which elements
2301201 3,1.25e5,325.0,0.,0.,0.,1
*
* DHX Outlet Mixer
* Component name; component type
2310000 DHXmix2 pipe
* Number of elements
2310001 1
```

```
* Volume flow area; which elements
2310101 6.11e-4,1
* Volume length; which elements
2310301 0.33000,1
* Volume azimuthal angle; which elements (optional card)
2310501 0.0,1
* Volume inclination angle; which elements (required)
2310601 90.0,1
* Wall roughness; hydraulic diameter; which elements
* Here for stainless steel: k=0.015mm
2310801 1.5e-5,2.79e-2,1
* tlpvbfe (see p.130 of Manual Appendix A); which elements
2311001 10,1
* ebt (initial conditions options); P; T; 0; 0; 0; which elements
2311201 3,1.25e5,325.0,0.,0.,0.,1
*
* DHX Shell Side (Primary)
* Component name; component type
2400000 DHXshell pipe
* Number of elements
2400001 11
* Volume flow area; which elements
2400101 9.43e-4,11
* Volume length; which elements
2400301 0.10795,11
* Volume azimuthal angle; which elements (optional card)
2400501 0.0,11
* Volume inclination angle; which elements (required)
2400601 90.0,11
* Wall roughness; hydraulic diameter; which elements
* Here for stainless steel: k=0.015mm
2400801 1.5e-5,5.65e-3,11
* tlpvbfe (see p.130 of Manual Appendix A); which elements
2401001 0,11
* jefvcahs (see p.132 of Manual Appendix A); which elements
2401101 0,10
* ebt (initial conditions options); P; T; 0; 0; 0; which elements
2401201 3,1.2e5,325.0,0.,0.,0.,11
* Junction initial conditions control option (0 for velocities, 1 for mass flow rates)
2401300 1
* Initial liquid velocity; initial gas velocity; interface velocity (enter 0.0); junction number
2401301 0.,0.,0.,10
*
* DHX Inlet Mixer Pipe
* Component name; component type
2500000 DHXmix3 pipe
* Number of elements
2500001 2
* Volume flow area; which elements
2500101 6.11e-4,2
* Volume length; which elements
2500301 0.11123,2
* Volume azimuthal angle; which elements (optional card)
2500501 0.0,2
* Volume inclination angle; which elements (required)
2500601 90.0,2
* Wall roughness; hydraulic diameter; which elements
* Here for stainless steel: k=0.015mm
2500801 1.5e-5,2.79e-2,2
* tlpvbfe (see p.130 of Manual Appendix A); which elements
2501001 0,2
* jefvcahs (see p.132 of Manual Appendix A); which elements
```

```
2501101 0,1
* ebt (initial conditions options); P; T; 0; 0; 0; which elements
2501201 3,1.2e5,325.0,0.,0.,0.,2
* Junction initial conditions control option (0 for velocities, 1 for mass flow rates)
2501300 1
* Initial liquid velocity; initial gas velocity; interface velocity (enter 0.0); junction number
2501301 0.,0.,0.,1
*
* DHX Inlet Mixer
* Component name; component type
2510000 DHXmix4 pipe
* Number of elements
2510001 1
* Volume flow area; which elements
2510101 6.11e-4,1
* Volume length; which elements
2510301 0.33000,1
* Volume azimuthal angle; which elements (optional card)
2510501 0.0,1
* Volume inclination angle; which elements (required)
2510601 90.0,1
* Wall roughness; hydraulic diameter; which elements
* Here for stainless steel: k=0.015mm
2510801 1.5e-5,2.79e-2,1
* tlpvbfe (see p.130 of Manual Appendix A); which elements
2511001 10,1
* ebt (initial conditions options); P; T; 0; 0; 0; which elements
2511201 3,1.2e5,325.0,0.,0.,0.,1
*
* DHX Leg 5
* Component name; component type
2600000 DHXleg5 pipe
* Number of elements
2600001 2
* Volume flow area; which elements
2600101 6.11e-4,2
* Volume length; which elements
2600301 0.10795,2
* Volume azimuthal angle; which elements (optional card)
2600501 0.0,2
* Volume inclination angle; which elements (required)
2600601 52.57199446,2
* Wall roughness; hydraulic diameter; which elements
* Here for stainless steel: k=0.015mm
2600801 1.5e-5,2.79e-2,2
* tlpvbfe (see p.130 of Manual Appendix A); which elements
2601001 0,2
* jefvcahs (see p.132 of Manual Appendix A); which elements
2601101 0,1
* ebt (initial conditions options); P; T; 0; 0; 0; which elements
2601201 3,1.15e5,325.0,0.,0.,0.,2
* Junction initial conditions control option (0 for velocities, 1 for mass flow rates)
2601300 1
* Initial liquid velocity; initial gas velocity; interface velocity (enter 0.0); junction number
2601301 0.,0.,0.,1
*
* DHX Tube Side (DRACS) Bottom
* Component name; component type
3010000 DHXbot pipe
* Number of elements
3010001 1
* Volume flow area; which elements
```

```
3010101 7.18e-4,1
* Volume length; which elements
3010301 0.11113,1
* Volume azimuthal angle; which elements (optional card)
3010501 0.0,1
* Volume inclination angle; which elements (required)
3010601 90.0,1
* Wall roughness; hydraulic diameter; which elements
* Here for stainless steel: k=0.015mm
3010801 1.5e-5,6.93e-3,1
* tlpvbfe (see p.130 of Manual Appendix A); which elements
3011001 0,1
* ebt (initial conditions options); P; T; 0; 0; 0; which elements
3011201 3,1.55e5,325.0,0.,0.,0.,1
*
* DHX Tube Side (DRACS)
* Component name; component type
3000000 DHXtube pipe
* Number of elements
3000001 11
* Volume flow area; which elements
3000101 7.18e-4,11
* Volume length; which elements
3000301 0.10795,11
* Volume azimuthal angle; which elements (optional card)
3000501 0.0,11
* Volume inclination angle; which elements (required)
3000601 90.0,11
* Wall roughness; hydraulic diameter; which elements
* Here for stainless steel: k=0.015mm
3000801 1.5e-5,6.93e-3,11
* tlpvbfe (see p.130 of Manual Appendix A); which elements
3001001 0,11
* jefvcahs (see p.132 of Manual Appendix A); which elements
3001101 0,10
* ebt (initial conditions options); P; T; 0; 0; 0; which elements
3001201 3,1.5e5,325.0,0.,0.,0.,11
* Junction initial conditions control option (0 for velocities, 1 for mass flow rates)
3001300 1
* Initial liquid velocity; initial gas velocity; interface velocity (enter 0.0); junction number
3001301 0.,0.,0.,10
*
* DHX Tube Side (DRACS) Top
* Component name; component type
3020000 DHXtop pipe
* Number of elements
3020001 2
* Volume flow area; which elements
3020101 7.18e-4,2
* Volume length; which elements
3020301 0.09208,2
* Volume azimuthal angle; which elements (optional card)
3020501 0.0,2
* Volume inclination angle; which elements (required)
3020601 90.0,2
* Wall roughness; hydraulic diameter; which elements
* Here for stainless steel: k=0.015mm
3020801 1.5e-5,6.93e-3,2
* tlpvbfe (see p.130 of Manual Appendix A); which elements
3021001 0,2
* jefvcahs (see p.132 of Manual Appendix A); which elements
3021101 0,1
```

```
* ebt (initial conditions options); P; T; 0; 0; 0; which elements
3021201 3,1.45e5,325.0,0.,0.,0.,2
* Junction initial conditions control option (0 for velocities, 1 for mass flow rates)
3021300 1
* Initial liquid velocity; initial gas velocity; interface velocity (enter 0.0); junction number
3021301 0.,0.,0.,1
*
* DHX Outlet Mixer Pipe (DRACS loop)
* Component name; component type
3100000 DHXmix5 pipe
* Number of elements
3100001 1
* Volume flow area; which elements
3100101 6.11e-4,1
* Volume length; which elements
3100301 0.14308,1
* Volume azimuthal angle; which elements (optional card)
3100501 0.0,1
* Volume inclination angle; which elements (required)
3100601 90.0,1
* Wall roughness; hydraulic diameter; which elements
* Here for stainless steel: k=0.015mm
3100801 1.5e-5,2.79e-2,1
* tlpvbfe (see p.130 of Manual Appendix A); which elements
3101001 0,1
* ebt (initial conditions options); P; T; 0; 0; 0; which elements
3101201 3,1.42e5,325.0,0.,0.,0.,1
*
* DHX Outlet Mixer (DRACS loop)
* Component name; component type
3110000 DHXmix6 pipe
* Number of elements
3110001 1
* Volume flow area; which elements
3110101 6.11e-4,1
* Volume length; which elements
3110301 0.33000,1
* Volume azimuthal angle; which elements (optional card)
3110501 0.0,1
* Volume inclination angle; which elements (required)
3110601 90.0,1
* Wall roughness; hydraulic diameter; which elements
* Here for stainless steel: k=0.015mm
3110801 1.5e-5,2.79e-2,1
* tlpvbfe (see p.130 of Manual Appendix A); which elements
3111001 10,1
* ebt (initial conditions options); P; T; 0; 0; 0; which elements
3111201 3,1.42e5,325.0,0.,0.,0.,1
*
* DRACS Hot Leg 1
* Component name; component type
3200000 DRACSh1 pipe
* Number of elements
3200001 2
* Volume flow area; which elements
3200101 6.11e-4,2
* Volume length; which elements
3200301 0.11906,2
* Volume azimuthal angle; which elements (optional card)
3200501 180.0,2
* Volume inclination angle; which elements (required)
3200601 54.42289745,2
```

```
* Wall roughness; hydraulic diameter; which elements
* Here for stainless steel: k=0.015mm
3200801 1.5e-5,2.79e-2,2
* tlpvbfe (see p.130 of Manual Appendix A); which elements
3201001 0,2
* jefvcahs (see p.132 of Manual Appendix A); which elements
3201101 0,1
* ebt (initial conditions options); P; T; 0; 0; 0; which elements
3201201 3,1.4e5,325.0,0.,0.,0.,2
* Junction initial conditions control option (0 for velocities, 1 for mass flow rates)
3201300 1
* Initial liquid velocity; initial gas velocity; interface velocity (enter 0.0); junction number
3201301 0.,0.,0.,1
*
* DRACS Hot Leg 2
* Component name; component type
3300000 DRACSh2 pipe
* Number of elements
3300001 28
* Volume flow area; which elements
3300101 6.11e-4,28
* Volume length; which elements
3300301 0.10750,28
* Volume azimuthal angle; which elements (optional card)
3300501 0.0,28
* Volume inclination angle; which elements (required)
3300601 90.0,28
* Wall roughness; hydraulic diameter; which elements
* Here for stainless steel: k=0.015mm
3300801 1.5e-5,2.79e-2,28
* tlpvbfe (see p.130 of Manual Appendix A); which elements
3301001 0,28
* jefvcahs (see p.132 of Manual Appendix A); which elements
3301101 0,27
* ebt (initial conditions options); P; T; 0; 0; 0; which elements
3301201 3,1.3e5,325.0,0.,0.,0.,28
* Junction initial conditions control option (0 for velocities, 1 for mass flow rates)
3301300 1
* Initial liquid velocity; initial gas velocity; interface velocity (enter 0.0); junction number
3301301 0.,0.,0.,27
*
* TCHX Horizontal
* Component name; component type
3510000 TCHX_hor pipe
* Number of elements
3510001 11
* Volume flow area; which elements
3510101 1.33e-3,11
* Volume length; which elements
3510301 0.10441,11
* Volume azimuthal angle; which elements (optional card)
3510501 180.0,11
* Volume inclination angle; which elements (required)
3510601 0.0,11
* Wall roughness; hydraulic diameter; which elements
* Here for stainless steel: k=0.015mm
3510801 1.5e-5,1.19e-2,11
* tlpvbfe (see p.130 of Manual Appendix A); which elements
3511001 10,11
* jefvcahs (see p.132 of Manual Appendix A); which elements
3511101 0,10
* ebt (initial conditions options); P; T; 0; 0; 0; which elements
```

```
3511201 3,1.15e5,325.0,0.,0.,0.,11
* Junction initial conditions control option (0 for velocities, 1 for mass flow rates)
3511300 1
* Initial liquid velocity; initial gas velocity; interface velocity (enter 0.0); junction number
3511301 0.,0.,0.,10
*
* TCHX Vertical
* Component name; component type
3520000 TCHX_ver pipe
* Number of elements
3520001 4
* Volume flow area; which elements
3520101 1.33e-3,4
* Volume length; which elements
3520301 0.10398,4
* Volume azimuthal angle; which elements (optional card)
3520501 0.0,4
* Volume inclination angle; which elements (required)
3520601 -90.0,4
* Wall roughness; hydraulic diameter; which elements
* Here for stainless steel: k=0.015mm
3520801 1.5e-5,1.19e-2,4
* tlpvbfe (see p.130 of Manual Appendix A); which elements
3521001 10,4
* jefvcahs (see p.132 of Manual Appendix A); which elements
3521101 0,3
* ebt (initial conditions options); P; T; 0; 0; 0; which elements
3521201 3,1.15e5,325.0,0.,0.,0.,4
* Junction initial conditions control option (0 for velocities, 1 for mass flow rates)
3521300 1
* Initial liquid velocity; initial gas velocity; interface velocity (enter 0.0); junction number
3521301 0.,0.,0.,3
*
* TCHX Outlet Mixer Pipe
* Component name; component type
3600000 TCHXmix1 pipe
* Number of elements
3600001 2
* Volume flow area; which elements
3600101 6.11e-4,2
* Volume length; which elements
3600301 0.10170,2
* Volume azimuthal angle; which elements (optional card)
3600501 0.0,2
* Volume inclination angle; which elements (required)
3600601 -58.99728087,2
* Wall roughness; hydraulic diameter; which elements
* Here for stainless steel: k=0.015mm
3600801 1.5e-5,2.79e-2,2
* tlpvbfe (see p.130 of Manual Appendix A); which elements
3601001 0,2
* jefvcahs (see p.132 of Manual Appendix A); which elements
3601101 0,1
* ebt (initial conditions options); P; T; 0; 0; 0; which elements
3601201 3,1.2e5,325.0,0.,0.,0.,2
* Junction initial conditions control option (0 for velocities, 1 for mass flow rates)
3601300 1
* Initial liquid velocity; initial gas velocity; interface velocity (enter 0.0); junction number
3601301 0.,0.,0.,1
*
* TCHX Outlet Mixer
* Component name; component type
```

```
3610000 TCHXmix2 pipe
* Number of elements
3610001 1
* Volume flow area; which elements
3610101 6.11e-4,1
* Volume length; which elements
3610301 0.33000,1
* Volume azimuthal angle; which elements (optional card)
3610501 0.0,1
* Volume inclination angle; which elements (required)
3610601 -58.99728087,1
* Wall roughness; hydraulic diameter; which elements
* Here for stainless steel: k=0.015mm
3610801 1.5e-5,2.79e-2,1
* tlpvbfe (see p.130 of Manual Appendix A); which elements
3611001 10,1
* ebt (initial conditions options); P; T; 0; 0; 0; which elements
3611201 3,1.2e5,325.0,0.,0.,0.,1
*
* DRACS Cold Leg 1
* Component name; component type
3700000 DRACSc1 pipe
* Number of elements
3700001 16
* Volume flow area; which elements
3700101 6.11e-4,16
* Volume length; which elements
3700301 0.11085,16
* Volume azimuthal angle; which elements (optional card)
3700501 0.0,16
* Volume inclination angle; which elements (required)
3700601 -90.0,16
* Wall roughness; hydraulic diameter; which elements
* Here for stainless steel: k=0.015mm
3700801 1.5e-5,2.79e-2,16
* tlpvbfe (see p.130 of Manual Appendix A); which elements
3701001 0,16
* jefvcahs (see p.132 of Manual Appendix A); which elements
3701101 0,15
* ebt (initial conditions options); P; T; 0; 0; 0; which elements
3701201 3,1.25e5,325.0,0.,0.,0.,16
* Junction initial conditions control option (0 for velocities, 1 for mass flow rates)
3701300 1
* Initial liquid velocity; initial gas velocity; interface velocity (enter 0.0); junction number
3701301 0.,0.,0.,15
*
* DRACS Flowmeter
* Component name; component type
3710000 DRACSflo pipe
* Number of elements
3710001 1
* Volume flow area; which elements
3710101 6.11e-4,1
* Volume length; which elements
3710301 0.36000,1
* Volume azimuthal angle; which elements (optional card)
3710501 0.0,1
* Volume inclination angle; which elements (required)
3710601 -90.0,1
* Wall roughness; hydraulic diameter; which elements
* Here for stainless steel: k=0.015mm
3710801 1.5e-5,2.79e-2,1
```

```
* tlpvbfe (see p.130 of Manual Appendix A); which elements
3711001 10,1
* ebt (initial conditions options); P; T; 0; 0; 0; which elements
3711201 3,1.3e5,325.0,0.,0.,0.,1
*
* DRACS Cold Leg 2
* Component name; component type
3800000 DRACSc2 pipe
* Number of elements
3800001 3
* Volume flow area; which elements
3800101 6.11e-4,3
* Volume length; which elements
3800301 0.11218,3
* Volume azimuthal angle; which elements (optional card)
3800501 0.0,3
* Volume inclination angle; which elements (required)
3800601 -52.41532675,3
* Wall roughness; hydraulic diameter; which elements
* Here for stainless steel: k=0.015mm
3800801 1.5e-5,2.79e-2,3
* tlpvbfe (see p.130 of Manual Appendix A); which elements
3801001 0,3
* jefvcahs (see p.132 of Manual Appendix A); which elements
3801101 0,2
* ebt (initial conditions options); P; T; 0; 0; 0; which elements
3801201 3,1.35e5,325.0,0.,0.,0.,3
* Junction initial conditions control option (0 for velocities, 1 for mass flow rates)
3801300 1
* Initial liquid velocity; initial gas velocity; interface velocity (enter 0.0); junction number
3801301 0.,0.,0.,2
*
* DRACS Cold Leg 3
* Component name; component type
3900000 DRACSc3 pipe
* Number of elements
3900001 18
* Volume flow area; which elements
3900101 6.11e-4,18
* Volume length; which elements
3900301 0.10619,18
* Volume azimuthal angle; which elements (optional card)
3900501 0.0,18
* Volume inclination angle; which elements (required)
3900601 -80.6488182,18
* Wall roughness; hydraulic diameter; which elements
* Here for stainless steel: k=0.015mm
3900801 1.5e-5,2.79e-2,18
* tlpvbfe (see p.130 of Manual Appendix A); which elements
3901001 0,18
* jefvcahs (see p.132 of Manual Appendix A); which elements
3901101 0,17
* ebt (initial conditions options); P; T; 0; 0; 0; which elements
3901201 3,1.45e5,325.0,0.,0.,0.,18
* Junction initial conditions control option (0 for velocities, 1 for mass flow rates)
3901300 1
* Initial liquid velocity; initial gas velocity; interface velocity (enter 0.0); junction number
3901301 0.,0.,0.,17
*
* Primary Loop Expansion Tank
* Component name; component type
4010000 tank1 tmdpvol
```

```
* Volume flow area; volume length; volume volume (calculated if 0); azimuthal angle; inclination angle; elevation
change; wall roughness (1e-9 times hydraulic diameter if 0); hydraulic diameter (calculated if 0); tlpvbfe
4010101 1.0 1.0 0.0 0.0 90.0 1.0 0.0 0.0 0
* ebt
4010200 3
* Search variable (time); P; T
4010201 0.0 101.33e3 320.0
*
* DRACS Loop Expansion Tank
* Component name; component type
4020000 tank2 tmdpvol
* Volume flow area; volume length; volume volume (calculated if 0); azimuthal angle; inclination angle; elevation
change; wall roughness (1e-9 times hydraulic diameter if 0); hydraulic diameter (calculated if 0); tlpvbfe
4020101 1.0 1.0 0.0 0.0 90.0 1.0 0.0 0.0 0
* ebt
4020200 3
* Search variable (time); P; T
4020201 0.0 101.33e3 320.0
*
* Junction 11-10
* Component name; component type
5000000 jn1110 sngljun
* From; to; junction area; A_f; A_r; jefvcahs
5000101 11010000 10000000 3.64e-4 3.95 3.95 0
* Control word (0 for velocities, 1 for mass flow rates); initial liquid velocity; initial gas velocity; interface velocity
(enter 0.0)
5000201 1 0.18 0.18 0.
*
* Junction 10-12
* Component name; component type
5010000 jn1012 sngljun
* From; to; junction area; A_f; A_r; jefvcahs
5010101 10010000 12000000 3.64e-4 0. 0. 0
* Control word (0 for velocities, 1 for mass flow rates); initial liquid velocity; initial gas velocity; interface velocity
(enter 0.0)
5010201 1 0.18 0.18 0.
*
* Junction 12-20
* Component name; component type
5020000 jn1220 sngljun
* From; to; junction area; A_f; A_r; jefvcahs
5020101 12010000 20000000 6.11e-4 3.75 3.75 0
* Control word (0 for velocities, 1 for mass flow rates); initial liquid velocity; initial gas velocity; interface velocity
(enter 0.0)
5020201 1 0.18 0.18 0.
*
* Junction 20-21
* Component name; component type
5030000 jn2021 sngljun
* From; to; junction area; A_f; A_r; jefvcahs
5030101 20010000 21000000 6.11e-4 22.8 22.8 0
* User-specified form loss coefficients: B_f; C_f; B_r; C_r
5030111 4000. 1. 4000. 1.
* Control word (0 for velocities, 1 for mass flow rates); initial liquid velocity; initial gas velocity; interface velocity
(enter 0.0)
5030201 1 0.18 0.18 0.
*
* Junction 21-30
* Component name; component type
5040000 jn2130 sngljun
* From; to; junction area; A_f; A_r; jefvcahs
5040101 21010000 30000000 6.11e-4 0. 0. 0
```

```
* Control word (0 for velocities, 1 for mass flow rates); initial liquid velocity; initial gas velocity; interface velocity
(enter 0.0)
5040201 1 0.18 0.18 0.
*
* Junction 30-40
* Component name; component type
5050000 jn3040 sngljun
* From; to; junction area; A_f; A_r; jefvcahs
5050101 30010000 40000000 6.11e-4 17.15 17.15 0
* Control word (0 for velocities, 1 for mass flow rates); initial liquid velocity; initial gas velocity; interface velocity
(enter 0.0)
5050201 1 0.18 0.18 0.
*
* Junction 60-61
* Component name; component type
5060000 jn6061 sngljun
* From; to; junction area; A_f; A_r; jefvcahs
5060101 60010000 61000000 6.11e-4 26.05 26.05 0
* User-specified form loss coefficients: B_f; C_f; B_r; C_r
5060111 4000. 1. 4000. 1.
* Control word (0 for velocities, 1 for mass flow rates); initial liquid velocity; initial gas velocity; interface velocity
(enter 0.0)
5060201 1 0.18 0.18 0.
*
* Junction 61-71
* Component name; component type
5070000 jn6171 sngljun
* From; to; junction area; A_f; A_r; jefvcahs
5070101 61010000 71000000 6.11e-4 0. 0. 0
* Control word (0 for velocities, 1 for mass flow rates); initial liquid velocity; initial gas velocity; interface velocity
(enter 0.0)
5070201 1 0.18 0.18 0.
*
* Junction 71-72
* Component name; component type
5080000 jn7172 sngljun
* From; to; junction area; A_f; A_r; jefvcahs
5080101 71010000 72000000 1.33e-3 391.4 391.4 0
* User-specified form loss coefficients: B_f; C_f; B_r; C_r
5080111 57202.3 1. 57202.3 1.
* Control word (0 for velocities, 1 for mass flow rates); initial liquid velocity; initial gas velocity; interface velocity
(enter 0.0)
5080201 1 0.18 0.18 0.
*
* Junction 72-81
* Component name; component type
5090000 jn7281 sngljun
* From; to; junction area; A_f; A_r; jefvcahs
5090101 72010000 81000000 6.11e-4 0. 0. 0
* Control word (0 for velocities, 1 for mass flow rates); initial liquid velocity; initial gas velocity; interface velocity
(enter 0.0)
5090201 1 0.18 0.18 0.
*
* Junction 81-80
* Component name; component type
5100000 jn8180 sngljun
* From; to; junction area; A_f; A_r; jefvcahs
5100101 81010000 80000000 6.11e-4 24.75 24.75 0
* User-specified form loss coefficients: B_f; C_f; B_r; C_r
5100111 4000. 1. 4000. 1.
* Control word (0 for velocities, 1 for mass flow rates); initial liquid velocity; initial gas velocity; interface velocity
(enter 0.0)
```

```
5100201 1 0.18 0.18 0.
*
* Junction 80-90
* Component name; component type
5110000 jn8090 sngljun
* From; to; junction area; A_f; A_r; jefvcahs
5110101 80010000 90000000 6.11e-4 0. 0. 0
* Control word (0 for velocities, 1 for mass flow rates); initial liquid velocity; initial gas velocity; interface velocity
(enter 0.0)
5110201 1 0.18 0.18 0.
*
* Junction 90-100
* Component name; component type
5120000 jn90100 sngljun
* From; to; junction area; A_f; A_r; jefvcahs
5120101 90010000 100000000 6.11e-4 0.8 0.8 0
* Control word (0 for velocities, 1 for mass flow rates); initial liquid velocity; initial gas velocity; interface velocity
(enter 0.0)
5120201 1 0.18 0.18 0.
*
* Junction 100-110
* Component name; component type
5130000 jn100110 sngljun
* From; to; junction area; A_f; A_r; jefvcahs
5130101 100010000 110000000 6.11e-4 0. 0. 0
* Control word (0 for velocities, 1 for mass flow rates); initial liquid velocity; initial gas velocity; interface velocity
(enter 0.0)
5130201 1 0.18 0.18 0.
*
* Junction 110-120
* Component name; component type
5140000 jn110120 sngljun
* From; to; junction area; A_f; A_r; jefvcahs
5140101 110010000 120000000 6.11e-4 13.23 13.23 0
* Control word (0 for velocities, 1 for mass flow rates); initial liquid velocity; initial gas velocity; interface velocity
(enter 0.0)
5140201 1 0.18 0.18 0.
*
* Junction 120-130
* Component name; component type
5150000 jn120130 tmdpjun
* From; to; junction area; A_f; A_r; jefvcahs
5150101 120010000 130000000 6.11e-4 0
* Control word (0 for velocities, 1 for mass flow rates)
5150200 1
* Time; Liquid velocity; Gas velocity; interface velocity (enter 0.0)
5150201 0.0000 0.18 0. 0.
5150202 10000.0 0.18 0. 0.
*
* Junction 130-140
* Component name; component type
5160000 jn130140 sngljun
* From; to; junction area; A_f; A_r; jefvcahs
5160101 130010000 140000000 6.11e-4 23.78 23.78 0
* Control word (0 for velocities, 1 for mass flow rates); initial liquid velocity; initial gas velocity; interface velocity
(enter 0.0)
5160201 1 0.18 0.18 0.
*
* Junction 140-141
* Component name; component type
5170000 jn140141 sngljun
* From; to; junction area; A_f; A_r; jefvcahs
```

```
5170101 140010000 141000000 6.11e-4 2.4 2.4 0
* Control word (0 for velocities, 1 for mass flow rates); initial liquid velocity; initial gas velocity; interface velocity
(enter 0.0)
5170201 1 0.18 0.18 0.
*
* Junction 141-150
* Component name; component type
5180000 jn141150 sngljun
* From; to; junction area; A_f; A_r; jefvcahs
5180101 141010000 150000000 6.11e-4 18.1 18.1 0
* User-specified form loss coefficients: B_f; C_f; B_r; C_r
5180111 93006.9 1.3476 93006.9 1.3476
* Control word (0 for velocities, 1 for mass flow rates); initial liquid velocity; initial gas velocity; interface velocity
(enter 0.0)
5180201 1 0.18 0.18 0.
*
* Junction 150-160
* Component name; component type
5190000 jn150160 sngljun
* From; to; junction area; A_f; A_r; jefvcahs
5190101 150010000 160000000 6.11e-4 0.8 0.8 0
* Control word (0 for velocities, 1 for mass flow rates); initial liquid velocity; initial gas velocity; interface velocity
(enter 0.0)
5190201 1 0.18 0.18 0.
*
* Junction 180-11
* Component name; component type
5200000 jn18011 sngljun
* From; to; junction area; A_f; A_r; jefvcahs
5200101 180010000 11000000 6.11e-4 5.15 5.15 0
* Control word (0 for velocities, 1 for mass flow rates); initial liquid velocity; initial gas velocity; interface velocity
(enter 0.0)
5200201 1 0.18 0.18 0.
*
* Junction 190-200
* Component name; component type
5210000 jn190200 sngljun
* From; to; junction area; A_f; A_r; jefvcahs
5210101 190010000 200000000 6.11e-4 7.5 7.5 0
* Control word (0 for velocities, 1 for mass flow rates); initial liquid velocity; initial gas velocity; interface velocity
(enter 0.0)
5210201 1 0. 0. 0.
*
* Junction 200-210
* Component name; component type
5220000 jn200210 sngljun
* From; to; junction area; A_f; A_r; jefvcahs
5220101 200010000 210000000 6.11e-4 0. 0. 0
* Control word (0 for velocities, 1 for mass flow rates); initial liquid velocity; initial gas velocity; interface velocity
(enter 0.0)
5220201 1 0. 0. 0.
*
* Junction 210-211
* Component name; component type
5230000 jn210211 sngljun
* From; to; junction area; A_f; A_r; jefvcahs
5230101 210010000 211000000 6.11e-4 4.4 4.4 0
* Control word (0 for velocities, 1 for mass flow rates); initial liquid velocity; initial gas velocity; interface velocity
(enter 0.0)
5230201 1 0. 0. 0.
*
* Junction 211-220
```

```
* Component name; component type
5240000 jn211220 sngljun
* From; to; junction area; A_f; A_r; jefvcahs
5240101 211010000 220000000 6.11e-4 18.1 18.1 0
* User-specified form loss coefficients: B_f; C_f; B_r; C_r
5240111 93006.9 1.3476 93006.9 1.3476
* Control word (0 for velocities, 1 for mass flow rates); initial liquid velocity; initial gas velocity; interface velocity
(enter 0.0)
5240201 1 0. 0. 0.
*
* Junction 220-231
* Component name; component type
5250000 jn220231 sngljun
* From; to; junction area; A_f; A_r; jefvcahs
5250101 220010000 231000000 6.11e-4 45.95 45.95 0
* Control word (0 for velocities, 1 for mass flow rates); initial liquid velocity; initial gas velocity; interface velocity
(enter 0.0)
5250201 1 0. 0. 0.
*
* Junction 231-230
* Component name; component type
5260000 jn231230 sngljun
* From; to; junction area; A_f; A_r; jefvcahs
5260101 231010000 230000000 6.11e-4 22.35 22.35 0
* User-specified form loss coefficients: B_f; C_f; B_r; C_r
5260111 4000. 1. 4000. 1.
* Control word (0 for velocities, 1 for mass flow rates); initial liquid velocity; initial gas velocity; interface velocity
(enter 0.0)
5260201 1 0. 0. 0.
*
* Junction 230-240
* Component name; component type
5270000 jn230240 sngljun
* From; to; junction area; A_f; A_r; jefvcahs
5270101 230010000 240000000 6.11e-4 0. 0. 0
* Control word (0 for velocities, 1 for mass flow rates); initial liquid velocity; initial gas velocity; interface velocity
(enter 0.0)
5270201 1 0. 0. 0.
*
* Junction 240-250
* Component name; component type
5280000 jn240250 sngljun
* From; to; junction area; A_f; A_r; jefvcahs
5280101 240010000 250000000 6.11e-4 23.9 23.9 0
* Control word (0 for velocities, 1 for mass flow rates); initial liquid velocity; initial gas velocity; interface velocity
(enter 0.0)
5280201 1 0. 0. 0.
*
* Junction 250-251
* Component name; component type
5290000 jn250251 sngljun
* From; to; junction area; A_f; A_r; jefvcahs
5290101 250010000 251000000 6.11e-4 22.35 22.35 0
* User-specified form loss coefficients: B_f; C_f; B_r; C_r
5290111 4000. 1. 4000. 1.
* Control word (0 for velocities, 1 for mass flow rates); initial liquid velocity; initial gas velocity; interface velocity
(enter 0.0)
5290201 1 0. 0. 0.
*
* Junction 251-260
* Component name; component type
5300000 jn251260 valve
```

* From; to; junction area; A_f; A_r; jefvcahs
5300101 251010000 260000000 6.11e-4 0. 0. 0
* Control word (0 for velocities, 1 for mass flow rates); initial liquid velocity; initial gas velocity; interface velocity (enter 0.0)
5300201 1 0. 0. 0.
* Valve type
5300300 trpvlv
* Trip number (false = closed; true = open)
5300301 401
*
* Junction 301-300
* Component name; component type
5310000 jn301300 sngljun
* From; to; junction area; A_f; A_r; jefvcahs
5310101 301010000 300000000 7.18e-4 0. 0. 0
* Control word (0 for velocities, 1 for mass flow rates); initial liquid velocity; initial gas velocity; interface velocity (enter 0.0)
5310201 1 0. 0. 0.
*
* Junction 300-302
* Component name; component type
5320000 jn300302 sngljun
* From; to; junction area; A_f; A_r; jefvcahs
5320101 300010000 302000000 7.18e-4 3.3 3.3 0
* Control word (0 for velocities, 1 for mass flow rates); initial liquid velocity; initial gas velocity; interface velocity (enter 0.0)
5320201 1 0. 0. 0.
*
* Junction 302-310
* Component name; component type
5330000 jn302310 sngljun
* From; to; junction area; A_f; A_r; jefvcahs
5330101 302010000 310000000 6.11e-4 0. 0. 0
* Control word (0 for velocities, 1 for mass flow rates); initial liquid velocity; initial gas velocity; interface velocity (enter 0.0)
5330201 1 0. 0. 0.
*
* Junction 310-311
* Component name; component type
5340000 jn310311 sngljun
* From; to; junction area; A_f; A_r; jefvcahs
5340101 310010000 311000000 6.11e-4 22.35 22.35 0
* User-specified form loss coefficients: B_f; C_f; B_r; C_r
5340111 4000. 1. 4000. 1.
* Control word (0 for velocities, 1 for mass flow rates); initial liquid velocity; initial gas velocity; interface velocity (enter 0.0)
5340201 1 0. 0. 0.
*
* Junction 311-320
* Component name; component type
5350000 jn311320 sngljun
* From; to; junction area; A_f; A_r; jefvcahs
5350101 311010000 320000000 6.11e-4 0. 0. 0
* Control word (0 for velocities, 1 for mass flow rates); initial liquid velocity; initial gas velocity; interface velocity (enter 0.0)
5350201 1 0. 0. 0.
*
* Junction 320-330
* Component name; component type
5360000 jn320330 sngljun
* From; to; junction area; A_f; A_r; jefvcahs
5360101 320010000 330000000 6.11e-4 0.8 0.8 0

* Control word (0 for velocities, 1 for mass flow rates); initial liquid velocity; initial gas velocity; interface velocity (enter 0.0)
5360201 1 0. 0. 0.
*
* Junction 351-352
* Component name; component type
5370000 jn351352 sngljun
* From; to; junction area; A_f; A_r; jefvcahs
5370101 351010000 352000000 1.33e-3 442.74 442.74 0
* User-specified form loss coefficients: B_f; C_f; B_r; C_r
5370111 48022.3 1. 48022.3 1.
* Control word (0 for velocities, 1 for mass flow rates); initial liquid velocity; initial gas velocity; interface velocity (enter 0.0)
5370201 1 0. 0. 0.
*
* Junction 352-360
* Component name; component type
5380000 jn352360 sngljun
* From; to; junction area; A_f; A_r; jefvcahs
5380101 352010000 360000000 6.11e-4 5.8 5.8 0
* Control word (0 for velocities, 1 for mass flow rates); initial liquid velocity; initial gas velocity; interface velocity (enter 0.0)
5380201 1 0. 0. 0.
*
* Junction 360-361
* Component name; component type
5390000 jn360361 sngljun
* From; to; junction area; A_f; A_r; jefvcahs
5390101 360010000 361000000 6.11e-4 24.75 24.75 0
* User-specified form loss coefficients: B_f; C_f; B_r; C_r
5390111 4000. 1. 4000. 1.
* Control word (0 for velocities, 1 for mass flow rates); initial liquid velocity; initial gas velocity; interface velocity (enter 0.0)
5390201 1 0. 0. 0.
*
* Junction 361-370
* Component name; component type
5400000 jn361370 sngljun
* From; to; junction area; A_f; A_r; jefvcahs
5400101 361010000 370000000 6.11e-4 0. 0. 0
* Control word (0 for velocities, 1 for mass flow rates); initial liquid velocity; initial gas velocity; interface velocity (enter 0.0)
5400201 1 0. 0. 0.
*
* Junction 370-371
* Component name; component type
5410000 jn370371 sngljun
* From; to; junction area; A_f; A_r; jefvcahs
5410101 370010000 371000000 6.11e-4 14. 14. 0
* Control word (0 for velocities, 1 for mass flow rates); initial liquid velocity; initial gas velocity; interface velocity (enter 0.0)
5410201 1 0. 0. 0.
*
* Junction 371-380
* Component name; component type
5420000 jn371380 sngljun
* From; to; junction area; A_f; A_r; jefvcahs
5420101 371010000 380000000 6.11e-4 18.1 18.1 0
* User-specified form loss coefficients: B_f; C_f; B_r; C_r
5420111 93006.9 1.3476 93006.9 1.3476
* Control word (0 for velocities, 1 for mass flow rates); initial liquid velocity; initial gas velocity; interface velocity (enter 0.0)

```
5420201 1 0. 0. 0.
*
* Junction 380-390
* Component name; component type
5430000 jn380390 sngljun
* From; to; junction area; A_f; A_r; jefvcahs
5430101 380010000 390000000 6.11e-4 0.8 0.8 0
* Control word (0 for velocities, 1 for mass flow rates); initial liquid velocity; initial gas velocity; interface velocity
(enter 0.0)
5430201 1 0. 0. 0.
*
* Junction 390-301
* Component name; component type
5440000 jn390301 sngljun
* From; to; junction area; A_f; A_r; jefvcahs
5440101 390010000 301000000 6.11e-4 2.65 2.65 0
* Control word (0 for velocities, 1 for mass flow rates); initial liquid velocity; initial gas velocity; interface velocity
(enter 0.0)
5440201 1 0. 0. 0.
*
* Branch 5
* Component name; component type
500000 branch5 branch
* Number of junctions; control word (0: velocities, 1: mass flow rates)
500001 4 1
* Volume flow area; volume length; volume of volume (calculated if 0.0); azimuthal angle; vertical angle; elevation
change; wall roughness; hydraulic diameter; tlpvbfe
500101 6.11e-4 0.74930 0. 0. 0. 0. 1.5e-5 2.79e-2 0
* ebt (initial conditions options); P; T
500200 3 1.1e5 325.0
* From; to; junction area; A_f; A_r; jefvcahs
501101  40010000  50000000 6.11e-4 2.4 2.4 0
502101  50010000  60000000 6.11e-4 0. 0. 0
503101  50010000 401000000 6.11e-4 0. 0. 100
504101 260010000  50000000 6.11e-4 1.75 1.75 0
* Initial liquid velocity; initial gas velocity;
* Interface velocity (enter 0.0)
501201  0.18  0.18 0.
502201  0.18  0.18 0.
503201  0.000  0.000 0.
504201  0.000  0.000 0.
*
* Branch 17
* Component name; component type
1700000 branch17 branch
* Number of junctions; control word (0: velocities, 1: mass flow rates)
1700001 3 1
* Volume flow area; volume length; volume of volume (calculated if 0.0); azimuthal angle; vertical angle; elevation
change; wall roughness; hydraulic diameter; tlpvbfe
1700101 6.11e-4 0.47308 0. 0. 0. 0. 1.5e-5 2.79e-2 0
* ebt (initial conditions options); P; T
1700200 3 1.4e5 325.0
* From; to; junction area; A_f; A_r; jefvcahs
1701101  160010000  170000000 6.11e-4 1.9 1.9 0
1702101  170010000  180000000 6.11e-4 0. 0. 0
1703101  170010000  190000000 6.11e-4 0. 0. 0
* Initial liquid velocity; initial gas velocity;
* Interface velocity (enter 0.0)
1701201  0.18  0.18 0.
1702201  0.18  0.18 0.
1703201 -0.000 -0.000 0.
*
```

```
* Branch 34
* Component name; component type
3400000 branch34 branch
* Number of junctions; control word (0: velocities, 1: mass flow rates)
3400001 3 1
* Volume flow area; volume length; volume of volume (calculated if 0.0); azimuthal angle; vertical angle; elevation
change; wall roughness; hydraulic diameter; tlpvbfe
3400101 6.11e-4 0.55245 0. 0. 0. 0. 1.5e-5 2.79e-2 0
* ebt (initial conditions options); P; T
3400200 3 1.15e5 325.0
* From; to; junction area; A_f; A_r; jefvcahs
3401101  330010000  340000000 6.11e-4 2.75 2.75 0
3402101  340000000  402000000 6.11e-4 0. 0. 100
3403101  340010000  351000000 6.11e-4 4.25 4.25 0
* Initial liquid velocity; initial gas velocity;
* Interface velocity (enter 0.0)
3401201  0.000  0.000 0.
3402201  0.000  0.000 0.
3403201  0.000  0.000 0.
*
*******************************************************
* Heat structures
*******************************************************
*
* Bottom of heater outer tube
* Number of axial heat structures; number of radial mesh points;
* Geometry type (2: cylindrical, coupled to hydrodynamic component);
* Steady-state initialization flag (1: initial T calculated by code);
* Left boundary coordinate; reflood condition
10111000 2 7 2 1 1.92e-2 0
* Mesh location flag; mesh format flag (see p.252 of Manual Appendix A)
10111100 0 2
* Mesh interval distance; interval number
10111101 9.525e-4 2
10111102 1.270e-2 6
* Composition (table number); interval number
10111201 100 2
10111202 120 6
* Power input proportion; mesh interval number
10111301 1.0 2
10111302 0.0 6
* Initial temperature; mesh point number
10111401 325.0  3
10111402 293.15 7
* Left boundary condition definition (here: vol number); increment;
* Boundary condition type (101: convection); surface area code (1: length);
* Length; heat structure number
10111501 11010000 10000 101 1 0.47828 2
* Right boundary condition, see above (-30: T defined in general table 30; 1000: T set in Word 1)
10111601 -30 0 1000 1 0.47828 2
* Power source (table number); internal source multiplier; direct mod heatin mult (left)
* Direct mod heatin mult (right); heat structure number
10111701 0 0.0 0.0 0.0 2
* Additional left boundary: heat transfer hydraulic diameter; heated length fwd (10.: ignore);
* Heated length rev (10.: ignore); grid spacer length fwd (0.: ignore); grid spacer length rev (0.: ignore);
* Grid loss coef fwd (0.: ignore); grid loss coef rev (0.: ignore); boiling factor (1.: subcooled liquid);
* Heat structure number
10111801 1.21e-2 10.0 10.0 0.0 0.0 0.0 0.0 1.0 2
*
* Bottom of heater inner tube
* Number of axial heat structures; number of radial mesh points;
* Geometry type (2: cylindrical, coupled to hydrodynamic component);
```

```
* Steady-state initialization flag (1: initial T calculated by code);
* Left boundary coordinate; reflood condition
10112000 2 3 2 1 1.33e-2 0
* Mesh location flag; mesh format flag (see p.252 of Manual Appendix A)
10112100 0 1
* Number of intervals; right coordinate
10112101 2 1.59e-2
* Composition (table number); interval number
10112201 100 2
* Power input proportion; mesh interval number
10112301 1.0 2
* Initial temperature; mesh point number
10112401 325.0 3
* Left boundary condition definition (0: adiabatic); increment;
* Boundary condition type (0: adiabatic); surface area code (1: length);
* Length; heat structure number
10112501 0 0 0 1 0.47828 2
* Right boundary condition, see above (101: convection)
10112601 11010000 10000 101 1 0.47828 2
* Power source (no source); internal source multiplier; direct mod heatin mult (left)
* Direct mod heatin mult (right); heat structure number
10112701 0 0.0 0.0 0.0 2
* Additional right boundary: heat transfer hydraulic diameter; heated length fwd (10.: ignore);
* Heated length rev (10.: ignore); grid spacer length fwd (0.: ignore); grid spacer length rev (0.: ignore);
* Grid loss coef fwd (0.: ignore); grid loss coef rev (0.: ignore); boiling factor (1.: subcooled liquid);
* Heat structure number
10112901 1.46e-2 10.0 10.0 0.0 0.0 0.0 0.0 1.0 2
*
* Heater outer tube
* Number of axial heat structures; number of radial mesh points;
* Geometry type (2: cylindrical, coupled to hydrodynamic component);
* Steady-state initialization flag (1: initial T calculated by code);
* Left boundary coordinate; reflood condition
10101000 15 3 2 1 1.92e-2 0
* Mesh location flag; mesh format flag (see p.252 of Manual Appendix A)
10101100 0 2
* Mesh interval distance; interval number
10101101 9.525e-4 2
* Composition (table number); interval number
10101201 100 2
* Power input proportion; mesh interval number
10101301 1.0 2
* Initial temperature; mesh point number
10101401 325.0  3
* Left boundary condition definition (here: vol number); increment;
* Boundary condition type (101: convection); surface area code (1: length);
* Length; heat structure number
10101501 10010000 10000 101 1 0.10922 15
* Right boundary condition, see above (0: adiabatic)
10101601 0 0 0 1 0.10922 15
* Power source (table number); internal source multiplier; direct mod heatin mult (left)
* Direct mod heatin mult (right); heat structure number
10101701 10 0.066666667 0.0 0.0 15
* Additional left boundary: heat transfer hydraulic diameter; heated length fwd (10.: ignore);
* Heated length rev (10.: ignore); grid spacer length fwd (0.: ignore); grid spacer length rev (0.: ignore);
* Grid loss coef fwd (0.: ignore); grid loss coef rev (0.: ignore); boiling factor (1.: subcooled liquid);
* Heat structure number
10101801 1.21e-2 10.0 10.0 0.0 0.0 0.0 0.0 1.0 15
*
* Heater inner tube
* Number of axial heat structures; number of radial mesh points;
* Geometry type (2: cylindrical, coupled to hydrodynamic component);
```

```
* Steady-state initialization flag (1: initial T calculated by code);
* Left boundary coordinate; reflood condition
10102000 15 3 2 1 1.33e-2 0
* Mesh location flag; mesh format flag (see p.252 of Manual Appendix A)
10102100 0 1
* Number of intervals; right coordinate
10102101 2 1.59e-2
* Composition (table number); interval number
10102201 100 2
* Power input proportion; mesh interval number
10102301 1.0 2
* Initial temperature; mesh point number
10102401 325.0 3
* Left boundary condition definition (0: adiabatic); increment;
* Boundary condition type (0: adiabatic); surface area code (1: length);
* Length; heat structure number
10102501 0 0 0 1 0.10922 15
* Right boundary condition, see above (101: convection)
10102601 10010000 10000 101 1 0.10922 15
* Power source (no source); internal source multiplier; direct mod heatin mult (left)
* Direct mod heatin mult (right); heat structure number
10102701 0 0.0 0.0 0.0 15
* Additional right boundary: heat transfer hydraulic diameter; heated length fwd (10.: ignore);
* Heated length rev (10.: ignore); grid spacer length fwd (0.: ignore); grid spacer length rev (0.: ignore);
* Grid loss coef fwd (0.: ignore); grid loss coef rev (0.: ignore); boiling factor (1.: subcooled liquid);
* Heat structure number
10102901 1.46e-2 10.0 10.0 0.0 0.0 0.0 0.0 1.0 15
*
* Top of heater outer tube
* Number of axial heat structures; number of radial mesh points;
* Geometry type (2: cylindrical, coupled to hydrodynamic component);
* Steady-state initialization flag (1: initial T calculated by code);
* Left boundary coordinate; reflood condition
10121000 1 7 2 1 1.92e-2 0
* Mesh location flag; mesh format flag (see p.252 of Manual Appendix A)
10121100 0 2
* Mesh interval distance; interval number
10121101 9.525e-4 2
10121102 1.270e-2 6
* Composition (table number); interval number
10121201 100 2
10121202 120 6
* Power input proportion; mesh interval number
10121301 1.0 2
10121302 0.0 6
* Initial temperature; mesh point number
10121401 325.0  3
10121402 293.15 7
* Left boundary condition definition (here: vol number); increment;
* Boundary condition type (101: convection); surface area code (1: length);
* Length; heat structure number
10121501 12010000 10000 101 1 0.40561 1
* Right boundary condition, see above (-30: T defined in general table 30; 1000: T set in Word 1)
10121601 -30 0 1000 1 0.40561 1
* Power source (table number); internal source multiplier; direct mod heatin mult (left)
* Direct mod heatin mult (right); heat structure number
10121701 0 0.0 0.0 0.0 1
* Additional left boundary: heat transfer hydraulic diameter; heated length fwd (10.: ignore);
* Heated length rev (10.: ignore); grid spacer length fwd (0.: ignore); grid spacer length rev (0.: ignore);
* Grid loss coef fwd (0.: ignore); grid loss coef rev (0.: ignore); boiling factor (1.: subcooled liquid);
* Heat structure number
10121801 1.21e-2 10.0 10.0 0.0 0.0 0.0 0.0 1.0 1
```

```
*
* Top of heater inner tube
* Number of axial heat structures; number of radial mesh points;
* Geometry type (2: cylindrical, coupled to hydrodynamic component);
* Steady-state initialization flag (1: initial T calculated by code);
* Left boundary coordinate; reflood condition
10122000 1 3 2 1 1.33e-2 0
* Mesh location flag; mesh format flag (see p.252 of Manual Appendix A)
10122100 0 1
* Number of intervals; right coordinate
10122101 2 1.59e-2
* Composition (table number); interval number
10122201 100 2
* Power input proportion; mesh interval number
10122301 1.0 2
* Initial temperature; mesh point number
10122401 325.0 3
* Left boundary condition definition (0: adiabatic); increment;
* Boundary condition type (0: adiabatic); surface area code (1: length);
* Length; heat structure number
10122501 0 0 0 1 0.40561 1
* Right boundary condition, see above (101: convection)
10122601 12010000 10000 101 1 0.40561 1
* Power source (no source); internal source multiplier; direct mod heatin mult (left)
* Direct mod heatin mult (right); heat structure number
10122701 0 0.0 0.0 0.0 1
* Additional right boundary: heat transfer hydraulic diameter; heated length fwd (10.: ignore);
* Heated length rev (10.: ignore); grid spacer length fwd (0.: ignore); grid spacer length rev (0.: ignore);
* Grid loss coef fwd (0.: ignore); grid loss coef rev (0.: ignore); boiling factor (1.: subcooled liquid);
* Heat structure number
10122901 1.46e-2 10.0 10.0 0.0 0.0 0.0 0.0 1.0 1
*
* Heater mixer pipe
* Number of axial heat structures; number of radial mesh points;
* Geometry type (2: cylindrical, coupled to hydrodynamic component);
* Steady-state initialization flag (1: initial T calculated by code);
* Left boundary coordinate; reflood condition
10201000 1 7 2 1 1.39e-2 0
* Mesh location flag; mesh format flag (see p.252 of Manual Appendix A)
10201100 0 2
* Mesh interval distance; interval number
10201101 5.426e-4 2
10201102 1.270e-2 6
* Composition (table number); interval number
10201201 100 2
10201202 120 6
* Power input proportion; mesh interval number
10201301 1.0 2
10201302 0.0 6
* Initial temperature; mesh point number
10201401 325.0  3
10201402 293.15 7
* Left boundary condition definition (here: vol number); increment;
* Boundary condition type (101: convection); surface area code (1: length);
* Length; heat structure number
10201501 20010000 10000 101 1 1.01674 1
* Right boundary condition, see above (-30: T defined in general table 30; 1000: T set in Word 1)
10201601 -30 0 1000 1 1.01674 1
* Power source (table number); internal source multiplier; direct mod heatin mult (left)
* Direct mod heatin mult (right); heat structure number
10201701 0 0.0 0.0 0.0 1
* Additional left boundary: heat transfer hydraulic diameter; heated length fwd (10.: ignore);
```

```
* Heated length rev (10.: ignore); grid spacer length fwd (0.: ignore); grid spacer length rev (0.: ignore);
* Grid loss coef fwd (0.: ignore); grid loss coef rev (0.: ignore); boiling factor (1.: subcooled liquid);
* Heat structure number
10201801 0.0 10.0 10.0 0.0 0.0 0.0 0.0 1.0 1
*
* Heater mixer
* Number of axial heat structures; number of radial mesh points;
* Geometry type (2: cylindrical, coupled to hydrodynamic component);
* Steady-state initialization flag (1: initial T calculated by code);
* Left boundary coordinate; reflood condition
10211000 1 7 2 1 1.39e-2 0
* Mesh location flag; mesh format flag (see p.252 of Manual Appendix A)
10211100 0 2
* Mesh interval distance; interval number
10211101 5.426e-4 2
10211102 1.270e-2 6
* Composition (table number); interval number
10211201 100 2
10211202 120 6
* Power input proportion; mesh interval number
10211301 1.0 2
10211302 0.0 6
* Initial temperature; mesh point number
10211401 325.0  3
10211402 293.15 7
* Left boundary condition definition (here: vol number); increment;
* Boundary condition type (101: convection); surface area code (1: length);
* Length; heat structure number
10211501 21010000 10000 101 1 2.24537 1
* Right boundary condition, see above (-30: T defined in general table 30; 1000: T set in Word 1)
10211601 -30 0 1000 1 2.24537 1
* Power source (table number); internal source multiplier; direct mod heatin mult (left)
* Direct mod heatin mult (right); heat structure number
10211701 0 0.0 0.0 0.0 1
* Additional left boundary: heat transfer hydraulic diameter; heated length fwd (10.: ignore);
* Heated length rev (10.: ignore); grid spacer length fwd (0.: ignore); grid spacer length rev (0.: ignore);
* Grid loss coef fwd (0.: ignore); grid loss coef rev (0.: ignore); boiling factor (1.: subcooled liquid);
* Heat structure number
10211801 0.0 10.0 10.0 0.0 0.0 0.0 0.0 1.0 1
*
* Hot leg 1
* Number of axial heat structures; number of radial mesh points;
* Geometry type (2: cylindrical, coupled to hydrodynamic component);
* Steady-state initialization flag (1: initial T calculated by code);
* Left boundary coordinate; reflood condition
10301000 12 7 2 1 1.39e-2 0
* Mesh location flag; mesh format flag (see p.252 of Manual Appendix A)
10301100 0 2
* Mesh interval distance; interval number
10301101 5.426e-4 2
10301102 1.270e-2 6
* Composition (table number); interval number
10301201 100 2
10301202 120 6
* Power input proportion; mesh interval number
10301301 1.0 2
10301302 0.0 6
* Initial temperature; mesh point number
10301401 325.0  3
10301402 293.15 7
* Left boundary condition definition (here: vol number); increment;
* Boundary condition type (101: convection); surface area code (1: length);
```

```
* Length; heat structure number
10301501 30010000 10000 101 1 0.72730 12
* Right boundary condition, see above (-30: T defined in general table 30; 1000: T set in Word 1)
10301601 -30 0 1000 1 0.72730 12
* Power source (table number); internal source multiplier; direct mod heatin mult (left)
* Direct mod heatin mult (right); heat structure number
10301701 0 0.0 0.0 0.0 12
* Additional left boundary: heat transfer hydraulic diameter; heated length fwd (10.: ignore);
* Heated length rev (10.: ignore); grid spacer length fwd (0.: ignore); grid spacer length rev (0.: ignore);
* Grid loss coef fwd (0.: ignore); grid loss coef rev (0.: ignore); boiling factor (1.: subcooled liquid);
* Heat structure number
10301801 0.0 10.0 10.0 0.0 0.0 0.0 0.0 1.0 12
*
* Hot leg 2
* Number of axial heat structures; number of radial mesh points;
* Geometry type (2: cylindrical, coupled to hydrodynamic component);
* Steady-state initialization flag (1: initial T calculated by code);
* Left boundary coordinate; reflood condition
10401000 2 7 2 1 1.39e-2 0
* Mesh location flag; mesh format flag (see p.252 of Manual Appendix A)
10401100 0 2
* Mesh interval distance; interval number
10401101 5.426e-4 2
10401102 1.270e-2 6
* Composition (table number); interval number
10401201 100 2
10401202 120 6
* Power input proportion; mesh interval number
10401301 1.0 2
10401302 0.0 6
* Initial temperature; mesh point number
10401401 325.0  3
10401402 293.15 7
* Left boundary condition definition (here: vol number); increment;
* Boundary condition type (101: convection); surface area code (1: length);
* Length; heat structure number
10401501 40010000 10000 101 1 0.82093 2
* Right boundary condition, see above (-30: T defined in general table 30; 1000: T set in Word 1)
10401601 -30 0 1000 1 0.82093 2
* Power source (table number); internal source multiplier; direct mod heatin mult (left)
* Direct mod heatin mult (right); heat structure number
10401701 0 0.0 0.0 0.0 2
* Additional left boundary: heat transfer hydraulic diameter; heated length fwd (10.: ignore);
* Heated length rev (10.: ignore); grid spacer length fwd (0.: ignore); grid spacer length rev (0.: ignore);
* Grid loss coef fwd (0.: ignore); grid loss coef rev (0.: ignore); boiling factor (1.: subcooled liquid);
* Heat structure number
10401801 0.0 10.0 10.0 0.0 0.0 0.0 0.0 1.0 2
*
* Branch 5
* Number of axial heat structures; number of radial mesh points;
* Geometry type (2: cylindrical, coupled to hydrodynamic component);
* Steady-state initialization flag (1: initial T calculated by code);
* Left boundary coordinate; reflood condition
10501000 1 7 2 1 1.39e-2 0
* Mesh location flag; mesh format flag (see p.252 of Manual Appendix A)
10501100 0 2
* Mesh interval distance; interval number
10501101 5.426e-4 2
10501102 1.270e-2 6
* Composition (table number); interval number
10501201 100 2
10501202 120 6
```

```
* Power input proportion; mesh interval number
10501301 1.0 2
10501302 0.0 6
* Initial temperature; mesh point number
10501401 325.0  3
10501402 293.15 7
* Left boundary condition definition (here: vol number); increment;
* Boundary condition type (101: convection); surface area code (1: length);
* Length; heat structure number
10501501 50010000 10000 101 1 5.09834 1
* Right boundary condition, see above (-30: T defined in general table 30; 1000: T set in Word 1)
10501601 -30 0 1000 1 5.09834 1
* Power source (table number); internal source multiplier; direct mod heatin mult (left)
* Direct mod heatin mult (right); heat structure number
10501701 0 0.0 0.0 0.0 1
* Additional left boundary: heat transfer hydraulic diameter; heated length fwd (10.: ignore);
* Heated length rev (10.: ignore); grid spacer length fwd (0.: ignore); grid spacer length rev (0.: ignore);
* Grid loss coef fwd (0.: ignore); grid loss coef rev (0.: ignore); boiling factor (1.: subcooled liquid);
* Heat structure number
10501801 0.0 10.0 10.0 0.0 0.0 0.0 0.0 1.0 1
*
* CTAH inlet mixer pipe
* Number of axial heat structures; number of radial mesh points;
* Geometry type (2: cylindrical, coupled to hydrodynamic component);
* Steady-state initialization flag (1: initial T calculated by code);
* Left boundary coordinate; reflood condition
10601000 1 7 2 1 1.39e-2 0
* Mesh location flag; mesh format flag (see p.252 of Manual Appendix A)
10601100 0 2
* Mesh interval distance; interval number
10601101 5.426e-4 2
10601102 1.270e-2 6
* Composition (table number); interval number
10601201 100 2
10601202 120 6
* Power input proportion; mesh interval number
10601301 1.0 2
10601302 0.0 6
* Initial temperature; mesh point number
10601401 325.0  3
10601402 293.15 7
* Left boundary condition definition (here: vol number); increment;
* Boundary condition type (101: convection); surface area code (1: length);
* Length; heat structure number
10601501 60010000 10000 101 1 1.03832 1
* Right boundary condition, see above (-30: T defined in general table 30; 1000: T set in Word 1)
10601601 -30 0 1000 1 1.03832 1
* Power source (table number); internal source multiplier; direct mod heatin mult (left)
* Direct mod heatin mult (right); heat structure number
10601701 0 0.0 0.0 0.0 1
* Additional left boundary: heat transfer hydraulic diameter; heated length fwd (10.: ignore);
* Heated length rev (10.: ignore); grid spacer length fwd (0.: ignore); grid spacer length rev (0.: ignore);
* Grid loss coef fwd (0.: ignore); grid loss coef rev (0.: ignore); boiling factor (1.: subcooled liquid);
* Heat structure number
10601801 0.0 10.0 10.0 0.0 0.0 0.0 0.0 1.0 1
*
* CTAH inlet mixer
* Number of axial heat structures; number of radial mesh points;
* Geometry type (2: cylindrical, coupled to hydrodynamic component);
* Steady-state initialization flag (1: initial T calculated by code);
* Left boundary coordinate; reflood condition
10611000 1 7 2 1 1.39e-2 0
```

```
* Mesh location flag; mesh format flag (see p.252 of Manual Appendix A)
10611100 0 2
* Mesh interval distance; interval number
10611101 5.426e-4 2
10611102 1.270e-2 6
* Composition (table number); interval number
10611201 100 2
10611202 120 6
* Power input proportion; mesh interval number
10611301 1.0 2
10611302 0.0 6
* Initial temperature; mesh point number
10611401 325.0  3
10611402 293.15 7
* Left boundary condition definition (here: vol number); increment;
* Boundary condition type (101: convection); surface area code (1: length);
* Length; heat structure number
10611501 61010000 10000 101 1 2.24536 1
* Right boundary condition, see above (-30: T defined in general table 30; 1000: T set in Word 1)
10611601 -30 0 1000 1 2.24536 1
* Power source (table number); internal source multiplier; direct mod heatin mult (left)
* Direct mod heatin mult (right); heat structure number
10611701 0 0.0 0.0 0.0 1
* Additional left boundary: heat transfer hydraulic diameter; heated length fwd (10.: ignore);
* Heated length rev (10.: ignore); grid spacer length fwd (0.: ignore); grid spacer length rev (0.: ignore);
* Grid loss coef fwd (0.: ignore); grid loss coef rev (0.: ignore); boiling factor (1.: subcooled liquid);
* Heat structure number
10611801 0.0 10.0 10.0 0.0 0.0 0.0 0.0 1.0 1
*
* CTAH 1
* Number of axial heat structures; number of radial mesh points;
* Geometry type (2: cylindrical, coupled to hydrodynamic component);
* Steady-state initialization flag (1: initial T calculated by code);
* Left boundary coordinate; reflood condition
10711000 3 5 2 1 5.95e-3 0
* Mesh location flag; mesh format flag (see p.252 of Manual Appendix A)
10711100 0 2
* Mesh interval distance; interval number
10711101 4.00e-4 4
* Composition (table number); interval number
10711201 110 4
* Power input proportion; mesh interval number
10711301 1.0 4
* Initial temperature; mesh point number
10711401 325.0  5
* Left boundary condition definition (here: vol number); increment;
* Boundary condition type (3060: HTC set in general table 60); surface area code (1: length);
* Length; heat structure number
10711501 71010000 10000 3060 1 0.11007 3
* Right boundary condition, see above (-40: T defined in general table 40; 1000: T set in Word 1)
10711601 -40 0 1000 1 0.11007 3
* Power source (table number); internal source multiplier; direct mod heatin mult (left)
* Direct mod heatin mult (right); heat structure number
10711701 0 0.0 0.0 0.0 3
* Additional left boundary: heat transfer hydraulic diameter; heated length fwd (10.: ignore);
* Heated length rev (10.: ignore); grid spacer length fwd (0.: ignore); grid spacer length rev (0.: ignore);
* Grid loss coef fwd (0.: ignore); grid loss coef rev (0.: ignore); boiling factor (1.: subcooled liquid);
* Heat structure number
10711801 0.0 10.0 10.0 0.0 0.0 0.0 0.0 1.0 3
*
* CTAH 2
* Number of axial heat structures; number of radial mesh points;
```

```
* Geometry type (2: cylindrical, coupled to hydrodynamic component);
* Steady-state initialization flag (1: initial T calculated by code);
* Left boundary coordinate; reflood condition
10721000 11 5 2 1 5.95e-3 0
* Mesh location flag; mesh format flag (see p.252 of Manual Appendix A)
10721100 0 2
* Mesh interval distance; interval number
10721101 4.00e-4 4
* Composition (table number); interval number
10721201 110 4
* Power input proportion; mesh interval number
10721301 1.0 4
* Initial temperature; mesh point number
10721401 325.0  5
* Left boundary condition definition (here: vol number); increment;
* Boundary condition type (3060: HTC set in general table 60); surface area code (1: length);
* Length; heat structure number
10721501 72010000 10000 3060 1 0.11220 11
* Right boundary condition, see above (-40: T defined in general table 40; 1000: T set in Word 1)
10721601 -40 0 1000 1 0.11220 11
* Power source (table number); internal source multiplier; direct mod heatin mult (left)
* Direct mod heatin mult (right); heat structure number
10721701 0 0.0 0.0 0.0 11
* Additional left boundary: heat transfer hydraulic diameter; heated length fwd (10.: ignore);
* Heated length rev (10.: ignore); grid spacer length fwd (0.: ignore); grid spacer length rev (0.: ignore);
* Grid loss coef fwd (0.: ignore); grid loss coef rev (0.: ignore); boiling factor (1.: subcooled liquid);
* Heat structure number
10721801 0.0 10.0 10.0 0.0 0.0 0.0 0.0 1.0 11
*
* CTAH outlet mixer pipe
* Number of axial heat structures; number of radial mesh points;
* Geometry type (2: cylindrical, coupled to hydrodynamic component);
* Steady-state initialization flag (1: initial T calculated by code);
* Left boundary coordinate; reflood condition
10801000 2 7 2 1 1.39e-2 0
* Mesh location flag; mesh format flag (see p.252 of Manual Appendix A)
10801100 0 2
* Mesh interval distance; interval number
10801101 1.384e-3 2
10801102 9.525e-3 6
* Composition (table number); interval number
10801201 100 2
10801202 120 6
* Power input proportion; mesh interval number
10801301 1.0 2
10801302 0.0 6
* Initial temperature; mesh point number
10801401 325.0  3
10801402 293.15 7
* Left boundary condition definition (here: vol number); increment;
* Boundary condition type (101: convection); surface area code (1: length);
* Length; heat structure number
10801501 80010000 10000 101 1 0.41528 2
* Right boundary condition, see above (-30: T defined in general table 30; 1000: T set in Word 1)
10801601 -30 0 1000 1 0.41528 2
* Power source (table number); internal source multiplier; direct mod heatin mult (left)
* Direct mod heatin mult (right); heat structure number
10801701 0 0.0 0.0 0.0 2
* Additional left boundary: heat transfer hydraulic diameter; heated length fwd (10.: ignore);
* Heated length rev (10.: ignore); grid spacer length fwd (0.: ignore); grid spacer length rev (0.: ignore);
* Grid loss coef fwd (0.: ignore); grid loss coef rev (0.: ignore); boiling factor (1.: subcooled liquid);
* Heat structure number
```

```
10801801 0.0 10.0 10.0 0.0 0.0 0.0 0.0 1.0 2
*
* CTAH outlet mixer
* Number of axial heat structures; number of radial mesh points;
* Geometry type (2: cylindrical, coupled to hydrodynamic component);
* Steady-state initialization flag (1: initial T calculated by code);
* Left boundary coordinate; reflood condition
10811000 1 7 2 1 1.39e-2 0
* Mesh location flag; mesh format flag (see p.252 of Manual Appendix A)
10811100 0 2
* Mesh interval distance; interval number
10811101 1.384e-3 2
10811102 9.525e-3 6
* Composition (table number); interval number
10811201 100 2
10811202 120 6
* Power input proportion; mesh interval number
10811301 1.0 2
10811302 0.0 6
* Initial temperature; mesh point number
10811401 325.0  3
10811402 293.15 7
* Left boundary condition definition (here: vol number); increment;
* Boundary condition type (101: convection); surface area code (1: length);
* Length; heat structure number
10811501 81010000 10000 101 1 1.23206 1
* Right boundary condition, see above (-30: T defined in general table 30; 1000: T set in Word 1)
10811601 -30 0 1000 1 1.23206 1
* Power source (table number); internal source multiplier; direct mod heatin mult (left)
* Direct mod heatin mult (right); heat structure number
10811701 0 0.0 0.0 0.0 1
* Additional left boundary: heat transfer hydraulic diameter; heated length fwd (10.: ignore);
* Heated length rev (10.: ignore); grid spacer length fwd (0.: ignore); grid spacer length rev (0.: ignore);
* Grid loss coef fwd (0.: ignore); grid loss coef rev (0.: ignore); boiling factor (1.: subcooled liquid);
* Heat structure number
10811801 0.0 10.0 10.0 0.0 0.0 0.0 0.0 1.0 1
*
* Cold leg 1
* Number of axial heat structures; number of radial mesh points;
* Geometry type (2: cylindrical, coupled to hydrodynamic component);
* Steady-state initialization flag (1: initial T calculated by code);
* Left boundary coordinate; reflood condition
10901000 7 7 2 1 1.39e-2 0
* Mesh location flag; mesh format flag (see p.252 of Manual Appendix A)
10901100 0 2
* Mesh interval distance; interval number
10901101 1.384e-3 2
10901102 9.525e-3 6
* Composition (table number); interval number
10901201 100 2
10901202 120 6
* Power input proportion; mesh interval number
10901301 1.0 2
10901302 0.0 6
* Initial temperature; mesh point number
10901401 325.0  3
10901402 293.15 7
* Left boundary condition definition (here: vol number); increment;
* Boundary condition type (101: convection); surface area code (1: length);
* Length; heat structure number
10901501 90010000 10000 101 1 0.37933 7
* Right boundary condition, see above (-30: T defined in general table 30; 1000: T set in Word 1)
```

```
10901601 -30 0 1000 1 0.37933 7
* Power source (table number); internal source multiplier; direct mod heatin mult (left)
* Direct mod heatin mult (right); heat structure number
10901701 0 0.0 0.0 0.0 7
* Additional left boundary: heat transfer hydraulic diameter; heated length fwd (10.: ignore);
* Heated length rev (10.: ignore); grid spacer length fwd (0.: ignore); grid spacer length rev (0.: ignore);
* Grid loss coef fwd (0.: ignore); grid loss coef rev (0.: ignore); boiling factor (1.: subcooled liquid);
* Heat structure number
10901801 0.0 10.0 10.0 0.0 0.0 0.0 0.0 1.0 7
*
* Cold leg 2
* Number of axial heat structures; number of radial mesh points;
* Geometry type (2: cylindrical, coupled to hydrodynamic component);
* Steady-state initialization flag (1: initial T calculated by code);
* Left boundary coordinate; reflood condition
11001000 22 7 2 1 1.39e-2 0
* Mesh location flag; mesh format flag (see p.252 of Manual Appendix A)
11001100 0 2
* Mesh interval distance; interval number
11001101 1.384e-3 2
11001102 9.525e-3 6
* Composition (table number); interval number
11001201 100 2
11001202 120 6
* Power input proportion; mesh interval number
11001301 1.0 2
11001302 0.0 6
* Initial temperature; mesh point number
11001401 325.0  3
11001402 293.15 7
* Left boundary condition definition (here: vol number); increment;
* Boundary condition type (101: convection); surface area code (1: length);
* Length; heat structure number
11001501 100010000 10000 101 1 0.41595 22
* Right boundary condition, see above (-30: T defined in general table 30; 1000: T set in Word 1)
11001601 -30 0 1000 1 0.41595 22
* Power source (table number); internal source multiplier; direct mod heatin mult (left)
* Direct mod heatin mult (right); heat structure number
11001701 0 0.0 0.0 0.0 22
* Additional left boundary: heat transfer hydraulic diameter; heated length fwd (10.: ignore);
* Heated length rev (10.: ignore); grid spacer length fwd (0.: ignore); grid spacer length rev (0.: ignore);
* Grid loss coef fwd (0.: ignore); grid loss coef rev (0.: ignore); boiling factor (1.: subcooled liquid);
* Heat structure number
11001801 0.0 10.0 10.0 0.0 0.0 0.0 0.0 1.0 22
*
* Cold leg 3
* Number of axial heat structures; number of radial mesh points;
* Geometry type (2: cylindrical, coupled to hydrodynamic component);
* Steady-state initialization flag (1: initial T calculated by code);
* Left boundary coordinate; reflood condition
11101000 4 7 2 1 1.39e-2 0
* Mesh location flag; mesh format flag (see p.252 of Manual Appendix A)
11101100 0 2
* Mesh interval distance; interval number
11101101 1.384e-3 2
11101102 9.525e-3 6
* Composition (table number); interval number
11101201 100 2
11101202 120 6
* Power input proportion; mesh interval number
11101301 1.0 2
11101302 0.0 6
```

```
* Initial temperature; mesh point number
11101401 325.0  3
11101402 293.15 7
* Left boundary condition definition (here: vol number); increment;
* Boundary condition type (101: convection); surface area code (1: length);
* Length; heat structure number
11101501 110010000 10000 101 1 0.45045 4
* Right boundary condition, see above (-30: T defined in general table 30; 1000: T set in Word 1)
11101601 -30 0 1000 1 0.45045 4
* Power source (table number); internal source multiplier; direct mod heatin mult (left)
* Direct mod heatin mult (right); heat structure number
11101701 0 0.0 0.0 0.0 4
* Additional left boundary: heat transfer hydraulic diameter; heated length fwd (10.: ignore);
* Heated length rev (10.: ignore); grid spacer length fwd (0.: ignore); grid spacer length rev (0.: ignore);
* Grid loss coef fwd (0.: ignore); grid loss coef rev (0.: ignore); boiling factor (1.: subcooled liquid);
* Heat structure number
11101801 0.0 10.0 10.0 0.0 0.0 0.0 0.0 1.0 4
*
* Pump suction
* Number of axial heat structures; number of radial mesh points;
* Geometry type (2: cylindrical, coupled to hydrodynamic component);
* Steady-state initialization flag (1: initial T calculated by code);
* Left boundary coordinate; reflood condition
11201000 3 7 2 1 1.39e-2 0
* Mesh location flag; mesh format flag (see p.252 of Manual Appendix A)
11201100 0 2
* Mesh interval distance; interval number
11201101 1.384e-3 2
11201102 1.270e-2 6
* Composition (table number); interval number
11201201 100 2
11201202 120 6
* Power input proportion; mesh interval number
11201301 1.0 2
11201302 0.0 6
* Initial temperature; mesh point number
11201401 325.0  3
11201402 293.15 7
* Left boundary condition definition (here: vol number); increment;
* Boundary condition type (101: convection); surface area code (1: length);
* Length; heat structure number
11201501 120010000 10000 101 1 0.41491 3
* Right boundary condition, see above (-30: T defined in general table 30; 1000: T set in Word 1)
11201601 -30 0 1000 1 0.41491 3
* Power source (table number); internal source multiplier; direct mod heatin mult (left)
* Direct mod heatin mult (right); heat structure number
11201701 0 0.0 0.0 0.0 3
* Additional left boundary: heat transfer hydraulic diameter; heated length fwd (10.: ignore);
* Heated length rev (10.: ignore); grid spacer length fwd (0.: ignore); grid spacer length rev (0.: ignore);
* Grid loss coef fwd (0.: ignore); grid loss coef rev (0.: ignore); boiling factor (1.: subcooled liquid);
* Heat structure number
11201801 0.0 10.0 10.0 0.0 0.0 0.0 0.0 1.0 3
*
* Pump discharge
* Number of axial heat structures; number of radial mesh points;
* Geometry type (2: cylindrical, coupled to hydrodynamic component);
* Steady-state initialization flag (1: initial T calculated by code);
* Left boundary coordinate; reflood condition
11301000 12 7 2 1 1.39e-2 0
* Mesh location flag; mesh format flag (see p.252 of Manual Appendix A)
11301100 0 2
* Mesh interval distance; interval number
```

```
11301101 1.384e-3 2
11301102 1.270e-2 6
* Composition (table number); interval number
11301201 100 2
11301202 120 6
* Power input proportion; mesh interval number
11301301 1.0 2
11301302 0.0 6
* Initial temperature; mesh point number
11301401 325.0  3
11301402 293.15 7
* Left boundary condition definition (here: vol number); increment;
* Boundary condition type (101: convection); surface area code (1: length);
* Length; heat structure number
11301501 130010000 10000 101 1 0.39612 12
* Right boundary condition, see above (-30: T defined in general table 30; 1000: T set in Word 1)
11301601 -30 0 1000 1 0.39612 12
* Power source (table number); internal source multiplier; direct mod heatin mult (left)
* Direct mod heatin mult (right); heat structure number
11301701 0 0.0 0.0 0.0 12
* Additional left boundary: heat transfer hydraulic diameter; heated length fwd (10.: ignore);
* Heated length rev (10.: ignore); grid spacer length fwd (0.: ignore); grid spacer length rev (0.: ignore);
* Grid loss coef fwd (0.: ignore); grid loss coef rev (0.: ignore); boiling factor (1.: subcooled liquid);
* Heat structure number
11301801 0.0 10.0 10.0 0.0 0.0 0.0 0.0 1.0 12
*
* Cold leg 4
* Number of axial heat structures; number of radial mesh points;
* Geometry type (2: cylindrical, coupled to hydrodynamic component);
* Steady-state initialization flag (1: initial T calculated by code);
* Left boundary coordinate; reflood condition
11401000 6 7 2 1 1.39e-2 0
* Mesh location flag; mesh format flag (see p.252 of Manual Appendix A)
11401100 0 2
* Mesh interval distance; interval number
11401101 1.384e-3 2
11401102 1.270e-2 6
* Composition (table number); interval number
11401201 100 2
11401202 120 6
* Power input proportion; mesh interval number
11401301 1.0 2
11401302 0.0 6
* Initial temperature; mesh point number
11401401 325.0  3
11401402 293.15 7
* Left boundary condition definition (here: vol number); increment;
* Boundary condition type (101: convection); surface area code (1: length);
* Length; heat structure number
11401501 140010000 10000 101 1 0.41610 6
* Right boundary condition, see above (-30: T defined in general table 30; 1000: T set in Word 1)
11401601 -30 0 1000 1 0.41610 6
* Power source (table number); internal source multiplier; direct mod heatin mult (left)
* Direct mod heatin mult (right); heat structure number
11401701 0 0.0 0.0 0.0 6
* Additional left boundary: heat transfer hydraulic diameter; heated length fwd (10.: ignore);
* Heated length rev (10.: ignore); grid spacer length fwd (0.: ignore); grid spacer length rev (0.: ignore);
* Grid loss coef fwd (0.: ignore); grid loss coef rev (0.: ignore); boiling factor (1.: subcooled liquid);
* Heat structure number
11401801 0.0 10.0 10.0 0.0 0.0 0.0 0.0 1.0 6
*
* CTAH flowmeter
```

```
* Number of axial heat structures; number of radial mesh points;
* Geometry type (2: cylindrical, coupled to hydrodynamic component);
* Steady-state initialization flag (1: initial T calculated by code);
* Left boundary coordinate; reflood condition
11411000 1 7 2 1 1.39e-2 0
* Mesh location flag; mesh format flag (see p.252 of Manual Appendix A)
11411100 0 2
* Mesh interval distance; interval number
11411101 1.384e-3 2
11411102 1.270e-2 6
* Composition (table number); interval number
11411201 100 2
11411202 120 6
* Power input proportion; mesh interval number
11411301 1.0 2
11411302 0.0 6
* Initial temperature; mesh point number
11411401 325.0  3
11411402 293.15 7
* Left boundary condition definition (here: vol number); increment;
* Boundary condition type (101: convection); surface area code (1: length);
* Length; heat structure number
11411501 141010000 10000 101 1 1.34407 1
* Right boundary condition, see above (-30: T defined in general table 30; 1000: T set in Word 1)
11411601 -30 0 1000 1 1.34407 1
* Power source (table number); internal source multiplier; direct mod heatin mult (left)
* Direct mod heatin mult (right); heat structure number
11411701 0 0.0 0.0 0.0 1
* Additional left boundary: heat transfer hydraulic diameter; heated length fwd (10.: ignore);
* Heated length rev (10.: ignore); grid spacer length fwd (0.: ignore); grid spacer length rev (0.: ignore);
* Grid loss coef fwd (0.: ignore); grid loss coef rev (0.: ignore); boiling factor (1.: subcooled liquid);
* Heat structure number
11411801 0.0 10.0 10.0 0.0 0.0 0.0 0.0 1.0 1
*
* Cold leg 5
* Number of axial heat structures; number of radial mesh points;
* Geometry type (2: cylindrical, coupled to hydrodynamic component);
* Steady-state initialization flag (1: initial T calculated by code);
* Left boundary coordinate; reflood condition
11501000 3 7 2 1 1.39e-2 0
* Mesh location flag; mesh format flag (see p.252 of Manual Appendix A)
11501100 0 2
* Mesh interval distance; interval number
11501101 1.384e-3 2
11501102 1.270e-2 6
* Composition (table number); interval number
11501201 100 2
11501202 120 6
* Power input proportion; mesh interval number
11501301 1.0 2
11501302 0.0 6
* Initial temperature; mesh point number
11501401 325.0  3
11501402 293.15 7
* Left boundary condition definition (here: vol number); increment;
* Boundary condition type (101: convection); surface area code (1: length);
* Length; heat structure number
11501501 150010000 10000 101 1 0.44253 3
* Right boundary condition, see above (-30: T defined in general table 30; 1000: T set in Word 1)
11501601 -30 0 1000 1 0.44253 3
* Power source (table number); internal source multiplier; direct mod heatin mult (left)
* Direct mod heatin mult (right); heat structure number
```

```
11501701 0 0.0 0.0 0.0 3
* Additional left boundary: heat transfer hydraulic diameter; heated length fwd (10.: ignore);
* Heated length rev (10.: ignore); grid spacer length fwd (0.: ignore); grid spacer length rev (0.: ignore);
* Grid loss coef fwd (0.: ignore); grid loss coef rev (0.: ignore); boiling factor (1.: subcooled liquid);
* Heat structure number
11501801 0.0 10.0 10.0 0.0 0.0 0.0 0.0 1.0 3
*
* Cold leg 6
* Number of axial heat structures; number of radial mesh points;
* Geometry type (2: cylindrical, coupled to hydrodynamic component);
* Steady-state initialization flag (1: initial T calculated by code);
* Left boundary coordinate; reflood condition
11601000 6 7 2 1 1.39e-2 0
* Mesh location flag; mesh format flag (see p.252 of Manual Appendix A)
11601100 0 2
* Mesh interval distance; interval number
11601101 1.384e-3 2
11601102 1.270e-2 6
* Composition (table number); interval number
11601201 100 2
11601202 120 6
* Power input proportion; mesh interval number
11601301 1.0 2
11601302 0.0 6
* Initial temperature; mesh point number
11601401 325.0  3
11601402 293.15 7
* Left boundary condition definition (here: vol number); increment;
* Boundary condition type (101: convection); surface area code (1: length);
* Length; heat structure number
11601501 160010000 10000 101 1 0.40106 6
* Right boundary condition, see above (-30: T defined in general table 30; 1000: T set in Word 1)
11601601 -30 0 1000 1 0.40106 6
* Power source (table number); internal source multiplier; direct mod heatin mult (left)
* Direct mod heatin mult (right); heat structure number
11601701 0 0.0 0.0 0.0 6
* Additional left boundary: heat transfer hydraulic diameter; heated length fwd (10.: ignore);
* Heated length rev (10.: ignore); grid spacer length fwd (0.: ignore); grid spacer length rev (0.: ignore);
* Grid loss coef fwd (0.: ignore); grid loss coef rev (0.: ignore); boiling factor (1.: subcooled liquid);
* Heat structure number
11601801 0.0 10.0 10.0 0.0 0.0 0.0 0.0 1.0 6
*
* Branch 17
* Number of axial heat structures; number of radial mesh points;
* Geometry type (2: cylindrical, coupled to hydrodynamic component);
* Steady-state initialization flag (1: initial T calculated by code);
* Left boundary coordinate; reflood condition
11701000 1 7 2 1 1.39e-2 0
* Mesh location flag; mesh format flag (see p.252 of Manual Appendix A)
11701100 0 2
* Mesh interval distance; interval number
11701101 1.384e-3 2
11701102 1.270e-2 6
* Composition (table number); interval number
11701201 100 2
11701202 120 6
* Power input proportion; mesh interval number
11701301 1.0 2
11701302 0.0 6
* Initial temperature; mesh point number
11701401 325.0  3
11701402 293.15 7
```

```
* Left boundary condition definition (here: vol number); increment;
* Boundary condition type (101: convection); surface area code (1: length);
* Length; heat structure number
11701501 170010000 10000 101 1 1.76625 1
* Right boundary condition, see above (-30: T defined in general table 30; 1000: T set in Word 1)
11701601 -30 0 1000 1 1.76625 1
* Power source (table number); internal source multiplier; direct mod heatin mult (left)
* Direct mod heatin mult (right); heat structure number
11701701 0 0.0 0.0 0.0 1
* Additional left boundary: heat transfer hydraulic diameter; heated length fwd (10.: ignore);
* Heated length rev (10.: ignore); grid spacer length fwd (0.: ignore); grid spacer length rev (0.: ignore);
* Grid loss coef fwd (0.: ignore); grid loss coef rev (0.: ignore); boiling factor (1.: subcooled liquid);
* Heat structure number
11701801 0.0 10.0 10.0 0.0 0.0 0.0 0.0 1.0 1
*
* Cold leg 7
* Number of axial heat structures; number of radial mesh points;
* Geometry type (2: cylindrical, coupled to hydrodynamic component);
* Steady-state initialization flag (1: initial T calculated by code);
* Left boundary coordinate; reflood condition
11801000 1 7 2 1 1.39e-2 0
* Mesh location flag; mesh format flag (see p.252 of Manual Appendix A)
11801100 0 2
* Mesh interval distance; interval number
11801101 1.384e-3 2
11801102 1.270e-2 6
* Composition (table number); interval number
11801201 100 2
11801202 120 6
* Power input proportion; mesh interval number
11801301 1.0 2
11801302 0.0 6
* Initial temperature; mesh point number
11801401 325.0  3
11801402 293.15 7
* Left boundary condition definition (here: vol number); increment;
* Boundary condition type (101: convection); surface area code (1: length);
* Length; heat structure number
11801501 180010000 10000 101 1 0.66382 1
* Right boundary condition, see above (-30: T defined in general table 30; 1000: T set in Word 1)
11801601 -30 0 1000 1 0.66382 1
* Power source (table number); internal source multiplier; direct mod heatin mult (left)
* Direct mod heatin mult (right); heat structure number
11801701 0 0.0 0.0 0.0 1
* Additional left boundary: heat transfer hydraulic diameter; heated length fwd (10.: ignore);
* Heated length rev (10.: ignore); grid spacer length fwd (0.: ignore); grid spacer length rev (0.: ignore);
* Grid loss coef fwd (0.: ignore); grid loss coef rev (0.: ignore); boiling factor (1.: subcooled liquid);
* Heat structure number
11801801 0.0 10.0 10.0 0.0 0.0 0.0 0.0 1.0 1
*
* DHX leg 1
* Number of axial heat structures; number of radial mesh points;
* Geometry type (2: cylindrical, coupled to hydrodynamic component);
* Steady-state initialization flag (1: initial T calculated by code);
* Left boundary coordinate; reflood condition
11901000 2 7 2 1 1.39e-2 0
* Mesh location flag; mesh format flag (see p.252 of Manual Appendix A)
11901100 0 2
* Mesh interval distance; interval number
11901101 1.384e-3 2
11901102 1.270e-2 6
* Composition (table number); interval number
```

```
11901201 100 2
11901202 120 6
* Power input proportion; mesh interval number
11901301 1.0 2
11901302 0.0 6
* Initial temperature; mesh point number
11901401 325.0  3
11901402 293.15 7
* Left boundary condition definition (here: vol number); increment;
* Boundary condition type (101: convection); surface area code (1: length);
* Length; heat structure number
11901501 190010000 10000 101 1 0.53227 2
* Right boundary condition, see above (-30: T defined in general table 30; 1000: T set in Word 1)
11901601 -30 0 1000 1 0.53227 2
* Power source (table number); internal source multiplier; direct mod heatin mult (left)
* Direct mod heatin mult (right); heat structure number
11901701 0 0.0 0.0 0.0 2
* Additional left boundary: heat transfer hydraulic diameter; heated length fwd (10.: ignore);
* Heated length rev (10.: ignore); grid spacer length fwd (0.: ignore); grid spacer length rev (0.: ignore);
* Grid loss coef fwd (0.: ignore); grid loss coef rev (0.: ignore); boiling factor (1.: subcooled liquid);
* Heat structure number
11901801 0.0 10.0 10.0 0.0 0.0 0.0 0.0 1.0 2
*
* DHX leg 2
* Number of axial heat structures; number of radial mesh points;
* Geometry type (2: cylindrical, coupled to hydrodynamic component);
* Steady-state initialization flag (1: initial T calculated by code);
* Left boundary coordinate; reflood condition
12001000 3 7 2 1 1.39e-2 0
* Mesh location flag; mesh format flag (see p.252 of Manual Appendix A)
12001100 0 2
* Mesh interval distance; interval number
12001101 1.384e-3 2
12001102 1.270e-2 6
* Composition (table number); interval number
12001201 100 2
12001202 120 6
* Power input proportion; mesh interval number
12001301 1.0 2
12001302 0.0 6
* Initial temperature; mesh point number
12001401 325.0  3
12001402 293.15 7
* Left boundary condition definition (here: vol number); increment;
* Boundary condition type (101: convection); surface area code (1: length);
* Length; heat structure number
12001501 200010000 10000 101 1 0.54510 3
* Right boundary condition, see above (-30: T defined in general table 30; 1000: T set in Word 1)
12001601 -30 0 1000 1 0.54510 3
* Power source (table number); internal source multiplier; direct mod heatin mult (left)
* Direct mod heatin mult (right); heat structure number
12001701 0 0.0 0.0 0.0 3
* Additional left boundary: heat transfer hydraulic diameter; heated length fwd (10.: ignore);
* Heated length rev (10.: ignore); grid spacer length fwd (0.: ignore); grid spacer length rev (0.: ignore);
* Grid loss coef fwd (0.: ignore); grid loss coef rev (0.: ignore); boiling factor (1.: subcooled liquid);
* Heat structure number
12001801 0.0 10.0 10.0 0.0 0.0 0.0 0.0 1.0 3
*
* DHX leg 3
* Number of axial heat structures; number of radial mesh points;
* Geometry type (2: cylindrical, coupled to hydrodynamic component);
* Steady-state initialization flag (1: initial T calculated by code);
```

```
* Left boundary coordinate; reflood condition
12101000 4 7 2 1 1.39e-2 0
* Mesh location flag; mesh format flag (see p.252 of Manual Appendix A)
12101100 0 2
* Mesh interval distance; interval number
12101101 1.384e-3 2
12101102 1.270e-2 6
* Composition (table number); interval number
12101201 100 2
12101202 120 6
* Power input proportion; mesh interval number
12101301 1.0 2
12101302 0.0 6
* Initial temperature; mesh point number
12101401 325.0  3
12101402 293.15 7
* Left boundary condition definition (here: vol number); increment;
* Boundary condition type (101: convection); surface area code (1: length);
* Length; heat structure number
12101501 210010000 10000 101 1 0.59247 4
* Right boundary condition, see above (-30: T defined in general table 30; 1000: T set in Word 1)
12101601 -30 0 1000 1 0.59247 4
* Power source (table number); internal source multiplier; direct mod heatin mult (left)
* Direct mod heatin mult (right); heat structure number
12101701 0 0.0 0.0 0.0 4
* Additional left boundary: heat transfer hydraulic diameter; heated length fwd (10.: ignore);
* Heated length rev (10.: ignore); grid spacer length fwd (0.: ignore); grid spacer length rev (0.: ignore);
* Grid loss coef fwd (0.: ignore); grid loss coef rev (0.: ignore); boiling factor (1.: subcooled liquid);
* Heat structure number
12101801 0.0 10.0 10.0 0.0 0.0 0.0 0.0 1.0 4
*
* DHX flowmeter
* Number of axial heat structures; number of radial mesh points;
* Geometry type (2: cylindrical, coupled to hydrodynamic component);
* Steady-state initialization flag (1: initial T calculated by code);
* Left boundary coordinate; reflood condition
12111000 1 7 2 1 1.39e-2 0
* Mesh location flag; mesh format flag (see p.252 of Manual Appendix A)
12111100 0 2
* Mesh interval distance; interval number
12111101 1.384e-3 2
12111102 1.270e-2 6
* Composition (table number); interval number
12111201 100 2
12111202 120 6
* Power input proportion; mesh interval number
12111301 1.0 2
12111302 0.0 6
* Initial temperature; mesh point number
12111401 325.0  3
12111402 293.15 7
* Left boundary condition definition (here: vol number); increment;
* Boundary condition type (101: convection); surface area code (1: length);
* Length; heat structure number
12111501 211010000 10000 101 1 1.74929 1
* Right boundary condition, see above (-30: T defined in general table 30; 1000: T set in Word 1)
12111601 -30 0 1000 1 1.74929 1
* Power source (table number); internal source multiplier; direct mod heatin mult (left)
* Direct mod heatin mult (right); heat structure number
12111701 0 0.0 0.0 0.0 1
* Additional left boundary: heat transfer hydraulic diameter; heated length fwd (10.: ignore);
* Heated length rev (10.: ignore); grid spacer length fwd (0.: ignore); grid spacer length rev (0.: ignore);
```

```
* Grid loss coef fwd (0.: ignore); grid loss coef rev (0.: ignore); boiling factor (1.: subcooled liquid);
* Heat structure number
12111801 0.0 10.0 10.0 0.0 0.0 0.0 0.0 1.0 1
*
* DHX leg 4
* Number of axial heat structures; number of radial mesh points;
* Geometry type (2: cylindrical, coupled to hydrodynamic component);
* Steady-state initialization flag (1: initial T calculated by code);
* Left boundary coordinate; reflood condition
12201000 6 7 2 1 1.39e-2 0
* Mesh location flag; mesh format flag (see p.252 of Manual Appendix A)
12201100 0 2
* Mesh interval distance; interval number
12201101 1.384e-3 2
12201102 1.270e-2 6
* Composition (table number); interval number
12201201 100 2
12201202 120 6
* Power input proportion; mesh interval number
12201301 1.0 2
12201302 0.0 6
* Initial temperature; mesh point number
12201401 325.0  3
12201402 293.15 7
* Left boundary condition definition (here: vol number); increment;
* Boundary condition type (101: convection); surface area code (1: length);
* Length; heat structure number
12201501 220010000 10000 101 1 0.56055 6
* Right boundary condition, see above (-30: T defined in general table 30; 1000: T set in Word 1)
12201601 -30 0 1000 1 0.56055 6
* Power source (table number); internal source multiplier; direct mod heatin mult (left)
* Direct mod heatin mult (right); heat structure number
12201701 0 0.0 0.0 0.0 6
* Additional left boundary: heat transfer hydraulic diameter; heated length fwd (10.: ignore);
* Heated length rev (10.: ignore); grid spacer length fwd (0.: ignore); grid spacer length rev (0.: ignore);
* Grid loss coef fwd (0.: ignore); grid loss coef rev (0.: ignore); boiling factor (1.: subcooled liquid);
* Heat structure number
12201801 0.0 10.0 10.0 0.0 0.0 0.0 0.0 1.0 6
*
* DHX outlet mixer pipe
* Number of axial heat structures; number of radial mesh points;
* Geometry type (2: cylindrical, coupled to hydrodynamic component);
* Steady-state initialization flag (1: initial T calculated by code);
* Left boundary coordinate; reflood condition
12301000 1 7 2 1 1.39e-2 0
* Mesh location flag; mesh format flag (see p.252 of Manual Appendix A)
12301100 0 2
* Mesh interval distance; interval number
12301101 1.384e-3 2
12301102 1.270e-2 6
* Composition (table number); interval number
12301201 100 2
12301202 120 6
* Power input proportion; mesh interval number
12301301 1.0 2
12301302 0.0 6
* Initial temperature; mesh point number
12301401 325.0  3
12301402 293.15 7
* Left boundary condition definition (here: vol number); increment;
* Boundary condition type (101: convection); surface area code (1: length);
* Length; heat structure number
```

```
12301501 230010000 10000 101 1 0.43295 1
* Right boundary condition, see above (-30: T defined in general table 30; 1000: T set in Word 1)
12301601 -30 0 1000 1 0.43295 1
* Power source (table number); internal source multiplier; direct mod heatin mult (left)
* Direct mod heatin mult (right); heat structure number
12301701 0 0.0 0.0 0.0 1
* Additional left boundary: heat transfer hydraulic diameter; heated length fwd (10.: ignore);
* Heated length rev (10.: ignore); grid spacer length fwd (0.: ignore); grid spacer length rev (0.: ignore);
* Grid loss coef fwd (0.: ignore); grid loss coef rev (0.: ignore); boiling factor (1.: subcooled liquid);
* Heat structure number
12301801 0.0 10.0 10.0 0.0 0.0 0.0 0.0 1.0 1
*
* DHX outlet mixer
* Number of axial heat structures; number of radial mesh points;
* Geometry type (2: cylindrical, coupled to hydrodynamic component);
* Steady-state initialization flag (1: initial T calculated by code);
* Left boundary coordinate; reflood condition
12311000 1 7 2 1 1.39e-2 0
* Mesh location flag; mesh format flag (see p.252 of Manual Appendix A)
12311100 0 2
* Mesh interval distance; interval number
12311101 1.384e-3 2
12311102 1.270e-2 6
* Composition (table number); interval number
12311201 100 2
12311202 120 6
* Power input proportion; mesh interval number
12311301 1.0 2
12311302 0.0 6
* Initial temperature; mesh point number
12311401 325.0  3
12311402 293.15 7
* Left boundary condition definition (here: vol number); increment;
* Boundary condition type (101: convection); surface area code (1: length);
* Length; heat structure number
12311501 231010000 10000 101 1 1.60351 1
* Right boundary condition, see above (-30: T defined in general table 30; 1000: T set in Word 1)
12311601 -30 0 1000 1 1.60351 1
* Power source (table number); internal source multiplier; direct mod heatin mult (left)
* Direct mod heatin mult (right); heat structure number
12311701 0 0.0 0.0 0.0 1
* Additional left boundary: heat transfer hydraulic diameter; heated length fwd (10.: ignore);
* Heated length rev (10.: ignore); grid spacer length fwd (0.: ignore); grid spacer length rev (0.: ignore);
* Grid loss coef fwd (0.: ignore); grid loss coef rev (0.: ignore); boiling factor (1.: subcooled liquid);
* Heat structure number
12311801 0.0 10.0 10.0 0.0 0.0 0.0 0.0 1.0 1
*
* DHX shell
* Number of axial heat structures; number of radial mesh points;
* Geometry type (2: cylindrical, coupled to hydrodynamic component);
* Steady-state initialization flag (1: initial T calculated by code);
* Left boundary coordinate; reflood condition
12401000 11 7 2 1 2.54e-2 0
* Mesh location flag; mesh format flag (see p.252 of Manual Appendix A)
12401100 0 2
* Mesh interval distance; interval number
12401101 8.000e-4 2
12401102 1.270e-2 6
* Composition (table number); interval number
12401201 110 2
12401202 120 6
* Power input proportion; mesh interval number
```

```
12401301 1.0 2
12401302 0.0 6
* Initial temperature; mesh point number
12401401 325.0  3
12401402 293.15 7
* Left boundary condition definition (here: vol number); increment;
* Boundary condition type (101: convection); surface area code (1: length);
* Length; heat structure number
12401501 240010000 10000 101 1 0.75129 11
* Right boundary condition, see above (-30: T defined in general table 30; 1000: T set in Word 1)
12401601 -30 0 1000 1 0.75129 11
* Power source (table number); internal source multiplier; direct mod heatin mult (left)
* Direct mod heatin mult (right); heat structure number
12401701 0 0.0 0.0 0.0 11
* Additional left boundary: heat transfer hydraulic diameter; heated length fwd (10.: ignore);
* Heated length rev (10.: ignore); grid spacer length fwd (0.: ignore); grid spacer length rev (0.: ignore);
* Grid loss coef fwd (0.: ignore); grid loss coef rev (0.: ignore); boiling factor (1.: subcooled liquid);
* Heat structure number
12401801 2.36e-2 10.0 10.0 0.0 0.0 0.0 0.0 1.0 11
*
* DHX inlet mixer pipe
* Number of axial heat structures; number of radial mesh points;
* Geometry type (2: cylindrical, coupled to hydrodynamic component);
* Steady-state initialization flag (1: initial T calculated by code);
* Left boundary coordinate; reflood condition
12501000 2 7 2 1 1.39e-2 0
* Mesh location flag; mesh format flag (see p.252 of Manual Appendix A)
12501100 0 2
* Mesh interval distance; interval number
12501101 1.384e-3 2
12501102 1.270e-2 6
* Composition (table number); interval number
12501201 100 2
12501202 120 6
* Power input proportion; mesh interval number
12501301 1.0 2
12501302 0.0 6
* Initial temperature; mesh point number
12501401 325.0  3
12501402 293.15 7
* Left boundary condition definition (here: vol number); increment;
* Boundary condition type (101: convection); surface area code (1: length);
* Length; heat structure number
12501501 250010000 10000 101 1 0.50749 2
* Right boundary condition, see above (-30: T defined in general table 30; 1000: T set in Word 1)
12501601 -30 0 1000 1 0.50749 2
* Power source (table number); internal source multiplier; direct mod heatin mult (left)
* Direct mod heatin mult (right); heat structure number
12501701 0 0.0 0.0 0.0 2
* Additional left boundary: heat transfer hydraulic diameter; heated length fwd (10.: ignore);
* Heated length rev (10.: ignore); grid spacer length fwd (0.: ignore); grid spacer length rev (0.: ignore);
* Grid loss coef fwd (0.: ignore); grid loss coef rev (0.: ignore); boiling factor (1.: subcooled liquid);
* Heat structure number
12501801 0.0 10.0 10.0 0.0 0.0 0.0 0.0 1.0 2
*
* DHX inlet mixer
* Number of axial heat structures; number of radial mesh points;
* Geometry type (2: cylindrical, coupled to hydrodynamic component);
* Steady-state initialization flag (1: initial T calculated by code);
* Left boundary coordinate; reflood condition
12511000 1 7 2 1 1.39e-2 0
* Mesh location flag; mesh format flag (see p.252 of Manual Appendix A)
```

```
12511100 0 2
* Mesh interval distance; interval number
12511101 1.384e-3 2
12511102 1.270e-2 6
* Composition (table number); interval number
12511201 100 2
12511202 120 6
* Power input proportion; mesh interval number
12511301 1.0 2
12511302 0.0 6
* Initial temperature; mesh point number
12511401 325.0  3
12511402 293.15 7
* Left boundary condition definition (here: vol number); increment;
* Boundary condition type (101: convection); surface area code (1: length);
* Length; heat structure number
12511501 251010000 10000 101 1 1.50563 1
* Right boundary condition, see above (-30: T defined in general table 30; 1000: T set in Word 1)
12511601 -30 0 1000 1 1.50563 1
* Power source (table number); internal source multiplier; direct mod heatin mult (left)
* Direct mod heatin mult (right); heat structure number
12511701 0 0.0 0.0 0.0 1
* Additional left boundary: heat transfer hydraulic diameter; heated length fwd (10.: ignore);
* Heated length rev (10.: ignore); grid spacer length fwd (0.: ignore); grid spacer length rev (0.: ignore);
* Grid loss coef fwd (0.: ignore); grid loss coef rev (0.: ignore); boiling factor (1.: subcooled liquid);
* Heat structure number
12511801 0.0 10.0 10.0 0.0 0.0 0.0 0.0 1.0 1
*
* DHX leg 5
* Number of axial heat structures; number of radial mesh points;
* Geometry type (2: cylindrical, coupled to hydrodynamic component);
* Steady-state initialization flag (1: initial T calculated by code);
* Left boundary coordinate; reflood condition
12601000 2 7 2 1 1.39e-2 0
* Mesh location flag; mesh format flag (see p.252 of Manual Appendix A)
12601100 0 2
* Mesh interval distance; interval number
12601101 1.384e-3 2
12601102 1.270e-2 6
* Composition (table number); interval number
12601201 100 2
12601202 120 6
* Power input proportion; mesh interval number
12601301 1.0 2
12601302 0.0 6
* Initial temperature; mesh point number
12601401 325.0  3
12601402 293.15 7
* Left boundary condition definition (here: vol number); increment;
* Boundary condition type (101: convection); surface area code (1: length);
* Length; heat structure number
12601501 260010000 10000 101 1 0.49252 2
* Right boundary condition, see above (-30: T defined in general table 30; 1000: T set in Word 1)
12601601 -30 0 1000 1 0.49252 2
* Power source (table number); internal source multiplier; direct mod heatin mult (left)
* Direct mod heatin mult (right); heat structure number
12601701 0 0.0 0.0 0.0 2
* Additional left boundary: heat transfer hydraulic diameter; heated length fwd (10.: ignore);
* Heated length rev (10.: ignore); grid spacer length fwd (0.: ignore); grid spacer length rev (0.: ignore);
* Grid loss coef fwd (0.: ignore); grid loss coef rev (0.: ignore); boiling factor (1.: subcooled liquid);
* Heat structure number
12601801 0.0 10.0 10.0 0.0 0.0 0.0 0.0 1.0 2
```

```
*
* DHX tubes
* Number of axial heat structures; number of radial mesh points;
* Geometry type (2: cylindrical, coupled to hydrodynamic component);
* Steady-state initialization flag (1: initial T calculated by code);
* Left boundary coordinate; reflood condition
13001000 11 5 2 1 3.47e-3 0
* Mesh location flag; mesh format flag (see p.252 of Manual Appendix A)
13001100 0 2
* Mesh interval distance; interval number
13001101 2.00025e-4 4
* Composition (table number); interval number
13001201 110 4
* Power input proportion; mesh interval number
13001301 1.0 4
* Initial temperature; mesh point number
13001401 325.0  5
* Left boundary condition definition (here: vol number); increment;
* Boundary condition type (101: convection); surface area code (1: length);
* Length; heat structure number
13001501 300010000 10000 101 1 1.17203 11
* Right boundary condition, see above
13001601 240010000 10000 101 1 1.17203 11
* Power source (table number); internal source multiplier; direct mod heatin mult (left)
* Direct mod heatin mult (right); heat structure number
13001701 0 0.0 0.0 0.0 11
* Additional left boundary: heat transfer hydraulic diameter; heated length fwd (10.: ignore);
* Heated length rev (10.: ignore); grid spacer length fwd (0.: ignore); grid spacer length rev (0.: ignore);
* Grid loss coef fwd (0.: ignore); grid loss coef rev (0.: ignore); boiling factor (1.: subcooled liquid);
* Heat structure number
13001801 6.93e-3 10.0 10.0 0.0 0.0 0.0 0.0 1.0 11
* Additional right boundary: heat transfer hydraulic diameter; heated length fwd (10.: ignore);
* Heated length rev (10.: ignore); grid spacer length fwd (0.: ignore); grid spacer length rev (0.: ignore);
* Grid loss coef fwd (0.: ignore); grid loss coef rev (0.: ignore); boiling factor (1.: subcooled liquid);
* Heat structure number
13001901 7.42e-3 10.0 10.0 0.0 0.0 0.0 0.0 1.0 11
*
* DHX outlet mixer pipe (DRACS loop)
* Number of axial heat structures; number of radial mesh points;
* Geometry type (2: cylindrical, coupled to hydrodynamic component);
* Steady-state initialization flag (1: initial T calculated by code);
* Left boundary coordinate; reflood condition
13101000 1 7 2 1 1.39e-2 0
* Mesh location flag; mesh format flag (see p.252 of Manual Appendix A)
13101100 0 2
* Mesh interval distance; interval number
13101101 1.384e-3 2
13101102 1.270e-2 6
* Composition (table number); interval number
13101201 100 2
13101202 120 6
* Power input proportion; mesh interval number
13101301 1.0 2
13101302 0.0 6
* Initial temperature; mesh point number
13101401 325.0  3
13101402 293.15 7
* Left boundary condition definition (here: vol number); increment;
* Boundary condition type (101: convection); surface area code (1: length);
* Length; heat structure number
13101501 310010000 10000 101 1 0.354312962 1
* Right boundary condition, see above (-30: T defined in general table 30; 1000: T set in Word 1)
```

```
13101601 -30 0 1000 1 0.354312962 1
* Power source (table number); internal source multiplier; direct mod heatin mult (left)
* Direct mod heatin mult (right); heat structure number
13101701 0 0.0 0.0 0.0 1
* Additional left boundary: heat transfer hydraulic diameter; heated length fwd (10.: ignore);
* Heated length rev (10.: ignore); grid spacer length fwd (0.: ignore); grid spacer length rev (0.: ignore);
* Grid loss coef fwd (0.: ignore); grid loss coef rev (0.: ignore); boiling factor (1.: subcooled liquid);
* Heat structure number
13101801 0.0 10.0 10.0 0.0 0.0 0.0 0.0 1.0 1
*
* DHX outlet mixer (DRACS loop)
* Number of axial heat structures; number of radial mesh points;
* Geometry type (2: cylindrical, coupled to hydrodynamic component);
* Steady-state initialization flag (1: initial T calculated by code);
* Left boundary coordinate; reflood condition
13111000 1 7 2 1 1.39e-2 0
* Mesh location flag; mesh format flag (see p.252 of Manual Appendix A)
13111100 0 2
* Mesh interval distance; interval number
13111101 1.384e-3 2
13111102 1.270e-2 6
* Composition (table number); interval number
13111201 100 2
13111202 120 6
* Power input proportion; mesh interval number
13111301 1.0 2
13111302 0.0 6
* Initial temperature; mesh point number
13111401 325.0  3
13111402 293.15 7
* Left boundary condition definition (here: vol number); increment;
* Boundary condition type (101: convection); surface area code (1: length);
* Length; heat structure number
13111501 311010000 10000 101 1 0.817188128 1
* Right boundary condition, see above (-30: T defined in general table 30; 1000: T set in Word 1)
13111601 -30 0 1000 1 0.817188128 1
* Power source (table number); internal source multiplier; direct mod heatin mult (left)
* Direct mod heatin mult (right); heat structure number
13111701 0 0.0 0.0 0.0 1
* Additional left boundary: heat transfer hydraulic diameter; heated length fwd (10.: ignore);
* Heated length rev (10.: ignore); grid spacer length fwd (0.: ignore); grid spacer length rev (0.: ignore);
* Grid loss coef fwd (0.: ignore); grid loss coef rev (0.: ignore); boiling factor (1.: subcooled liquid);
* Heat structure number
13111801 0.0 10.0 10.0 0.0 0.0 0.0 0.0 1.0 1
*
* DRACS hot leg 1
* Number of axial heat structures; number of radial mesh points;
* Geometry type (2: cylindrical, coupled to hydrodynamic component);
* Steady-state initialization flag (1: initial T calculated by code);
* Left boundary coordinate; reflood condition
13201000 2 7 2 1 1.39e-2 0
* Mesh location flag; mesh format flag (see p.252 of Manual Appendix A)
13201100 0 2
* Mesh interval distance; interval number
13201101 1.384e-3 2
13201102 1.270e-2 6
* Composition (table number); interval number
13201201 100 2
13201202 120 6
* Power input proportion; mesh interval number
13201301 1.0 2
13201302 0.0 6
```

```
* Initial temperature; mesh point number
13201401 325.0  3
13201402 293.15 7
* Left boundary condition definition (here: vol number); increment;
* Boundary condition type (101: convection); surface area code (1: length);
* Length; heat structure number
13201501 320010000 10000 101 1 0.294831571 2
* Right boundary condition, see above (-30: T defined in general table 30; 1000: T set in Word 1)
13201601 -30 0 1000 1 0.294831571 2
* Power source (table number); internal source multiplier; direct mod heatin mult (left)
* Direct mod heatin mult (right); heat structure number
13201701 0 0.0 0.0 0.0 2
* Additional left boundary: heat transfer hydraulic diameter; heated length fwd (10.: ignore);
* Heated length rev (10.: ignore); grid spacer length fwd (0.: ignore); grid spacer length rev (0.: ignore);
* Grid loss coef fwd (0.: ignore); grid loss coef rev (0.: ignore); boiling factor (1.: subcooled liquid);
* Heat structure number
13201801 0.0 10.0 10.0 0.0 0.0 0.0 0.0 1.0 2
*
* DRACS hot leg 2
* Number of axial heat structures; number of radial mesh points;
* Geometry type (2: cylindrical, coupled to hydrodynamic component);
* Steady-state initialization flag (1: initial T calculated by code);
* Left boundary coordinate; reflood condition
13301000 28 7 2 1 1.39e-2 0
* Mesh location flag; mesh format flag (see p.252 of Manual Appendix A)
13301100 0 2
* Mesh interval distance; interval number
13301101 1.384e-3 2
13301102 1.270e-2 6
* Composition (table number); interval number
13301201 100 2
13301202 120 6
* Power input proportion; mesh interval number
13301301 1.0 2
13301302 0.0 6
* Initial temperature; mesh point number
13301401 325.0  3
13301402 293.15 7
* Left boundary condition definition (here: vol number); increment;
* Boundary condition type (101: convection); surface area code (1: length);
* Length; heat structure number
13301501 330010000 10000 101 1 0.266205223 28
* Right boundary condition, see above (-30: T defined in general table 30; 1000: T set in Word 1)
13301601 -30 0 1000 1 0.266205223 28
* Power source (table number); internal source multiplier; direct mod heatin mult (left)
* Direct mod heatin mult (right); heat structure number
13301701 0 0.0 0.0 0.0 28
* Additional left boundary: heat transfer hydraulic diameter; heated length fwd (10.: ignore);
* Heated length rev (10.: ignore); grid spacer length fwd (0.: ignore); grid spacer length rev (0.: ignore);
* Grid loss coef fwd (0.: ignore); grid loss coef rev (0.: ignore); boiling factor (1.: subcooled liquid);
* Heat structure number
13301801 0.0 10.0 10.0 0.0 0.0 0.0 0.0 1.0 28
*
* Branch 34
* Number of axial heat structures; number of radial mesh points;
* Geometry type (2: cylindrical, coupled to hydrodynamic component);
* Steady-state initialization flag (1: initial T calculated by code);
* Left boundary coordinate; reflood condition
13401000 1 7 2 1 1.39e-2 0
* Mesh location flag; mesh format flag (see p.252 of Manual Appendix A)
13401100 0 2
* Mesh interval distance; interval number
```

```
13401101 1.384e-3 2
13401102 1.270e-2 6
* Composition (table number); interval number
13401201 100 2
13401202 120 6
* Power input proportion; mesh interval number
13401301 1.0 2
13401302 0.0 6
* Initial temperature; mesh point number
13401401 325.0  3
13401402 293.15 7
* Left boundary condition definition (here: vol number); increment;
* Boundary condition type (101: convection); surface area code (1: length);
* Length; heat structure number
13401501 340010000 10000 101 1 1.368047216 1
* Right boundary condition, see above (-30: T defined in general table 30; 1000: T set in Word 1)
13401601 -30 0 1000 1 1.368047216 1
* Power source (table number); internal source multiplier; direct mod heatin mult (left)
* Direct mod heatin mult (right); heat structure number
13401701 0 0.0 0.0 0.0 1
* Additional left boundary: heat transfer hydraulic diameter; heated length fwd (10.: ignore);
* Heated length rev (10.: ignore); grid spacer length fwd (0.: ignore); grid spacer length rev (0.: ignore);
* Grid loss coef fwd (0.: ignore); grid loss coef rev (0.: ignore); boiling factor (1.: subcooled liquid);
* Heat structure number
13401801 0.0 10.0 10.0 0.0 0.0 0.0 0.0 1.0 1
*
* TCHX 1
* Number of axial heat structures; number of radial mesh points;
* Geometry type (2: cylindrical, coupled to hydrodynamic component);
* Steady-state initialization flag (1: initial T calculated by code);
* Left boundary coordinate; reflood condition
13511000 11 5 2 1 5.95e-3 0
* Mesh location flag; mesh format flag (see p.252 of Manual Appendix A)
13511100 0 2
* Mesh interval distance; interval number
13511101 4.00e-4 4
* Composition (table number); interval number
13511201 110 4
* Power input proportion; mesh interval number
13511301 1.0 4
* Initial temperature; mesh point number
13511401 325.0  5
* Left boundary condition definition (here: vol number); increment;
* Boundary condition type (3070: HTC set in general table 70); surface area code (1: length);
* Length; heat structure number
13511501 351010000 10000 3070 1 0.10441 11
* Right boundary condition, see above (-50: T defined in general table 50; 1000: T set in Word 1)
13511601 -50 0 1000 1 0.10441 11
* Power source (table number); internal source multiplier; direct mod heatin mult (left)
* Direct mod heatin mult (right); heat structure number
13511701 0 0.0 0.0 0.0 11
* Additional left boundary: heat transfer hydraulic diameter; heated length fwd (10.: ignore);
* Heated length rev (10.: ignore); grid spacer length fwd (0.: ignore); grid spacer length rev (0.: ignore);
* Grid loss coef fwd (0.: ignore); grid loss coef rev (0.: ignore); boiling factor (1.: subcooled liquid);
* Heat structure number
13511801 0.0 10.0 10.0 0.0 0.0 0.0 0.0 1.0 11
*
* TCHX 2
* Number of axial heat structures; number of radial mesh points;
* Geometry type (2: cylindrical, coupled to hydrodynamic component);
* Steady-state initialization flag (1: initial T calculated by code);
* Left boundary coordinate; reflood condition
```

```
13521000 4 5 2 1 5.95e-3 0
* Mesh location flag; mesh format flag (see p.252 of Manual Appendix A)
13521100 0 2
* Mesh interval distance; interval number
13521101 4.00e-4 4
* Composition (table number); interval number
13521201 110 4
* Power input proportion; mesh interval number
13521301 1.0 4
* Initial temperature; mesh point number
13521401 325.0  5
* Left boundary condition definition (here: vol number); increment;
* Boundary condition type (3070: HTC set in general table 70); surface area code (1: length);
* Length; heat structure number
13521501 352010000 10000 3070 1 0.10398 4
* Right boundary condition, see above (-50: T defined in general table 50; 1000: T set in Word 1)
13521601 -50 0 1000 1 0.10398 4
* Power source (table number); internal source multiplier; direct mod heatin mult (left)
* Direct mod heatin mult (right); heat structure number
13521701 0 0.0 0.0 0.0 4
* Additional left boundary: heat transfer hydraulic diameter; heated length fwd (10.: ignore);
* Heated length rev (10.: ignore); grid spacer length fwd (0.: ignore); grid spacer length rev (0.: ignore);
* Grid loss coef fwd (0.: ignore); grid loss coef rev (0.: ignore); boiling factor (1.: subcooled liquid);
* Heat structure number
13521801 0.0 10.0 10.0 0.0 0.0 0.0 0.0 1.0 4
*
* TCHX outlet mixer pipe
* Number of axial heat structures; number of radial mesh points;
* Geometry type (2: cylindrical, coupled to hydrodynamic component);
* Steady-state initialization flag (1: initial T calculated by code);
* Left boundary coordinate; reflood condition
13601000 2 7 2 1 1.39e-2 0
* Mesh location flag; mesh format flag (see p.252 of Manual Appendix A)
13601100 0 2
* Mesh interval distance; interval number
13601101 1.384e-3 2
13601102 1.270e-2 6
* Composition (table number); interval number
13601201 100 2
13601202 120 6
* Power input proportion; mesh interval number
13601301 1.0 2
13601302 0.0 6
* Initial temperature; mesh point number
13601401 325.0  3
13601402 293.15 7
* Left boundary condition definition (here: vol number); increment;
* Boundary condition type (101: convection); surface area code (1: length);
* Length; heat structure number
13601501 360010000 10000 101 1 0.202040244 2
* Right boundary condition, see above (-30: T defined in general table 30; 1000: T set in Word 1)
13601601 -30 0 1000 1 0.202040244 2
* Power source (table number); internal source multiplier; direct mod heatin mult (left)
* Direct mod heatin mult (right); heat structure number
13601701 0 0.0 0.0 0.0 2
* Additional left boundary: heat transfer hydraulic diameter; heated length fwd (10.: ignore);
* Heated length rev (10.: ignore); grid spacer length fwd (0.: ignore); grid spacer length rev (0.: ignore);
* Grid loss coef fwd (0.: ignore); grid loss coef rev (0.: ignore); boiling factor (1.: subcooled liquid);
* Heat structure number
13601801 0.0 10.0 10.0 0.0 0.0 0.0 0.0 1.0 2
*
* TCHX outlet mixer
```

```
* Number of axial heat structures; number of radial mesh points;
* Geometry type (2: cylindrical, coupled to hydrodynamic component);
* Steady-state initialization flag (1: initial T calculated by code);
* Left boundary coordinate; reflood condition
13611000 1 7 2 1 1.39e-2 0
* Mesh location flag; mesh format flag (see p.252 of Manual Appendix A)
13611100 0 2
* Mesh interval distance; interval number
13611101 1.384e-3 2
13611102 1.270e-2 6
* Composition (table number); interval number
13611201 100 2
13611202 120 6
* Power input proportion; mesh interval number
13611301 1.0 2
13611302 0.0 6
* Initial temperature; mesh point number
13611401 325.0  3
13611402 293.15 7
* Left boundary condition definition (here: vol number); increment;
* Boundary condition type (101: convection); surface area code (1: length);
* Length; heat structure number
13611501 361010000 10000 101 1 0.655587814 1
* Right boundary condition, see above (-30: T defined in general table 30; 1000: T set in Word 1)
13611601 -30 0 1000 1 0.655587814 1
* Power source (table number); internal source multiplier; direct mod heatin mult (left)
* Direct mod heatin mult (right); heat structure number
13611701 0 0.0 0.0 0.0 1
* Additional left boundary: heat transfer hydraulic diameter; heated length fwd (10.: ignore);
* Heated length rev (10.: ignore); grid spacer length fwd (0.: ignore); grid spacer length rev (0.: ignore);
* Grid loss coef fwd (0.: ignore); grid loss coef rev (0.: ignore); boiling factor (1.: subcooled liquid);
* Heat structure number
13611801 0.0 10.0 10.0 0.0 0.0 0.0 0.0 1.0 1
*
* DRACS cold leg 1
* Number of axial heat structures; number of radial mesh points;
* Geometry type (2: cylindrical, coupled to hydrodynamic component);
* Steady-state initialization flag (1: initial T calculated by code);
* Left boundary coordinate; reflood condition
13701000 16 7 2 1 1.39e-2 0
* Mesh location flag; mesh format flag (see p.252 of Manual Appendix A)
13701100 0 2
* Mesh interval distance; interval number
13701101 1.384e-3 2
13701102 1.270e-2 6
* Composition (table number); interval number
13701201 100 2
13701202 120 6
* Power input proportion; mesh interval number
13701301 1.0 2
13701302 0.0 6
* Initial temperature; mesh point number
13701401 325.0  3
13701402 293.15 7
* Left boundary condition definition (here: vol number); increment;
* Boundary condition type (101: convection); surface area code (1: length);
* Length; heat structure number
13701501 370010000 10000 101 1 0.220217907 16
* Right boundary condition, see above (-30: T defined in general table 30; 1000: T set in Word 1)
13701601 -30 0 1000 1 0.220217907 16
* Power source (table number); internal source multiplier; direct mod heatin mult (left)
* Direct mod heatin mult (right); heat structure number
```

```
13701701 0 0.0 0.0 0.0 16
* Additional left boundary: heat transfer hydraulic diameter; heated length fwd (10.: ignore);
* Heated length rev (10.: ignore); grid spacer length fwd (0.: ignore); grid spacer length rev (0.: ignore);
* Grid loss coef fwd (0.: ignore); grid loss coef rev (0.: ignore); boiling factor (1.: subcooled liquid);
* Heat structure number
13701801 0.0 10.0 10.0 0.0 0.0 0.0 0.0 1.0 16
*
* DRACS flowmeter
* Number of axial heat structures; number of radial mesh points;
* Geometry type (2: cylindrical, coupled to hydrodynamic component);
* Steady-state initialization flag (1: initial T calculated by code);
* Left boundary coordinate; reflood condition
13711000 1 7 2 1 1.39e-2 0
* Mesh location flag; mesh format flag (see p.252 of Manual Appendix A)
13711100 0 2
* Mesh interval distance; interval number
13711101 1.384e-3 2
13711102 1.270e-2 6
* Composition (table number); interval number
13711201 100 2
13711202 120 6
* Power input proportion; mesh interval number
13711301 1.0 2
13711302 0.0 6
* Initial temperature; mesh point number
13711401 325.0  3
13711402 293.15 7
* Left boundary condition definition (here: vol number); increment;
* Boundary condition type (101: convection); surface area code (1: length);
* Length; heat structure number
13711501 371010000 10000 101 1 0.715186706 1
* Right boundary condition, see above (-30: T defined in general table 30; 1000: T set in Word 1)
13711601 -30 0 1000 1 0.715186706 1
* Power source (table number); internal source multiplier; direct mod heatin mult (left)
* Direct mod heatin mult (right); heat structure number
13711701 0 0.0 0.0 0.0 1
* Additional left boundary: heat transfer hydraulic diameter; heated length fwd (10.: ignore);
* Heated length rev (10.: ignore); grid spacer length fwd (0.: ignore); grid spacer length rev (0.: ignore);
* Grid loss coef fwd (0.: ignore); grid loss coef rev (0.: ignore); boiling factor (1.: subcooled liquid);
* Heat structure number
13711801 0.0 10.0 10.0 0.0 0.0 0.0 0.0 1.0 1
*
* DRACS cold leg 2
* Number of axial heat structures; number of radial mesh points;
* Geometry type (2: cylindrical, coupled to hydrodynamic component);
* Steady-state initialization flag (1: initial T calculated by code);
* Left boundary coordinate; reflood condition
13801000 3 7 2 1 1.39e-2 0
* Mesh location flag; mesh format flag (see p.252 of Manual Appendix A)
13801100 0 2
* Mesh interval distance; interval number
13801101 1.384e-3 2
13801102 1.270e-2 6
* Composition (table number); interval number
13801201 100 2
13801202 120 6
* Power input proportion; mesh interval number
13801301 1.0 2
13801302 0.0 6
* Initial temperature; mesh point number
13801401 325.0  3
13801402 293.15 7
```

```
* Left boundary condition definition (here: vol number); increment;
* Boundary condition type (101: convection); surface area code (1: length);
* Length; heat structure number
13801501 380010000 10000 101 1 0.222860124 3
* Right boundary condition, see above (-30: T defined in general table 30; 1000: T set in Word 1)
13801601 -30 0 1000 1 0.222860124 3
* Power source (table number); internal source multiplier; direct mod heatin mult (left)
* Direct mod heatin mult (right); heat structure number
13801701 0 0.0 0.0 0.0 3
* Additional left boundary: heat transfer hydraulic diameter; heated length fwd (10.: ignore);
* Heated length rev (10.: ignore); grid spacer length fwd (0.: ignore); grid spacer length rev (0.: ignore);
* Grid loss coef fwd (0.: ignore); grid loss coef rev (0.: ignore); boiling factor (1.: subcooled liquid);
* Heat structure number
13801801 0.0 10.0 10.0 0.0 0.0 0.0 0.0 1.0 3
*
* DRACS cold leg 3
* Number of axial heat structures; number of radial mesh points;
* Geometry type (2: cylindrical, coupled to hydrodynamic component);
* Steady-state initialization flag (1: initial T calculated by code);
* Left boundary coordinate; reflood condition
13901000 18 7 2 1 1.39e-2 0
* Mesh location flag; mesh format flag (see p.252 of Manual Appendix A)
13901100 0 2
* Mesh interval distance; interval number
13901101 1.384e-3 2
13901102 1.270e-2 6
* Composition (table number); interval number
13901201 100 2
13901202 120 6
* Power input proportion; mesh interval number
13901301 1.0 2
13901302 0.0 6
* Initial temperature; mesh point number
13901401 325.0  3
13901402 293.15 7
* Left boundary condition definition (here: vol number); increment;
* Boundary condition type (101: convection); surface area code (1: length);
* Length; heat structure number
13901501 390010000 10000 101 1 0.210960212 18
* Right boundary condition, see above (-30: T defined in general table 30; 1000: T set in Word 1)
13901601 -30 0 1000 1 0.210960212 18
* Power source (table number); internal source multiplier; direct mod heatin mult (left)
* Direct mod heatin mult (right); heat structure number
13901701 0 0.0 0.0 0.0 18
* Additional left boundary: heat transfer hydraulic diameter; heated length fwd (10.: ignore);
* Heated length rev (10.: ignore); grid spacer length fwd (0.: ignore); grid spacer length rev (0.: ignore);
* Grid loss coef fwd (0.: ignore); grid loss coef rev (0.: ignore); boiling factor (1.: subcooled liquid);
* Heat structure number
13901801 0.0 10.0 10.0 0.0 0.0 0.0 0.0 1.0 18
*
*******************************************************
*  Material properties
*******************************************************
*
* Stainless steel
* Material type (user supplied table); thermal conductivity format flag;
* Volumetric heat capacity format flag (see p.227 of Manual Appendix A)
20110000   tbl/fctn  1  1
* Stainless steel thermal conductivity (T; k) from k=14.6+0.0127*T[°C]
* (http://www.mace.manchester.ac.uk/project/research/structures/strucfire/
* materialInFire/Steel/StainlessSteel/thermalProperties.htm)
20110001   250.0   14.31
```

```
20110002   300.0   14.94
20110003   350.0   15.58
20110004   400.0   16.21
20110005   450.0   16.85
20110006   500.0   17.48
20110007   700.0   20.02
20110008   1000.0   23.83
* Stainless steel volumetric heat capacity (T; rho*cp)
* From cp=450+0.28*T[°C]-2.91E-4*T[°C]^2+1.34E-7*T[°C]^3 (same source)
* and rho=8030[kg/m^3] (http://www.lenntech.com/stainless-steel-304.htm)
20110051   250.0   3.56e6
20110052   300.0   3.67e6
20110053   350.0   3.77e6
20110054   400.0   3.86e6
20110055   450.0   3.94e6
20110056   500.0   4.02e6
20110057   700.0   4.23e6
20110058   1000.0   4.43e6
*
* Copper
* Material type (user supplied table); thermal conductivity format flag;
* Volumetric heat capacity format flag (see p.227 of Manual Appendix A)
20111000   tbl/fctn  1  1
* Copper thermal conductivity (T; k)
* From http://www.efunda.com/materials/elements/TC_Table.cfm?Element_ID=Cu
20111001   250.0   406.
20111002   300.0   401.
20111003   350.0   396.
20111004   400.0   393.
20111005   500.0   386.
20111006   1000.0   352.
* Copper volumetric heat capacity (T; rho*cp)
* cp from http://www.efunda.com/materials/elements/HC_Table.cfm?Element_ID=Cu
* rho=8940[kg/m^3]
20111051   200.0   3.18e6
20111052   250.0   3.34e6
20111053   298.15   3.44e6
20111054   350.0   3.51e6
20111055   400.0   3.56e6
20111056   500.0   3.64e6
20111057   600.0   3.73e6
*
* Fiberglass insulation
* Material type (user supplied table); thermal conductivity format flag;
* Volumetric heat capacity format flag (see p.227 of Manual Appendix A)
20112000   tbl/fctn  1  1
* Fiberglass insulation thermal conductivity (T; k) from k=7.702E-4*T[°C]+0.206
* (CIET-DESIGN-141_Properties_PSHT2_Materials)
20112001   250.0   0.028616
20112002   293.15   0.033060
20112003   350.0   0.038916
20112004   400.0   0.044066
20112005   500.0   0.054366
20112006   600.0   0.064666
* Fiberglass insulation volumetric heat capacity (T; rho*cp)
* From cp=844[J/kg-K] and rho=20[kg/m^3]
20112051   250.0   1.69e4
20112052   293.15   1.69e4
20112053   350.0   1.69e4
20112054   400.0   1.69e4
20112055   500.0   1.69e4
20112056   600.0   1.69e4
```

```
*
*****************************************************
*  General tables
*****************************************************
* Heater power
* Table type
20201000  power
* Time; power [W]
20201001 0.     2512.9
20201002 3361.  2512.9
20201003 3362.  4218.7
20201004 4050.  4218.7
20201005 4051.  6072.5
20201006 4702.  6072.5
20201007 4703.  7085.2
20201008 5406.  7085.2
20201009 5407.  7598.2
20201010 6069.  7598.2
20201011 6070.  7156.4
20201012 6895.  7156.4
20201013 6896.  5435.0
20201014 7551.  5435.0
20201015 7552.  2710.1
20201016 10000. 2710.1
*
* Ambient temperature
* Table type
20203000  temp
* Time; temperature [K]
20203001  0.00000  298.15
20203002  10000.0   298.15
*
* CTAH outlet temperature
* Table type
20204000  temp
* Time; temperature [K]
20204001  0.00000  353.10
20204002  10000.0   353.10
*
* TCHX outlet temperature
* Table type
20205000  temp
* Time; temperature [K]
20205001  0.00000  308.4
20205002  10000.0   308.4
*
* CTAH heat transfer coefficient
* Table type
20206000  htc-t
* Time; heat transfer coefficient [W/m^2-K]
20206001  0.00000  80000.
20206002  10000.0   80000.
*
* TCHX heat transfer coefficient
* Table type
20207000  htc-t
* Time; heat transfer coefficient [W/m^2-K]
20207001  0.00000  8000.
20207002  10000.0   8000.
*
*****************************************************
*  Trips
```

```
*****************************************************
* Variable code; parameter (0 if variable code is time); relationship;
* Variable code; parameter; additive constant; latch indicator
401 time 0 ge null 0 20000. l
*
* End of input
.
```

Appendix B RELAP5-3D Model of the Mk1 PB-FHR

This Appendix lists all parameters – for both hydrodynamic components and heat structures – used to build the equivalent model of the Mk1 PB-FHR in RELAP5-3D, represented by the nodalization diagram in Figure 3-3. In particular, details about modeling of the Mk1 core in RELAP5-3D are provided in Section B.2. For reproducibility purposes, the RELAP5-3D input deck used to generate the results shown in Figure 3-4 and Figure 3-5 is also included in Section B.3.

B.1 List of Parameters Used in the RELAP5-3D Mk1 PB-FHR Equivalent Model

Table B-1. Hydrodynamic component parameters of the RELAP5-3D Mk1 model.

Component	Number on diagram	RELAP volume number	Length (m)	Vertical angle (°)	Hydraulic diameter (m)	Flow area (m²)
Core branch (bottom to top)						
Active core region	1	10	4.58	90	3.00E-02	1.33E+00
Core bypass	2	20	4.58	90	1.00E-02	1.33E-01
Hot salt collection ring	3	30	3.96	0	5.67E-01	2.52E-01
Hot salt extraction pipe	4	40	3.77	90	5.66E-01	2.51E-01
Branch	26	260	0.50	0	5.80E-01	2.64E-01
CTAH branch (top to bottom)						
Reactor vessel to hot salt well	5	50	3.73	1.24432251	5.80E-01	2.64E-01
Hot salt well	6	60	2.00	9.78781906	1.45E+00	3.31E+00
Hot salt well to CTAH	7	70	3.23	-0.81600463	4.40E-01	3.04E-01
CTAH hot manifold	8	80	3.418	-90	2.80E-01	4.93E-01
CTAH salt side	9	90	18.47	-0.50875102	4.57E-03	4.49E-01
CTAH cold manifold	10	100	3.418	-90	1.75E-01	1.92E-01
CTAH to drain tank	11	110	3.48	-1.23491845	4.38E-01	3.02E-01
Stand pipe	12	120	6.51	90	4.38E-01	3.02E-01
Stand pipe to reactor vessel	13	130	6.603338	1.21484167	4.38E-01	3.02E-01
Injection plenum	14	140	3.04	-90	4.38E-01	3.02E-01
Branch	27	270	0.50	-90	5.60E-02	3.04E-01
Downcomer	15	150	4.76	-90	5.60E-02	3.04E-01
Inlet plenum	28	280	0.20	0	3.00E-02	1.33E+00
DHX branch (bottom to top)						
Downcomer to DHX	16	160	0.58	90	1.50E-01	3.53E-02
DHX shell side	17	170	2.50	90	1.09E-02	2.22E-01
DHX to hot leg	18	180	3.008	9.76153245	1.50E-01	3.53E-02
DRACS loop (counterclockwise)						
DHX tube side	19	190	2.50	90	1.09E-02	1.84E-01

Component	Number on diagram	RELAP volume number	Length (m)	Vertical angle (°)	Hydraulic diameter (m)	Flow area (m²)
DRACS hot leg 1	20	200	3.45	90	1.50E-01	3.53E-02
DRACS hot leg 2	21	210	3.67	0	1.50E-01	3.53E-02
TCHX manifold	22	220	2.60	90	1.50E-01	3.53E-02
TCHX salt tube	23	230	6.00	-25.6792886	1.09E-02	1.75E-01
DRACS cold leg 1	24	240	4.43	0	1.50E-01	3.53E-02
DRACS cold leg 2	25	250	5.95	-90	1.50E-01	3.53E-02

Table B-2. Heat structure parameters of the RELAP5-3D Mk1 model.

Component	Number on diagram	RELAP volume number	Length (m)	Left boundary (m)	Pipe wall thickness (m)
CTAH salt side	9	90	18.47	2.286E-03	8.89E-04
DHX tube side	19	190	2.50	5.450E-03	9.00E-04
TCHX salt tube	23	230	6.00	5.450E-03	9.00E-04

B.2 Modeling of the Mk1 PB-FHR Core in RELAP5-3D

While details on RELAP5 modeling of pebble fuel heat structures in PB-FHR cores are documented in an earlier publication [36], this Section develops the methodology used to model the Mk1 core hydrodynamic components in RELAP5-3D.

B.2.1 Geometric Parameters for the Hydrodynamic Components

Because natural circulation, which is a key phenomenon to be modeled for the Mk1 PB-FHR passive safety systems, depends on relative elevations of heat sources and sinks in the reactor, the RELAP5-3D model of the Mk1 core preserves its elevation, used as the total length and elevation of the core hydrodynamic component. To also preserve total coolant inventory – and therefore residence time – in the Mk1 core, the flow area of the core hydrodynamic component is adjusted so that the total fluid volume in the active region of the core is the same between the model and the Mk1 design (6.09 m³).

B.2.2 Porous Media Flow Modeling

Another key phenomenon to model in RELAP5-3D is porous media flow in the Mk1 pebble-bed core. The study of porous media flow requires the introduction of some useful, specific parameters in addition to standard thermal hydraulic parameters, which are listed here:

- Porosity φ, defined as the fraction of the total volume of the medium that is occupied by "void space" (coolant in this case). The porosity for randomly packed beds of spheres is usually assumed to be 40% [85];
- Permeability K (in m²), defined by:

$$K = \frac{\varphi^3 d_p^2}{180(1-\varphi)^2} \quad \text{(B-1)}$$

where d_p is the pebble diameter;

- Reynolds number, defined in this context by:

$$Re_d = \frac{\rho_f u_D d_p}{\mu_f} \quad \text{(B-2)}$$

or:

$$Re_K = \frac{\rho_f u_D K^{1/2}}{\mu_f} \quad \text{(B-3)}$$

where ρ_f is the density of the fluid, u_D the superficial velocity, and μ_f the dynamic viscosity of the fluid. The Reynolds number uses a characteristic length that can be defined in two ways, one using the pebble diameter, and one (more frequently used for porous media flow studies) using permeability of the bed. The ratio between the two Reynolds numbers is given, for a randomly packed bed of spheres, using 40% porosity as a reference value, by:

$$Re_d / Re_K \approx 32 \quad \text{(B-4)}$$

- Friction factor f_K, defined in this context by:

$$f_K = \frac{K^{1/2}}{\rho_f u_D^2}\left(-\frac{dp}{dz}\right) \quad \text{(B-5)}$$

where dp is the pressure drop over flow length dz;

- Energy loss coefficient in RELAP5-3D, f_{RELAP}, defined by:

$$-dp = \frac{\rho_f u_D^2}{2} f_{RELAP} \Rightarrow f_{RELAP} = \frac{2 f_K}{K^{1/2}} dz \quad \text{(B-6)}$$

The most common deterministic correlation used to quantify pressure drop for flow across porous beds is Ergun's correlation, defined by [85]:

$$f_K = \frac{1}{Re_K} + \frac{1.75}{\sqrt{180\varphi^3}} \quad \text{(B-7)}$$

For a randomly packed bed of spheres, this correlation is approximated by:

$$f_K \approx \frac{1}{Re_K} + 0.5156 \quad \text{(B-8)}$$

Finally, the energy loss coefficient f_{RELAP} can be implemented in RELAP5-3D as:

$$f_{RELAP} = A + B \cdot Re^{-C} \quad \text{(B-9)}$$

where A, B and C are defined by the user. Knowing f_K from Eq. (B-8) and K from Eq. (B-1), an expression for f_{RELAP} can be derived from Eq. (B-6), which is how coefficients A, B and C are obtained.

Once the flow distribution in the Mk1 annular core has been optimized using other software such as COMSOL Multiphysics (e.g. to minimize pressure drop across the core to enhance natural circulation), parameters A, B and C can be modified to adjust pressure drop to the right value across the RELAP5-3D one-dimensional component.

B.3 Example of a RELAP5-3D Input Deck Used to Model an LOFC Transient on the Mk1 PB-FHR

```
=Mk1 PB-FHR Equivalent Model for LOFC Analysis
* Using equivalent CTAH (2 in 1) and DRACS (2 in 1) loops
* Using idealized boundary conditions on CTAH and TCHX secondary sides
* Parameters to be adjusted before each run:
* - Forward form loss coefficient for fluidic diode (card 6070101)
* - Pump coast down parameters (search 'tmdpjun')
* - Power distribution in core (cards 101017NN and 202010NN)
* Future updates:
* - Implement actual heat transfer correlations for CTAH and TCHX
* - Implement radiative heat transfer for TCHX
* - Implement point kinetics model
* - Include physical model for the pump
* - Add heat structures for structural materials, reflectors, etc.
* New problem using non-standard fluid; transient mode
100 newath transnt
* SI units for input; SI units for output
102 si si
* Reference volume; reference elevation; fluid (flibe)
120   10010000 0.0000  ms1
121  190010000 5.3400  ms1
* End time; min time step; max time step; control option;
* Minor edit frequency; major edit frequency; restart frequency
201   1000.0  1.0e-7 0.1  15011  1000  10000 10000
202  10000.0  1.0e-7 0.1  15011  10    10000 10000
* Minor edit requests: variable request code; parameter
301  mflowfj  10010000
302  mflowfj  20010000
303  mflowfj 170010000
304  mflowfj 190010000
305  tempf   280010000
306  tempf    30010000
307  tempf   160030000
308  tempf   180010000
309  tempf   250340000
310  tempf   200010000
311  tempf   220150000
312  tempf   240010000
*******************************************************
* Hydrodynamic components
*******************************************************
*
* Active core region
* Component name; component type
100000 core pipe
```

```
* Number of elements
100001 26
* Volume flow area; volume number
100101 1.327511,26
* Volume length; volume number
100301 0.17615385,26
* Volume inclination angle; volume number (required)
100601 90.0,26
* Wall roughness; hydraulic diameter; volume number
* Here for graphite: k=0.015mm
100801 1.5e-5,3.00e-2,26
* A_f; A_r; junction number
100901 32.1,32.1,25
* tlpvbfe (see p.130 of Manual Appendix A); volume number
101001 10,26
* jefvcahs (see p.132 of Manual Appendix A); junction number
101101 0,25
* ebt (initial conditions options); P; T; 0; 0; 0; volume number
101201 3,1.80e5,873.0,0.,0.,0.,26
* Junction initial conditions control option
* 0 for velocities, 1 for mass flow rates
101300 1
* Initial liquid velocity; initial gas velocity;
* Interface velocity (enter 0.0); junction number
101301 977.,977.,0.,25
* Hydraulic diameter; flooding correlation (enter 0.0); vapor/gas
* intercept (enter 1.0); slope (enter 1.0);junction number
101401 3.00e-2,0.,1.,1.,25
* B_f; C_f; B_r; C_r; junction number
103001 4974.4,1.0,4974.4,1.0,25
*
* Core bypass
* Component name; component type
200000 bypass pipe
* Number of elements
200001 26
* Volume flow area; volume number
200101 0.065,26
* Volume length; volume number
200301 0.17615385,26
* Volume inclination angle; volume number (required)
200601 90.0,26
* Wall roughness; hydraulic diameter; volume number
* Here for graphite: k=0.015mm
200801 1.5e-5,1.00e-2,26
* tlpvbfe (see p.130 of Manual Appendix A); volume number
201001 0,26
* jefvcahs (see p.132 of Manual Appendix A); junction number
201101 0,25
* ebt (initial conditions options); P; T; 0; 0; 0; volume number
201201 3,1.80e5,873.0,0.,0.,0.,26
* Junction initial conditions control option
* 0 for velocities, 1 for mass flow rates
201300 1
```

```
* Initial liquid velocity; initial gas velocity;
* Interface velocity (enter 0.0); junction number
201301 97.7,97.7,0.,25
*
* Hot salt collection ring
* Component name; component type
300000 hotring branch
* Number of junctions; control word (0: velocities, 1: mass flow rates)
300001 3 1
* Volume flow area; volume length; volume of volume (calculated if 0.0)
* Azimuthal angle; vertical angle; elevation change; wall roughness
* Hydraulic diameter; tlpvbfe
300101 2.524495e-1 3.960000 0. 0. 0. 0. 1.5e-5 5.669468e-1 0
* ebt (initial conditions options); P; T
300200 3 1.76e5 973.0
* From; to; junction area; A_f; A_r; jefvcahs
301101  10010000  30000000 2.524495e-1 0. 0. 100
302101  20010000  30000000 0.065      0. 0. 100
303101  30010000  40000000 2.512732e-1 0. 0. 100
* Initial liquid velocity; initial gas velocity;
* Interface velocity (enter 0.0)
301201   977.   977.  0.
302201    97.7   97.7 0.
303201  1074.7 1074.7 0.
*
* Hot salt extraction pipe
* Component name; component type
400000 extract pipe
* Number of elements
400001 21
* Volume flow area; volume number
400101 2.512732e-1,21
* Volume length; volume number
400301 0.17952381,21
* Volume inclination angle; volume number (required)
400601 90.0,21
* Wall roughness; hydraulic diameter; volume number
* Here for stainless steel: k=0.015mm
400801 1.5e-5,5.656244e-1,21
* tlpvbfe (see p.130 of Manual Appendix A); volume number
401001 0,21
* jefvcahs (see p.132 of Manual Appendix A); junction number
401101 0,20
* ebt (initial conditions options); P; T; 0; 0; 0; volume number
401201 3,1.08e5,973.0,0.,0.,0.,21
* Junction initial conditions control option
* 0 for velocities, 1 for mass flow rates
401300 1
* Initial liquid velocity; initial gas velocity;
* Interface velocity (enter 0.0); junction number
401301 1074.7,1074.7,0.,20
*
* Reactor vessel to hot salt well
* Component name; component type
```

```
500000 vesswell pipe
* Number of elements
500001 21
* Volume flow area; volume number
500101 2.642080e-1,21
* Volume length; volume number
500301 0.17761905,21
* Volume inclination angle; volume number (required)
500601 1.24432251,21
* Wall roughness; hydraulic diameter; volume number
* Here for stainless steel: k=0.015mm
500801 1.5e-5,5.800001e-1,21
* tlpvbfe (see p.130 of Manual Appendix A); volume number
501001 0,21
* jefvcahs (see p.132 of Manual Appendix A); junction number
501101 0,20
* ebt (initial conditions options); P; T; 0; 0; 0; volume number
501201 3,1.06e5,973.0,0.,0.,0.,21
* Junction initial conditions control option
* 0 for velocities, 1 for mass flow rates
501300 1
* Initial liquid velocity; initial gas velocity;
* Interface velocity (enter 0.0); junction number
501301 1084.47,1084.47,0.,20
*
* Hot salt well
* Component name; component type
600000 hotwell pipe
* Number of elements
600001 11
* Volume flow area; volume number
600101 3.314500,11
* Volume length; volume number
600301 0.18181818,11
* Volume inclination angle; volume number (required)
600601 9.78781906,11
* Wall roughness; hydraulic diameter; volume number
* Here for stainless steel: k=0.015mm
600801 1.5e-5,1.452610,11
* tlpvbfe (see p.130 of Manual Appendix A); volume number
601001 0,11
* jefvcahs (see p.132 of Manual Appendix A); junction number
601101 0,10
* ebt (initial conditions options); P; T; 0; 0; 0; volume number
601201 3,1.00e5,973.0,0.,0.,0.,11
* Junction initial conditions control option
* 0 for velocities, 1 for mass flow rates
601300 1
* Initial liquid velocity; initial gas velocity;
* Interface velocity (enter 0.0); junction number
601301 1084.47,1084.47,0.,10
*
* Hot salt well to CTAH
* Component name; component type
```

```
700000 wellctah pipe
* Number of elements
700001 18
* Volume flow area; volume number
700101 3.041000e-1,18
* Volume length; volume number
700301 0.17944444,18
* Volume inclination angle; volume number (required)
700601 -0.81600463,18
* Wall roughness; hydraulic diameter; volume number
* Here for stainless steel: k=0.015mm
700801 1.5e-5,4.399955e-1,18
* tlpvbfe (see p.130 of Manual Appendix A); volume number
701001 0,18
* jefvcahs (see p.132 of Manual Appendix A); junction number
701101 0,17
* ebt (initial conditions options); P; T; 0; 0; 0; volume number
701201 3,4.81e5,973.0,0.,0.,0.,18
* Junction initial conditions control option
* 0 for velocities, 1 for mass flow rates
701300 1
* Initial liquid velocity; initial gas velocity;
* Interface velocity (enter 0.0); junction number
701301 1084.47,1084.47,0.,17
*
* CTAH hot manifold
* Component name; component type
800000 ctahhot pipe
* Number of elements
800001 19
* Volume flow area; volume number
800101 4.926017e-1,19
* Volume length; volume number
800301 0.17989474,19
* Volume inclination angle; volume number (required)
800601 -90.0,19
* Wall roughness; hydraulic diameter; volume number
* Here for stainless steel: k=0.015mm
800801 1.5e-5,2.800000e-1,19
* tlpvbfe (see p.130 of Manual Appendix A); volume number
801001 0,19
* jefvcahs (see p.132 of Manual Appendix A); junction number
801101 0,18
* ebt (initial conditions options); P; T; 0; 0; 0; volume number
801201 3,5.43e5,973.0,0.,0.,0.,19
* Junction initial conditions control option
* 0 for velocities, 1 for mass flow rates
801300 1
* Initial liquid velocity; initial gas velocity;
* Interface velocity (enter 0.0); junction number
801301 1084.47,1084.47,0.,18
*
* CTAH tubes (salt side)
* Component name; component type
```

```
900000 ctahtube pipe
* Number of elements
900001 99
* Volume flow area; volume number
900101 4.491779e-1,99
* Volume length; volume number
900301 0.18656566,99
* Volume inclination angle; volume number (required)
900601 -0.50875102,99
* Wall roughness; hydraulic diameter; volume number
* Here for stainless steel: k=0.015mm
900801 1.5e-5,4.572000e-3,99
* tlpvbfe (see p.130 of Manual Appendix A); volume number
901001 0,99
* jefvcahs (see p.132 of Manual Appendix A); junction number
901101 0,98
* ebt (initial conditions options); P; T; 0; 0; 0; volume number
901201 3,2.92e5,923.0,0.,0.,0.,99
* Junction initial conditions control option
* 0 for velocities, 1 for mass flow rates
901300 1
* Initial liquid velocity; initial gas velocity;
* Interface velocity (enter 0.0); junction number
901301 1084.47,1084.47,0.,98
*
* CTAH cold manifold
* Component name; component type
1000000 ctahcold pipe
* Number of elements
1000001 19
* Volume flow area; volume number
1000101 1.924226e-1,19
* Volume length; volume number
1000301 0.17989474,19
* Volume inclination angle; volume number (required)
1000601 -90.0,19
* Wall roughness; hydraulic diameter; volume number
* Here for stainless steel: k=0.015mm
1000801 1.5e-5,1.750000e-1,19
* tlpvbfe (see p.130 of Manual Appendix A); volume number
1001001 0,19
* jefvcahs (see p.132 of Manual Appendix A); junction number
1001101 0,18
* ebt (initial conditions options); P; T; 0; 0; 0; volume number
1001201 3,3.53e5,873.0,0.,0.,0.,19
* Junction initial conditions control option
* 0 for velocities, 1 for mass flow rates
1001300 1
* Initial liquid velocity; initial gas velocity;
* Interface velocity (enter 0.0); junction number
1001301 1084.47,1084.47,0.,18
*
* CTAH to drain tank
* Component name; component type
```

```
1100000 ctahdrn pipe
* Number of elements
1100001 20
* Volume flow area; volume number
1100101 3.019068e-1,20
* Volume length; volume number
1100301 0.17400000,20
* Volume inclination angle; volume number (required)
1100601 -1.23491845,20
* Wall roughness; hydraulic diameter; volume number
* Here for stainless steel: k=0.015mm
1100801 1.5e-5,4.384060e-1,20
* tlpvbfe (see p.130 of Manual Appendix A); volume number
1101001 0,20
* jefvcahs (see p.132 of Manual Appendix A); junction number
1101101 0,19
* ebt (initial conditions options); P; T; 0; 0; 0; volume number
1101201 3,3.54e5,873.0,0.,0.,0.,20
* Junction initial conditions control option
* 0 for velocities, 1 for mass flow rates
1101300 1
* Initial liquid velocity; initial gas velocity;
* Interface velocity (enter 0.0); junction number
1101301 1084.47,1084.47,0.,19
*
* Stand pipe
* Component name; component type
1200000 stdpipe pipe
* Number of elements
1200001 37
* Volume flow area; volume number
1200101 3.019068e-1,37
* Volume length; volume number
1200301 0.17594595,37
* Volume inclination angle; volume number (required)
1200601 90.0,37
* Wall roughness; hydraulic diameter; volume number
* Here for stainless steel: k=0.015mm
1200801 1.5e-5,4.384060e-1,37
* tlpvbfe (see p.130 of Manual Appendix A); volume number
1201001 0,37
* jefvcahs (see p.132 of Manual Appendix A); junction number
1201101 0,36
* ebt (initial conditions options); P; T; 0; 0; 0; volume number
1201201 3,2.30e5,873.0,0.,0.,0.,37
* Junction initial conditions control option
* 0 for velocities, 1 for mass flow rates
1201300 1
* Initial liquid velocity; initial gas velocity;
* Interface velocity (enter 0.0); junction number
1201301 1084.47,1084.47,0.,36
*
* Stand pipe to reactor vessel
* Component name; component type
```

```
1300000 stdvess pipe
* Number of elements
1300001 37
* Volume flow area; volume number
1300101 3.019068e-1,37
* Volume length; volume number
1300301 0.17846859,37
* Volume inclination angle; volume number (required)
1300601 1.21484167,37
* Wall roughness; hydraulic diameter; volume number
* Here for stainless steel: k=0.015mm
1300801 1.5e-5,4.384060e-1,37
* tlpvbfe (see p.130 of Manual Appendix A); volume number
1301001 0,37
* jefvcahs (see p.132 of Manual Appendix A); junction number
1301101 0,36
* ebt (initial conditions options); P; T; 0; 0; 0; volume number
1301201 3,2.26e5,873.0,0.,0.,0.,37
* Junction initial conditions control option
* 0 for velocities, 1 for mass flow rates
1301300 1
* Initial liquid velocity; initial gas velocity;
* Interface velocity (enter 0.0); junction number
1301301 1084.47,1084.47,0.,36
*
* Injection plenum
* Component name; component type
1400000 plenum pipe
* Number of elements
1400001 17
* Volume flow area; volume number
1400101 3.019068e-1,17
* Volume length; volume number
1400301 0.17882353,17
* Volume inclination angle; volume number (required)
1400601 -90.0,17
* Wall roughness; hydraulic diameter; volume number
* Here for stainless steel: k=0.015mm
1400801 1.5e-5,4.384060e-1,17
* tlpvbfe (see p.130 of Manual Appendix A); volume number
1401001 0,17
* jefvcahs (see p.132 of Manual Appendix A); junction number
1401101 0,16
* ebt (initial conditions options); P; T; 0; 0; 0; volume number
1401201 3,2.82e5,873.0,0.,0.,0.,17
* Junction initial conditions control option
* 0 for velocities, 1 for mass flow rates
1401300 1
* Initial liquid velocity; initial gas velocity;
* Interface velocity (enter 0.0); junction number
1401301 1084.47,1084.47,0.,16
*
* Downcomer
* Component name; component type
```

```
1500000 dwncmr pipe
* Number of elements
1500001 27
* Volume flow area; volume number
1500101 3.038791e-1,27
* Volume length; volume number
1500301 0.17629630,27
* Volume inclination angle; volume number (required)
1500601 -90.0,27
* Wall roughness; hydraulic diameter; volume number
* Here for stainless steel: k=0.015mm
1500801 1.5e-5,5.602840e-2,27
* tlpvbfe (see p.130 of Manual Appendix A); volume number
1501001 0,27

* jefvcahs (see p.132 of Manual Appendix A); junction number
1501101 0,26
* ebt (initial conditions options); P; T; 0; 0; 0; volume number
1501201 3,3.65e5,873.0,0.,0.,0.,27
* Junction initial conditions control option
* 0 for velocities, 1 for mass flow rates
1501300 1
* Initial liquid velocity; initial gas velocity;
* Interface velocity (enter 0.0); junction number
1501301 1074.7,1074.7,0.,26
*
* Downcomer to DHX
* Component name; component type
1600000 dwndhx pipe
* Number of elements
1600001 3
* Volume flow area; volume number
1600101 3.534292e-2,3
* Volume length; volume number
1600301 0.19333333,3
* Volume inclination angle; volume number (required)
1600601 90.0,3
* Wall roughness; hydraulic diameter; volume number
* Here for stainless steel: k=0.015mm
1600801 1.5e-5,1.500000e-1,3
* tlpvbfe (see p.130 of Manual Appendix A); volume number
1601001 0,3
* jefvcahs (see p.132 of Manual Appendix A); junction number
1601101 0,2
* ebt (initial conditions options); P; T; 0; 0; 0; volume number
1601201 3,1.64e5,873.0,0.,0.,0.,3
* Junction initial conditions control option
* 0 for velocities, 1 for mass flow rates
1601300 1
* Initial liquid velocity; initial gas velocity;
* Interface velocity (enter 0.0); junction number
1601301 9.77,9.77,0.,2
*
* DHX shell side
```

```
* Component name; component type
1700000 dhxshell pipe
* Number of elements
1700001 14
* Volume flow area; volume number
1700101 2.224163e-1,14
* Volume length; volume number
1700301 0.17857143,14
* Volume inclination angle; volume number (required)
1700601 90.0,14
* Wall roughness; hydraulic diameter; volume number
* Here for stainless steel: k=0.015mm
1700801 1.5e-5,1.085449e-2,14
* tlpvbfe (see p.130 of Manual Appendix A); volume number
1701001 0,14
* jefvcahs (see p.132 of Manual Appendix A); junction number
1701101 0,13
* ebt (initial conditions options); P; T; 0; 0; 0; volume number
1701201 3,1.18e5,853.0,0.,0.,0.,14
* Junction initial conditions control option
* 0 for velocities, 1 for mass flow rates
1701300 1
* Initial liquid velocity; initial gas velocity;
* Interface velocity (enter 0.0); junction number
1701301 9.77,9.77,0.,13
*
* DHX to hot leg
* Component name; component type
1800000 dhxtohot pipe
* Number of elements
1800001 17
* Volume flow area; volume number
1800101 3.534292e-2,17
* Volume length; volume number
1800301 0.17694118,17
* Volume inclination angle; volume number (required)
1800601 9.76153245,17
* Wall roughness; hydraulic diameter; volume number
* Here for stainless steel: k=0.015mm
1800801 1.5e-5,1.500000e-1,17
* tlpvbfe (see p.130 of Manual Appendix A); volume number
1801001 0,17
* jefvcahs (see p.132 of Manual Appendix A); junction number
1801101 0,16
* ebt (initial conditions options); P; T; 0; 0; 0; volume number
1801201 3,1.08e5,833.0,0.,0.,0.,17
* Junction initial conditions control option
* 0 for velocities, 1 for mass flow rates
1801300 1
* Initial liquid velocity; initial gas velocity;
* Interface velocity (enter 0.0); junction number
1801301 9.77,9.77,0.,16
*
* DHX tube side
```

```
* Component name; component type
1900000 dhxtube pipe
* Number of elements
1900001 14
* Volume flow area; volume number
1900101 1.836403e-1,14
* Volume length; volume number
1900301 0.17857143,14
* Volume inclination angle; volume number (required)
1900601 90.0,14
* Wall roughness; hydraulic diameter; volume number
* Here for stainless steel: k=0.015mm
1900801 1.5e-5,1.090000e-2,14
* tlpvbfe (see p.130 of Manual Appendix A); volume number
1901001 0,14
* jefvcahs (see p.132 of Manual Appendix A); junction number
1901101 0,13
* ebt (initial conditions options); P; T; 0; 0; 0; volume number
1901201 3,1.64e5,839.0,0.,0.,0.,14
* Junction initial conditions control option
* 0 for velocities, 1 for mass flow rates
1901300 1
* Initial liquid velocity; initial gas velocity;
* Interface velocity (enter 0.0); junction number
1901301 11.9,11.9,0.,13
*
* DRACS hot leg 1
* Component name; component type
2000000 dracsh1 pipe
* Number of elements
2000001 20
* Volume flow area; volume number
2000101 3.534292e-2,20
* Volume length; volume number
2000301 0.17250000,20
* Volume inclination angle; volume number (required)
2000601 90.0,20
* Wall roughness; hydraulic diameter; volume number
* Here for stainless steel: k=0.015mm
2000801 1.5e-5,1.500000e-1,20
* tlpvbfe (see p.130 of Manual Appendix A); volume number
2001001 0,20
* jefvcahs (see p.132 of Manual Appendix A); junction number
2001101 0,19
* ebt (initial conditions options); P; T; 0; 0; 0; volume number
2001201 3,1.00e5,881.0,0.,0.,0.,20
* Junction initial conditions control option
* 0 for velocities, 1 for mass flow rates
2001300 1
* Initial liquid velocity; initial gas velocity;
* Interface velocity (enter 0.0); junction number
2001301 11.9,11.9,0.,19
*
* DRACS hot leg 2
```

```
* Component name; component type
2100000 dracsh2 pipe
* Number of elements
2100001 21
* Volume flow area; volume number
2100101 3.534292e-2,21
* Volume length; volume number
2100301 0.17476190,21
* Volume inclination angle; volume number (required)
2100601 0.0,21
* Wall roughness; hydraulic diameter; volume number
* Here for stainless steel: k=0.015mm
2100801 1.5e-5,1.500000e-1,21
* tlpvbfe (see p.130 of Manual Appendix A); volume number
2101001 0,21
* jefvcahs (see p.132 of Manual Appendix A); junction number
2101101 0,20
* ebt (initial conditions options); P; T; 0; 0; 0; volume number
2101201 3,1.00e5,881.0,0.,0.,0.,21
* Junction initial conditions control option
* 0 for velocities, 1 for mass flow rates
2101300 1
* Initial liquid velocity; initial gas velocity;
* Interface velocity (enter 0.0); junction number
2101301 11.9,11.9,0.,20
*
* TCHX manifold
* Component name; component type
2200000 tchxman pipe
* Number of elements
2200001 15
* Volume flow area; volume number
2200101 3.534292e-2,15
* Volume length; volume number
2200301 0.17333333,15
* Volume inclination angle; volume number (required)
2200601 90.0,15
* Wall roughness; hydraulic diameter; volume number
* Here for stainless steel: k=0.015mm
2200801 1.5e-5,1.500000e-1,15
* tlpvbfe (see p.130 of Manual Appendix A); volume number
2201001 0,15
* jefvcahs (see p.132 of Manual Appendix A); junction number
2201101 0,14
* ebt (initial conditions options); P; T; 0; 0; 0; volume number
2201201 3,4.69e4,881.0,0.,0.,0.,15
* Junction initial conditions control option
* 0 for velocities, 1 for mass flow rates
2201300 1
* Initial liquid velocity; initial gas velocity;
* Interface velocity (enter 0.0); junction number
2201301 11.9,11.9,0.,14
*
* TCHX salt tube
```

```
* Component name; component type
2300000 tchxsalt pipe
* Number of elements
2300001 34
* Volume flow area; volume number
2300101 1.746822e-1,34
* Volume length; volume number
2300301 0.17647059,34
* Volume inclination angle; volume number (required)
2300601 -25.67928862,34
* Wall roughness; hydraulic diameter; volume number
* Here for stainless steel: k=0.015mm
2300801 1.5e-5,1.090000e-2,34
* tlpvbfe (see p.130 of Manual Appendix A); volume number
2301001 0,34
* jefvcahs (see p.132 of Manual Appendix A); junction number
2301101 0,33
* ebt (initial conditions options); P; T; 0; 0; 0; volume number
2301201 3,9.58e4,839.0,0.,0.,0.,34
* Junction initial conditions control option
* 0 for velocities, 1 for mass flow rates
2301300 1
* Initial liquid velocity; initial gas velocity;
* Interface velocity (enter 0.0); junction number
2301301 11.9,11.9,0.,33
*
* DRACS cold leg 1
* Component name; component type
2400000 dracsc1 pipe
* Number of elements
2400001 25
* Volume flow area; volume number
2400101 3.534292e-2,25
* Volume length; volume number
2400301 0.17720000,25
* Volume inclination angle; volume number (required)
2400601 0.0,25
* Wall roughness; hydraulic diameter; volume number
* Here for stainless steel: k=0.015mm
2400801 1.5e-5,1.500000e-1,25
* tlpvbfe (see p.130 of Manual Appendix A); volume number
2401001 0,25
* jefvcahs (see p.132 of Manual Appendix A); junction number
2401101 0,24
* ebt (initial conditions options); P; T; 0; 0; 0; volume number
2401201 3,9.57e4,799.0,0.,0.,0.,25
* Junction initial conditions control option
* 0 for velocities, 1 for mass flow rates
2401300 1
* Initial liquid velocity; initial gas velocity;
* Interface velocity (enter 0.0); junction number
2401301 11.9,11.9,0.,24
*
* DRACS cold leg 2
```

```
* Component name; component type
2500000 dracsc2 pipe
* Number of elements
2500001 34
* Volume flow area; volume number
2500101 3.534292e-2,34
* Volume length; volume number
2500301 0.17500000,34
* Volume inclination angle; volume number (required)
2500601 -90.0,34
* Wall roughness; hydraulic diameter; volume number
* Here for stainless steel: k=0.015mm
2500801 1.5e-5,1.500000e-1,34
* tlpvbfe (see p.130 of Manual Appendix A); volume number
2501001 0,34
* jefvcahs (see p.132 of Manual Appendix A); junction number
2501101 0,33
* ebt (initial conditions options); P; T; 0; 0; 0; volume number
2501201 3,2.10e5,799.0,0.,0.,0.,34
* Junction initial conditions control option
* 0 for velocities, 1 for mass flow rates
2501300 1
* Initial liquid velocity; initial gas velocity;
* Interface velocity (enter 0.0); junction number
2501301 11.9,11.9,0.,33
*
* Top branch
* Component name; component type
2600000 branch26 branch
* Number of junctions; control word (0: velocities, 1: mass flow rates)
2600001 3 1
* Volume flow area; volume length; volume of volume (calculated if 0.0)
* Azimuthal angle; vertical angle; elevation change; wall roughness
* Hydraulic diameter; tlpvbfe
2600101 2.642080e-1 0.500000 0. 0. 0. 0. 1.5e-5 5.800001e-1 0
* ebt (initial conditions options); P; T
2600200 3 1.08e5 973.0
* From; to; junction area; A_f; A_r; jefvcahs
2601101   40010000  260000000 2.512732e-1 0. 0. 0
2602101  180010000  260000000 3.534292e-2 0. 0. 100
2603101  260010000   50000000 2.642080e-1 0. 0. 100
* Initial liquid velocity; initial gas velocity;
* Interface velocity (enter 0.0)
2601201  1074.7 1074.7  0.
2602201    9.77   9.77 0.
2603201  1084.47 1084.47 0.
*
* Middle branch
* Component name; component type
2700000 branch27 branch
* Number of junctions; control word (0: velocities, 1: mass flow rates)
2700001 3 1
* Volume flow area; volume length; volume of volume (calculated if 0.0)
* Azimuthal angle; vertical angle; elevation change; wall roughness
```

```
* Hydraulic diameter; tlpvbfe
2700101 3.038791e-1 0.50000 0. 0. -90. -0.50000 1.5e-5 5.602840e-2 0
* ebt (initial conditions options); P; T
2700200 3 2.82e5 873.0
* From; to; junction area; A_f; A_r; jefvcahs
2701101  140010000  270000000 3.019068e-1 0. 0. 0
2702101  270010000  150000000 3.038791e-1 0. 0. 100
2703101  270010000  160000000 3.534292e-2 0. 0. 100
* Initial liquid velocity; initial gas velocity;
* Interface velocity (enter 0.0)
2701201  1084.47 1084.47 0.
2702201  1074.7  1074.7  0.
2703201    9.77    9.77 0.
*
* Bottom branch
* Component name; component type
2800000 branch28 branch
* Number of junctions; control word (0: velocities, 1: mass flow rates)
2800001 3 1
* Volume flow area; volume length; volume of volume (calculated if 0.0)
* Azimuthal angle; vertical angle; elevation change; wall roughness
* Hydraulic diameter; tlpvbfe
2800101 1.327511 0.200000 0. 0. 0. 0. 1.5e-5 3.000000e-2 0
* ebt (initial conditions options); P; T
2800200 3 3.65e5 873.0
* From; to; junction area; A_f; A_r; jefvcahs
2801101  150010000  280000000 3.038791e-1 0. 0. 100
2802101  280010000   10000000 1.327511    0. 0. 0
2803101  280010000   20000000 0.065       0. 0. 100
* Initial liquid velocity; initial gas velocity;
* Interface velocity (enter 0.0)
2801201  1074.7 1074.7 0.
2802201   977.   977.  0.
2803201    97.7   97.7 0.
*
* Primary Loop Expansion Tank
* Component name; component type
4010000 tank1 tmdpvol
* Volume flow area; volume length; volume volume (calculated if 0);
* Azimuthal angle; inclination angle; elevation change;
* Wall roughness (1e-9 times hydraulic diameter if 0);
* Hydraulic diameter (calculated if 0); tlpvbfe
4010101 1.0 1.0 0.0 0.0 90.0 1.0 0.0 0.0 0
* ebt
4010200 3
* Search variable (time); P; T
4010201 0.0 1.00e5 973.15
*
* Primary tank branch
* Component name; component type
5010000 tank1br branch
* Number of junctions; control word (0: velocities, 1: mass flow rates)
5010001 3 1
* Volume flow area; volume length; volume of volume (calculated if 0.0)
```

```
* Azimuthal angle; vertical angle; elevation change; wall roughness
* Hydraulic diameter; tlpvbfe
5010101 2.642080e-1 0.100000 0. 0. 0. 0. 1.5e-5 5.800001e-1 0
* ebt (initial conditions options); P; T
5010200 3 1.00e5 973.0
* From; to; junction area; A_f; A_r; jefvcahs
5011101   50010000  501000000 2.642080e-1 0. 0. 100
5012101  501010000   60000000 2.642080e-1 0. 0. 100
5013101  501010000  401000000 2.642080e-1 0. 0. 100
* Initial liquid velocity; initial gas velocity;
* Interface velocity (enter 0.0)
5011201  1084.47 1084.47 0.
5012201  1084.47 1084.47 0.
5013201    0.0    0.0  0.
*
* DRACS Loop Expansion Tank
* Component name; component type
4020000 tank2 tmdpvol
* Volume flow area; volume length; volume volume (calculated if 0);
* Azimuthal angle; inclination angle; elevation change;
* Wall roughness (1e-9 times hydraulic diameter if 0);
* Hydraulic diameter (calculated if 0); tlpvbfe
4020101 1.0 1.0 0.0 0.0 90.0 1.0 0.0 0.0 0
* ebt
4020200 3
* Search variable (time); P; T
4020201 0.0 1.00e5 881.15
*
* DRACS tank branch
* Component name; component type
5020000 tank2br branch
* Number of junctions; control word (0: velocities, 1: mass flow rates)
5020001 3 1
* Volume flow area; volume length; volume of volume (calculated if 0.0)
* Azimuthal angle; vertical angle; elevation change; wall roughness
* Hydraulic diameter; tlpvbfe
5020101 3.534292e-2 0.100000 0. 0. 0. 0. 1.5e-5 1.500000e-1 0
* ebt (initial conditions options); P; T
5020200 3 1.00e5 881.0
* From; to; junction area; A_f; A_r; jefvcahs
5021101  200010000  502000000 3.534292e-2 0. 0. 0
5022101  502010000  210000000 3.534292e-2 0. 0. 0
5023101  502010000  402000000 3.534292e-2 0. 0. 100
* Initial liquid velocity; initial gas velocity;
* Interface velocity (enter 0.0)
5021201  11.9 11.9 0.
5022201  11.9 11.9 0.
5023201   0.0  0.0 0.
*
* Junction 70-80
* Component name; component type
6010000 jn7080 sngljun
* From; to; junction area; A_f; A_r; jefvcahs
6010101 70010000 80000000 3.041000e-1 0. 0. 100
```

```
* Control word (0 for velocities, 1 for mass flow rates)
* Initial liquid velocity; initial gas velocity;
* Interface velocity (enter 0.0)
6010201 1 1084.47 1084.47 0.
*
* Junction 80-90
* Component name; component type
6020000 jn8090 sngljun
* From; to; junction area; A_f; A_r; jefvcahs
6020101 80010000 90000000 4.491779e-1 0. 0. 100
* Control word (0 for velocities, 1 for mass flow rates)
* Initial liquid velocity; initial gas velocity;
* Interface velocity (enter 0.0)
6020201 1 1084.47 1084.47 0.
*
* Junction 90-100
* Component name; component type
6030000 jn90100 sngljun
* From; to; junction area; A_f; A_r; jefvcahs
6030101 90010000 100000000 1.924226e-1 0. 0. 100
* Control word (0 for velocities, 1 for mass flow rates)
* Initial liquid velocity; initial gas velocity;
* Interface velocity (enter 0.0)
6030201 1 1084.47 1084.47 0.
*
* Junction 100-110
* Component name; component type
6040000 jn100110 sngljun
* From; to; junction area; A_f; A_r; jefvcahs
6040101 100010000 110000000 1.924226e-1 0. 0. 100
* Control word (0 for velocities, 1 for mass flow rates)
* Initial liquid velocity; initial gas velocity;
* Interface velocity (enter 0.0)
6040201 1 1084.47 1084.47 0.
*
* Junction 110-120
* Component name; component type
6050000 jn110120 sngljun
* From; to; junction area; A_f; A_r; jefvcahs
6050101 110010000 120000000 3.019068e-1 0. 0. 0
* Control word (0 for velocities, 1 for mass flow rates)
* Initial liquid velocity; initial gas velocity;
* Interface velocity (enter 0.0)
6050201 1 1084.47 1084.47 0.
*
* Junction 120-130
* Component name; component type
6060000 jn120130 sngljun
* From; to; junction area; A_f; A_r; jefvcahs
6060101 120010000 130000000 3.019068e-1 0. 0. 0
* Control word (0 for velocities, 1 for mass flow rates)
* Initial liquid velocity; initial gas velocity;
* Interface velocity (enter 0.0)
6060201 1 1084.47 1084.47 0.
```

```
*
* Junction 130-140
* Component name; component type
6070000 jn130140 sngljun
* From; to; junction area; A_f; A_r; jefvcahs
6070101 130010000 140000000 3.019068e-1 0. 0. 0
* Control word (0 for velocities, 1 for mass flow rates)
* Initial liquid velocity; initial gas velocity;
* Interface velocity (enter 0.0)
6070201 1 1084.47 1084.47 0.
*
* Junction 160-170
* Component name; component type
6080000 diode sngljun
* From; to; junction area; A_f; A_r; jefvcahs
6080101 160010000 170000000 3.534292e-2 50. 1. 0
* Control word (0 for velocities, 1 for mass flow rates)
* Initial liquid velocity; initial gas velocity;
* Interface velocity (enter 0.0)
6080201 1 9.77 9.77 0.
*
* Junction 170-180
* Component name; component type
6090000 jn170180 sngljun
* From; to; junction area; A_f; A_r; jefvcahs
6090101 170010000 180000000 3.534292e-2 100. 100. 100
* Control word (0 for velocities, 1 for mass flow rates)
* Initial liquid velocity; initial gas velocity;
* Interface velocity (enter 0.0)
6090201 1 9.77 9.77 0.
*
* Junction 190-200
* Component name; component type
6100000 jn190200 sngljun
* From; to; junction area; A_f; A_r; jefvcahs
6100101 190010000 200000000 3.534292e-2 50. 50. 100
* Control word (0 for velocities, 1 for mass flow rates)
* Initial liquid velocity; initial gas velocity;
* Interface velocity (enter 0.0)
6100201 1 11.9 11.9 0.
*
* Junction 210-220
* Component name; component type
6110000 jn210220 sngljun
* From; to; junction area; A_f; A_r; jefvcahs
6110101 210010000 220000000 3.534292e-2 0. 0. 0
* Control word (0 for velocities, 1 for mass flow rates)
* Initial liquid velocity; initial gas velocity;
* Interface velocity (enter 0.0)
6110201 1 11.9 11.9 0.
*
* Junction 220-230
* Component name; component type
6120000 jn220230 sngljun
```

```
* From; to; junction area; A_f; A_r; jefvcahs
6120101 220010000 230000000 3.534292e-2 0. 0. 100
* Control word (0 for velocities, 1 for mass flow rates)
* Initial liquid velocity; initial gas velocity;
* Interface velocity (enter 0.0)
6120201 1 11.9 11.9 0.
*
* Junction 230-240
* Component name; component type
6130000 jn230240 sngljun
* From; to; junction area; A_f; A_r; jefvcahs
6130101 230010000 240000000 3.534292e-2 0. 0. 100
* Control word (0 for velocities, 1 for mass flow rates)
* Initial liquid velocity; initial gas velocity;
* Interface velocity (enter 0.0)
6130201 1 11.9 11.9 0.
*
* Junction 240-250
* Component name; component type
6140000 jn240250 sngljun
* From; to; junction area; A_f; A_r; jefvcahs
6140101 240010000 250000000 3.534292e-2 0. 0. 0
* Control word (0 for velocities, 1 for mass flow rates)
* Initial liquid velocity; initial gas velocity;
* Interface velocity (enter 0.0)
6140201 1 11.9 11.9 0.
*
* Junction 250-190
* Component name; component type
6150000 jn250190 sngljun
* From; to; junction area; A_f; A_r; jefvcahs
6150101 250010000 190000000 3.534292e-2 0. 0. 100
* Control word (0 for velocities, 1 for mass flow rates)
* Initial liquid velocity; initial gas velocity;
* Interface velocity (enter 0.0)
6150201 1 11.9 11.9 0.
*
* Primary pump
* Component name; component type
7010000 pripump tmdpjun
* From; to; junction area; jefvcahs
7010101 60010000 70000000 3.041000e-1 0
* Control word (0 for velocities, 1 for mass flow rates)
7010200 1
* Time; Liquid velocity; Gas velocity; Interface velocity (enter 0.0)
7010201 0.00000 1084.47 0. 0.
7010202 1000.0  1084.47 0. 0.
7010203 1004.5  542.24  0. 0.
7010204 1009.0  271.12  0. 0.
7010205 1013.5  135.56  0. 0.
7010206 1018.0  67.78   0. 0.
7010207 1022.5  33.89   0. 0.
7010208 1027.0  16.94   0. 0.
7010209 1031.5  8.47    0. 0.
```

```
7010210 1036.0  4.24    0. 0.
7010211 1040.5  2.12    0. 0.
7010212 1045.0  1.06    0. 0.
7010213 1049.5  0.53    0. 0.
7010214 1054.0  0.26    0. 0.
7010215 1058.5  0.13    0. 0.
7010216 1063.0  0.07    0. 0.
7010217 1067.5  0.03    0. 0.
7010218 1072.0  0.02    0. 0.
7010219 1076.5  0.01    0. 0.
7010220 1081.0  0.00    0. 0.
7010220 10000.  0.00    0. 0.
*
************************************************************
* Heat structures
************************************************************
*
* Active core
* Number of axial heat structures; number of radial mesh points;
* Geometry type (3: spherical, coupled to hydrodynamic component);
* Steady-state initialization flag (1: initial T calculated by code);
* Left boundary coordinate; reflood condition
10101000 26 13 3 1 0.0 0
* Mesh location flag; mesh format flag (see p.252 of Manual Appendix A)
10101100 0 1
* Number of intervals; right coordinate
10101101 5 0.0125
10101102 5 0.0140
10101103 2 0.0150
* Composition (table number); interval number
10101201  101 5
10101202  102 10
10101203  101 12
* Power input proportion; mesh interval number
10101301 0.0 5
10101302 1.0 10
10101303 0.0 12
* Initial temperature; mesh point number
10101401 1000.0  13
* Left boundary condition definition (0: adiabatic); increment;
* Boundary condition type (0: adiabatic); surface area code (1: number of spheres);
* Number of spheres; heat structure number
10101501 0 0 0 1 24824.4 26
* Right boundary condition, see above (111: vertical bundle with cross flow, used as approximation)
10101601 10010000 10000 111 1 24824.4 26
* Power source (table number); internal source multiplier; direct mod heatin mult (left)
* Direct mod heatin mult (right); heat structure number
10101701 10 0.003614854 0.0 0.0 1
10101702 10 0.010187315 0.0 0.0 2
10101703 10 0.016102530 0.0 0.0 3
10101704 10 0.022674992 0.0 0.0 4
10101705 10 0.029576076 0.0 0.0 5
10101706 10 0.034834045 0.0 0.0 6
10101707 10 0.037791653 0.0 0.0 7
```

```
10101708 10 0.038777522 0.0 0.0 8
10101709 10 0.039106145 0.0 0.0 9
10101710 10 0.039106145 0.0 0.0 10
10101711 10 0.040420638 0.0 0.0 11
10101712 10 0.043706868 0.0 0.0 12
10101713 10 0.046335853 0.0 0.0 13
10101714 10 0.046993099 0.0 0.0 14
10101715 10 0.047321722 0.0 0.0 15
10101716 10 0.048307591 0.0 0.0 16
10101717 10 0.047650345 0.0 0.0 17
10101718 10 0.046007230 0.0 0.0 18
10101719 10 0.043378245 0.0 0.0 19
10101720 10 0.040420638 0.0 0.0 20
10101721 10 0.041735130 0.0 0.0 21
10101722 10 0.043049622 0.0 0.0 22
10101723 10 0.045678607 0.0 0.0 23
10101724 10 0.048636214 0.0 0.0 24
10101725 10 0.051922445 0.0 0.0 25
10101726 10 0.046664476 0.0 0.0 26
* Additional right boundary: heat transfer hydraulic diameter; heated length fwd (10.: ignore);
* Heated length rev (10.: ignore); grid spacer length fwd (0.: ignore); grid spacer length rev (0.: ignore);
* Grid loss coef fwd (0.: ignore); grid loss coef rev (0.: ignore); boiling factor (1.: subcooled liquid);
* Heat structure number
10101901 3.00e-2 10.0 10.0 0.0 0.0 0.0 0.0 1.0 26
*
* CTAH
* Number of axial heat structures; number of radial mesh points;
* Geometry type (2: cylindrical, coupled to hydrodynamic component);
* Steady-state initialization flag (1: initial T calculated by code);
* Left boundary coordinate; reflood condition
10901000 99 4 2 1 2.286e-3 0
* Mesh location flag; mesh format flag (see p.252 of Manual Appendix A)
10901100 0 2
* Mesh interval distance; interval number
10901101 2.2225e-4 3
* Composition (table number); interval number
10901201 100 3
* Power input proportion; mesh interval number
10901301 1.0 3
* Initial temperature; mesh point number
10901401 923.0  4
* Left boundary condition definition (here: vol number); increment;
* Boundary condition type (3060: HTC set in general table 60); surface area code (1: length);
* Length; heat structure number
10901501 90010000 10000 3060 1 5104.44 99
* Right boundary condition, see above (-40: T defined in general table 40; 1000: T set in Word 1)
10901601 -40 0 1000 1 5104.44 99
* Power source (table number); internal source multiplier; direct mod heatin mult (left)
* Direct mod heatin mult (right); heat structure number
10901701 0 0.0 0.0 0.0 99
* Additional left boundary: heat transfer hydraulic diameter; heated length fwd (10.: ignore);
* Heated length rev (10.: ignore); grid spacer length fwd (0.: ignore); grid spacer length rev (0.: ignore);
* Grid loss coef fwd (0.: ignore); grid loss coef rev (0.: ignore); boiling factor (1.: subcooled liquid);
* Heat structure number
```

```
10901801 0.0 10.0 10.0 0.0 0.0 0.0 0.0 1.0 99
*
* DHX tubes
* Number of axial heat structures; number of radial mesh points;
* Geometry type (2: cylindrical, coupled to hydrodynamic component);
* Steady-state initialization flag (1: initial T calculated by code);
* Left boundary coordinate; reflood condition
11901000 14 4 2 1 5.450e-3 0
* Mesh location flag; mesh format flag (see p.252 of Manual Appendix A)
11901100 0 2
* Mesh interval distance; interval number
11901101 2.2500e-4 3
* Composition (table number); interval number
11901201 100 3
* Power input proportion; mesh interval number
11901301 1.0 3
* Initial temperature; mesh point number
11901401 844.0  4
* Left boundary condition definition (here: vol number); increment;
* Boundary condition type (101: convection); surface area code (1: length);
* Length; heat structure number
11901501 190010000 10000 101 1 351.43 14
* Right boundary condition, see above
11901601 170010000 10000 101 1 351.43 14
* Power source (table number); internal source multiplier; direct mod heatin mult (left)
* Direct mod heatin mult (right); heat structure number
11901701 0 0.0 0.0 0.0 14
* Additional left boundary: heat transfer hydraulic diameter; heated length fwd (10.: ignore);
* Heated length rev (10.: ignore); grid spacer length fwd (0.: ignore); grid spacer length rev (0.: ignore);
* Grid loss coef fwd (0.: ignore); grid loss coef rev (0.: ignore); boiling factor (1.: subcooled liquid);
* Heat structure number
11901801 0.0 10.0 10.0 0.0 0.0 0.0 0.0 1.0 14
* Additional right boundary: heat transfer hydraulic diameter; heated length fwd (10.: ignore);
* Heated length rev (10.: ignore); grid spacer length fwd (0.: ignore); grid spacer length rev (0.: ignore);
* Grid loss coef fwd (0.: ignore); grid loss coef rev (0.: ignore); boiling factor (1.: subcooled liquid);
* Heat structure number
11901901 1.13e-2 10.0 10.0 0.0 0.0 0.0 0.0 1.0 14
*
* TCHX
* Number of axial heat structures; number of radial mesh points;
* Geometry type (2: cylindrical, coupled to hydrodynamic component);
* Steady-state initialization flag (1: initial T calculated by code);
* Left boundary coordinate; reflood condition
12301000 34 4 2 1 5.450e-3 0
* Mesh location flag; mesh format flag (see p.252 of Manual Appendix A)
12301100 0 2
* Mesh interval distance; interval number
12301101 2.2500e-4 3
* Composition (table number); interval number
12301201 100 3
* Power input proportion; mesh interval number
12301301 1.0 3
* Initial temperature; mesh point number
12301401 844.0  4
```

```
* Left boundary condition definition (here: vol number); increment;
* Boundary condition type (3070: HTC set in general table 70); surface area code (1: length);
* Length; heat structure number
12301501 230010000 10000 3070 1 330.35 34
* Right boundary condition, see above (-50: T defined in general table 50; 1000: T set in Word 1)
12301601 -50 0 1000 1 330.35 34
* Power source (table number); internal source multiplier; direct mod heatin mult (left)
* Direct mod heatin mult (right); heat structure number
12301701 0 0.0 0.0 0.0 34
* Additional left boundary: heat transfer hydraulic diameter; heated length fwd (10.: ignore);
* Heated length rev (10.: ignore); grid spacer length fwd (0.: ignore); grid spacer length rev (0.: ignore);
* Grid loss coef fwd (0.: ignore); grid loss coef rev (0.: ignore); boiling factor (1.: subcooled liquid);
* Heat structure number
12301801 0.0 10.0 10.0 0.0 0.0 0.0 0.0 1.0 34
*
*******************************************************
*  Material properties
*******************************************************
*
* Stainless steel
* Material type (user supplied table); thermal conductivity format flag;
* Volumetric heat capacity format flag (see p.227 of Manual Appendix A)
20110000  tbl/fctn  1  1
* Stainless steel thermal conductivity (T; k)
20110001   250.0   40.00
20110002  3000.0   40.00
* Stainless steel volumetric heat capacity (T; rho*cp)
20110051   250.0  3.50e6
20110052  3000.0  3.50e6
*
* H-451 graphite
* Material type (user supplied table); thermal conductivity format flag;
* Volumetric heat capacity format flag (see p.227 of Manual Appendix A)
20110100  tbl/fctn  1  1
* Stainless steel thermal conductivity (T; k)
20110101   250.0   80.00
20110102  3000.0   80.00
* Stainless steel volumetric heat capacity (T; rho*cp)
20110151   250.0  3.00e6
20110152  3000.0  3.00e6
*
* Graphite fuel
* Material type (user supplied table); thermal conductivity format flag;
* Volumetric heat capacity format flag (see p.227 of Manual Appendix A)
20110200  tbl/fctn  1  1
* Stainless steel thermal conductivity (T; k)
20110201   250.0   15.00
20110202  3000.0   15.00
* Stainless steel volumetric heat capacity (T; rho*cp)
20110251   250.0  3.00e6
20110252  3000.0  3.00e6
*
*******************************************************
*  General tables
```

```
*******************************************************
*
* Core power (from decay heat curve)
* Table type
20201000  power
* Time; power [W]
20201001 0.      2.36e8
20201002 1000.   2.36e8
20201003 1.001e3 1.25e7
20201004 1.002e3 1.20e7
20201005 1.004e3 1.13e7
20201006 1.008e3 1.04e7
20201007 1.016e3 9.51e6
20201008 1.024e3 8.93e6
20201009 1.032e3 8.51e6
20201010 1.040e3 8.19e6
20201011 1.048e3 7.92e6
20201012 1.060e3 7.59e6
20201013 1.120e3 6.59e6
20201014 1.240e3 5.72e6
20201015 1.480e3 4.96e6
20201016 1.960e3 4.23e6
20201017 2.440e3 3.80e6
20201018 2.920e3 3.49e6
20201019 3.400e3 3.25e6
20201020 3.880e3 3.07e6
20201021 4.360e3 2.92e6
20201022 4.600e3 2.85e6
20201023 1.320e4 1.92e6
*
* CTAH outlet temperature
* Table type
20204000  temp
* Time; temperature [K]
20204001  0.00000  873.15
20204002  10000.0  873.15
*
* TCHX outlet temperature
* Table type
20205000  temp
* Time; temperature [K]
20205001  0.00000  799.15
20205002  10000.0  799.15
*
* CTAH heat transfer coefficient
* Table type
20206000  htc-t
* Time; heat transfer coefficient [W/m^2-K]
20206001  0.00000  2000.
20206002  10000.0  2000.
*
* TCHX heat transfer coefficient
* Table type
20207000  htc-t
```

```
* Time; heat transfer coefficient [W/m^2-K]
20207001  0.00000  1000.
20207002  10000.0  1000.
* End of input
.
```

Appendix C Mathematical Description of aPC and Implementation through a Generic Example

This Appendix presents a summary of the mathematical description of aPC underlying the implementation algorithm of Figure 3-8, and provides a simple, generic example using a 2nd order polynomial expansion for a model with two input parameters, which can be generalized to higher-order, larger-dimension cases.

C.1 Mathematical Description of aPC

This Section provides a mathematical description of the aPC framework developed in Section 3.2.

C.1.1 Polynomial Chaos Expansion

Let $\omega = \{\omega_1, \dots, \omega_N\}$ represent the vector of N input parameters for some model $\Omega = f(\omega)$. To perform passive system reliability assessment, sensitivity analysis and uncertainty quantification, we wish to investigate the influence of all parameters ω on the model output Ω.

The aPC method consists in approximating the model response by a truncated polynomial expansion, using polynomials $\Psi_k(\omega)$:

$$\Omega(\omega) \approx \sum_{k=1}^{M} c_k \Psi_k(\omega) \tag{C-1}$$

where the number M of polynomials depends on the total number N of analyzed input parameters and the order d of the polynomial representation, according to the combinatoric formula [1]:

$$M = \frac{(N+d)!}{N!d!} \tag{C-2}$$

The coefficients c_k in Eq. (3-7) quantify the dependence of the model output Ω on the input parameters ω. The symbol Ψ_k is a simplified notation of the multivariate orthonormal polynomial basis for ω including all cross-terms between different parameters, as explained below.

---

[1] For a 2nd order polynomial expansion ($d = 2$), the number of polynomials in the expansion, and therefore the number of parameter sets at which the original model must be run (see Section C.1.3), is on the order of $N^2/2$, while for a 3rd order polynomial expansion ($d = 3$), it is on the order of $N^3/6$. For a large number of input parameters ($N > 100$), to remain within an acceptable computation time range, this limits the analysis to a 2nd order expansion.

C.1.2 Construction of the Orthonormal Polynomial Basis

Let us define the set of polynomials $\left\{P_j^{(0)}, \dots, P_j^{(d)}\right\}$ of degree d for the parameters ω_j as an orthonormal basis in the parameter space. The polynomial $P_j^{(k)}(\omega_j)$ of degree k in an individual parameter ω_j can be written as a simple linear combination of the different powers i of ω_j:

$$P_j^{(k)}(\omega_j) = \sum_{i=0}^{k} p_{i,j}^{(k)} \omega_j^i, \;\; k = 0 \dots d, \;\; j = 1 \dots N \tag{C-3}$$

Here $p_{i,j}^{(k)}$ are the coefficients within the polynomial $P_j^{(k)}(\omega_j)$. Assuming that the input parameters within ω are independent, the multi-dimensional basis can be constructed as a simple product of the corresponding univariate polynomials:

$$\Psi_k(\omega) = \prod_{j=1}^{N} P_j^{\left(\alpha_j^k\right)}(\omega_j), \;\; \sum_{j=1}^{N} \alpha_j^k \le d, \;\; k = 1 \dots M \tag{C-4}$$

where α_j^k is a multivariate index that contains the combinatoric information on how to enumerate all possible products of individual univariate basis functions. In other words, the index α can be seen as a $M \times N$ matrix that contains the corresponding degree for parameter number j in expansion term k.

We can now show how to construct the data-driven orthogonal polynomial basis for each individual component ω_j from vector ω. The coefficients $p_{i,j}^{(k)}$ in Eq. (C-3) must be constructed in such a way that the polynomials in Eq. (C-3) form a basis that is orthonormal in the given input distribution of model parameter ω_j.

As mentioned before, an orthogonal polynomial basis up to order d can be constructively defined for any arbitrary probability measure, given that ω_j has finite statistical moments up to order $2d-1$. The unknown polynomial coefficients $p_{i,j}^{(k)}$ can be defined through the following linear equation:

$$\begin{bmatrix} \mu_{0,j} & \mu_{1,j} & \dots & \mu_{k,j} \\ \mu_{1,j} & \mu_{2,j} & \dots & \mu_{k+1,j} \\ \dots & \dots & \dots & \dots \\ \mu_{k-1,j} & \mu_{k,j} & \dots & \mu_{2k-1,j} \\ 0 & 0 & \dots & 1 \end{bmatrix} \begin{bmatrix} p_{0,j}^{(k)} \\ p_{1,j}^{(k)} \\ \dots \\ p_{k-1,j}^{(k)} \\ p_{k,j}^{(k)} \end{bmatrix} = \begin{bmatrix} 0 \\ 0 \\ \dots \\ 0 \\ 1 \end{bmatrix} \tag{C-5}$$

Here, $\mu_{i,j}$ are the i^{th} non-central (raw) statistical moments for random variable ω_j:

$$\mu_{i,j} = E\left(\omega_j^i\right) \tag{C-6}$$

It becomes evident from Eq. (C-5) that these statistical moments are the only required form of information on the input distributions.

The above orthogonal polynomial basis can be used directly for analysis. However, a normalized basis has further useful properties. For example, the mean and variance of $\Omega(\omega)$, according to Eq. (3-7), are given by simple analytical relations, by virtue of the orthonormality property:

$$mean(\Omega) = c_1, \;\; Var(\Omega) = \sum_{k=2}^{M} c_k^2 \tag{C-7}$$

In the space of events Λ with probability measure Γ, $\hat{P}_j^{(k)}(\omega_j)$ is an orthonormal basis if:

$$\int_{\omega_j \in \Lambda} \hat{P}_j^{(k)}(\omega_j)\hat{P}_j^{(l)}(\omega_j) d\Gamma(\omega_j) = \delta_{kl} \quad \forall k, l = \overline{0, d} \tag{C-8}$$

The orthonormal polynomial basis can be obtained as:

$$\hat{P}_j^{(k)}(\omega_j) = \frac{P_j^{(k)}}{\left\| P_j^{(k)} \right\|}, \;\; \left\| P_j^{(k)} \right\|^2 = \int_{\omega_j \in \Lambda} \left[P_j^{(k)}(\omega_j) \right]^2 d\Gamma(\omega_j) \tag{C-9}$$

Because the square of a polynomial of order k yields a polynomial of order $2k$, normalization according to Eq. (C-9) requires the statistical moments of ω up to order $2d$. Using the definition of the i^{th} raw moment of the random variable ω_j: $\mu_{i,j} = \int_{\omega_j \in \Lambda} \omega_j^i d\Gamma(\omega_j)$, it can be proven that:

$$\left\| P_j^{(k)} \right\|^2 = \sum_{l=0}^{k} \sum_{m=0}^{k} p_{l,j}^{(k)} p_{m,j}^{(k)} \mu_{(l+m),j} \tag{C-10}$$

C.1.3 Determination of the Coefficients

The remaining task is to evaluate the coefficients c_k in Eq. (3-7). We use the non-intrusive probabilistic collocation method (PCM), which only requires knowledge on how to obtain the model output for a given set of input parameters, thus treating the model Ω like a "black-box". The idea of PCM is to evaluate the model exactly M times, which allows to directly fit the polynomial representation of Ω with its M unknown coefficients c_k to the obtained M model results. The M model evaluations are performed with M different parameter sets $\left\{\omega_1^{(i)}, \dots, \omega_N^{(i)}\right\}, i = 1, \dots, M$, or *collocation points*.

This leads to the following system of linear equations:

$$M_\Psi(\omega) V_c = V_\Omega(\omega) \tag{C-11}$$

where V_c is the $M \times 1$ vector of unknown coefficients c_k in Eq. (3-7), the $M \times 1$ vector V_Ω contains the model output for each collocation point, and the $M \times M$ matrix M_Ψ contains the polynomials evaluated at the collocation points:

$$\begin{cases} M_\Psi = \left\{ \Psi_k \left(\omega_1^{(i)}, \dots, \omega_N^{(i)} \right) \right\}, \;\; i = 1 \dots M, k = 1 \dots M \\ V_\Omega = \left\{ \Omega(\omega_1^{(i)}, \dots, \omega_N^{(i)}) \right\}, \;\; i = 1 \dots M \\ V_c = \{c_k\}, \;\; k = 1 \dots M \end{cases} \tag{C-12}$$

The solution V_c of Eq. (C-11) depends on the selection of collocation points. According to the literature, the optimal choice of collocation points corresponds to the roots of the polynomial of one degree higher $(d+1)$ than the order used in the chaos expansion (d) [86]. For multi-parameter analysis, the number of available points is therefore $(d+1)^N$, which is usually larger than the necessary number M of collocation points. In that case, a smart choice of a sparse subset of the tensor grid, from the most probable regions of the input parameters distribution, becomes necessary.

C.2 Implementation of aPC through a Generic Example

In this Section, we develop a step-by-step algorithm to implement aPC for practical studies such as passive system reliability assessment. For demonstration purposes, here we limit ourselves to a 2nd order polynomial expansion $(d=2)$ and only 2 input parameters ω_1, ω_2 $(N=2)$, although typical passive system reliability assessment studies would include many more input parameters.

1. From Eq. (C-2), the number of polynomials in the expansion is:

$$M = \frac{(2+2)!}{2!\,2!} = 6$$

and the aPC can be written as:

$$\Omega(\omega_1, \omega_2) \approx \sum_{k=1}^{6} c_k \, \Psi_k(\omega_1, \omega_2)$$

2. From Eq. (C-5), the unknown polynomial coefficients $p_{i,j}^{(k)}$ can be defined through:

$$p_{0,1}^{(0)} = p_{0,2}^{(0)} = 1$$

$$\begin{bmatrix} p_{0,1}^{(1)} \\ p_{1,1}^{(1)} \end{bmatrix} = \begin{bmatrix} \mu_{0,1} & \mu_{1,1} \\ 0 & 1 \end{bmatrix}^{-1} \begin{bmatrix} 0 \\ 1 \end{bmatrix}$$

$$\begin{bmatrix} p_{0,2}^{(1)} \\ p_{1,2}^{(1)} \end{bmatrix} = \begin{bmatrix} \mu_{0,2} & \mu_{1,2} \\ 0 & 1 \end{bmatrix}^{-1} \begin{bmatrix} 0 \\ 1 \end{bmatrix}$$

$$\begin{bmatrix} p_{0,1}^{(2)} \\ p_{1,1}^{(2)} \\ p_{2,1}^{(2)} \end{bmatrix} = \begin{bmatrix} \mu_{0,1} & \mu_{1,1} & \mu_{2,1} \\ \mu_{1,1} & \mu_{2,1} & \mu_{3,1} \\ 0 & 0 & 1 \end{bmatrix}^{-1} \begin{bmatrix} 0 \\ 0 \\ 1 \end{bmatrix}$$

$$\begin{bmatrix} p_{0,2}^{(2)} \\ p_{1,2}^{(2)} \\ p_{2,2}^{(2)} \end{bmatrix} = \begin{bmatrix} \mu_{0,2} & \mu_{1,2} & \mu_{2,2} \\ \mu_{1,2} & \mu_{2,2} & \mu_{3,2} \\ 0 & 0 & 1 \end{bmatrix}^{-1} \begin{bmatrix} 0 \\ 0 \\ 1 \end{bmatrix}$$

$$\begin{bmatrix} p_{0,1}^{(3)} \\ p_{1,1}^{(3)} \\ p_{2,1}^{(3)} \\ p_{3,1}^{(3)} \end{bmatrix} = \begin{bmatrix} \mu_{0,1} & \mu_{1,1} & \mu_{2,1} & \mu_{3,1} \\ \mu_{1,1} & \mu_{2,1} & \mu_{3,1} & \mu_{4,1} \\ \mu_{2,1} & \mu_{3,1} & \mu_{4,1} & \mu_{5,1} \\ 0 & 0 & 0 & 1 \end{bmatrix}^{-1} \begin{bmatrix} 0 \\ 0 \\ 0 \\ 1 \end{bmatrix}$$

$$\begin{bmatrix} p_{0,2}^{(3)} \\ p_{1,2}^{(3)} \\ p_{2,2}^{(3)} \\ p_{3,2}^{(3)} \end{bmatrix} = \begin{bmatrix} \mu_{0,2} & \mu_{1,2} & \mu_{2,2} & \mu_{3,2} \\ \mu_{1,2} & \mu_{2,2} & \mu_{3,2} & \mu_{4,2} \\ \mu_{2,2} & \mu_{3,2} & \mu_{4,2} & \mu_{5,2} \\ 0 & 0 & 0 & 1 \end{bmatrix}^{-1} \begin{bmatrix} 0 \\ 0 \\ 0 \\ 1 \end{bmatrix}$$

3. From Eq. (C-3), the univariate polynomial bases $P_1^{(k)}(\omega_1)$ and $P_2^{(k)}(\omega_2)$ can be written as linear combinations of the different powers of ω_1 and ω_2 ($P_1^{(3)}(\omega_1)$ and $P_2^{(3)}(\omega_2)$ will be used to determine the optimal collocation points):

$$P_1^{(0)}(\omega_1) = p_{0,1}^{(0)}$$

$$P_1^{(1)}(\omega_1) = p_{0,1}^{(1)} + p_{1,1}^{(1)}\omega_1$$

$$P_1^{(2)}(\omega_1) = p_{0,1}^{(2)} + p_{1,1}^{(2)}\omega_1 + p_{2,1}^{(2)}\omega_1^2$$

$$P_1^{(3)}(\omega_1) = p_{0,1}^{(3)} + p_{1,1}^{(3)}\omega_1 + p_{2,1}^{(3)}\omega_1^2 + p_{3,1}^{(3)}\omega_1^3$$

$$P_2^{(0)}(\omega_2) = p_{0,2}^{(0)}$$

$$P_2^{(1)}(\omega_2) = p_{0,2}^{(1)} + p_{1,2}^{(1)}\omega_2$$

$$P_2^{(2)}(\omega_2) = p_{0,2}^{(2)} + p_{1,2}^{(2)}\omega_2 + p_{2,2}^{(2)}\omega_2^2$$

$$P_2^{(3)}(\omega_2) = p_{0,2}^{(3)} + p_{1,2}^{(3)}\omega_2 + p_{2,2}^{(3)}\omega_2^2 + p_{3,2}^{(3)}\omega_2^3$$

4. From Eqs. (C-9) and (C-10), the orthonormal polynomial basis $\hat{P}_j^{(k)}(\omega_j)$ can be obtained from the previously built orthogonal basis $P_j^{(k)}(\omega_j)$, using the statistical moments of ω up to order 4 to calculate each polynomial's norm:

$$\left\| P_1^{(0)} \right\|^2 = \left\| P_2^{(0)} \right\|^2 = 1$$

$$\left\|P_1^{(1)}\right\|^2 = {p_{0,1}^{(1)}}^2 \mu_{0,1} + 2p_{0,1}^{(1)} p_{1,1}^{(1)} \mu_{1,1} + {p_{1,1}^{(1)}}^2 \mu_{2,1}$$

$$\left\|P_2^{(1)}\right\|^2 = {p_{0,2}^{(1)}}^2 \mu_{0,2} + 2p_{0,2}^{(1)} p_{1,2}^{(1)} \mu_{1,2} + {p_{1,2}^{(1)}}^2 \mu_{2,2}$$

$$\left\|P_1^{(2)}\right\|^2 = {p_{0,1}^{(2)}}^2 \mu_{0,1} + 2p_{0,1}^{(2)} p_{1,1}^{(2)} \mu_{1,1} + \left({p_{1,1}^{(2)}}^2 + 2p_{0,1}^{(2)} p_{2,1}^{(2)}\right) \mu_{2,1} + 2p_{1,1}^{(2)} p_{2,1}^{(2)} \mu_{3,1} + {p_{2,1}^{(2)}}^2 \mu_{4,1}$$

$$\left\|P_2^{(2)}\right\|^2 = {p_{0,2}^{(2)}}^2 \mu_{0,2} + 2p_{0,2}^{(2)} p_{1,2}^{(2)} \mu_{1,2} + \left({p_{1,2}^{(2)}}^2 + 2p_{0,2}^{(2)} p_{2,2}^{(2)}\right) \mu_{2,2} + 2p_{1,2}^{(2)} p_{2,2}^{(2)} \mu_{3,2} + {p_{2,2}^{(2)}}^2 \mu_{4,2}$$

5. From Eq. (C-4), the multivariate polynomial basis $\Psi_k(\omega_1, \omega_2)$ can be expanded in terms of univariate polynomials:

$$\Psi_1(\omega_1, \omega_2) = \hat{P}_1^{(0)}(\omega_1) \cdot \hat{P}_2^{(0)}(\omega_2)$$

$$\Psi_2(\omega_1, \omega_2) = \hat{P}_1^{(0)}(\omega_1) \cdot \hat{P}_2^{(1)}(\omega_2)$$

$$\Psi_3(\omega_1, \omega_2) = \hat{P}_1^{(1)}(\omega_1) \cdot \hat{P}_2^{(0)}(\omega_2)$$

$$\Psi_4(\omega_1, \omega_2) = \hat{P}_1^{(1)}(\omega_1) \cdot \hat{P}_2^{(1)}(\omega_2)$$

$$\Psi_5(\omega_1, \omega_2) = \hat{P}_1^{(0)}(\omega_1) \cdot \hat{P}_2^{(2)}(\omega_2)$$

$$\Psi_6(\omega_1, \omega_2) = \hat{P}_1^{(2)}(\omega_1) \cdot \hat{P}_2^{(0)}(\omega_2)$$

6. The roots of polynomials $P_1^{(3)}(\omega_1)$ and $P_2^{(3)}(\omega_2)$ can be calculated, and $M = 6$ combinations of these roots can be used as optimal collocation points $\omega^{(i)} \equiv \left(\omega_1^{(i)}, \omega_2^{(i)}\right),\ i = 1 \ldots 6$.
7. Once the collocation points have been chosen, the coefficients of the aPC can be determined using Eq. (C-11):

$$\begin{bmatrix} c_1 \\ c_2 \\ \ldots \\ c_6 \end{bmatrix} = \begin{bmatrix} \Psi_1\left(\omega^{(1)}\right) & \Psi_2\left(\omega^{(1)}\right) & \ldots & \Psi_6\left(\omega^{(1)}\right) \\ \Psi_1\left(\omega^{(2)}\right) & \Psi_2\left(\omega^{(2)}\right) & \ldots & \Psi_6\left(\omega^{(2)}\right) \\ \ldots & \ldots & \ldots & \ldots \\ \Psi_1\left(\omega^{(6)}\right) & \Psi_2\left(\omega^{(6)}\right) & \ldots & \Psi_6\left(\omega^{(6)}\right) \end{bmatrix}^{-1} \begin{bmatrix} \Omega\left(\omega^{(1)}\right) \\ \Omega\left(\omega^{(2)}\right) \\ \ldots \\ \Omega\left(\omega^{(6)}\right) \end{bmatrix}$$

C.3 Mathematical Description of Global Sensitivity Indices and Implementation through a Generic Example

This Section presents a summary of the mathematical description of global sensitivity indices introduced in Section 3.2.4 and provides a simple, generic example using a 2nd order polynomial expansion for a model with two input parameters, which can be generalized to higher-order, larger-dimension cases.

C.3.1 Sobol Sensitivity Indices

The Sobol index indicates what fraction of the total variance of Ω can be traced back to the joint contributions of parameters $\omega_{i_1}, \dots, \omega_{i_s}$. Using aPC, this can be expressed as:

$$S_{i_1,\dots,i_s} = \frac{\sum_{k=2}^{M} \chi_k c_k^2}{\sum_{k=2}^{M} c_k^2}, \quad \chi_k = \begin{Bmatrix} 1 & if\ \alpha_j^k > 0,\ \ \forall j \in (i_1, \dots, i_s)\ and\ \alpha_j^k = 0,\ \ \forall j \notin (i_1, \dots, i_s) \\ 0 & if\ \alpha_j^k = 0,\ \ \exists j \in (i_1, \dots, i_s)\ or\ \alpha_j^k > 0,\ \ \exists j \notin (i_1, \dots, i_s) \end{Bmatrix} \quad \text{(C-13)}$$

where c_k and α_j^k are defined in Eqs. (3-7) and (C-4), respectively. The index selection operator χ_k indicates where the chosen parameters $\omega_{i_1}, \dots, \omega_{i_s}$ have simultaneous contributions within the overall expansion.

The Total Index expresses the total contribution to the variance of the model output Ω due to the uncertainty of an individual parameter ω_j in all cross-combinations with other parameters:

$$S_{\omega_j}^T = \sum_{(i_1,\dots,i_s):j\in(i_1,\dots,i_s)} S_{(i_1,\dots,i_s)} \quad \text{(C-14)}$$

$S_{\omega_j}^T$ sums up all Sobol indices in which the variable ω_j appears, both as univariate and joint influences.

C.3.2 Weighted Sensitivity Indices

The weighted sensitivity indices reflect the square slope $\partial\Omega/\partial\omega_j$ averaged over the statistical distributions or weighing functions of $\omega_1, \dots, \omega_N$:

$$S_{\omega_j}^2 = \int_{\omega_1\in\Lambda} \dots \int_{\omega_N\in\Lambda} \left[\frac{\partial\Omega(\omega)}{\partial\omega_j}\right]^2 d\Gamma(\omega_1) \dots d\Gamma(\omega_N) \quad \text{(C-15)}$$

Using aPC, the averaged sensitivity index S_{ω_j} can be explicitly expressed as:

$$S_{\omega_j}^2 = \sum_{k=2}^{M} c_k^2 \sum_{i=0}^{\alpha_j^k-1} \left[b_{i,j}^{\left(\alpha_j^k-1\right)}\right]^2 \quad \text{(C-16)}$$

where the re-collection coefficients $b_{i,j}^{\left(\alpha_j^k-1\right)}$ are defined as solution of the following linear system:

$$\begin{bmatrix} p_{0,j}^{(0)} & 0 & 0 & 0 \\ p_{0,j}^{(1)} & p_{1,j}^{(1)} & \dots & 0 \\ \dots & \dots & \dots & \dots \\ p_{0,j}^{(\alpha_j^k-1)} & p_{1,j}^{(\alpha_j^k-1)} & \dots & p_{\alpha_j^k-1,j}^{(\alpha_j^k-1)} \end{bmatrix}^T \begin{bmatrix} b_{0,j}^{\left(\alpha_j^k-1\right)} \\ b_{1,j}^{\left(\alpha_j^k-1\right)} \\ \dots \\ b_{\alpha_j^k-1,j}^{\left(\alpha_j^k-1\right)} \end{bmatrix} = \begin{bmatrix} p_{1,j}^{(\alpha_j^k)} \\ 2p_{2,j}^{(\alpha_j^k)} \\ \dots \\ \alpha_j^k p_{\alpha_j^k,j}^{(\alpha_j^k)} \end{bmatrix} \quad \text{(C-17)}$$

C.3.3 Implementation of Weighted Sensitivity Indices through a Generic Example

Here, we derive the weighted sensitivity indices from the 2nd order, 2-parameter aPC developed in the simple aPC implementation algorithm detailed in Section C.2.

As seen previously, in this case, $M = 6$ and the weighted sensitivity indices are:

$$S^2_{\omega_1} = \sum_{k=1}^{6} c_k^2 \sum_{i=0}^{\alpha_1^k - 1} \left[b_{i,1}^{(\alpha_1^k - 1)} \right]^2 = c_3^2 \left[b_{0,1}^{(0)} \right]^2 + c_4^2 \left[b_{0,1}^{(0)} \right]^2 + c_6^2 \left[\left[b_{0,1}^{(1)} \right]^2 + \left[b_{1,1}^{(1)} \right]^2 \right]$$

$$S^2_{\omega_2} = \sum_{k=1}^{6} c_k^2 \sum_{i=0}^{\alpha_2^k - 1} \left[b_{i,2}^{(\alpha_2^k - 1)} \right]^2 = c_2^2 \left[b_{0,2}^{(0)} \right]^2 + c_4^2 \left[b_{0,2}^{(0)} \right]^2 + c_5^2 \left[\left[b_0^{(1)} \right]^2 + \left[b_1^{(1)} \right]^2 \right]$$

with:

$$p_{0,1}^{(0)} b_{0,1}^{(0)} = p_{1,1}^{(1)}$$

$$p_{0,2}^{(0)} b_{0,2}^{(0)} = p_{1,2}^{(1)}$$

$$\begin{bmatrix} p_{0,1}^{(0)} & 0 \\ p_{0,1}^{(1)} & p_{1,1}^{(1)} \end{bmatrix}^T \begin{bmatrix} b_{0,1}^{(1)} \\ b_{1,1}^{(1)} \end{bmatrix} = \begin{bmatrix} p_{1,1}^{(2)} \\ 2p_{2,1}^{(2)} \end{bmatrix}$$

$$\begin{bmatrix} p_{0,2}^{(0)} & 0 \\ p_{0,2}^{(1)} & p_{1,2}^{(1)} \end{bmatrix}^T \begin{bmatrix} b_{0,2}^{(1)} \\ b_{1,2}^{(1)} \end{bmatrix} = \begin{bmatrix} p_{1,2}^{(2)} \\ 2p_{2,2}^{(2)} \end{bmatrix}$$

C.4 aPC Implementation Algorithm in Matlab

This Section contains the complete Matlab algorithm used to calculate response surfaces based on the mathematical descriptions provided in the previous Sections. The first part of the algorithm is used to calculate the multivariate polynomials Ψ_k, based on the probability distributions of the input parameters. The second part of the algorithm takes the vector of values calculated by the best-estimate code (outside of the script) and calculates the aPC expansion coefficients c_k. The custom functions used in these algorithms are also listed below. Finally, the last algorithm calculates the Total Index and weighted sensitivity index for each parameters and ranks them in decreasing order of importance (useful for cases with a large number of parameters).

C.4.1 Part 1 of the aPC Algorithm

```
clear all % Remove all variables and functions from the workspace
format shortE % All numbers displayed with 5 significant digits, scientific notation
prompt='What is the desired order of the polynomial expansion?\nEnter 1 or 2: ';
```

```
result=input(prompt); % Order of polynomial expansion - can be modified by user
while result~=1 && result~=2
  disp('This is not a valid entry.');
  result=input(prompt);
end
d=result;

%% Load input parameters cell array
% Input array contains inputs with for each line: Parameter Name, mu_0, mu_1, ... , mu_(2d+1).

load('Input');
N=size(Input,1); % Number of input parameters

%% Step 1 of algorithm

% Calculate number of polynomials in the expansion.
% Using explicit expression instead of factorial to avoid NaN error for large N.
% MUST BE UPDATED FOR d>2.

if d==1
   M=N+1;
elseif d==2
   M=(N+2)*(N+1)/2;
end

%% Step 2-3 of algorithm. WARNING: risk of inaccuracy when inverting matrix.

% Calculate polynomial coefficients
% p(i+1,k+1,j)= p_(i,j)^((k))

p=zeros(d+2,d+2,N);
for k=0:d+1
   unit=zeros(k+1,1); % Build vector [0,...,0,1], see Eq. (C-5)
   unit(k+1,1)=1; % Build vector [0,...,0,1], see Eq. (C-5)
   for j=1:N
      mu=zeros(k+1,k+1); % Build matrix of raw moments, see Eq. (C-5)
      for m=0:k-1
         for l=0:k
            mu(m+1,l+1)=Input{j,m+l+2}; % Build matrix of raw moments, see Eq. (C-5)
         end
      end
      mu(k+1,k+1)=1; % Build matrix of raw moments, see Eq. (C-5)
      p_temp=inv(mu)*unit; % Temporary vector to build polynomial coefficients, see Eq. (C-5)
```

```
      for i=0:k
        p(i+1,k+1,j)=p_temp(i+1,1); % Fill the (d+2)*(d+2)*N array of polynomial coefficients
      end
    end
end

%% Step 4 of algorithm

% Calculate polynomial norms
% norm_P(j,k+1)=||P_j^((k))||

norm_P=zeros(N,d+1);
for k=0:d
  for j=1:N
    norm_P_temp=0; % Temporary variable to calculate norm of P, see Eq. (C-10)
    for l=0:k
      for m=0:k
        norm_P_temp=norm_P_temp+p(l+1,k+1,j)*p(m+1,k+1,j)*Input{j,l+m+2};
      end
    end
    norm_P(j,k+1)=sqrt(norm_P_temp); % Fill the N*(d+1) array of polynomial norms
  end
end

% Normalize polynomial coefficients, except order d+1

for i=0:d
  for k=0:d
    for j=1:N
      p(i+1,k+1,j)=p(i+1,k+1,j)/norm_P(j,k+1);
    end
  end
end

%% Step 5 of algorithm

% Build N*M matrix alpha_j^(k) for 1st and 2nd order expansions. MUST BE UPDATED FOR
d>2.
% alpha(j,k)=alpha_j^(k)

alpha=zeros(N,M);
for k=2:N+1
  alpha(k-1,k)=1; % First order polynomial terms
end
```

```
if d==2
   for k=N+2:2*N+1
      alpha(k-1-N,k)=2; % Second order polynomial terms
   end
   k=2*N+2;
   for j=1:N-1
      for m=k:k+N-j-1
         alpha(j,m)=1; % Cross-parameter terms
         alpha(m-k+j+1,m)=1; % Cross-parameter terms
      end
      k=k+N-j;
   end
end

%% Step 6 of algorithm

% Build N*(d+2) array of polynomial coefficients for the P_j^((d+1))
% pol_coef(j,i+1)=p_(d+1-i,j)^((d+1))

pol_coef=zeros(N,d+2);
for j=1:N
   for i=0:d+1
      pol_coef(j,i+1)=p(d+2-i,d+2,j);
   end
end

% Build (d+1)*N array of roots of P_j^((d+1)) for j=1:N

Roots=zeros(d+1,N);
for j=1:N
   Roots(:,j)=real(roots(pol_coef(j,:))); % Eliminates cases where there are imaginary roots
end

% Build M*N array of random indices in [1:d+1] with no repetition

Rand=zeros(M,N);
for j=1:N
   Rand(1,j)=d+1; % First row: collocation point closest to mean values
end
Rand_temp_num=Rand(1,:);
Rand_temp_str=num2str(Rand_temp_num);
key={Rand_temp_str};
value={1};
Rand_dic=containers.Map(key,value); % Dictionary to verify that each new row is unique
```

```
for i=2:M % Add one row at a time until array is complete
   while Rand_dic.isKey(Rand_temp_str) % Try new values until additional row is unique
      Rand_temp_num=randi([d,d+1],1,N); % Collocation points close to mean values.
WARNING: for d=2, only works if N>=4.
      Rand_temp_str=num2str(Rand_temp_num);
   end
   Rand(i,:)=Rand_temp_num; % Add row to array
   Rand_dic(Rand_temp_str)=1; % Add key to dictionary
end

% Build M*N array of unique collocation points
% collocation(i,j)=omega_j^((i))

collocation=zeros(M,N);
for i=1:M
   for j=1:N
      collocation(i,j)=Roots(Rand(i,j),j);
   end
end

%% Step 7 of algorithm

% Build M*M matrix M_Psi
% M_Psi(i,k)=Psi_k(omega^((i)))

M_Psi=zeros(M,M);
for i=1:M
   for k=1:M
      M_Psi(i,k)=Psi(p,k,alpha,collocation(i,:),N);
   end
end
```

C.4.2 Part 2 of the aPC Algorithm

```
% Calculate coefficients c_k after creating a column array 'omega' with results from RELAP5-
3D, using input parameters from collocation matrix

load('omega');
c=M_Psi\omega;

%% Information on response function, see Eq. (C-7)

mean=c(1);
```

```
Var=0;
for k=2:M
   Var=Var+c(k)^2;
end
StDev=sqrt(Var);

info_mean=['Mean = ', num2str(mean)];
disp(info_mean);
info_StDev=['Standard deviation = ', num2str(StDev)];
disp(info_StDev);
```

C.4.3 Functions Used in the aPC Algorithm

```
function P_j_k=P(p,j,k,omega_j)
% Build polynomials P_j^((k))
% P(p,j,k,omega_j)=P_j^((k)) (omega_j)
P_j_k=0;
for i=0:k
   P_j_k=P_j_k+p(i+1,k+1,j)*omega_j^i;
end

function Psi_k=Psi(p,k,alpha,omega,N) % omega is a vector
% Build polynomials Psi_k
% Psi(p,k,alpha,omega,N)=Psi_k(omega)
Psi_k=1;
for j=1:N
   Psi_k=Psi_k*P(p,j,alpha(j,k),omega(j));
end

function aPC_k=aPC(c,p,alpha,omega,N,M)
% Build response surface
aPC_k=0;
for k=1:M
  aPC_k=aPC_k+c(k)*Psi(p,k,alpha,omega,N);
end
```

C.4.4 Sensitivity Indices Algorithm

```
%% Sensitivity indices

% Build N*N matrix Sobol(j,m) for 1st and 2nd order expansions.
% MUST BE UPDATED FOR d>2.
% Sobol(j,l)=S_j if j=l or S_j,l if j~=l.

Sobol=zeros(N,N);
```

```
for j=1:N
  Sobol(j,j)=c(j+1)^2/Var; % First order terms
end
if d==2
  for j=1:N
    Sobol(j,j)=Sobol(j,j)+c(j+N+1)^2/Var; % Second order terms
  end
  k=2*N+2;
  for j=1:N-1
    for l=j+1:N
      Sobol(j,l)=c(l-j+k-1)^2/Var; % Cross-parameter terms
      Sobol(l,j)=c(l-j+k-1)^2/Var; % Sobol(l,j)=Sobol(j,l)
    end
    k=k+N-j;
  end
end

% Build 1*N vector Total_Index(j) for 1st and 2nd order expansions.
% MUST BE UPDATED FOR d>2.
% Total_Index(j)=S_j^(T).

Total_Index=zeros(1,N);
for j=1:N
  for l=1:N
    Total_Index(j)=Total_Index(j)+Sobol(j,l); % See Eq. (C-14)
  end
end

[Total_Index_sorted,Total_Index_indices]=sort(Total_Index,'descend');
prompt_Sobol='How many of the highest Sobol Total Index parameters would you like to
display? ';
result_Sobol=input(prompt_Sobol);
while result_Sobol>N
  disp('This is not a valid entry.');
  result_Sobol=input(prompt_Sobol);
end
disp('The highest Sobol Total Index parameters are:');
disp(Total_Index_indices(1:result_Sobol));
disp('The corresponding Sobol Total Indices are:');
disp(Total_Index_sorted(1:result_Sobol));

% Build 1*N vector S_weighted(j)
% S_weighted(j)=S_(omega_j)^2
```

```
S_weighted=zeros(1,N);
for j=1:N
  for k=2:M
    b=0;
    if alpha(j,k)>0
      P_temp=zeros(alpha(j,k),alpha(j,k));
      p_temp=zeros(alpha(j,k),1);
      for l=0:alpha(j,k)-1
        p_temp(l+1)=(l+1)*p(l+2,alpha(j,k)+1,j);
        for m=0:l
          P_temp(l+1,m+1)=p(m+1,l+1,j);
        end
      end
      b_temp=P_temp'\p_temp;
      for i=0:alpha(j,k)-1
        b=b+b_temp(i+1)^2;
      end
    end
    S_weighted(j)=S_weighted(j)+c(k)^2*b;
  end
end

[S_weighted_sorted,S_weighted_indices]=sort(S_weighted,'descend');
prompt_S_weighted='How many of the highest weighted sensitivity index parameters would
you like to display? ';
result_S_weighted=input(prompt_S_weighted);
while result_S_weighted>N
  disp('This is not a valid entry.');
  result_S_weighted=input(prompt_S_weighted);
end
disp('The highest weighted sensitivity index parameters are:');
disp(S_weighted_indices(1:result_S_weighted));
disp('The corresponding weighted sensitivity indices are:');
disp(S_weighted_sorted(1:result_S_weighted));
```